

Developments in Dynamic Field Gradient Focusing: Microfluidics and Integration

Thesis submitted in accordance with the requirements of the
University of Liverpool for the degree of Doctor in Philosophy

by

Thomas Robert Wray

August 2012



UNIVERSITY OF
LIVERPOOL

Acknowledgements

I would like to express my thanks to my supervisor Professor Peter Myers for his excellent guidance and ideas throughout this project and most importantly for all of the real ale and granting me the opportunity to undertake this project.

Thanks are also extended to all the members of the Myers group particularly fellow PhD student Dr Kevin Skinley for making the lab a great place to work.

I would also like to thank Thermo Fisher Scientific for sponsoring the DTA awards and providing funding for this research through Dr Harold Ritchie. Thanks also go to Pfizer for providing further funding through Dr Melissa Hannah-Brown.

I also thank all of the staff within the University Of Liverpool Department Of Chemistry for any support over all of my time studying here.

For collaborations during the project I would like to thank Dr Tony Edge and his team from Thermo Fisher Scientific and Dr Jetinder Singh and David Atkinson from the University Of Liverpool Department Of Engineering.

I am grateful to my family for all of their support and understanding during all of my studies. A big thanks to all my friends, especially everyone at the BKJJA, for all of their enduring encouragement.

Special thanks go to my partner Kate for all of her continued support and always being there for me, helping me through the hard times and making the good times the best. Thanks to Kate, I have got to where I am now which I couldn't have done without her.

Developments in Dynamic Field Gradient Focusing: Microfluidics and Integration

Abstract

By Thomas Robert Wray,

University of Liverpool, August 2012

Advances in modern science require the development of more robust and improved systems for electroseparations in chromatography. In response, the progress of a new analytical platform is discussed. DFGF (Dynamic Field Gradient Focusing) is a separation technique, first described in 1998, which exploits the differences in electrophoretic mobility and hydrodynamic area of analytes to result in separation. This is achieved by taking a channel and applying a hydrodynamic flow in one direction and a counteracting electric field gradient acting in the opposite direction, resulting in analytes reaching a focal point according to their electrophoretic mobility.

Work through this project has seen innovations to improve existing DFGF devices, including the design and manufacture of a novel packing material, while developing the latest DFGF system. This incorporates a microfluidic separation channel, eliminating the need for packing material or monolith. The new microfluidic device also features whole-on-column UV detection. Improvements through the developments of this device are discussed, most notably the utilisation of a new rapid prototyping technique. Examples of applications undertaken with the new device are demonstrated including novel samples and integration with mass spectrometry and 2D-HPLC.

Contents

Acknowledgements	i
Abstract	ii
Table of Contents	iii
List of Tables	vii
List of Figures	ix
1. Introduction	1
1.1 Background	1
1.2 Separation of Proteins	4
1.2.1 Chromatographic Protein Separation Techniques	5
1.2.2 Electrophoretic Protein Separation Techniques	9
1.2.3 Electrofocusing Techniques	10
1.3 References	15
2. DFGF	18
2.1 Theory	18
2.2 DFGF Set Up	21
2.2.1. DFGF Configuration	22
2.2.2. Packing Method	23
2.2.3. General Operation	25
2.2.4. Dynamic Flow Control: Flux Instruments Rheos Pumps and Janeiro 3.0	25
2.2.5. Dynamic Electric Field: Power Supply and Control	27
2.2.6. Data collection and presentation	30
2.3. Experimental with First Generation Device	35
2.3.1. First generation DFGF Device	35
2.3.2 Separation of two component test mixture: Bromophenol Blue and Amaranth	35
2.3.3 Separations of the Bio-Rad Kaleidoscope pre-stained standards test mixture	39

2.4	Experimentation with the Protasis DFGF device	47
2.4.1	The Protasis DFGF device: An Overview	47
2.4.2	Protasis Experimentation with a single analyte	48
2.4.3	Protasis separation of a two component test mixture	48
2.4.4	Protasis separation of Bio-Rad Kaleidoscope pre-stained standards test mixture	49
2.5	Discussion	55
2.6	Novel packing material for DFGF	59
2.6.1	Development of Particles for DFGF	59
2.6.2	Procedure for manufacture of macroporous monodispersed spherical silica	60
2.6.3	Droplet Generation	61
2.6.3.1	Fused Silica Tubing and a pump	61
2.6.3.2	Spraying with water misters and pneumatic sprayer	62
2.6.3.3	Inkjet and Domino Printer controlled droplet generation	64
2.6.4	Testing the particles with Gas Chromatography	69
2.6.5	DFGF experimentation with 80 μ m Silica particles	72
2.6.5.1	Packing the DFGF with the 80 μ m Silica particles	72
2.6.5.2	DFGF separations with novel packing material	74
2.7	Conclusions	81
2.8	References	85
3.	Microfluidic DFGF	87
3.1	Microfluidics	87
3.2	The New Microfluidic DFGF	88
3.2.1	Microfluidic DFGF design	88
3.2.2	DFGF Quartz Chip	89
3.2.3	The microfluidic DFGF device design	92
3.3	Experimental	94
3.3.1	Integration with power supply	94
3.3.2	Microfluidic DFGF -Instructions for Use	96
3.3.3	First Separation using the microfluidic DFGF	97
3.3.4	Electrode decomposition, New Gold electrodes	100
3.3.5	Separation of a three component test mixture	104

3.3.6 Separation using lower voltages	108
3.3.7 Sample leakage issues	111
3.3.8 Rapid Prototyping (RP)	122
3.3.9 Stereolithography Rapid Prototyping	122
3.3.10 RP Mask for Electrode Manufacture	124
3.3.11 RP Modified Electrode channels	128
3.3.12 Testing with the 100 μ m Electrode Channel	132
3.3.13 Testing with the 200 μ m Electrode Channel	134
3.3.14 PDA Detection	143
3.4 Conclusions	154
3.5 References	157
4. Applications using the microfluidic DFGF	159
4.1 DFGF Applications	159
4.2 Functionalised Gold Nano Particle Separation	159
4.2.1 Gold Nano Particle separation in a packed column using the first gen. DFGF	161
4.2.2. Microfluidic DFGF GNP Separation	165
4.3 Post column Detection	170
4.3.1 Capacitively Coupled Contactless Conductivity Detection (C ⁴ D)	171
4.3.2 Microfluidic DFGF post column detection	171
4.3.3 Results with all detection	175
4.4 Applications with Analytical Instrumentation	191
4.4.1. 2D-HPLC	191
4.4.2 HPLC-DFGF-MS: Single Valve Work	192
4.4.2 2D-HPLC: Dual Valve Set Up	199
4.5 Conclusions	206
4.6 References	211
5. Final Conclusions	212
5.1 Conclusions	212
5.2 Further work	217
5.3 References	223

Appendix	225
Appendix A. List of Abbreviations	225
Appendix B. Protasis voltage array and control software	228
Appendix C. ImageJ Visual Basic script	247
Appendix D. VBA MS Excel based system for graph generation	248
Appendix E. First generation DFGF construction	251
Appendix F. LabView C4D and UV DAQ System	252
Appendix G. List of Software	255

List of Tables

<i>Table 1.1. Summary of the properties of purification techniques utilised for proteins.</i>	4
<i>Table 2.3.1. Kaleidoscope Pre-Stained Standards Test Mixture.</i>	40
<i>Table 2.3.2. Voltage profile for Kaleidoscope separation in figure 2.3.8.</i>	45
<i>Table 2.4.1. Summary of voltage profiles used to separate 40μL Kaleidoscope mixture.</i>	50
<i>Table 2.4.2. EFG and flow rates applied to separate the Kaleidoscope mixture in figure 2.4.5.</i>	54
<i>Table 2.6.2. Particles manufactured using the hand spray and pneumatic spray.</i>	63
<i>Table 2.6.3. EFG Applied to separate the mixture of BPB and AM.</i>	76
<i>Table 2.6.4. Experimental conditions applied to the device to separate the Kaleidoscope test mixture with the monodispersed packing material.</i>	79
<i>Table 3.3.1. Summary of conditions for a microfluidic DFGF test separation of BPB and AM.</i>	98
<i>Table 3.3.2. Conditions for the separation of BPB, AM and AY in figure 3.3.9.</i>	105
<i>Table 3.3.3. Conditions used to result in the focusing of the 3 component mixture of AM and BPB and Acid Yellow.</i>	109
<i>Table 3.3.4. Experimental parameters for the separation of 5μL of 10% BPB AM and AY test mixture.</i>	112
<i>Table 3.3.5. Conditions for the separation of the Bio-Rad Kaleidoscope Pre-stain Standards in figure 3.3.16.</i>	120
<i>Table 3.3.6. Conditions used to separate AM and BPB testing the 200μm electrode channel.</i>	136
<i>Table 3.3.7. Optimised Microfluidic DFGF device.</i>	138
<i>Table 3.3.8. Conditions the separation of Kaleidoscope Proteins in figure 3.3.28.</i>	139

<i>Table 3.3.9. Table of voltage profiles and flow rates for the repeat separation of the kaleidoscope test mixture using the optimised microfluidic DFGF.</i>	142
<i>Table 3.3.10. Summary of controlling parameters and features available in data acquisition from the PDA using the bespoke software.</i>	144
<i>Table 3.3.11. Optimum PDA Detection parameter using the LCD backlight.</i>	149
<i>Table 3.3.12. Separation of the kaleidoscope mixture detected with the PDA detector in figure 3.3.35.</i>	150
<i>Table 3.3.13. UV light source stability issues.</i>	154
<i>Table 4.2.1. Voltage profiles and flow rates applied to separate the functionalised GNPs.</i>	162
<i>Table 4.2.2. Parameters used in separating the GNPs in the microfluidic DFGF.</i>	168
<i>Table 4.3.1. Optimal conditions for detection by C⁴D from the profiling for BPB.</i>	173
<i>Table 4.3.2. Changes in EFG for the separation of AM and BPB in figure 4.3.8.</i>	182
<i>Table 4.3.3. Conditions for the separation of AM and BPB monitored by C⁴D and UV. The detection data is shown in figure 4.3.9.</i>	184
<i>Table 4.3.4. Conditions for repeat separation of the Kaleidoscope proteins in figure 4.3.11.</i>	187
<i>Table 4.4.1. Timings for the application of the EFG in the microfluidic device during 2D method.</i>	204

List of Figures

<i>Figure 1.1.1. Protein structure of Lysozyme.</i>	3
<i>Figure 1.2.1. Configuration of the EFGF device.</i>	13
<i>Figure 2.1.1. Theoretical model for DFGF.</i>	19
<i>Equation 2.1.1. The Flux equation.</i>	19
<i>Equation 2.1.2. The flux equation solved for C, where M_i is the total number of moles of analyte.</i>	19
<i>Equation 2.1.3. X_i defines a point along the length of the separation channel where an analyte will come into focus.</i>	20
<i>Equation 2.1.4. Variance of the width of a focused band of analyte.</i>	20
<i>Figure 2.2.1. DFGF Set Up and supporting equipment.</i>	21
<i>Figure 2.2.2. DFGF Channel Configuration.</i>	22
<i>Figure 2.2.3. DFGF packing apparatus.</i>	24
<i>Figure 2.2.4. Flux Instruments Rheos Janeiro 3.0 software.</i>	26
<i>Figure 2.2.5. Protasis Power supply schematic.</i>	27
<i>Figure 2.2.6. Protasis UController HV Control Software.</i>	28
<i>Figure 2.2.7. An example of a linear EFG generated by the Labview Protasis Ucontroller software in Automatic Mode.</i>	29

<i>Figure 2.2.8. An example of the EFGs which can be applied by the Labview Ucontroller software in Manual Mode.</i>	30
<i>Figure 2.2.9. A) Nikon D80 with a 60mm 1:2.8D macro lens configured to take images of the separation channel with the addition of a LED ring illuminator. B) Nikon Camera Control Pro software user interface.</i>	31
<i>Figure 2.2.10. A) Detection using GIMP to subtract images highlighting any changes in the positions of analytes with a corresponding profile measurement. B) Next a profile plot is generated using ImageJ, in this instance, FIJI¹⁶, a rich featured version of ImageJ.</i>	32
<i>Figure 2.2.11. 1) Data Interpretation. 2) The cropped image stack is loaded into ImageJ and all the profiles are measured. 3) This data was loaded into the MS Excel 'Profile Generator' producing a graph of the separation.</i>	34
<i>Figure 2.3.1. Structure of Bromophenol Blue (BPB) 4,4'-(1,1-dioxido-3H-2,1-benzoxathiole-3,3-diyl)bis(2,6-dibromophenol).</i>	35
<i>Figure 2.3.2. Structure of Amaranth (AM) trisodium (4E)-3-oxo-4-[(4-sulfonato-1-naphthyl)hydrazono]naphthalene-2,7-disulfonate.</i>	36
<i>Figure 2.3.3. Separation and focusing of Bromophenol Blue (BPB) and Amaranth (AM).</i>	37
<i>Figure 2.3.4. Injection of BPB with a static linear EFG.</i>	38
<i>Figure 2.3.5. BPB focusing as shown in the form of a Montage. Constructed by taking the cropped images and stacking them in order.</i>	39
<i>Figure 2.3.6. Kaleidoscope bands migrating back and forth along the separation channel in a focused band of the protein mixture.</i>	41
<i>Figure 2.3.7. A) Graphical representation of kaleidoscope mixture focused in the first gen. device. B) Montage of the images displaying the movement of the bands along the separation channel.</i>	42
<i>Figure 2.3.8. A) 'Run1' From Table2.3.2 Displaying the kaleidoscope test mixture being manipulated in the separation channel. B) 'Run2' From Table2.3.2 An immediate follow up experiment injecting the sample and focusing again. Three separated bands can be seen in the plot.</i>	46
<i>Figure 2.4.1. Construction and image of the Protasis DFGF device.</i>	47

<i>Figure 2.4.2. More than 20μL of 10% v/v Lissamine green solution being injected and focused into a tight band.</i>	48
<i>Figure 2.4.3. A mixture of Amaranth and BPB separated and focused.</i>	49
<i>Figure 2.4.4. A) Graphical representation of the separation of 40μL Kaleidoscope mixture. B) Single plot at 147mins displaying at least four bands.</i>	51
<i>Figure 2.4.5. The separation of Kaleidoscope test mixture displayed graphically. Five component peaks are observed during the separation.</i>	54
<i>Figure 2.5.1. LEFT: Displays the Protasis device. RIGHT: top area of separation channel with the blemishing of the acrylic after running at the maximum 1000V without cooling.</i>	57
<i>Figure 2.5.2. Optical Microscope image of polyacrylamide packing material in DFGF channel. Void spaces and irregular interstitial spacing are visible across the entire bed.</i>	58
<i>Figure 2.5.3. Left to right, images displaying a bed rearrangement leading to the collapse of the membrane.</i>	59
<i>Figure 2.6.1. Drop generator system.</i>	62
<i>Figure 2.6.2. Printer Head of the Domino printer.</i>	65
<i>Figure 2.6.3. Optimal 'Break Up' of droplets from the spray head on the Domino printer.</i>	66
<i>Figure 2.6.4. Spraying monodispersed particles using the modified Domino printer.</i>	67
<i>Figure 2.6.5. Mercury Porosimetry of the 80μm silica particles.</i>	68
<i>Figure 2.6.6. SEM images of the drop by drop 80μm silica particles.</i>	69
<i>Figure 2.6.7. Optical microscopy of the packed GC column.</i>	70
<i>Figure 2.6.8. GC separation of Petroleum Ether and DCM at 60$^{\circ}$C using the 1.2m column packed with 80μm silica.</i>	71

<i>Figure 2.6.9. FTIR analysis of the 80μm particles before and after treatment at 1000°C.</i>	72
<i>Figure 2.6.10. First Gen. DFGF packed with 80μm porous silica particles.</i>	73
<i>Figure 2.6.11. A) Graphical representation of a flow through of 10% BPB AM mixture at 1μLmin⁻¹. B) Montage of images displaying the mixture as purple in colour, showing no derivation of red or blue corresponding to BPB or AM.</i>	75
<i>Figure 2.6.12. Separation of BPB and AM in a faster time utilising the larger pore monodispersed packing material.</i>	77
<i>Figure 2.6.13. A) Graph of the separation of the Kaleidoscope test mixture. B) Montage of the Kaleidoscope separation.</i>	80
<i>Figure 3.2.1. Initial design of a microfluidic DFGF from Dolomite.</i>	89
<i>Figure 3.2.2. Design of the Microfluidic DFGF separation channel chip and electrode chip.</i>	90
<i>Figure 3.2.3. Microfluidic DFGF device exploded view.</i>	91
<i>Figure 3.2.4. Microfluidic DFGF device design summary.</i>	93
<i>Figure 3.3.1. Prototype Electrode connector made from IDC connector.</i>	94
<i>Figure 3.3.2. A) Microfluidic DFGF Electrode Connector. B) Connector inserted in the recess at the back of the microfluidic DFGF. C) All HV connections in place using IDC connectors.</i>	95
<i>Figure 3.3.3. Dolomite User Guide for the microfluidic DFGF.</i>	96
<i>Figure 3.3.4. Initial Separation of BPB and AM with the microfluidic DFGF.</i>	99
<i>Figure 3.3.5. Severe degradation of the platinum electrodes on the microfluidic DFGF electrode chip.</i>	100
<i>Figure 3.3.6. Structure of Nafion.</i>	101

<i>Figure 3.3.7. Gold electrode array on an existing electrode chip.</i>	102
<i>Figure 3.3.8. Completed gold electrode array and chip holder base with fixed connector.</i>	103
<i>Figure 3.3.9. The molecular structure of Acid Yellow, Disodium 2,5-dichloro-4-[3-methyl-5-oxo-4-(4-sulfonatophenyl)diazenyl-4H-pyrazol-1-yl]benzenesulfonate.</i>	104
<i>Figure 3.3.10. Separation and focusing of BPB, AM and AY.</i>	107
<i>Figure 3.3.11. A) Graphical representation of the focusing of the 3 component mixture of AM and BPB and Acid Yellow. B) Image of the separation channel of the focused band where it is apparent that some of the sample has leaked from the separation channel.</i>	110
<i>Figure 3.3.12. Graph showing the separation and focusing of a 5μL injection of the BPB AM and AY.</i>	113
<i>Figure 3.3.13. Membrane from experiment in figure 3.3.11.</i>	114
<i>Figure 3.3.14. Enlarged cross section of the microfluidic DFGF detailing the issue with the channel dimensions and leakage issue.</i>	116
<i>Figure 3.3.15. Prototype Teflon insert to provide a narrower electrode channel and better support for the membrane in comparison to the original PEEK electrode channel and gasket.</i>	117
<i>Figure 3.3.16. Prototype Platinum Electrodes on a plastic chip with holes drilled for the flow of electrode channel buffer and an IDC connector to interface with the Protasis Power Supply.</i>	118
<i>Figure 3.3.17. Separation and focusing of the Bio-Rad Kaleidoscope test mixture in the microfluidic DFGF using the prototype platinum electrode array and prototype Teflon electrode channel.</i>	121
<i>Figure 3.3.18. Schematic displaying the setup of Stereolithography Apparatus.</i>	123
<i>Figure 3.3.19. Electrode chip mask design drawn in CAD software.</i>	125
<i>Figure 3.3.20. PVD Platinum electrode plate and the RP mask.</i>	126

<i>Figure 3.3.21. Decomposed PVD electrodes after 20mins at 200Vcm⁻².</i>	127
<i>Figure 3.3.22. Final Electrode chip. Houses five platinum electrodes on a glass chip with IDC connector.</i>	127
<i>Figure 3.3.23. A, B & C) 'Gasket Holder' drawn in CAD ready for SLA manufacture. Top, Base, and Front elevations respectively. D) Manufacture of 'Gasket Holder' using SLA RP.</i>	128
<i>Figure 3.3.24. Cross section schematics of the 'Gasket Holder' with channel widths of 100µm and 200µm respectively.</i>	130
<i>Figure 3.3.25. A) This graph displays the need to collect images at a shorter time intervals as the analyte comes into focus seemingly instantaneously where this effect in actual is a gradual phenomenon. B) The montage also displays this as the AM and BPB are observed.</i>	132
<i>Figure 3.3.26. Separation of BPB and AM using 100µm electrode channel.</i>	133
<i>Figure 3.3.27. Graph of separation using the 200µm electrode channel.</i>	136
<i>Figure 3.3.28. Separation of Kaleidoscope test mixture displaying a region of focused proteins.</i>	140
<i>Figure 3.3.29. Separation of the kaleidoscope test mixture using the optimised microfluidic DFGF with enhanced imaging.</i>	142
<i>Figure 3.3.30. Toshiba TC101 PDA Detector.</i>	144
<i>Figure 3.3.31. PDA Software user interface with option to collect single samples or collect a sequence which are stored in the capture buffer before writing to a *.CSV file.</i>	144
<i>Figure 3.3.32. PDA DFGF configuration using ambient light. Left: Image illustrates the setup. Right: Cross section of the chip and the PDA.</i>	145
<i>Figure 3.3.33. PDA detector graph showing three peaks corresponding to the three markers on the separation channel.</i>	146
<i>Figure 3.3.34. PDA Light sources.</i>	148
<i>Figure 3.3.35. Separation attempt of the Kaleidoscope protein mixture.</i>	151

<i>Figure 3.3.36. Test displaying the introduction of a Test mixture into the separation channel.</i>	152
<i>Figure 4.2.1. CPS Analysis of the functionalised GNPs.</i>	160
<i>Figure 4.2.2. Graphical representation and Montage of the separation of the functionalised GNPs in the first gen. DFGF device.</i>	163
<i>Figure 4.2.3. SEM of the packing material from the band 40mm along the channel displaying singular GNPs on the surface of the polyacrylamide spheres.</i>	164
<i>Figure 4.2.4. SEM of the packing material from the band 55mm along the channel displaying aggregates of the GNPs on the surface of the polyacrylamide spheres.</i>	165
<i>Figure 4.2.5. Graphical representation of the open channel microfluidic DFGF separation of the GNPs.</i>	168
<i>Figure 4.2.6. Image of the separation channel with the GNP's separated from the aggregates.</i>	169
<i>Figure 4.3.1. UV and C⁴D set up.</i>	172
<i>Figure 4.3.2. Profile of condition for C⁴D detection of BPB.</i>	173
<i>Figure 4.3.3. Labview DAQ System for C⁴D and UV detectors.</i>	174
<i>Figure 4.3.4. The first data successfully collected from the DAQ system showing a flat base line for each detector.</i>	175
<i>Figure 4.3.5. Graphical representation of the whole column reflectance data displaying the BPB moving through the microfluidic DFGF.</i>	177
<i>Figure 4.3.6. BPB injected and brought into focus and detected.</i>	178
<i>Figure 4.3.7. Elution detection from the microfluidic DFGF separation of AM and BPB.</i>	179
<i>Figure 4.3.8. Separation of AM and BPB with post column detection.</i>	183
<i>Figure 4.3.9. Separation of AM and BPB over three injection with C⁴D and UV detection.</i>	184

<i>Figure 4.3.10. Post separation channel detection for the separation of kaleidoscope test mixture in chapter three figure3.3.28.</i>	185
<i>Figure 4.3.11. Graph displaying the PDA data for the separation of the kaleidoscope test mixture with C⁴D and UV detection.</i>	188
<i>Figure 4.3.12. Post separation channel detection for the separation of the Kaleidoscope test mixture described in chapter three figure33.34.</i>	190
<i>Figure 4.4.1. HPLC-DFGF-MS Set up.</i>	193
<i>Figure 4.4.2. Injection of insulin pumped at 100uLmin⁻¹ without applied electric field.</i>	194
<i>Figure 4.4.3. Injection of insulin pumped at 100uLmin⁻¹ with the electric field applied between 1min and 6.5min with 1000V on each electrode.</i>	195
<i>Figure 4.4.4. Overlaid chromatograms from the test injection of insulin with and without the use of the electric field.</i>	195
<i>Figure 4.4.5. Injection and flow through of the sample without a column at 2μLm⁻¹ with no electric field applied.</i>	197
<i>Figure 4.4.6. Injection and flow through of the sample without a column at 2μLm⁻¹ with an electric field applied from 0mins until the end of the run.</i>	197
<i>Figure 4.4.7. Overlaid chromatograms for focusing effect without a column in place.</i>	198
<i>Figure 4.4.8. Integration of the microfluidic DFGF with a 2D HPLC valve switching array.</i>	199
<i>Figure 4.4.9. Switching valve positions and flow of sample for the DFGF assisted 2D HPLC procedure.</i>	202
<i>Figure 4.4.10. The DFGF assisted 2D HPLC procedure running without the use of the EFG for comparison.</i>	203
<i>Figure 4.4.11. Chromatogram from the DFGF assisted 2D HPLC separation with the EFG in operation.</i>	204
<i>Figure 4.4.12. Overlaid chromatograms from the DFGF assisted 2D HPLC separations with and without the pre-concentration of the electric field.</i>	205
<i>Figure 5.2.1. NanoFlex Electrode chip design.</i>	220

Chapter 1. Introduction

1.1 Background

Advancements in cellular research and the completion of the human genome project have driven the demand on the analysis of biomacromolecules to reach a point outstretching current abilities. As the coding of human and other genomes are now understood, the next step is to identify and characterise specific proteins and determine which processes and pathways regulate their production at a cellular level. For the last decade many chromatographic techniques have been extensively developed but still fail to deliver the efficiency and selectivity required for separations and purification of proteins in the areas of biological, medical and physical sciences. This can be attributed to proteins themselves being a challenging matrix for separation.

Proteins are the most abundant macromolecules occurring naturally. These macromolecules range from small peptides to massive polymers and are found in thousands of diverse forms. These varieties of proteins, regardless of origin, are made up from the same twenty standard amino acids. Despite twenty fundamental building blocks the range of proteins and their application in organisms is vast. From the silk from spiders, feathers of a bird, poisons in mushrooms, to more specific and novel proteins namely Enzymes. Enzymes, all of which being proteins, are the most diverse and specialised¹.

There are twenty amino acid components which are composed of a primary amine ($-\text{NH}_3^+$), a carboxylic acid ($-\text{COOH}$) group bonded to a central alpha carbon, and a variable side chain ($-\text{R}$) group also bonded to the central alpha carbon atom.

However, there is one exception to this general structure, namely proline, which has a secondary cyclic amine and is therefore characterised as an imino acid². A protein itself is formed by linking different combinations of these side chains by a covalent peptide bond formed between the amino group of one, and the alpha carbon of the next amino acid. This gives proteins their characteristic of having a rigid back bone, from planar peptide groups, and suspended side chains.

As a result of this complicated macromolecular arrangement, a protein's structure is described in terms of four levels of intricacy¹. The primary structure of a protein is the linear chain of amino acids linked by the covalent peptide bonds. Also included in the primary structure are other covalent bonds such as disulphide bonds from cysteine residues that are in close proximity but not part of the linear chain.

The secondary protein structure is dependent on the nature of 'folding' within sections of the polypeptide chain. Protein folding is a rearrangement in space of the polypeptide structure into a lower energy conformation.

There are two common types of folding, α -helix and β -pleated sheets. The formation of an α -helix is a result of the carbonyl oxygen of each peptide bond hydrogen bonding to the hydrogen of the amino group of the amino acid four units along the chain. These bonds run parallel to the axis of helix and depending on the interactions of the amino acid R-groups this conformation can be stabilised or destabilised. The β -pleated sheets occur where polypeptide bonds, from the same chain or different chains, have hydrogen bonds between them. This bonding is planar and has a slight twist which in some cases can result in a β -barrel².

The tertiary structural elements of proteins refer to the three-dimensional arrangement of the whole chain.

For example, when introduced to water, a protein will fold as to expose the hydrophilic elements of the chain and protect the hydrophobic species. Interestingly, once the protein has folded in its natural media it is held in place by electrostatic interaction of the side chains and by hydrogen bonding with the disulphides.

Quaternary protein structures are where proteins are made up of more than one polypeptide chains. This therefore refers to the spatial arrangement of different polypeptide units and the interactions between them.



Figure 1.1.1. Protein structure of lysozyme displaying; the protein backbone in white, α -helix in pink, β -sheets in yellow, disulphide coordination in cyan.

1.2 Separation of Proteins

These different elements of the proteins structure generate a number of properties which can be exploited to result in successful and efficient separations and purification. A summary of the most common methods of purification techniques and the properties exploited are listed in table 1.1 below.

Technique	Property Exploited	Capacity	Resolution	Yield	Cost
pH precipitation	Charge	High	Very Low	Medium	Low
Ammonium sulphate precipitation	Hydrophobicity	High	Very Low	High	Low
Aq. Two phase extraction	Mixture, Bip-Affinity	High	Very Low	High	Low
Ion exchange chromatography	Charge	Medium	Medium	Medium	Medium
Hydrophobic interaction chromatography	Hydrophobicity	Medium	Medium	Medium	Medium
Isoelectric focusing	Charge/ pI	Low	High	Medium	High
Dye Affinity chromatography	Mixture	Medium	High	Medium	Medium
Ligand affinity chromatography	Bio-Activity	Medium-Low	Very High	Low	High
Size Exclusion Chromatography	Size	Very Low	Low	High	Medium

Table 1.1. Summary of the properties of purification techniques utilised for proteins³.

Common procedures for the purification of proteins will include a number of steps utilising two or more of the techniques in table 1.1.

Initially, the most important factors are a high capacity and low cost to yield the highest volume of protein from its source.

After this, or additional steps, the resolution is most important to enable the determination and identification of individual proteins from a complex mixture. There are many existing methods for a range of separation techniques which are applicable to proteins. These can be described as two types of technique. Firstly, chromatographic techniques where separation occurs by partitioning between the mobile and stationary phase. Secondly, electrophoretic separations where electric fields are used to mobilise individual proteins to unique points within a gel or channel.

1.2.1 Chromatographic Protein Separation Techniques

The most effective and commonly used chromatographic separation techniques include Size Exclusion, Ion Exchange, Affinity chromatography, High Performance Liquid Chromatography and Liquid Chromatography Mass Spectrometry (LC/MS)⁴.

Size Exclusion Chromatography (SEC), or gel filtration, exploits the differences in the overall size of proteins to result in separation⁵. This is achieved by packing a column with a porous spherical insoluble polymer particle, typically porous polyacrylamide beads, and pumping the sample through this packed bed. This packing results in a range of pathways through the column. Smaller species and small impurities flow through the column and diffuse in and out of the pores and smaller interstitial spaces taking longer to elute.

Larger species, i.e. the desired proteins, are too large to flow through the pores of the packing material and flow through the column following a path only through the interstitial space and elute from the column faster. As shown in table 1.1 size exclusion is a low resolution and low capacity technique.

Ion Exchange Chromatography separates proteins according to net charge. Anion exchange utilises a positively charged stationary phase packed into a column^{6,7}. A protein sample is introduced and pumped through the column by the mobile phase, typically buffered solution at pH 7. The result of this is that any proteins with a negative charge will have bound to the stationary phase and any neutral or positively charged species will have passed straight through the column. To elute the negatively charged species, the mobile phase is changed from a buffer solution to a salt solution of NaCl. The chloride ions then outcompete the protein for charged sites on the stationary phase resulting in displacement and elution. Cation exchange is the opposite, running a negatively charged stationary phase. Elution can be controlled in both polarities by changing the pH of the buffer solution resulting in changes to the net charge of the proteins. Ion Exchange provides a separation technique which can deliver separation of large mixtures; however the reproducibility of separations using these columns is poor due to the differences in efficiency of ligand coverage over the stationary phase and packing of the charged material being difficult.

Affinity Chromatography, AC, utilises the binding specificities of a given protein to another molecule, the ligand, to result in separation^{8,9}. Once a suitable ligand has been identified to function as a binding site, it is covalently bonded to the stationary phase, which is then packed into a column.

Next a sample mixture containing the desired protein is mobilised through the column with mobile phase favouring the conditions for absorption of the protein to the ligand. Only the specific desired protein will interact with the carefully chosen ligand and the other undesired proteins and impurities are flushed out of the column. To elute the desired protein the mobile phase is changed to favour desorption and the protein is collected in high purity.

Despite the high resolution there are difficulties in scale up of this separation technique. Most importantly AC is a highly labour intensive and costly approach because of the work involved in identifying and creating a specific stationary phase, as a result this process is more commonly used in areas such as pharmaceuticals where purity is considered paramount and far outweighs the cost.

High Performance Liquid Chromatography, HPLC, utilises high pressure pumps and smaller particle sizes to increase the migration of samples through a column¹⁰. The decrease in particle size facilitates faster separations by increasing the surface area of the stationary phase and providing a shorter diffusion pathway through the particles. This results in the ability to operate at higher flow rates further increasing the speed of separation and reducing the diffusion of samples¹¹.

Reverse Phase High Performance Liquid Chromatography, RP-HPLC, separates analytes according to differences in hydrophobic interaction. A functionalised hydrophobic stationary phase is packed into the column and a polar mobile phase is passed through at high pressure. Conversely 'Normal Phase' HPLC consists of the opposite, with a polar stationary phase and non-polar mobile phase, the separation occurs as a result of the sample having an affinity to the mobile or stationary phases, causing partitioning.

RP-HPLC is preferred for the analysis of proteins and biological samples as the resolution is very high, facilitating the separation of polypeptides of the same mass with differing sequences. Furthermore the aqueous mobile phase used in RP-HPLC is more compatible with biological samples compared to the high organic content used for Normal Phase HPLC. For larger polypeptides and, even larger proteins, the retention mechanism in RP-HPLC differs from that of smaller molecules. When smaller molecules flow through the column the species are constantly partitioning between the mobile and stationary phase.

Yet proteins and polypeptides are too large to continually partition and simply absorb to the hydrophobic surface of the stationary phase until the concentration of organic modifier in the mobile phase is increased to reach a critical point which causes desorption¹². At this point the species flows through the column with minimal interaction with the stationary phase. Though this technique provides separations with good resolution, there are shortcomings with the ability of the technique to handle complex samples. Furthermore the protein sample will often be denatured in RP-HPLC conditions removing any biological activity of recovered protein¹³.

To overcome the issue of sample complexity a second dimension of separation can be added before separation by RP-HPLC. Two Dimensional HPLC, 2D-HPLC, introduces an Ion Exchange column to fractionate the sample before further separation by RP-HPLC, improving the resolution and selectivity of separations by combining retention mechanisms¹⁴⁻¹⁸. Where 2D-HPLC is implemented, Mass Spectrometry is the *de-facto* detection method falling under the category of Liquid Chromatography/ Mass Spectrometer, LC/MS.

LC/MS is a powerful tool in protein characterisation as the molecular weight of a given sample is determined while also deciphering sequence information by the detected mass fragments^{4,14}. As the MS provides an increase in resolving power and reduced analysis time, separations can be run in less time, making MS more favourable than other detection methods such as refractive index or UV detection.

1.2.2 Electrophoretic Protein Separation Techniques

The most widely used electrophoretic separation techniques include; 2-D Gel - Electrophoresis Mass Spectrometry (2-DGE/MS)¹⁹, and Capillary Electrophoresis Mass Spectrometry (CE/MS)²⁰. Commercial instrumentation has been developed for CE/MS, LC/MS and GE/MS²¹. The most widely implemented technique appears to be 2-DGE/MS⁴. This is due to this method facilitating the separation of different proteins yielding sufficient quantities for further analysis.

State-of-the-art 2-D gel operations use precision robotics to dissect the gels, enabling the bands of protein to be analysed further by mass spectrometry. Having run an electrophoretic separation by applying an electric field over a polyacrylamide gel, migrations of individual proteins form bands at different lengths along the gel. These bands are then fed into optical readers and analysed by a computer to give a chromatogram, before being further analysed by MS. This process can sample thousands of proteins a day, but in spite of this, it can still take months to determine the proteins native structural elements. It is fundamental that in proteome research proteins from cells and tissues need to be isolated in high purity and quantity for analysis.

Chromatography and electrophoresis are most extensively used in high-resolution purification^{22,23}. As a result work has been conducted to combine these techniques in hope of devising a hybrid of the advantages of both²⁴.

Electroseparation methods have long been required and developed, but with the complexity of Isotachophoresis (ITP), the sample limitations of Capillary Electrophoresis (CE) and the mobile phase and support problems in Capillary Electrokinetic Chromatography (CEC), High Performance Liquid Chromatography (HPLC) is still the major liquid separation technique. This is despite the major problems and limitations in the analysis time and resolution, e.g. chiral separations²⁵⁻²⁷, and isoform fractionation²⁸. Therefore alternative methods and instrumentation are needed. Research has continued on the combined development of these electrophoretic techniques by combining the new developments of; microfabrication, detection, and computer controlled fluidics and voltages. This has seen new electrophoretic techniques emerge that remove key disadvantages of the individual techniques. These techniques are known as electro- chromatography (EC)²⁴. The most recent advancements utilise electrophoretic mobilisation at the same time as a hydrodynamic flow making these focusing techniques. Advances in this area began with Counteracting Chromatographic Electrophoresis (CACE)²⁹.

1.2.3 Electrofocusing Techniques

In CACE, different grades of chromatographic media are setup up in the direction of flow. Simultaneously an electric field is applied in the opposing direction to the mobile phase. This field can then be manipulated to counteract the hydrodynamic flow resulting in a protein analyte focusing into a band.

This work by O'Farrell *et al.*²⁹ focused proteins into bands using an electric field, without the use of a pH gradient. However, this method of separation showed poor performance with mixtures of proteins and had issues with scale up³⁰.

Comparing electrofocusing techniques described above with CE, the performance is similar. However, the gains made in complex and costly modifications to CE are inherently encompassed in electrofocusing technologies. This introduces significant advantages for challenging analytical separations, providing high resolution and high concentration of samples, lending itself to small scale applications³¹. Isoelectric focusing (IEF) however enables scale up at the cost of large increases in time for separations to occur.

IEF is a form of zone electrophoresis which separates analytes across a static pH gradient resulting in separation according to isoelectric point. Though IEF offers very high resolution, it has inherent problems with the complexity of stabilising the pH gradient under running conditions, particularly at preparative and large scales. At the isoelectric point (pI), many samples become insoluble. Furthermore some groups of samples are unable to be focused by this method either because degradation occurs at their isoelectric point; for example, nucleic acids. Moreover, IEF is a batch technique which is analogous to other chromatographic techniques presenting difficulties in implementing a continuous flow system. In addition to these issues the ampholytes which are key to stabilising the pH gradient, contribute a high cost to the recovery of protein purified to the cost of focusing³⁰.

Flow counterbalanced capillary electrophoresis (FCCE)³² developed by Jorgenson *et al.* provides separation by CE. The difference with this approach is that a counter flow is induced in the opposite direction to the electrokinetic migration.

The effect of the this counteracting flow is that the separation occurs more gradually over the length of the capillary which has the same effect as increasing the length of the column. Improvements in resolution and efficiency of a given CE separation were demonstrated by using FCCE without modification of the buffer, field strength, or method of detection.

Even though there are two opposing forces within the capillary, this is not a true focusing device as the analytes do not become stationary at any point in the separation. To fully concentrate a desired protein the opposing forces must control the flow movement of the species in both directions.

Electric Field Gradient Focusing, EFGF, described by Lee *et al.*^{33,34}, is a true electrofocusing technique. A capillary is placed inside a secondary reservoir constructed from a conductive polymer. The configuration of the EFGF device is shown in figure 1.2.1. As a hydrodynamic flow is applied in one direction through the capillary, an electrokinetic force is applied in the secondary reservoir acting in the opposite direction. The conductive polymer allows the propagation of the electric field, but not the sample. This results in analytes reaching focal points at unique points along the capillary, causing separation.

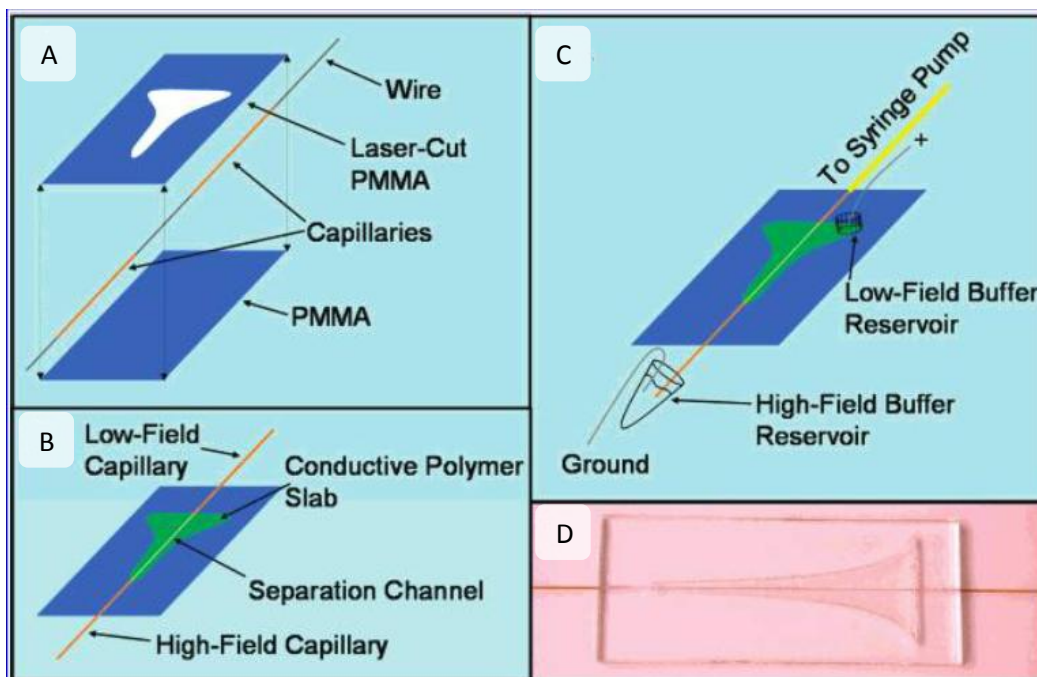


Figure 1.2.1. Configuration of the EFGF device. A) Exploded view of components made from Poly(methyl methacrylate), (PMMA). B) Assembled device. C) Assembled device with buffer reservoirs. D) Image of actual EFGF device.

It is noted that this is a static electric field gradient acting across the full length of the device. This configuration allows for the separation of analytes; however the electric field either retains all of the samples or allows them to elute. To solve this issue and facilitate the stacking of a concentrated sample, a tandem EFGF was redeveloped to isolate and re-focus a target protein once separated from a matrix³⁵.

Further work on EFGF saw the evaluation of the influence of the hydrogel used to form the channels³⁶. This work raised questions over the shape of the reservoir channel which was later changed to facilitate a more stable electric field. Improvements to this system saw the use of polyethylene glycol for the construction of the reservoir and therefore an increase in the effectiveness of the electric field propagation³⁷.

Key observations were made in a theoretical study³⁸ which indicated that the shape of the channel had a direct effect on the propagation of the electric field. A bi-linear EFGF³⁹ was developed which is a step towards the similar technique of Dynamic Field Gradient Focusing, DFGF. The main difference between the EFGF technique and DFGF is that in EFGF only a linear electric field gradient is applied to result in separation, where as DFGF allows adjustments to be made to the electric field at multiple points *in situ* to accurately manipulate and refine a separation in real time.

Dynamic Field Gradient Focusing is described and demonstrated throughout this thesis with the aim of performing separations of proteins similar to those of the devices listed above with improved performance.

1.3 References

1. D. Nelson and M. Cox, *Principles of Biochemistry*, 3rd Ed., 2000.
2. C. Brandon and J. Tooze, *Introduction to Protein Structure*, 2nd Ed., 1999.
3. P. G. Tuñón, University of Leeds, 2006.
4. S. P. Gygi and R. Aebersold, *Current Opinion in Chemical Biology*, 2000, **4**, 489-494.
5. J. O. Baker, W. S. Adney, M. Chen, and M. E. Himmel, *Handbook Of Size Exclusion Chromatography And Related Techniques*, CRC Press, 2003.
6. F. E. Regnier, *Analytical Biochemistry*, 1982, **126**, 1-7.
7. T. Hanai, *Journal of Liquid Chromatography & Related Technologies*, 2007, **30**, 1251-1275.
8. C.-H. Chen and W.-C. Lee, *Journal of Chromatography A*, 2001, **921**, 31-37.
9. W.-C. Lee and K. H. Lee, *Analytical Biochemistry*, 2004, **324**, 1-10.
10. GRACE VYDAC, *The Handbook of Analysis and Purification of Peptides and Proteins by Reversed-Phase HPLC*, 3rd Ed., 2002.
11. T. Macko and D. Berek, *Journal of Liquid Chromatography & Related Technologies*, 1998, **21**, 2265-2279.
12. G. Xindu and F. E. Regnier, *Journal of Chromatography A*, 1984, **296**, 15-30.
13. M. Rubinstein, *Analytical Biochemistry*, 1979, **98**, 1-7.
14. J. Tang, M. Gao, C. Deng, and X. Zhang, *Journal of chromatography. B, Analytical technologies in the biomedical and life sciences*, 2008, **866**, 123-32.
15. H. Wang and S. Hanash, *Journal of Chromatography B*, 2003, **787**, 11-18.

16. Y. Li, X. Fang, S. Zhao, T. Zhai, X. Sun, and J. J. Bao, *Chemistry Letters*, 2010, **39**, 983-985.
17. Y. Yang, J. Chae, Y. Yang, and J. Chae, in *2007 IEEE 20th International Conference on Micro Electro Mechanical Systems (MEMS)*, IEEE, 2007, pp. 421-424.
18. A. W. Moore and J. W. Jorgenson, *Analytical Chemistry*, 1995, **67**, 3448-3455.
19. S. D. Patterson and R. Aebbersold, *Electrophoresis*, 1995, **16**, 1791-1814.
20. P. K. Jensen, L. Pasa-Tolić, K. K. Peden, S. Martinović, M. S. Lipton, G. A. Anderson, N. Tolić, K. K. Wong, and R. D. Smith, *Electrophoresis*, 2000, **21**, 1372-80.
21. Y. Li, D. L. DeVoe, and C. S. Lee, *Electrophoresis*, 2003, **24**, 193-9.
22. C. F. Ivory, *Separation Science and Technology*, 1988, **23**, 875-912.
23. P. Righetti and C. Secchi, *Journal of Chromatography A*, 1972, **72**, 165-175.
24. A. L. Crego, A. González, and M. L. Marina, *Critical Reviews in Analytical Chemistry*, 1996, **26**, 261-304.
25. B. Preinerstorfer, M. Lammerhofer, and W. Lindner, *Electrophoresis*, 2009, **30**, 100-132.
26. G. Gübitz and M. G. Schmid, *Journal of Chromatography A*, 2008, **1204**, 140-156.
27. B. Chankvetadze, *Journal of Chromatography A*, 2007, **1168**, 45-70; discussion 44.
28. W. W. P. Chang, C. Hobson, D. C. Bomberger, and L. V. Schneider, *Electrophoresis*, 2005, **26**, 2179-2186.
29. P. H. O'farrell, *Science (New York, N.Y.)*, 1985, **227**, 1586-9.
30. C. F. IVORY, *Separation Science and Technology*, 2000, **35**, 1777-1793.
31. J. G. Shackman and D. Ross, *Electrophoresis*, 2007, **28**, 556-71.

32. W. H. Henley, R. T. Wilburn, A. M. Crouch, and J. W. Jorgenson, *Analytical chemistry*, 2005, **77**, 7024-31.
33. S. L. Lin, H. D. Tolley, and M. L. Lee, *Chromatographia*, 2005, **62**, 277-281.
34. P. H. Humble, R. T. Kelly, A. T. Woolley, H. D. Tolley, and M. L. Lee, *Analytical chemistry*, 2004, **76**, 5641-8.
35. S.-L. Lin, Y. Li, H. D. Tolley, P. H. Humble, and M. L. Lee, *Journal of chromatography. A*, 2006, **1125**, 254-62.
36. P. H. Humble, J. N. Harb, H. D. Tolley, A. T. Woolley, P. B. Farnsworth, and M. L. Lee, *Journal of Chromatography A*, 2007, **1160**, 311-319.
37. X. Sun, P. B. Farnsworth, A. T. Woolley, H. D. Tolley, K. F. Warnick, and M. L. Lee, *Analytical chemistry*, 2008, **80**, 451-60.
38. D. Maynes, J. Tenny, B. W. Webb, and M. L. Lee, *Electrophoresis*, 2008, **29**, 549-60.
39. X. Sun, D. Li, A. T. Woolley, P. B. Farnsworth, H. D. Tolley, K. F. Warnick, and M. L. Lee, *Journal of Chromatography A*, 2009, **1216**, 6532-6538.

Chapter 2. Dynamic Field Gradient Focusing

2.1 Theory

Dynamic Field Gradient Focusing (DFGF) is a relatively new separation technique which exploits the differences in electrophoretic mobility and hydrodynamic radius of analytes to result in a separation¹. This is achieved by taking a channel and applying a hydrodynamic flow in one direction and a counteracting electric field gradient (EFG) causing an electrophoretic force acting in the opposite direction, resulting in analytes reaching unique focal points across the length of the channel. At these focal points the sample is concentrated into a tight band giving separation and concentration in a single step². This is described graphically in, figure 2.1.1.

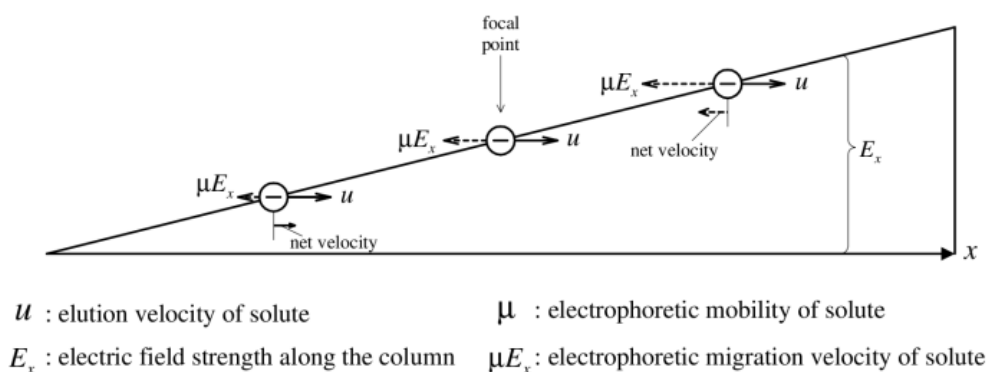


Figure 2.1.1. Theoretical model for DFGF³. The counteracting dynamic field gradient gives rise to inertia and a net force on the charged species bringing components of a given sample to unique focal points regardless of their initial location in the column.

From the model above the behaviour of a given analyte in a known electric field can be interpreted using the basic flux equation (equation 2.1.1).

$$J_i(x) = \underbrace{-D_i \frac{dC_i}{dx}}_{\text{Diffusion}} + \underbrace{[u_i + \mu_i E(x)]}_{\substack{\text{Electrophoretic} \\ \text{Migration}}} C_i$$

Hydrodynamic
Velocity

Equation 2.1.1. The Flux equation, where; J is the molar flux, D is the dispersion coefficient, C is the concentration, u is the velocity of the buffer, μ is the electrophoretic mobility of species, and E is the strength of the electric field⁴.

For an analyte to be considered focused, the molar flux must be zero, indicating the species is stationary, i.e. the opposing forces cancel each other. As seen in the flux equation, there are a number of conditions which in turn can be manipulated to focus an analyte into a band. This is also applicable for isoelectric focusing⁵, and EFGF⁴. The flux equation can be solved for C , concentration of a band of analyte, giving a Gaussian distribution shown, by Zheng³, below in equation 2.1.2.

$$C_i(x) = \frac{1}{\sqrt{2\pi}} \frac{M_i}{\sigma_i A} \exp\left[-\frac{(x - \chi_{f,i})^2}{2\sigma_i^2}\right]$$

Equation 2.1.2. The flux equation solved for C , where M_i is the total number of moles of analyte, A is the cross section area of the channel and σ is variance³.

From equation 2.1.2 for the concentration of a band, the focal point X at which the band will be stationary along the length of the channel and the variance σ , the area either side of X a sample could focus, can be derived. These are shown below in equation 2.1.3. and equation 2.1.4.

$$\chi_i = -\frac{u_i + \mu_i E_0}{\mu_i E_1}$$

Equation 2.1.3. X_i defines a point along the length of the separation channel where an analyte will come into focus³.

$$\sigma_i^2 = -\frac{D_i}{\mu_i E_1}$$

Equation 2.1.4. Variance of the width of a focused band of analyte³.

From equation 2.1.3 it is observed that increasing the electric field gradient will decrease the separation between bands. However from equation 2.1.4 increasing the electric field gradient will make the bands narrower. Therefore to increase separation and decrease variance both higher fields and flow rates are required. From the diffusion contribution (D_i) to variance, equation 2.1.4, it is apparent that focusing is indeed caused by the forces of hydrodynamic flow (μ_i) and electrophoretic mobility, from the applied EFG (E_1), counteracting one another. This shows the technique is independent of channel length focusing the sample in a position relative to the strength of these forces, particularly the EFG. In addition, the effect of focusing increases the concentration of the bands over time^{2,5}.

2.2 DFGF Set Up

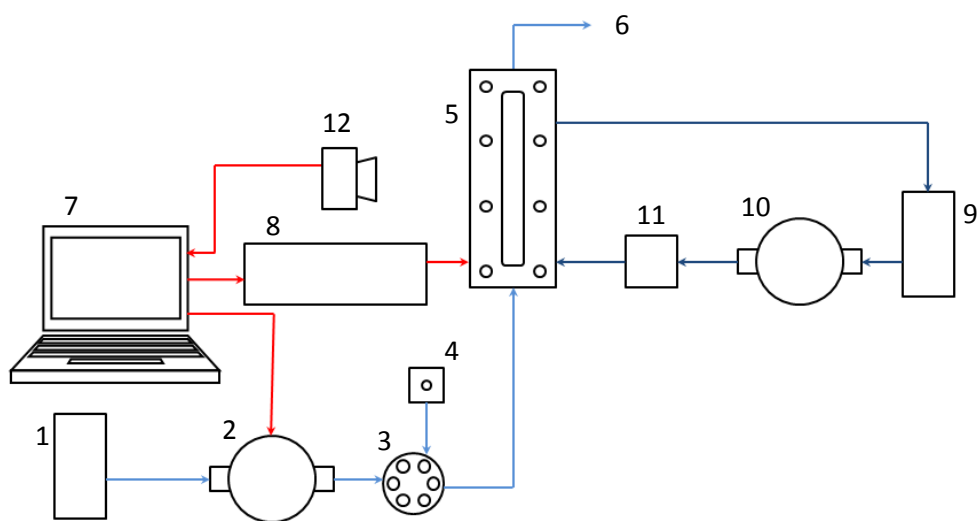
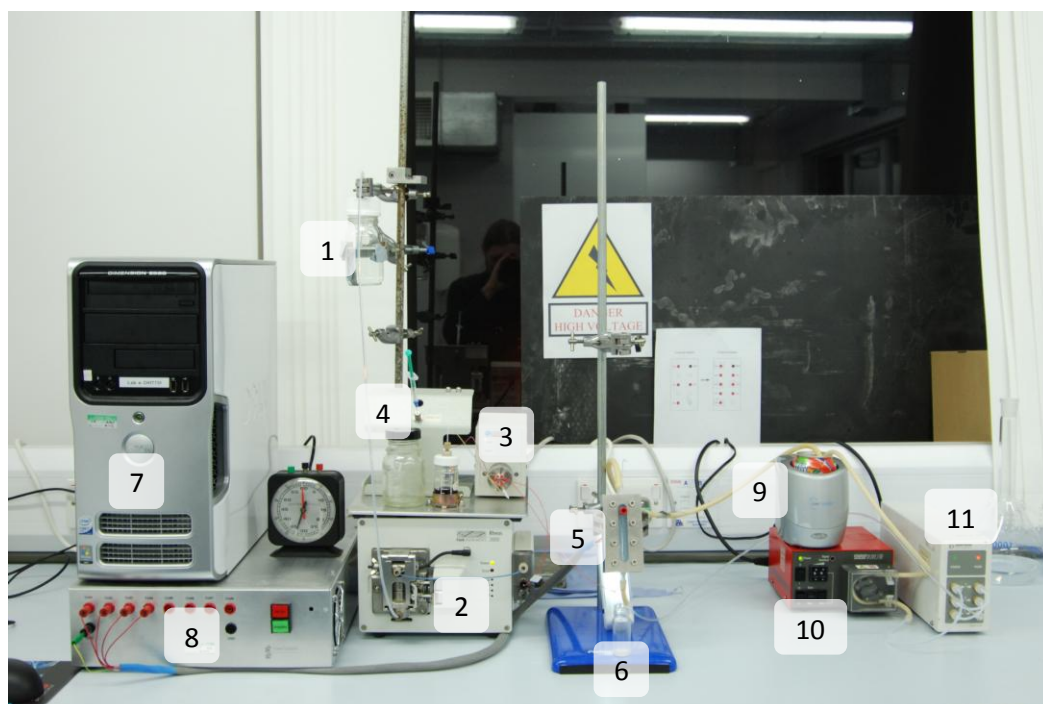


Figure 2.2.1. DFGF set up with electrical connections in red, separation channel fluid flow in light blue and electrode channel fluid flow in dark blue. Supporting equipment: 1) Separation channel buffer reservoir. 2) Computer controlled Flux Instruments Rheos2200 Pump. 3) 6 Port switching valve. 4) Injection port. 5) DFGF device. 6) Outlet for sample collection. 7) Computer. 8) Computer controlled high voltage power supply. 9) Electrode channel buffer reservoir with cooler. 10) Peristaltic pump. 11) De-gasser 12) Nikon D80 digital SLR camera with 60mm macro lens.

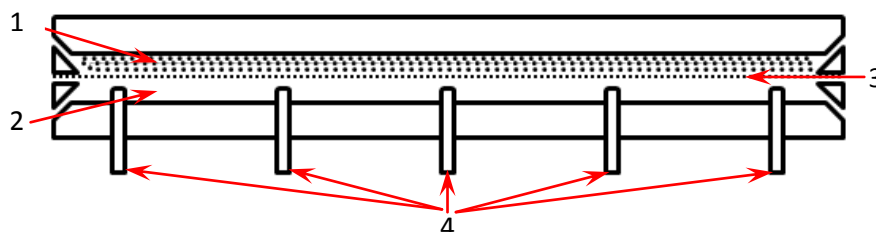


Figure 2.2.2. Side view of the DFGF channel configuration. Consisting of; 1) Packed separation channel. 2) Separate purge channel housing the electrodes. 3) Cellulose Dialysis Membrane dividing the two channels. 4) Platinum electrodes.

2.2.1. DFGF Configuration

The DFGF was setup as shown above in figure 2.2.1. The DFGF cell itself is composed of two acrylic layers which combine to form two channels divided by strip of cellulose dialysis membrane, detailed in figure 2.2.2. This dual channel arrangement eliminates pH changes and gas evolution from the separation channel which can be detrimental to separation⁶. Cellulose dialysis membrane⁷ is used as it allows the EFG to propagate through into the separation channel by allowing small ions to pass through. However large species, i.e. the sample, cannot permeate the membrane, therefore are trapped in the separation channel preventing them from being electrolysed. Gases and other electrolysis products are also unable to pass through the membrane from the electrode channel. Constant flow of buffer through electrode channel flushes away these species. The computer controlled Flux Instruments Rheos 2200⁸ pump drives the hydrodynamic flow of buffer through the injection valve into the cell and on to collection or further detection. The peristaltic pump circulates buffer solution around the electrode channel via a degasser to remove any electrolysis gasses.

The dynamic electric field gradient is supplied and manipulated from the Protasis⁹ voltage array using Labview control software (appendix B). Detection is performed by a Nikon D80 digital SLR camera with 60mm Macro lens¹⁰.

Separations are monitored and controlled in real time using the computer and an assortment of software. Before the DFGF is operated the separation channel must be packed with a packing media to provide a narrower diffusion pathway through the separation channel and to lower the solvent volume present. As the dimensions of these channels are at the millimetre scale, any focusing would require an extremely high voltage to apply an EFG capable of counteracting such a larger volume without a packing material or monolith.

2.2.2. Packing Method

The DFGF was prepared for packing by rinsing components with deionised water. Regenerated cellulose dialysis membrane with a molecular weight cut off (MWCO) twice that of the intended analyte was cut to the dimensions 20mm wide and 90mm in length. With the membrane in place on the Teflon gasket the two halves of the DFGF cell are bolted together, tightening the bolts sequentially across opposite corners. The separation and purge channels were then tested for leaks. A 1/16" in line frit and 0.030" ID PEEK capillary tubing was connected to the outlet of the separation channel. The same ID PEEK tubing was also connected to the inlet having been connected to the packing reservoir and vibrating packing apparatus. The cell was then immersed in the sonic bath and the reservoir charged with 500mg of Bio-Rad 45-90 μ m spherical polyacrylamide¹¹ packing material suspended in 10mL 50mM Tris HCl buffer.

Compressed air was used to charge the separation channel with the packing slurry. Packing solvent was pushed through the channel for 3 hours at a constant pressure of 4 bar. The system was then equilibrated for 24 hours at $1\mu\text{Lmin}^{-1}$ with Flux Instruments Rheos 2200 pump⁸. The DFGF packing apparatus configuration is shown below, figure 2.2.3.

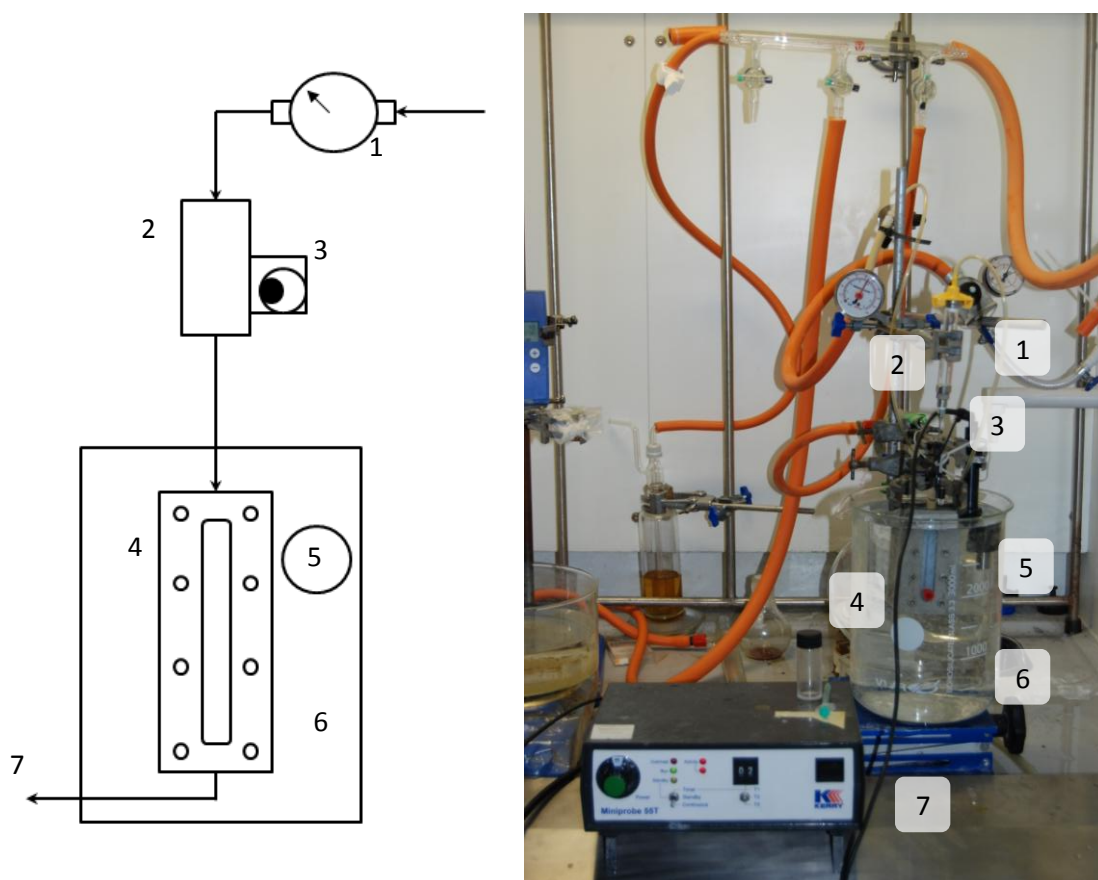


Figure 2.2.3. DFGF packing apparatus. 1) Compressed Air Supply with Pressure Gauge. 2) Slurry Reservoir. 3) Vibrating Motor. 4) DFGF Device. 5) Sonic Probe. 6) Beaker with DFGF submerged in water and sonic probe. 7) DFGF Outlet.

2.2.3. General Operation

In general the operation of the device would follow this standard procedure. A linear EFG of around 80% of the maximum field, using $\sim 800\text{V}$ across the length of the separation channel, was applied for 20mins before each experiment to ensure equilibration of the packed bed. The hydrodynamic flow of 50mM tris HCl buffer solution was pumped through the separation channel at $1\mu\text{Lmin}^{-1}$. Next the sample was loaded into the sample loop which was then switched in.

Once the sample was visible in the cell $\sim 30\text{mins}$ was left for the sample to reach a stable focal point. Typically, the linear EFG would be adjusted with the aim of separation. If samples were separated the electric field was manipulated manually, meaning overriding a linear gradient to produce bespoke voltage profiles, to hold a single species back and allow the others to elute off the device. Alternatively, the bands would be moved back down the column to refocus and increase the separation by increasing the EFG. Additionally, the flow rate was altered to further focus bands of sample giving dynamic flow as well as dynamic field. On injection of the sample, images of the separation channel were collection at regular intervals to record the separation. Each aspect of this control is explained in more detail below.

2.2.4. Dynamic Flow Control: Flux Instruments Rheos Pumps and Janeiro 3.0

Incorporating the Flux Instruments Rheos 2200 pump⁸ into the DFGF set up adds dynamic control over the flow rate used resulting in the technique being Dynamic Flow Dynamic Field Gradient Focusing. These pumps are controlled over RS232 protocol using the Flux Instruments Janeiro 3.0 software.

This computer control enables the flow rate to be adjusted in the order of $\pm 0.1 \mu\text{Lmin}^{-1}$. Most piston pumps used in chromatographic techniques give a pulsing flow which worsens as the flow rate is lowered¹². The Rheos 2200 pump⁸ utilises a pulse dampening system to result in a stable flow even at flow rates as low as $0.1 \mu\text{Lmin}^{-1}$.

The Flux Instruments Janeiro control software allows control over a number of parameters which are advantageous for DFGF. Figure 2.2.4 displays the user interface of Janeiro. The flow rate can be set by adjusting the dial controller or by entering a value into the flow rate input. Also the maximum pressure and warning pressure can be set to stop the pump in the event of a sudden increase in pressure which could cause the packing or membrane to fail.

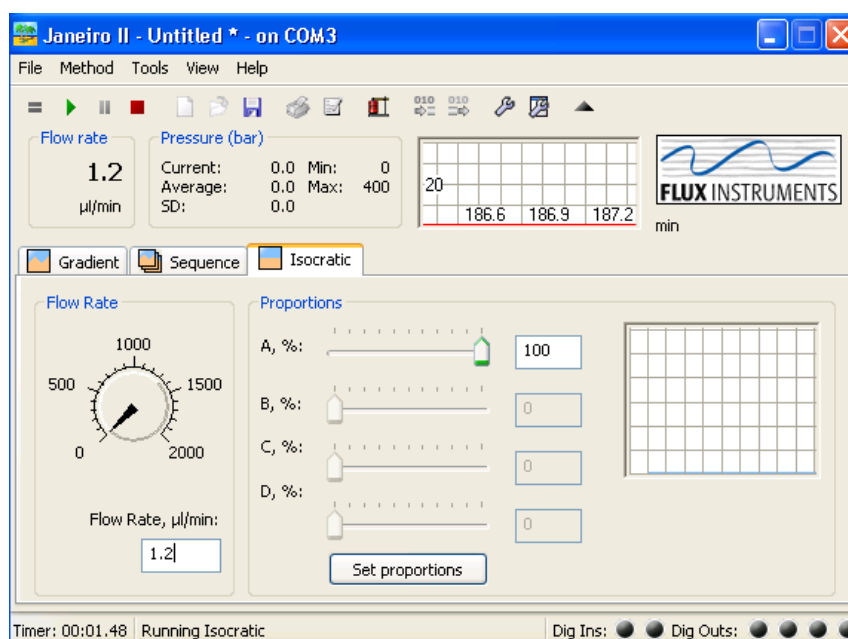


Figure 2.2.4. Flux Rheos Janeiro 3.0 software. The user interface is shown, the features used for running the pump for DFGF include the maximum and warning pressure settings to prevent a build up pressure from damaging the membrane.

2.2.5. Dynamic Electric Field: Power Supply and Control

The supporting equipment for the Protasis device, figure 2.4.1, is the equipment which has been used for all of the experimentation throughout this thesis. The power supply consists of four individual UltraVolt High Voltage generators¹³ connected to respective high voltage (HV) outputs sharing a common ground rail with a designated HV connection.

The HV generators were controlled independently by analogue signals from a universal serial bus (USB) interface board, shown in figure 2.2.5.

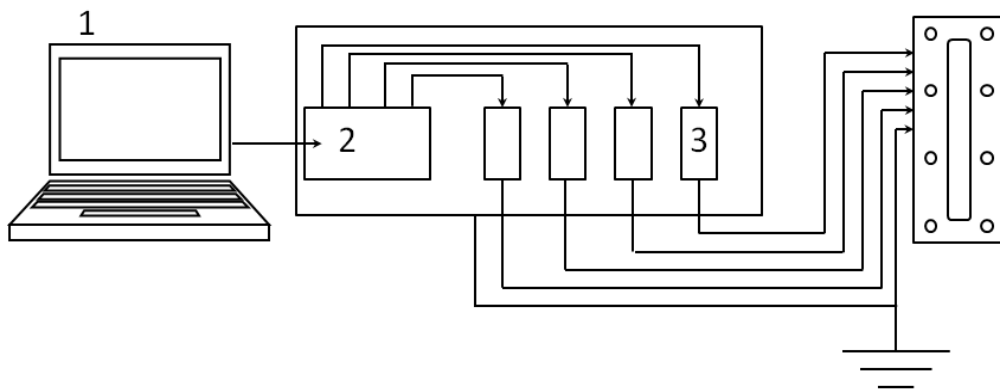


Figure 2.2.5. Protasis Power supply schematic. 1) Computer running Labview Software. 2) "Measurement Computing USB-3103" interface. 3) 4x Independent "Ultra Volt" power supplies. The arrow leading out of these represent individual control over each electrode of the five electrodes used in the DFGF device.

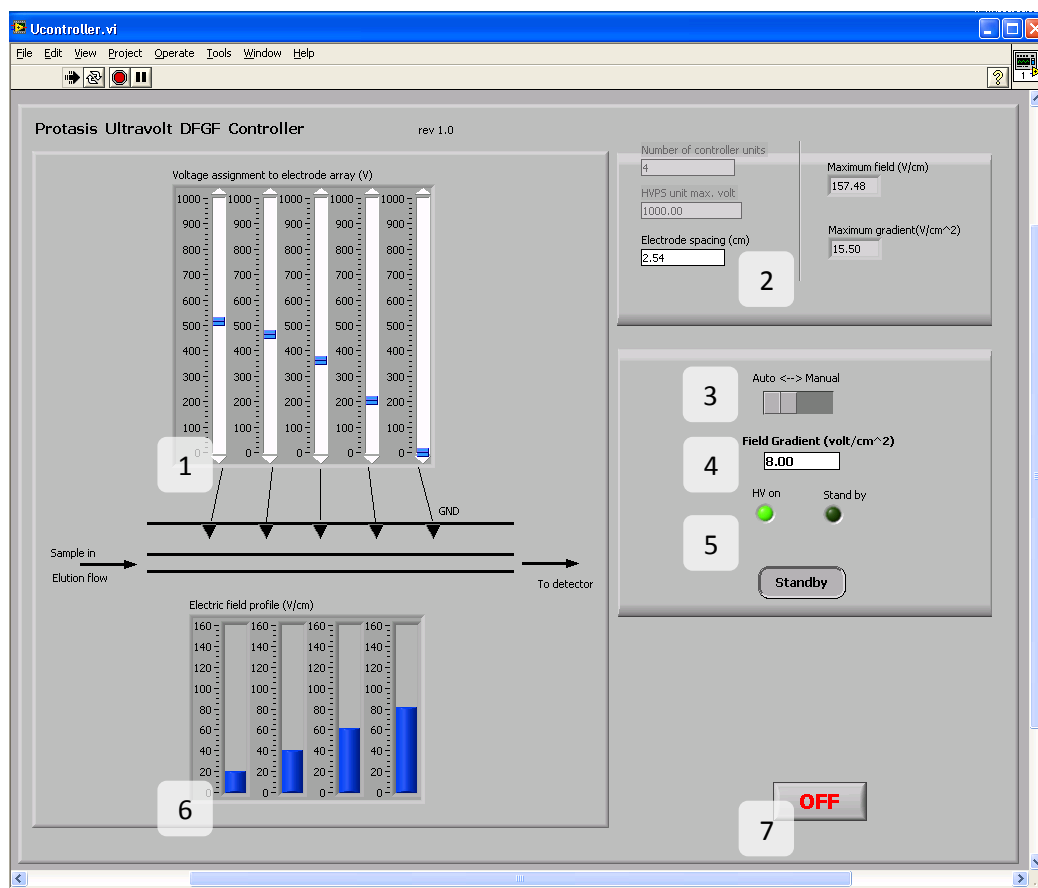


Figure 2.2.6. Protasis UController HV Control Software. 1) Voltages supplied to electrodes. 2) Electrode Spacing. 3) Mode selector switch. 4) EFG Value. 5) Indicator Lights. 6) Electric field profile. 7) Power off button.

The Protasis DFGF Power Supply Unit was controlled by bespoke software (appendix B) written in National Instruments LabView. The user interface, figure 2.2.6, enables control of the system in two modes, manual and automatic. Firstly, in automatic mode, the software uses the value entered for electrode spacing to calculate the maximum electric field gradient and uses this to calculate the required voltage for each of the four positive electrodes to generate the gradient entered by the user. In this mode the system designates the voltages applied to the electrodes according to the linear EFG entered.

A linear EFG is where the slope of the gradient is the same between all of the electrodes. An example of a linear EFG is shown in figure 2.2.7 with the corresponding applied voltages and electrode spacing. The specified gradient is plotted on a histogram shown in the bottom left of the interface, figure 2.2.6.

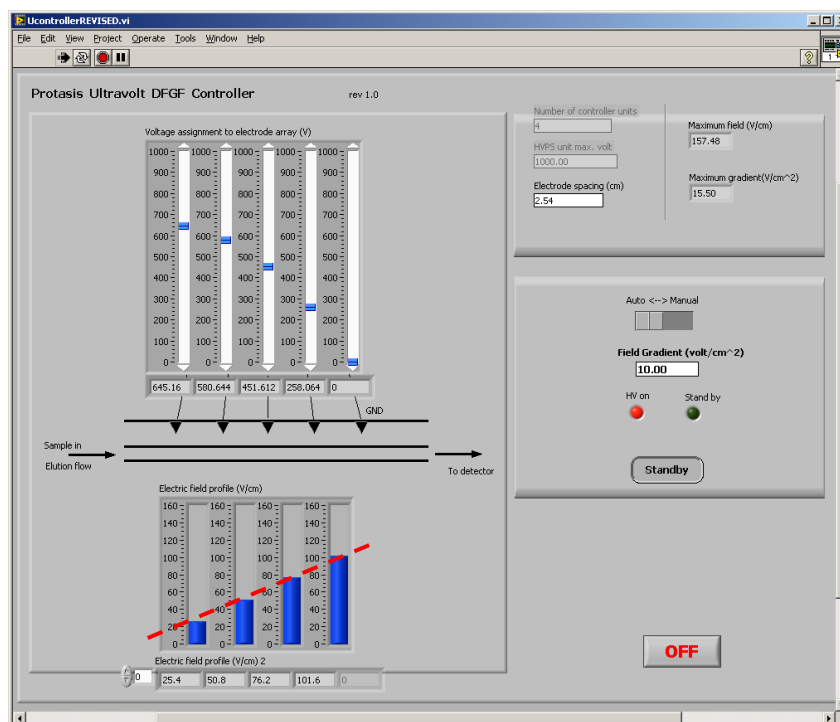


Figure 2.2.7. An example of a linear EFG generated by the Protasis Labview Ucontroller software in Automatic Mode. The dashed red line highlights the linear Electric Field Gradient.

In manual mode the software enables direct control of each electrode independently using the sliders in the top left of the interface (figure 2.2.6), to apply different gradients in different regions of the device, i.e. the EFG between each of the electrodes can be different, figure 2.2.8. This level of control enables focused bands of analyte to be manipulated with a higher degree of control.

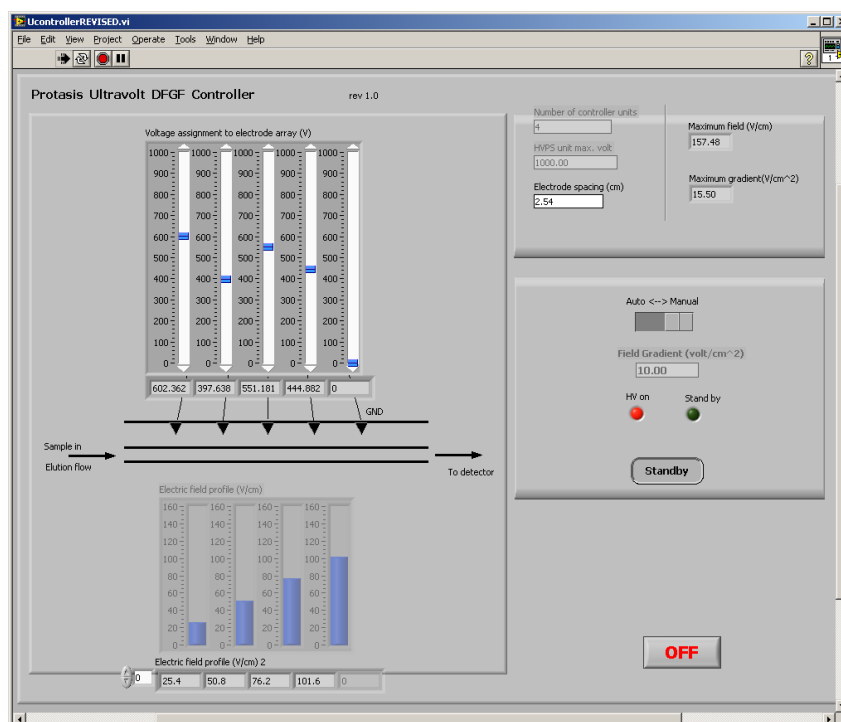


Figure 2.2.8. An example of the EFGs which can be applied by the Labview Ucontroller software in Manual Mode. Notice the electric field gradient is no longer linear therefore the area on the bottom left is shaded out.

2.2.6. Data collection and presentation

A simple method of detection with DFGF was to use reflectance measurements from digital exposures to monitor the position of bands in the separation channel. Utilising a Nikon D80 DSLR camera¹⁰ with a 60mm 1:2.8D macro lens, exposures were taken at set intervals incorporating the full length of the separation channel using Camera Control Pro¹⁴ software, figure 2.2.9.

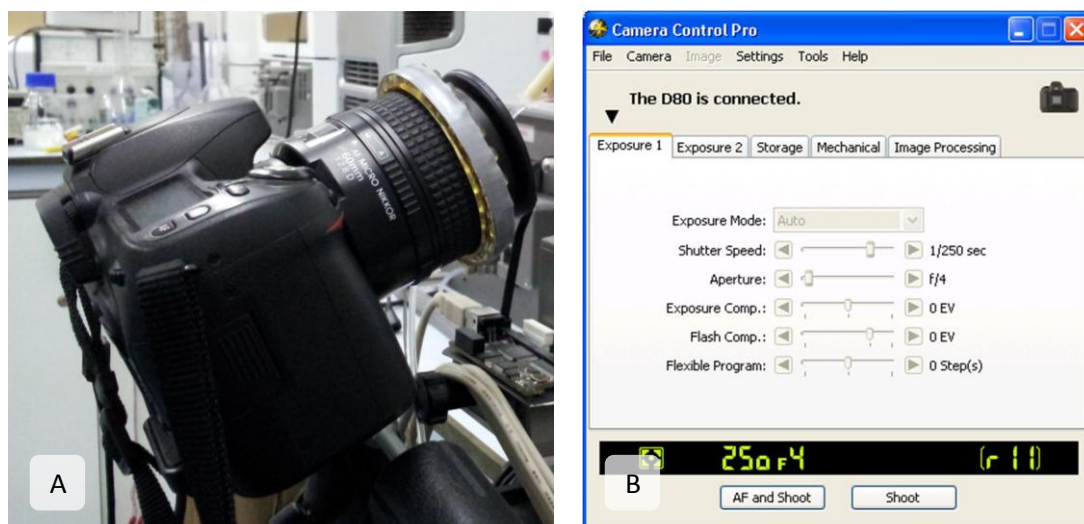


Figure 2.2.9. A) Nikon D80 with a 60mm 1:2.8D macro lens configured to take images of the separation channel with the addition of a LED ring illuminator. B) Nikon Camera Control Pro software user interface.

By stacking these images in an image editing software, namely Adobe Photoshop or GNU Image Manipulation Program (GIMP), it was possible to observe differences, hence the position of a given analyte, by subtracting the first background image from an image collected later. This preceding detection method is shown in figure 2.2.10A. For analysis of these subtracted images, “image analysis” software ImageJ¹⁵ was used to generate a ‘Profile Plot’ of the separation channel, shown in figure 2.2.10B.

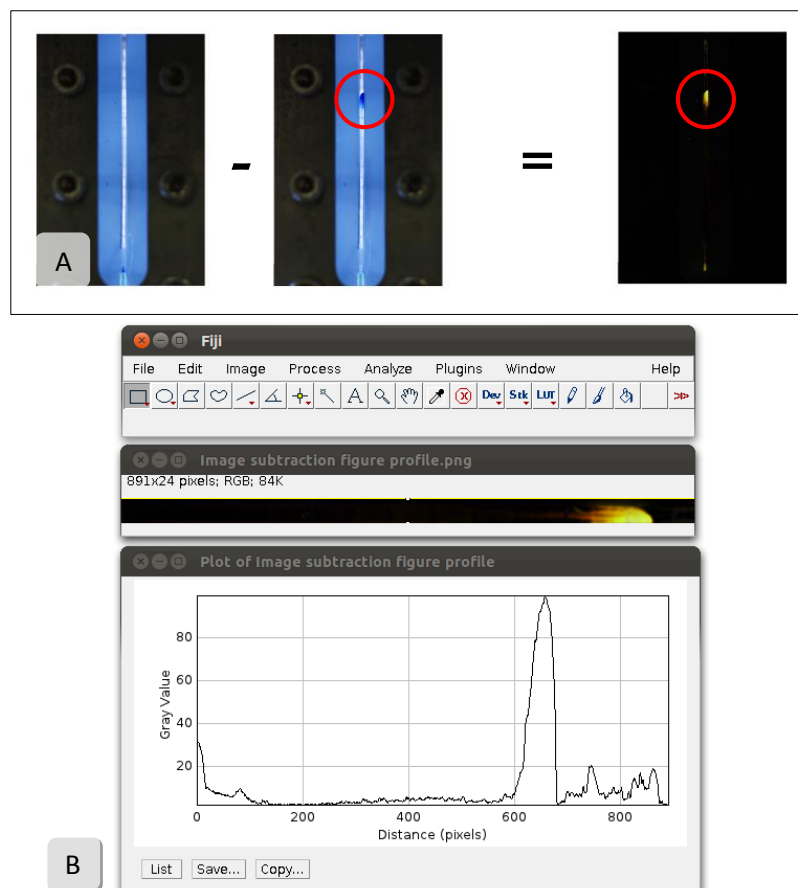
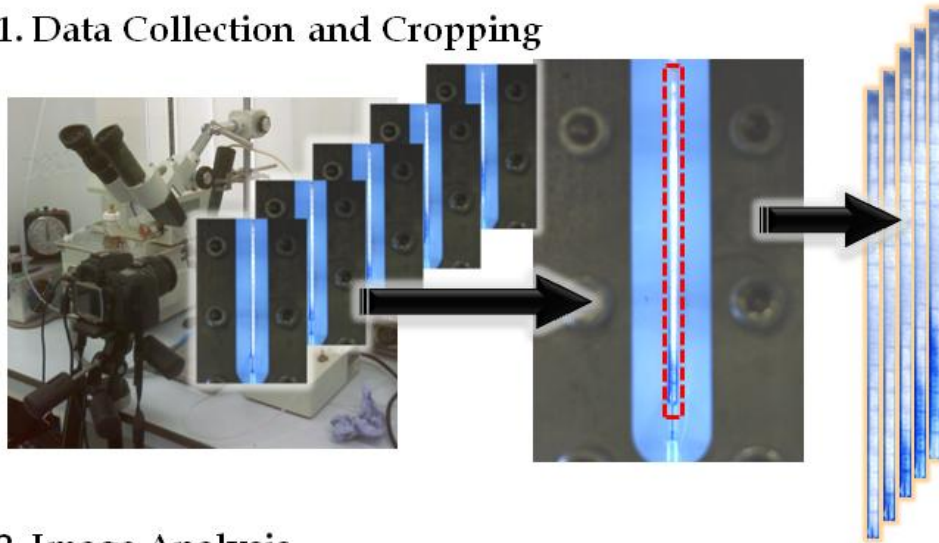


Figure 2.2.10. A) Detection using GIMP to subtract images highlighting any changes in the positions of analytes with a corresponding profile measurement. B) Next a profile plot is generated using Fiji¹⁶, a rich featured version of ImageJ.

Developing this process further, images were taken and interpreted in full post experiment yielding a plot of the whole separation over time. To generate a graphical representation of a separation a collection or 'stack' of images was cropped to display only the area of interest, the separation channel, using a Linux command line image editing tool, ImageMagik¹⁷. The image stack was then loaded into 'image analysis' software ImageJ¹⁵.

Using a bespoke Visual Basic script (appendix C) a 'Profile Plot' of each image was taken and the numerical analysis data of each individual image was saved to a Microsoft Excel spreadsheet, *.xls file. This data was then loaded into a VBA Microsoft Excel based system (appendix D) where each profile was plotted to give the final graph of the separation. This interpretation process is summarised in figure 2.2.11. The graph shows the length of the separation channel along the x-axis with the corresponding reflectance measured as 'grey value' on the y-axis. The z-axis is time, as each profile is arranged behind the previous one to build up a graphical representation of the entire separation occurring. An additional presentation method utilises a feature of ImageJ¹⁵, called the 'Montage', which is similar to graphs plotted by Lee *et al.* for EFGF¹⁸. This provides the equivalent of a top down view of the plotted graph with a qualitative measure of the positions of analytes by arranging the cropped images into a single column, with each image occupying a row. An example of this is shown in figure 2.3.5. These plots of the complete separation give a view of the capability of the technique to hold back samples and pre-concentrate analytes before eluting them from the device.

1. Data Collection and Cropping



2. Image Analysis



3. Graphical Presentation

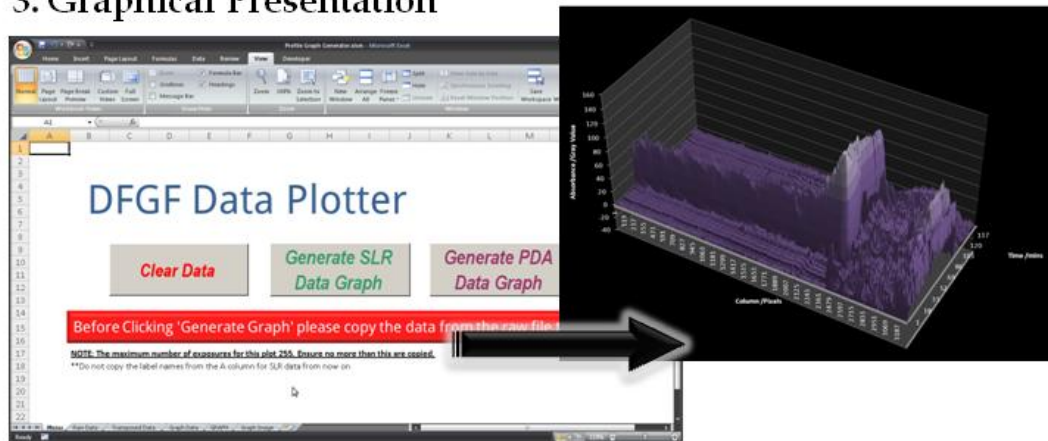


Figure 2.2.11. 1) Data Interpretation. Moving from left to right, Images were cropped to show only the separation channel. 2) The cropped image stack is loaded into ImageJ and all the profiles are measured. 3) This data was loaded into the Microsoft Excel 'Profile Generator' producing a graph of the separation.

2.3. Experimental with First Generation Device

2.3.1. First generation DFGF Device

The first generation DFGF device was devised by Ivory *et al.* at the University of Washington¹⁹. This device, though many advances have been made since its conception, was used to perform separations on a smaller scale than that of the Myers groups existing Protasis⁹ DFGF device. These experiments were carried out in anticipation of the microfluidic DFGF (chapter 3). In the following experiments the take off point remained closed and only five of the fifteen electrodes were used. Additionally, a Teflon gasket has been added to this first generation device in place of using a supporting ceramic for the membrane, as described in the construction of the first generation DFGF (appendix E).

2.3.2 Separation of a two component test mixture

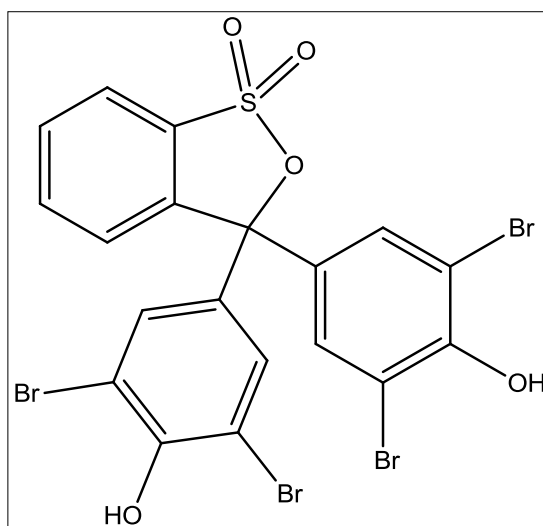


Figure 2.3.1. Structure of Bromophenol Blue (BPB) 4,4'-(1,1-dioxido-3H-2,1-benzoxathiole-3,3-diyl)bis(2,6-dibromophenol).

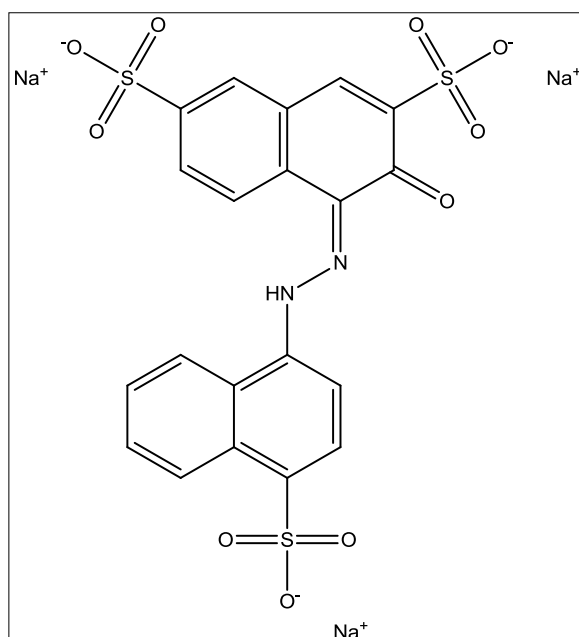


Figure 2.3.2. Structure of Amaranth (AM) trisodium (4E)-3-oxo-4-[(4-sulfonato-1-naphthyl)hydrazono]naphthalene-2,7-disulfonate.

At a flow rate of $1\mu\text{Lmin}^{-1}$, $10\mu\text{L}$ of a mixture of 10%v/v Bromophenol Blue (BPB) and Amaranth (AM) was injected. The structures for these analytes are shown in figures 2.3.1 and 2.3.2. A linear EFG of 100Vcm^{-2} was applied initially to prevent the sample from flowing through the channel. Having reached an initial focal point (figure 2.3.3A) the electric field strength was dropped to 80Vcm^{-2} and the components came to individual focal points around the middle of the channel. Next, the field was altered manually to bring the bands into sharper focus as shown in figure 2.3.3B. To prove the concept of full control over positions in the column, the field was increased again to 100Vcm^{-2} bringing the analytes into focus lower down in the channel (figure 2.3.3C).

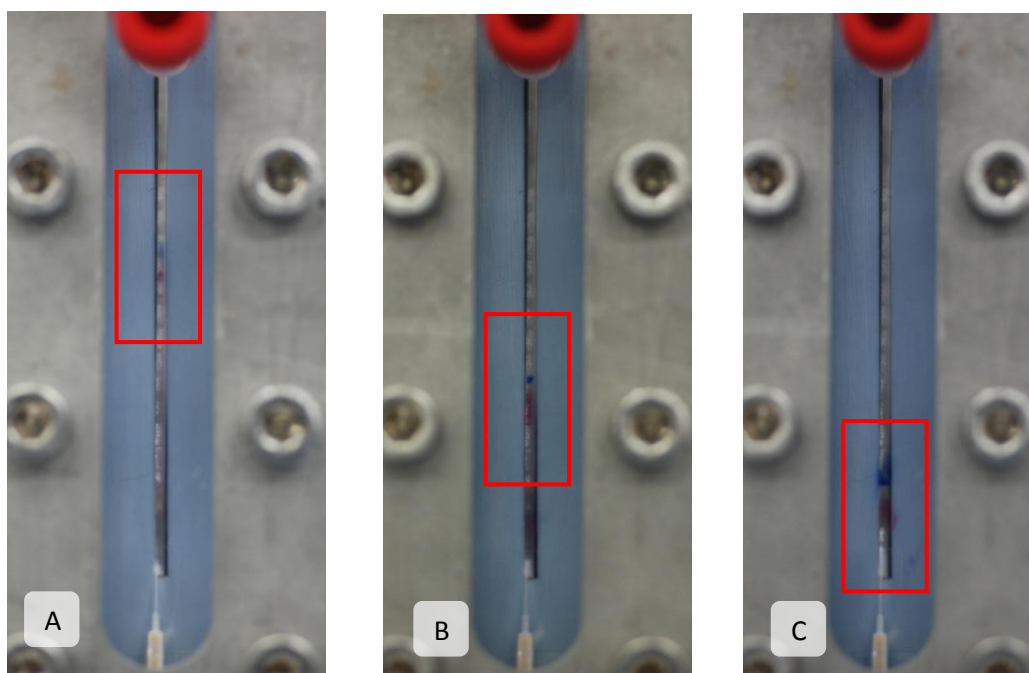


Figure 2.3.3. Separation and focusing of Bromophenol Blue (BPB) and Amaranth (AM). A) Sample comes into an initial focus point after injection. B) EFG is increased to focus analytes further. C) EFG is increased again resulting in two focused bands back at the beginning of the separation channel.

Having demonstrated the operation of the DFGF the next experiment displays the method of data capture and analysis. A sample of BPB was injected at $1\mu\text{Lmin}^{-1}$ and retained by an EFG of 55Vcm^{-2} . The analyte migrated to focal point, was held, and then released. This was then plotted using the image processing method described in figure 2.2.11, and is shown in figure 2.3.4. Another feature of using ImageJ is that an image montage can be generated from the image stack. The montage gives a view of the separation with time moving from bottom to top of the image. The montage is useful as it can be used to identify peaks in the graphs by colour of the corresponding band with time and channel position in the montage. The corresponding montage for figure 2.3.4 is shown in figure 2.3.5.

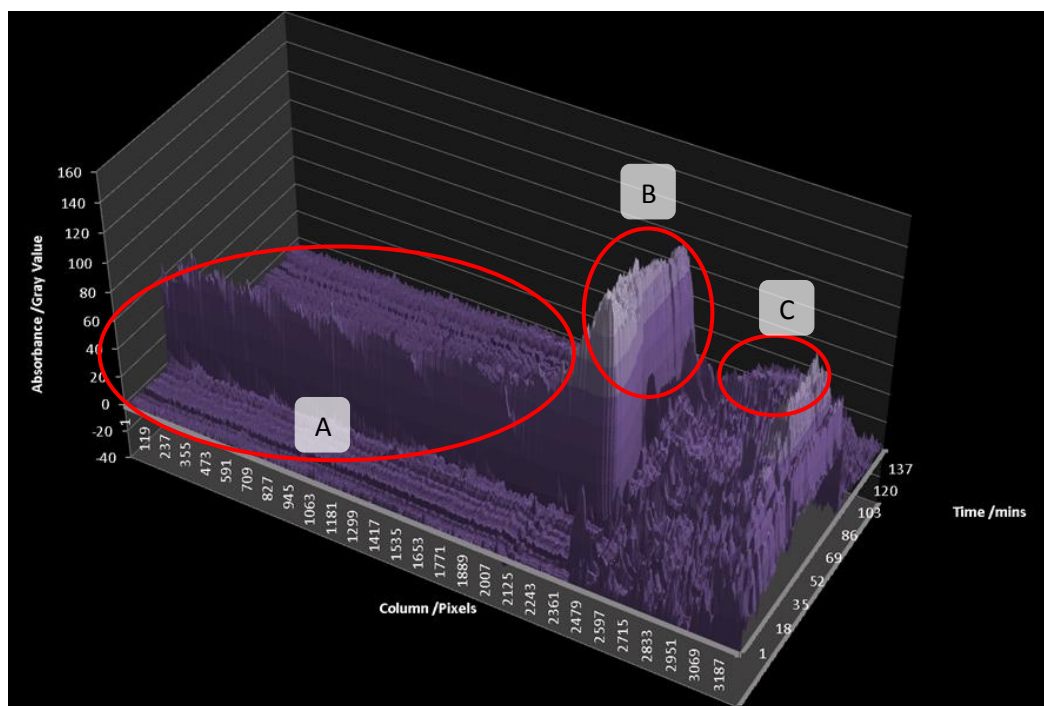


Figure 2.3.4. Focusing of BPB into a band using a static linear EFG. The sample of BPB flowed along the separation channel, where it was diffuse, as seen by the relatively lower intensity (y-value) after focusing, with time, the sample concentrates, as observed by the relatively high intensity of the peak. Following the movement of the sample over time, the graph displays: A) the entry and initial migration; B) focusing and concentration of the sample; and C) the eluting of the BPB.

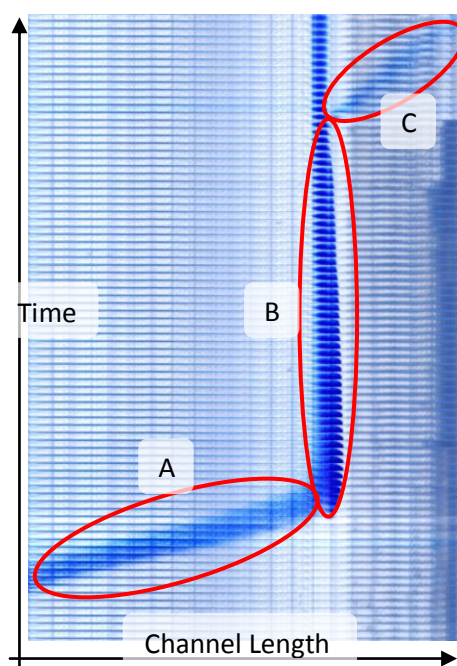


Figure 2.3.5. BPB focusing as shown in the form of a Montage. This was constructed by taking the cropped images and stacking them in order. Time runs upwards with injection at the bottom and elution near the top. In this case a higher flow rate would be required to elute the entire sample out of the packed channel. Following the movement of the sample over time, the montage displays: A) the entry and initial migration; B) focusing and concentration of the sample; and C) the eluting of the BPB.

2.3.3 Separations of the Bio-Rad Kaleidoscope pre-stained standards test mixture.

Having completed separations of simple test mixtures, experiments with protein cocktails were undertaken. The Bio-Rad Kaleidoscope²⁰ mixture was chosen as it is a mixture of seven uniquely coloured proteins with molecular weights ranging from approximately 7 to 200kDaltons, (table 2.3.1). Additionally, this protein mixture has been stained with covalently bonded coloured markers making it detectable with this DFGF set up; i.e. using reflectance measurements.

Protein	Molecular Weight (Da)	Stain
Myosin	202,000	Blue
β -galactosidase	133,000	Magenta
Bovine serum albumin	71,000	Green
Carbonic anhydrase	41,800	Violet
Soybean trypsin inhibitor	30,600	Orange
Lysozyme	17,800	Red
Aprotinin	6,900	Blue

Table 2.3.1. Kaleidoscope Pre-Stained Standards Test Mixture²⁰

At a flow of $1\mu\text{Lmin}^{-1}$ buffer solution was pumped through delivering $5\mu\text{L}$ of 10%v/v Kaleidoscope mixture to the separation channel. Prior to injection the EFG was set to 55Vcm^{-2} to equilibrate the packing. The mixture then came into focus around the middle of the channel. The sample was left to focus for 60mins. A longer time was left to ensure a second injection of sample reached the same focal point as the first before beginning separation. A second injection was added to improve the visibility of the sample in the separation channel also demonstrating the ability to stack and load further sample. After 60mins the field was increased to 60Vcm^{-2} to move the sample back down column. After 100mins into the separation, the flow rate was decreased to $0.5\mu\text{Lmin}^{-1}$ and the sample migrated back down the column. A voltage profile similar to the profile used by Myers *et al.*²¹ was applied in attempt to separate the mixture. Unfortunately, a separation was not observed due to the EFG being too steep. However, the mixture was successfully controlled as shown by the migration back and forth along the column, (figure 2.3.6).

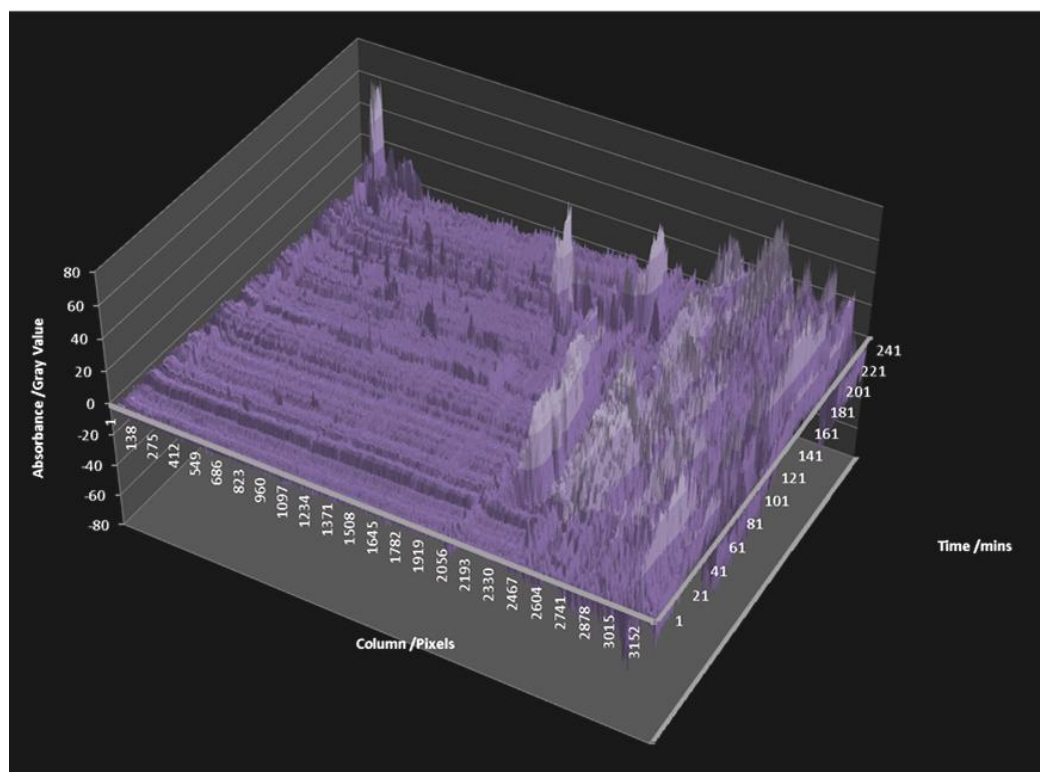


Figure 2.3.6. Kaleidoscope mixture migrating back and forth along the separation channel in a focused band of the protein mixture caused by changes in the EFG. The area on the far of the x-axis is noise caused by shadows of bubbles in the electrode channel.

In the above experiment a number of issues were identified with the configuration of the device. The flow rate of the peristaltic pump was set too high which, though more effective at removing gaseous products from the electrode channel, reduced the stability of the electric field³. A repeat experiment reverted back to a lower flow rate of $\sim 5 \text{ ml min}^{-1}$.

Again, at a flow rate of $1 \mu\text{L min}^{-1}$, a $5 \mu\text{L}$ injection of 10%v/v Kaleidoscope mixture was made. A second injection was made after 30mins to improve detection. The opposing EFG was initially set at 50 V cm^{-2} and lowered to 35 V cm^{-2} after 60mins. The mixture migrated and a slight separation was observed. Unfortunately as analytes separate the saturation in detection decreases.

After a further 15mins another linear EFG was applied of 20Vcm^{-2} . The mixture was observed migrating further up the channel. However, the sample was very difficult to detect. Some focal points are visible in the plot below (figure 2.3.7A) though where the sample had begun to separate, the bands became undetectable. This is also shown in the image stack on the right, in figure 2.3.7B. In addition, from figure 2.3.7B, the presence of small precipitate is visible forming in the channel. These could be caused by the protein mixture crystallising amongst the packing material. In further experiments, low concentrations of sodium dodecyl sulfate and cetyltrimethylammonium bromide, 0.035mM and 0.105mM respectively, were added to the buffer to aid solubility of the sample.

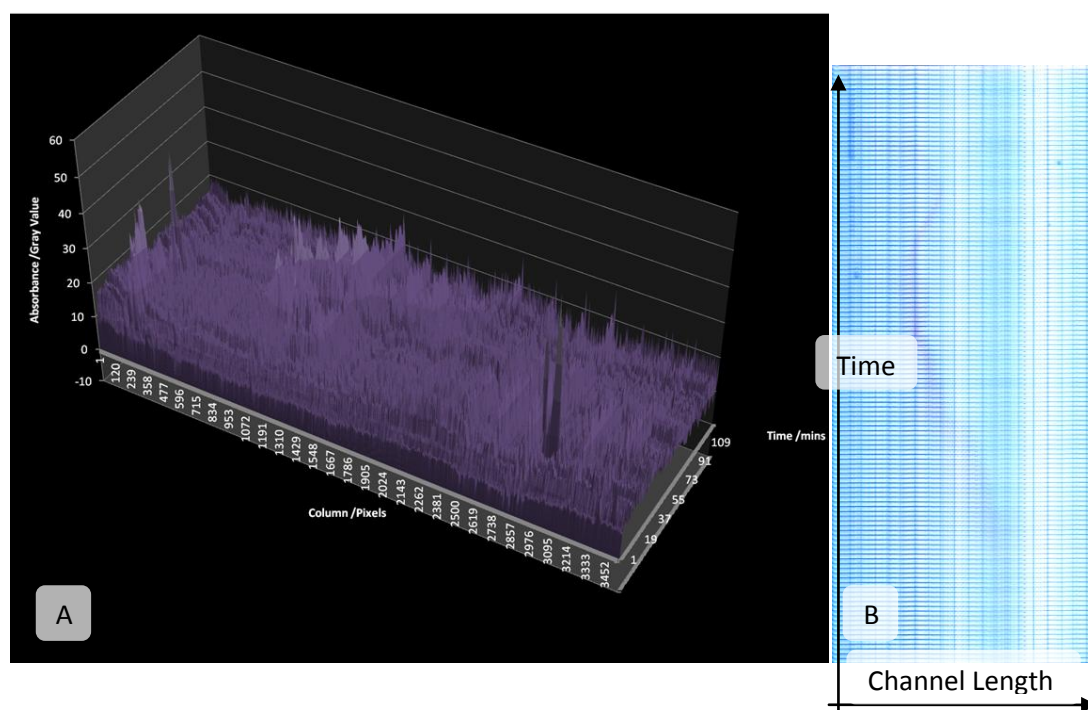


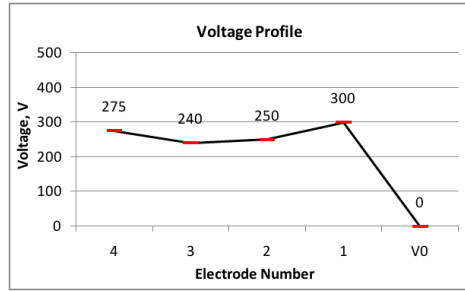
Figure 2.3.7. A) Graphical representation of kaleidoscope mixture focused in the first generation device. B) Montage of the images displaying the movement of the bands along the separation channel.

The final example of Kaleidoscope mixture using the first generation DFGF device displays a separation of three bands out of the seven components (figure 2.3.8).

An injection was made after 1min and a second injection made after 25mins. Following the data in table 2.3.2 below shows the changes made to the applied EFG.

Time (mins)	EFG (Vcm ⁻²) and Voltage Profile	Flow(μLmin ⁻¹)												
1	<p style="text-align: center;">G=50</p> <table border="1"> <caption>Voltage Profile Data (1 min, G=50)</caption> <thead> <tr> <th>Electrode Number</th> <th>Voltage, V</th> </tr> </thead> <tbody> <tr> <td>4</td> <td>844</td> </tr> <tr> <td>3</td> <td>760</td> </tr> <tr> <td>2</td> <td>590</td> </tr> <tr> <td>1</td> <td>338</td> </tr> <tr> <td>V0</td> <td>0</td> </tr> </tbody> </table>	Electrode Number	Voltage, V	4	844	3	760	2	590	1	338	V0	0	1.0
Electrode Number	Voltage, V													
4	844													
3	760													
2	590													
1	338													
V0	0													
25	<p style="text-align: center;">G=50</p> <table border="1"> <caption>Voltage Profile Data (25 min, G=50)</caption> <thead> <tr> <th>Electrode Number</th> <th>Voltage, V</th> </tr> </thead> <tbody> <tr> <td>4</td> <td>844</td> </tr> <tr> <td>3</td> <td>760</td> </tr> <tr> <td>2</td> <td>590</td> </tr> <tr> <td>1</td> <td>338</td> </tr> <tr> <td>V0</td> <td>0</td> </tr> </tbody> </table>	Electrode Number	Voltage, V	4	844	3	760	2	590	1	338	V0	0	1.0
Electrode Number	Voltage, V													
4	844													
3	760													
2	590													
1	338													
V0	0													
60	<p style="text-align: center;">G=25</p> <table border="1"> <caption>Voltage Profile Data (60 min, G=25)</caption> <thead> <tr> <th>Electrode Number</th> <th>Voltage, V</th> </tr> </thead> <tbody> <tr> <td>4</td> <td>422</td> </tr> <tr> <td>3</td> <td>380</td> </tr> <tr> <td>2</td> <td>295</td> </tr> <tr> <td>1</td> <td>169</td> </tr> <tr> <td>V0</td> <td>0</td> </tr> </tbody> </table>	Electrode Number	Voltage, V	4	422	3	380	2	295	1	169	V0	0	1.0
Electrode Number	Voltage, V													
4	422													
3	380													
2	295													
1	169													
V0	0													
97	<p style="text-align: center;">G=20</p> <table border="1"> <caption>Voltage Profile Data (97 min, G=20)</caption> <thead> <tr> <th>Electrode Number</th> <th>Voltage, V</th> </tr> </thead> <tbody> <tr> <td>4</td> <td>337.6</td> </tr> <tr> <td>3</td> <td>304</td> </tr> <tr> <td>2</td> <td>236</td> </tr> <tr> <td>1</td> <td>135.2</td> </tr> <tr> <td>V0</td> <td>0</td> </tr> </tbody> </table>	Electrode Number	Voltage, V	4	337.6	3	304	2	236	1	135.2	V0	0	1.0
Electrode Number	Voltage, V													
4	337.6													
3	304													
2	236													
1	135.2													
V0	0													
126	<table border="1"> <caption>Voltage Profile Data (126 min)</caption> <thead> <tr> <th>Electrode Number</th> <th>Voltage, V</th> </tr> </thead> <tbody> <tr> <td>4</td> <td>300</td> </tr> <tr> <td>3</td> <td>250</td> </tr> <tr> <td>2</td> <td>295</td> </tr> <tr> <td>1</td> <td>169</td> </tr> <tr> <td>V0</td> <td>0</td> </tr> </tbody> </table>	Electrode Number	Voltage, V	4	300	3	250	2	295	1	169	V0	0	1.0
Electrode Number	Voltage, V													
4	300													
3	250													
2	295													
1	169													
V0	0													

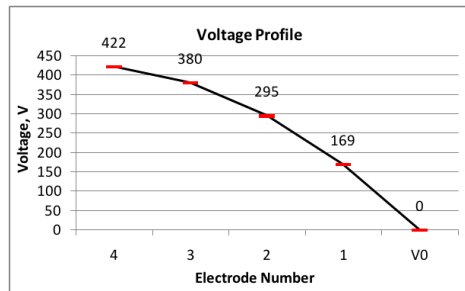
166



1.5

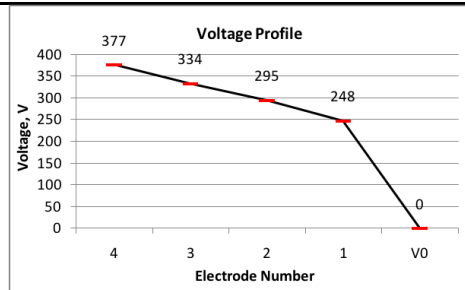
G=25

177



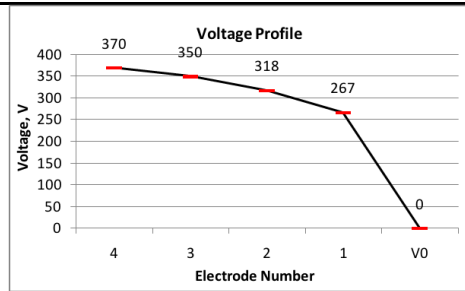
1.5

203



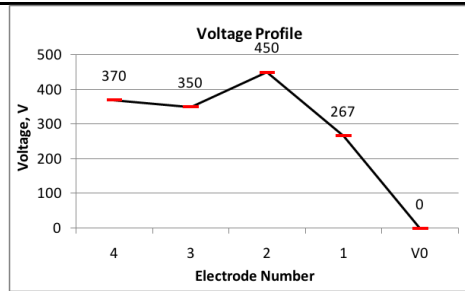
1.5

230



1.5

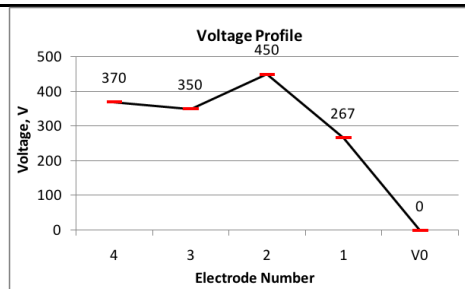
246



1.5

Run2

1



1

8	<p>Voltage Profile</p> <table border="1"> <thead> <tr> <th>Electrode Number</th> <th>Voltage, V</th> </tr> </thead> <tbody> <tr> <td>4</td> <td>400</td> </tr> <tr> <td>3</td> <td>450</td> </tr> <tr> <td>2</td> <td>400</td> </tr> <tr> <td>1</td> <td>267</td> </tr> <tr> <td>V0</td> <td>0</td> </tr> </tbody> </table>	Electrode Number	Voltage, V	4	400	3	450	2	400	1	267	V0	0	1
Electrode Number	Voltage, V													
4	400													
3	450													
2	400													
1	267													
V0	0													
23	<p>Voltage Profile</p> <table border="1"> <thead> <tr> <th>Electrode Number</th> <th>Voltage, V</th> </tr> </thead> <tbody> <tr> <td>4</td> <td>600</td> </tr> <tr> <td>3</td> <td>400</td> </tr> <tr> <td>2</td> <td>325</td> </tr> <tr> <td>1</td> <td>300</td> </tr> <tr> <td>V0</td> <td>0</td> </tr> </tbody> </table>	Electrode Number	Voltage, V	4	600	3	400	2	325	1	300	V0	0	1
Electrode Number	Voltage, V													
4	600													
3	400													
2	325													
1	300													
V0	0													
28	<p>Voltage Profile</p> <table border="1"> <thead> <tr> <th>Electrode Number</th> <th>Voltage, V</th> </tr> </thead> <tbody> <tr> <td>4</td> <td>650</td> </tr> <tr> <td>3</td> <td>400</td> </tr> <tr> <td>2</td> <td>325</td> </tr> <tr> <td>1</td> <td>275</td> </tr> <tr> <td>V0</td> <td>0</td> </tr> </tbody> </table>	Electrode Number	Voltage, V	4	650	3	400	2	325	1	275	V0	0	1
Electrode Number	Voltage, V													
4	650													
3	400													
2	325													
1	275													
V0	0													
35	<p>Voltage Profile</p> <table border="1"> <thead> <tr> <th>Electrode Number</th> <th>Voltage, V</th> </tr> </thead> <tbody> <tr> <td>4</td> <td>650</td> </tr> <tr> <td>3</td> <td>450</td> </tr> <tr> <td>2</td> <td>325</td> </tr> <tr> <td>1</td> <td>275</td> </tr> <tr> <td>V0</td> <td>0</td> </tr> </tbody> </table>	Electrode Number	Voltage, V	4	650	3	450	2	325	1	275	V0	0	1
Electrode Number	Voltage, V													
4	650													
3	450													
2	325													
1	275													
V0	0													
38	<p>Voltage Profile</p> <table border="1"> <thead> <tr> <th>Electrode Number</th> <th>Voltage, V</th> </tr> </thead> <tbody> <tr> <td>4</td> <td>700</td> </tr> <tr> <td>3</td> <td>450</td> </tr> <tr> <td>2</td> <td>325</td> </tr> <tr> <td>1</td> <td>275</td> </tr> <tr> <td>V0</td> <td>0</td> </tr> </tbody> </table>	Electrode Number	Voltage, V	4	700	3	450	2	325	1	275	V0	0	1
Electrode Number	Voltage, V													
4	700													
3	450													
2	325													
1	275													
V0	0													
47	<p>Voltage Profile</p> <table border="1"> <thead> <tr> <th>Electrode Number</th> <th>Voltage, V</th> </tr> </thead> <tbody> <tr> <td>4</td> <td>800</td> </tr> <tr> <td>3</td> <td>500</td> </tr> <tr> <td>2</td> <td>325</td> </tr> <tr> <td>1</td> <td>275</td> </tr> <tr> <td>V0</td> <td>0</td> </tr> </tbody> </table>	Electrode Number	Voltage, V	4	800	3	500	2	325	1	275	V0	0	1
Electrode Number	Voltage, V													
4	800													
3	500													
2	325													
1	275													
V0	0													

63

0

5

Table 2.3.2 Voltage profile for Kaleidoscope separation in figure 2.3.8.

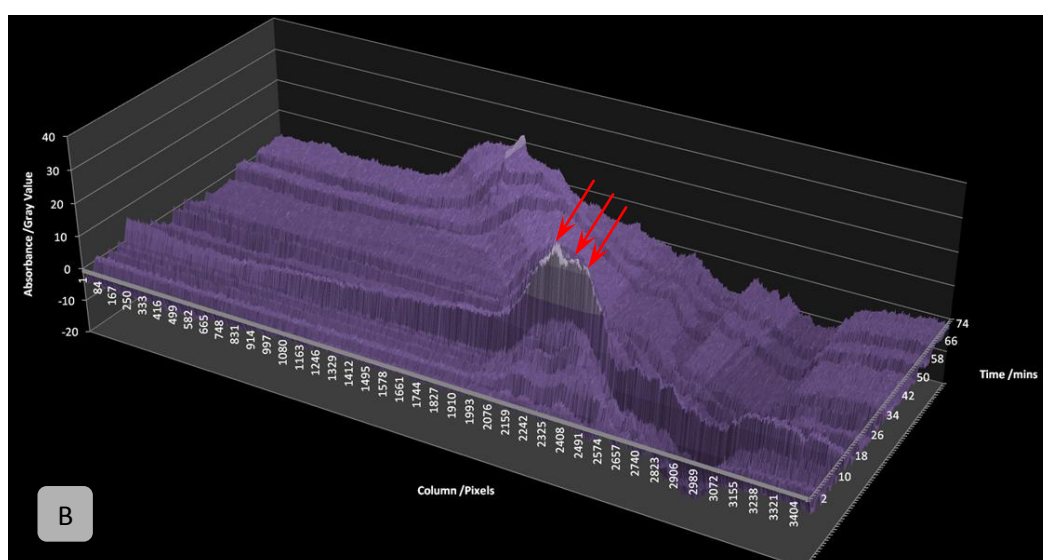
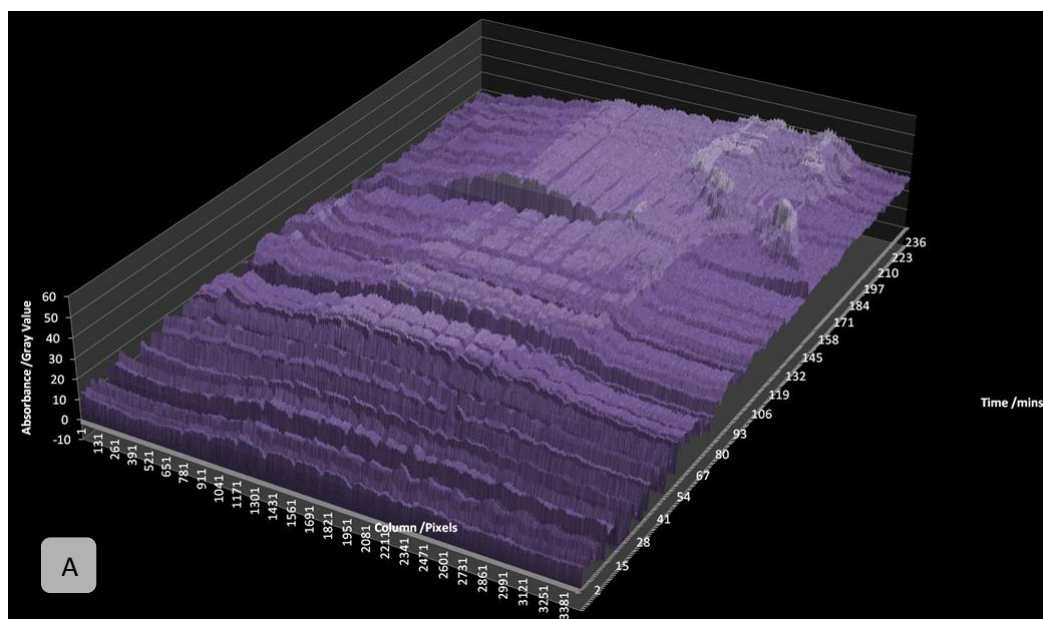


Figure 2.3.8. A) 'Run1' From Table 2.3.2 displaying the kaleidoscope test mixture being manipulated in the separation channel. B) 'Run2' From Table 2.3.2 an immediate follow up experiment injecting the sample and focusing again. Three separated bands can be seen in the plot (red arrows).

Following the profiles down table 2.3.2, as the separation progresses, a high voltage was applied to electrode 1 to cause further separation of the analytes at that point in the channel. This is seen by the faint blue and yellow (figure 2.3.8B) becoming more concentrated to give two of the three partially separated components.

In figure 2.3.8B, after 58mins, a very tightly focused band of protein is visible. These runs demonstrate the ability of DFGF to focus and separate large charged protein samples.

2.4 Experimentation with the Protasis DFGF device

2.4.1 The Protasis DFGF device: An Overview

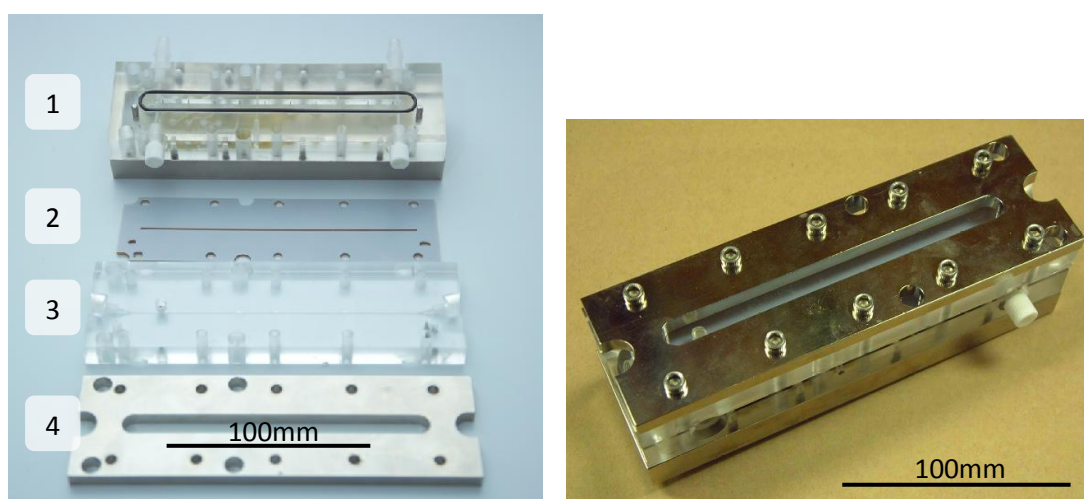


Figure 2.4.1. Construction and image of the Protasis DFGF device showing: 1) electrode channel; 2) membrane support; 3) separation channel; and 4) mounting plate.

The Protasis⁹ DFGF (figure 2.4.1) is a second generation device which is constructed in the same form factor as the previous first generation device from Ivory *et al.*²². The Protasis device was designed as a larger scale system equipped with a larger separation channel at 1mm wide, 0.4mm deep and 130mm long.

Though not a preparative scale DFGF, the Protasis device aims to handle larger sample loadings than previous systems. The device houses fewer electrodes as the resolution of field was not as critical as in analytical applications.

2.4.2 Protasis Experimentation with a single analyte.

The device was packed with Bio-Rad P4 polyacrylamide beads¹¹, ~45-90 μm in diameter, using 100MWCO cellulose membrane. A linear EFG of 5Vcm^{-2} and flow rate of $1\mu\text{Lmin}^{-1}$ was applied and the cell equilibrated for 20mins. A $20\mu\text{L}$ injection of 10%v/v lissamine green was made. The sample moved up the cell to a focal point at ~4cm, shown in figure 2.4.2 below. This focal point was consistent with observations from repeat experiments using the same conditions.

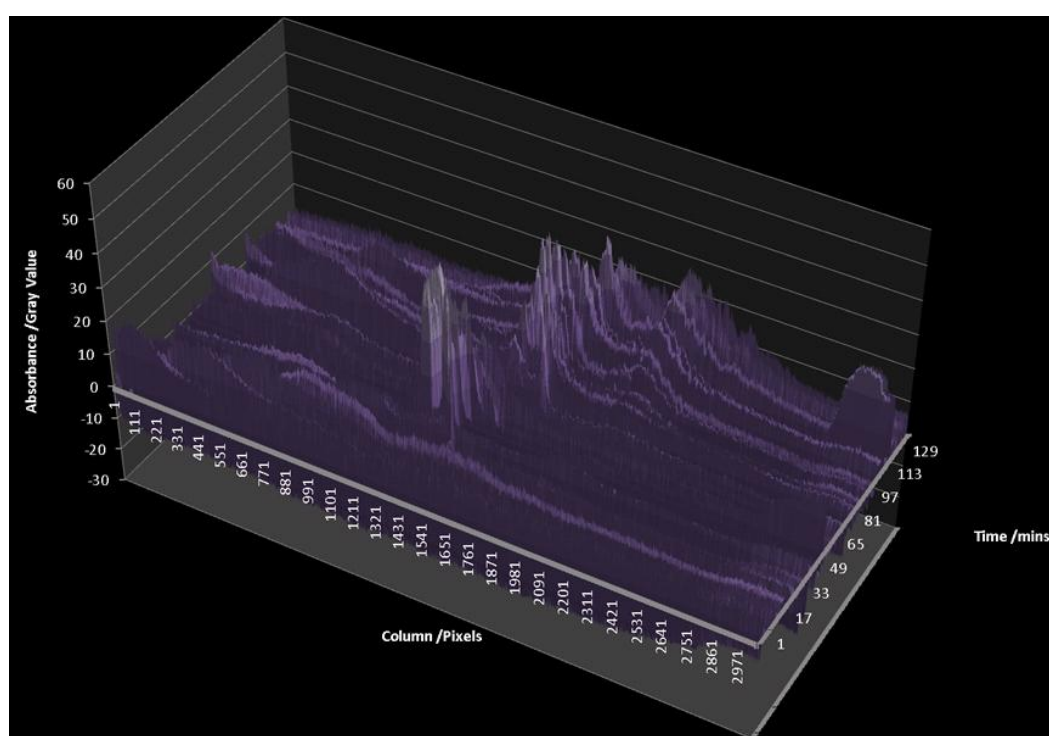


Figure 2.4.2. More than $20\mu\text{L}$ of 10% Lissamine green solution being injected and focused into a tight band by a linear EFG of 5Vcm^{-2} and flow rate of $1\mu\text{Lmin}^{-1}$.

2.4.3 Protasis separation of a two component test mixture

Moving to a two component test mixture of 10%v/v BPB and AM, the mixture was separated initially by an EFG of 5Vcm^{-2} and a flow rate of $1\mu\text{Lmin}^{-1}$. The separation displayed well focused bands of the individual analytes (figure 2.4.3).

To demonstrate the control with this device, after 13mins, the flow rate was increased to $1.5\mu\text{Lmin}^{-1}$ to push the bands further up the channel while maintaining their concentration. At 15mins the flow was increased again to $2\mu\text{Lmin}^{-1}$. This caused the sample to move up the channel as expected without any loss in the resolution of the focused bands. From these increments in flow rate, it can also be deduced that the technique is not electro-trapping, but is dynamic flow dynamic field gradient focusing, as demonstrated by the analytes moving further up the channel with the increases in flow rate.

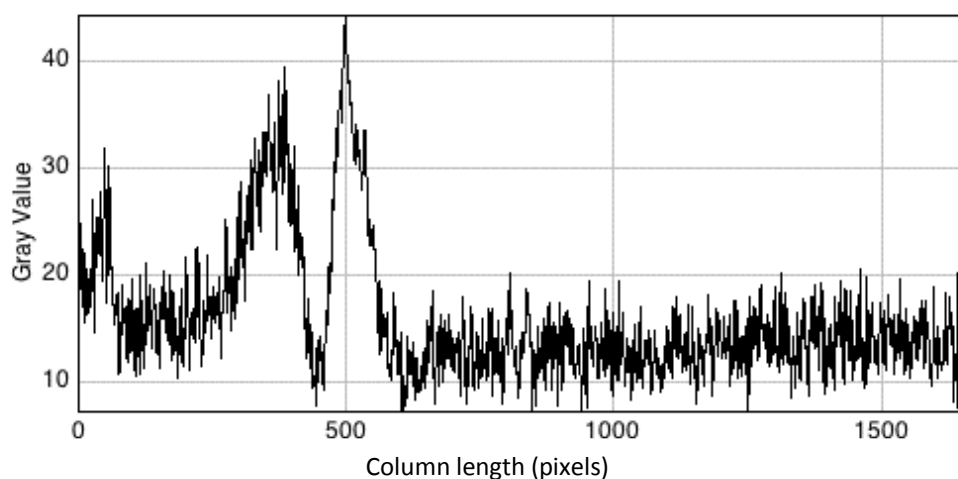


Figure 2.4.3. A mixture of AM and BPB separated and focused observed by the two peaks respectively. A single image analysis is shown as the full separation graph does not clearly show the separation.

2.4.4 Protasis separation of Bio-Rad Kaleidoscope test mixture

As with the first generation device earlier, once successful separations had been carried out with simple dyes, experiments with protein mixtures were performed, also using the Bio-Rad Kaleidoscope mixture²⁰ (table 2.3.1).

Starting the experiment with the flow rate set at $1\mu\text{Lmin}^{-1}$ and a linear EFG of 7Vcm^{-2} , $20\mu\text{L}$ of $10\%v/v$ Kaleidoscope test mixture²⁰ was injected. After 20mins the sample was present in the device. However, as the sample was difficult to see, even when concentrated, to improve the detection of the sample, a second $20\mu\text{L}$ injection was made. The mixture came into focus after $\sim 100\text{mins}$. Upon initial focusing the sample then began to form bands as the individual proteins began to separate. Four peaks were observed after 234mins and the EFG was lowered to 6.5Vcm^{-2} . The separation achieved is shown in figure 2.4.4. with the voltage profiles used to generate the EFGs displayed in table 2.4.1 below. After 318mins the field was switched off and the sample eluted from the device. This can be observed in the graph of the separation in figure 2.4.4. where a long flat area is visible after 318mins. This corresponds to the sample defocusing and eluting.

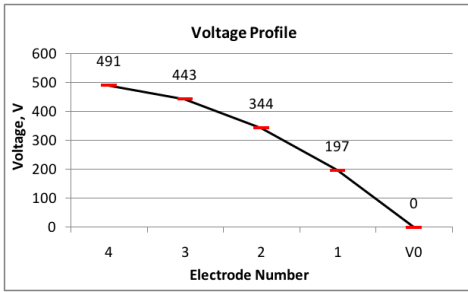
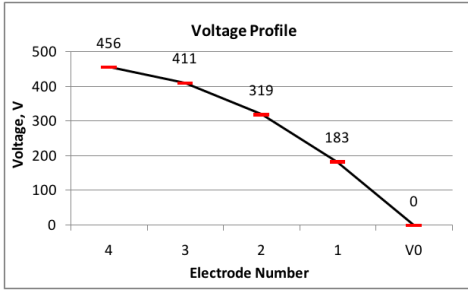
Time (mins)	EFG (Vcm^{-2}) and Voltage Profile	Flow(μLmin^{-1})
1	<p style="text-align: center;">$G=7$</p> 	1.0
234	<p style="text-align: center;">$G=6.5$</p> 	1.0
318	Off	1.0

Table 2.4.1. Summary of voltage profiles applied the electrodes to separate $40\mu\text{L}$ Kaleidoscope mixture.

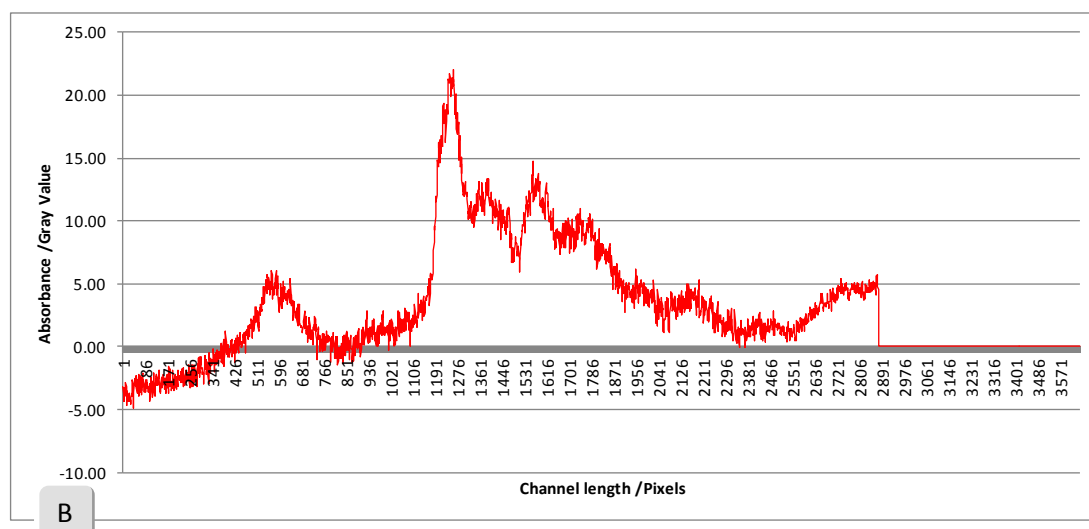
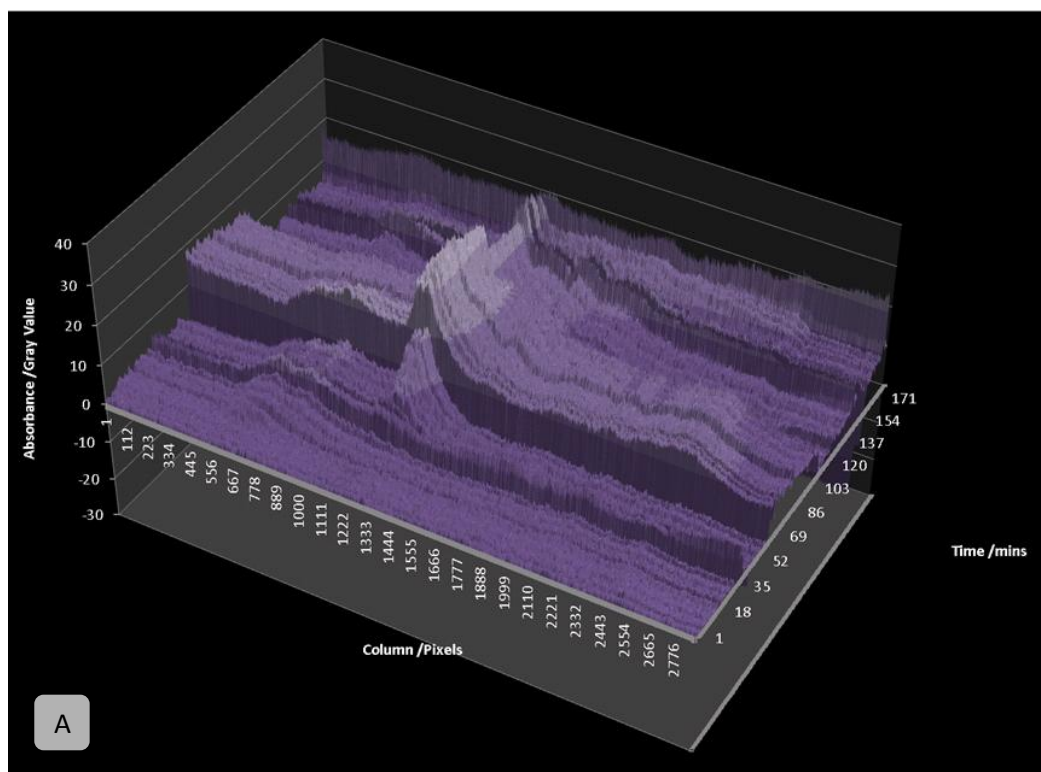
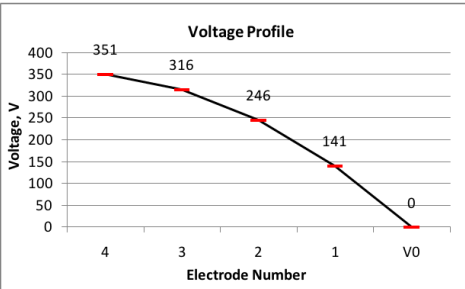
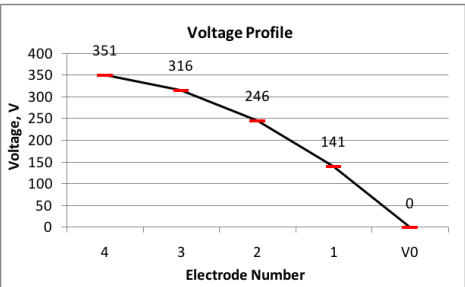
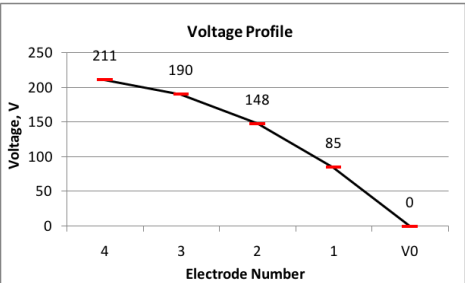


Figure 2.4.4. Kaleidoscope separation in the Protasis DFGF using the conditions in table 2.4.1. A) Graphical representation of the separation of 40 μ L Kaleidoscope mixture. B) Single plot at 147mins displaying at least four bands.

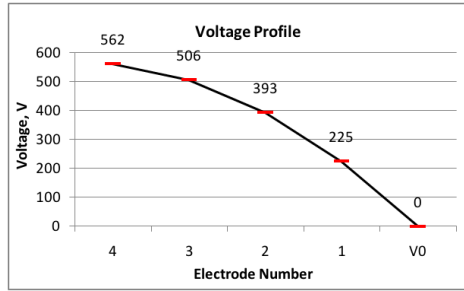
A repeat experiment of the kaleidoscope mixture demonstrated the sample being successfully controlled in the device for 4hours and 52 minutes.

In that time the sample was held lower in the column and then a number profiles were used in attempt to separate the mixture and improve on the previous four resolved proteins. As seen in figure 2.4.5, the best separation shows five species separated and the mixture recombined and separated again into five components. The progression of the experiment is summarised in table 2.4.2. The corresponding images are shown from later during the separation so analytes had time to migrate to new focal points as changes were made to the electric field profile.

Time (mins)	EFG (Vcm^{-2}) and Voltage Profile	Flow($\mu Lmin^{-1}$)
0	<p style="text-align: center;">G=5</p> 	1.5
26	<p style="text-align: center;">G=5</p> 	1.5
27	<p style="text-align: center;">G=3</p> 	1.5

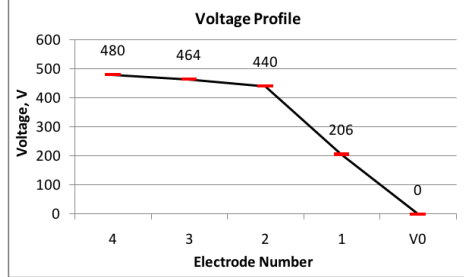
G=8

44



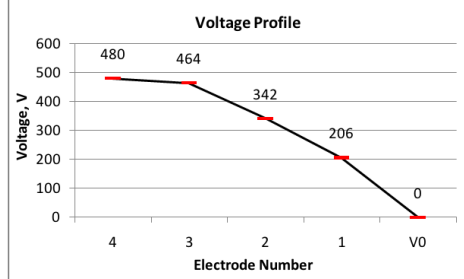
1.5

125



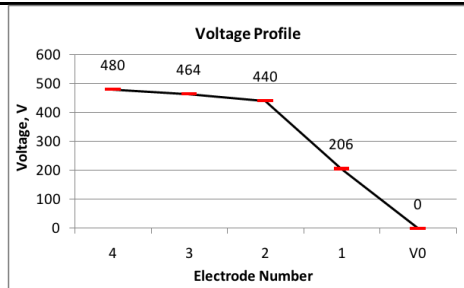
1.5

151



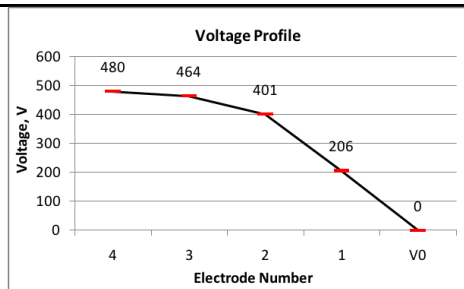
1.5

176



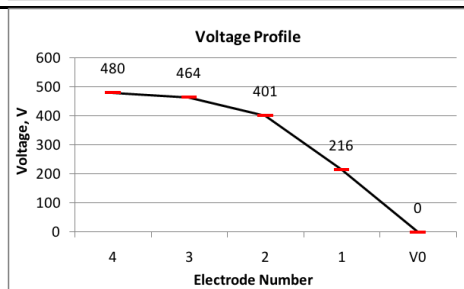
1.5

226



1.5

235



1.5

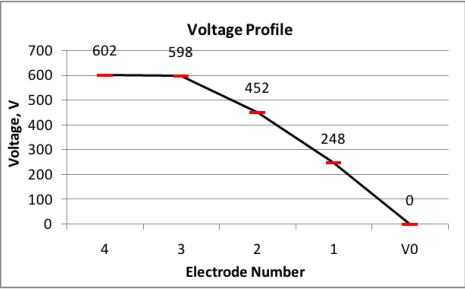
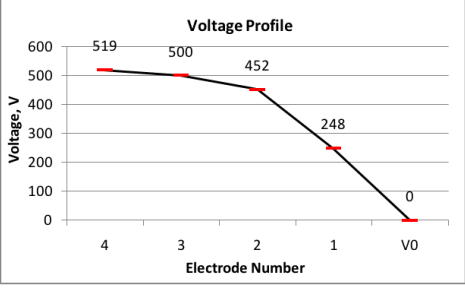
253		1.5
262		1.5
293	Off	1.5

Table 2.4.2. EFG and flow rates applied to separate the Kaleidoscope mixture in figure 2.4.5.

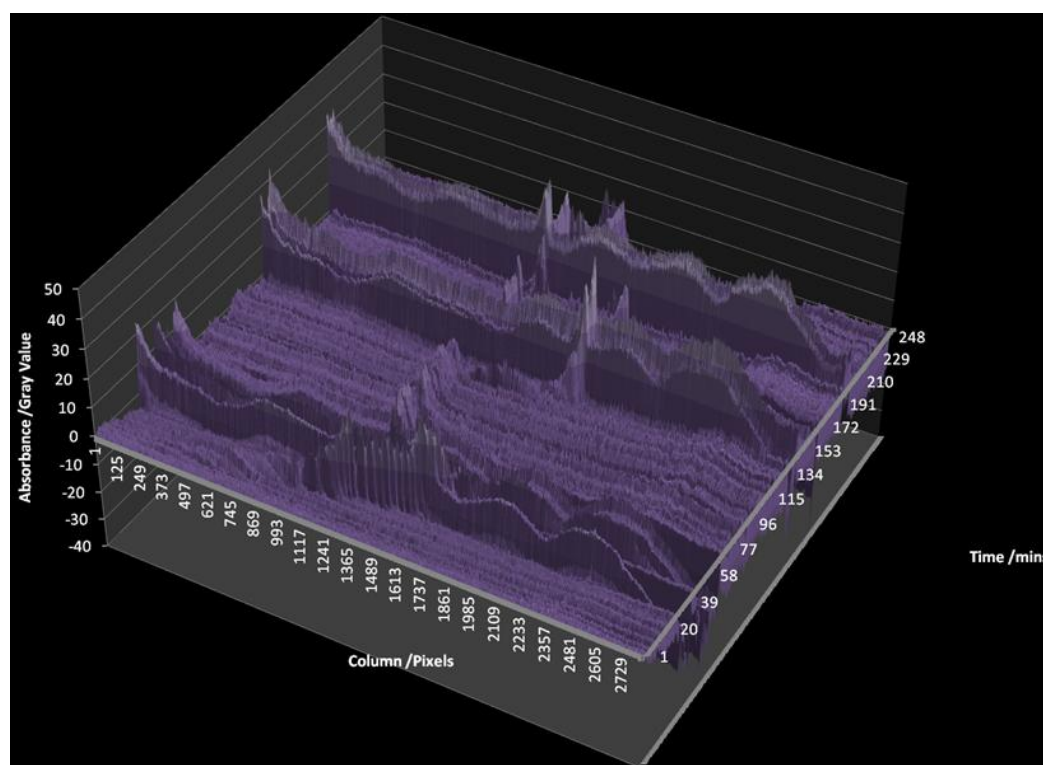


Figure 2.4.5. The separation of Kaleidoscope test mixture²⁰ using the conditions in table 2.4.2 displayed graphically. Five component peaks are observed during the separation.

From the above data it is apparent that the Protasis⁹ DFGF device is capable of separating greater volumes of sample and mixtures of proteins covering a large size range. From these images it is clear that there is a de-focusing region around each of the bands where the sample has not come into a highly focused sharp band. This is due to the deterioration of the electric field as the distance perpendicular to the channel length is increased. Previous work by Burke and Ivory²³ has seen the use of a subsidiary high voltage supply to apply a voltage of -200V to an electrode adjacent to the ground electrode. In this case the solution is complicated by the depth of the channel minimising the effect of the stabilising voltage. Furthermore, in other examples of DFGF¹⁹, higher resolutions were achieved by increasing the control over the electric field by using up to 15 individually controlled electrodes. As mentioned above, the Protasis system was designed in the knowledge that only four electrodes would be used and the resolution of the field would be less. However, effective separations are still achievable as indicated by this experiment.

The Protasis DFGF device was tested with a number of dyes and then finally with larger injections ca 40-60 μ L of protein cocktails.

2.5 Discussion

While these cells have advantages in loading capacity, there are a number of key faults of their design and layout. These key areas are; Joule heating, UV transparency, membrane failure, and all the problems associated with the requirement of a packing material²⁴. During testing of these devices, key experiments have displayed these flaws.

Firstly, the main limitation of these test devices is the acrylic construction which is not transparent to UV light. Below around 365nm the transmission is negligible. This poses a major issue as the target application for DFGF are larger molecules and proteins which do not absorb visible light. A solution to this was to alter the device to house a quartz window in front and behind the separation channel to allow a UV light source to propagate through the device onto a detector²⁵. This solution works well for this type of cell, however, further issues still remain. One of the most prevalent is the joule heating generated by the use of high voltage in the electrode channel. Figure 2.5.1 displays the result of driving these high voltages. The heat generated by the electrodes has caused the buffer to heat to such an extent that it has permanently damaged the upper area of the separation channel turning the acrylic white. To combat this effect, a cooling system is used for the electrode buffer. However, in advancing with this system less supporting equipment is much more favourable as it reduces the laboratory footprint of the instrument. Also having less supporting equipment reduces complexity in operation.

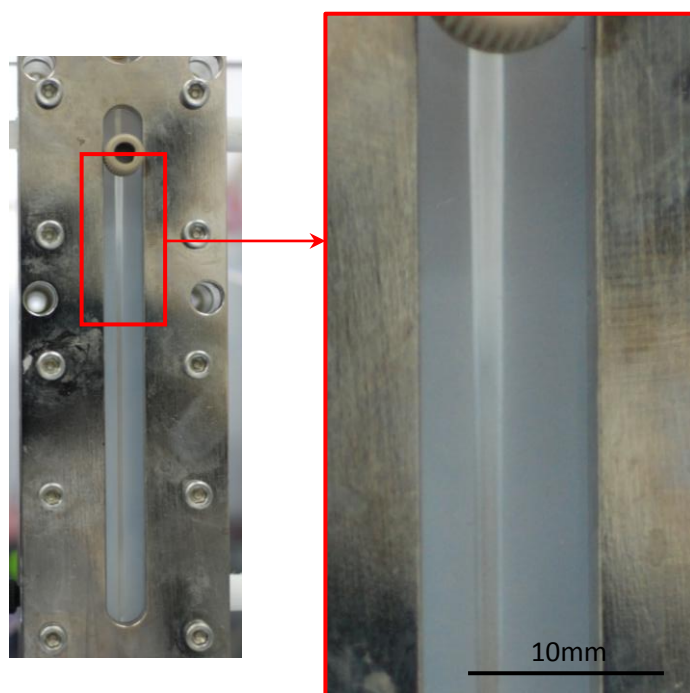


Figure 2.5.1. Protasis device irreversibly damaged by joule heating after running at the maximum 1000V without cooling. LEFT: Displays the Protasis device. RIGHT: top area of the separation channel turned white by the damage to the acrylic.

As listed above, the packing material presents problems in the key areas of set up, operation and longevity. When preparing either of these DFGF devices it is necessary to pack them with a material or monolith to provide a narrow diffusion pathway through the device. This results in a 24hour period, or more, depending on the success of the packing process, before the device is operational. Packing the separation channel itself is not a facile task. As with other packing methods for chromatography, there is a high deviation in success and failure when packing the channel. This is due to the complex system of solvent and material turbulent interactions resulting in artefacts and blockages, such as 'key stoning' where a group of particles form an arch, creating voids. These effects are worsened when using polydispersed packing materials. Polyacrylamide beads are used as a standard as they were determined experimentally to be optimal for EFGF⁶, though a major issue in packing them is the polydispersity.

An optical microscope image of the DFGF channel packed with polyacrylamide is shown in figure 2.5.2.

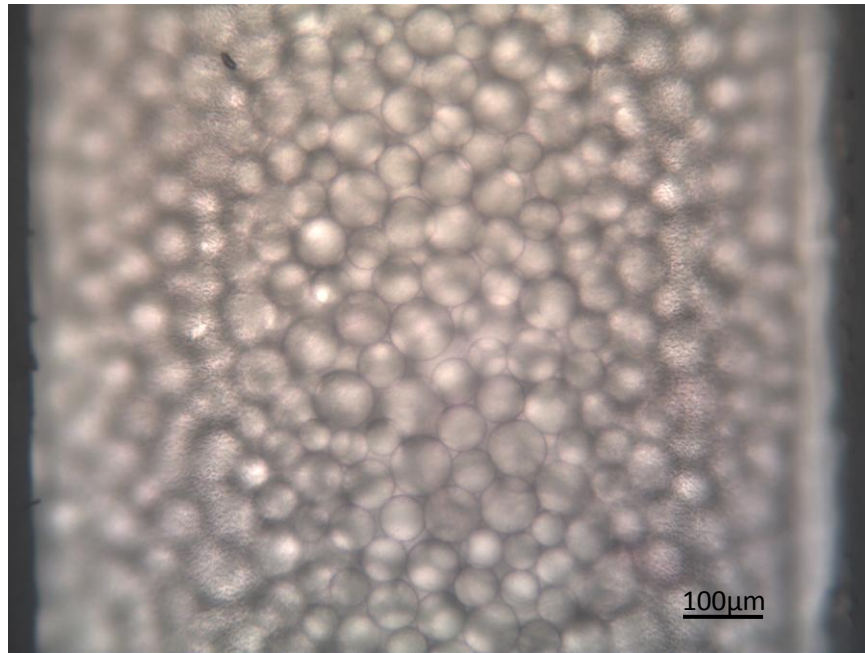


Figure 2.5.2. Optical Microscope image of polyacrylamide packing material in DFGF channel. Void spaces and irregular interstitial spacing are visible across the entire bed.

Changes to the packing methodology evolved with each packing completed until the final method, (described earlier in this chapter), with the addition of sonic and vibrational agitation, was devised. Additionally, the packing process relies on using continuous pressures of 4-5bar which applies stress to the cellulose membrane, therefore increasing the risk of membrane collapse. If a monodispersed material inert to samples and unaffected by the electric field were developed, this would significantly improve these issues. During operation of the DFGF device the packing presents problems in requiring more time for system equilibration, but mainly due to bed rearrangements or a poorly packed channel. This resulted in the device needing to be stripped down, the membrane replaced, and the device repacked.

Experimental observations clearly show this by gradual increase in the back pressure of the bed over time. In such cases the pressure increase at low flow rates leads to terminal membrane rupture with the packing material leaking into the electrode channel. An example of this is shown in figure 2.5.3.

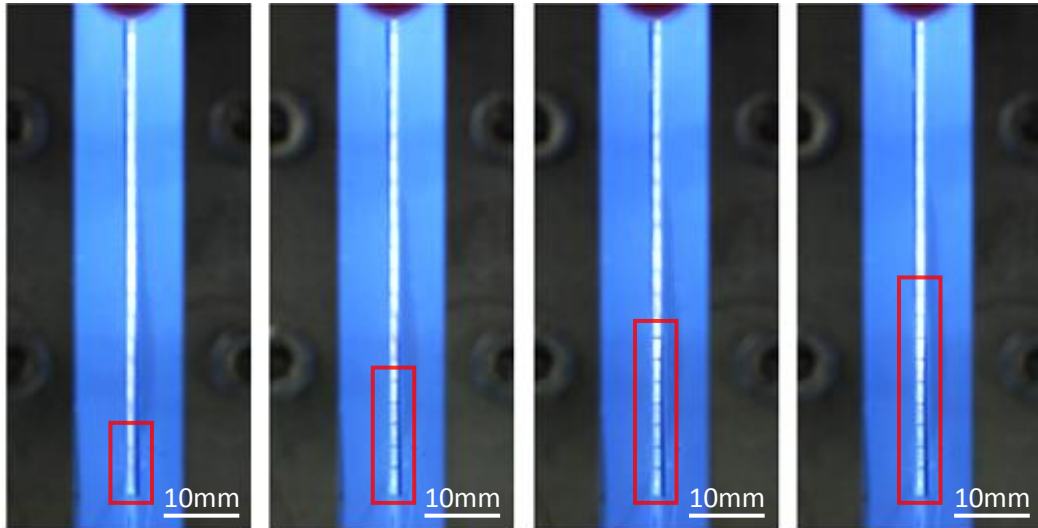


Figure 2.5.3. Left to right, images displaying a bed rearrangement leading to the collapse of the membrane. This can be observed by the translucent packing material moving up the channel to leave behind a transparent void (red rectangles) which increases in severity over time.

2.6 Novel packing material for DFGF

2.6.1 Development of Particles for DFGF

Development of the packing material began by addressing the issues surrounding the packing of the polyacrylamide material. Polydispersed materials are more difficult to pack due to the differing sizes of packing particles preventing a uniform flow of slurry into channels and the increased chance of 'key-stoning' by the hydrodynamic forces and Eddy currents which form when moving a solution around spheres of differing size²⁶.

Furthermore, work by van Deemter indicates that monodispersed packing materials result in a more uniform diffusion along the column²⁷. Previously, the assessment of monodispersed particles for DFGF deemed it unnecessary as the two opposing forces prevented longitudinal diffusion. However, in view the difficulties experienced in packing the polydispersed materials, and the heterogeneous diffusion pathways observed, the advantage of utilising monodispersed materials was highlighted as the solution to these issues.

2.6.2 Procedure for manufacture of macroporous monodispersed spherical silica

100mL of Syton X30 colloidal silica²⁸ were decanted through a 100 μ m sieve. The solution was acidified by addition of 0.5ml, 0.5% by volume, of 1.0M hydrochloric acid. A drop by drop technique was used to form spheres of the destabilised silica sol solution which were collected in a vessel containing liquid nitrogen. Batch sizes were determined by the size of the collection vessel as to not allow a dense layer of particles to form, as this causes coagulation. The collected material was transferred to the freezer, at -30°C, for 24 hours to complete gelation. Completed gelation was confirmed by the presence of free flowing particles which were then removed from a freezer and washed with cool de-ionised water. Washes were repeated and the particle submerged in water to float off any 'fines' having let the particles settle. This mixture was then decanted and the particles collected. The collected particles were then placed in an oven with no vacuum at 80-100°C to harden and dry the silica. Having dried, the crucible was placed in a furnace and slowly ramped at 2°Cmin⁻¹ and held at 850°C for 18hours before slowly cooling back to room temperature.

2.6.3 Droplet Generation

2.6.3.1 Fused Silica Tubing and a pump

A range of approaches were explored in developing a stable drop forming device. The first and most simple were to use fused silica tubing with a range of internal diameters, IDs. This involved charging a syringe with the destabilised sol solution which was then moved through the fused silica tubing at a constant flow rate using a syringe pump. Flow rates were typically 0.5mLmin^{-1} for tubing of diameters over $50\mu\text{m}$, and lower flow rates were used for smaller ID tubing. It was postulated that changing the ID of the tubing would have an effect on the diameter of the droplets formed. However, it was found that at these flow rates the sol would form a large droplet at the opening until the surface tension could no longer support the mass the drop and then it would fall. This was, therefore, an affect independent of the ID of the tubing. Modifying this setup to create a spray utilised a vibration motor. A 1amp micro electric motor was attached to the tubing to cause resonance of the tubing. When the sol was forced through the tubing the force of the vibration would overcome that of the surface tension and resulted in the droplets falling into the liquid nitrogen as required. This experimental setup is shown in figure 2.6.1.

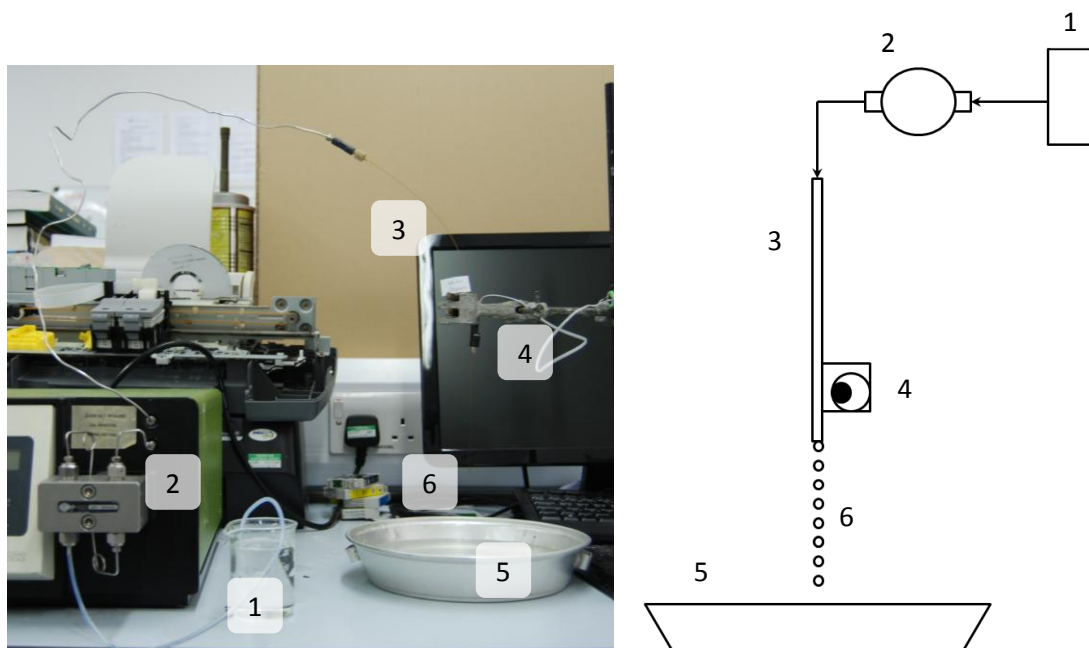


Figure 2.6.1. Drop generator using: 1) Precursor solution reservoir 2) Syringe pump 3) fused silica tubing 4) Vibrating motor. 5) Collection vessel containing $N_2(l)$ 6) Droplets of Precursor solution. Destabilised Sol solution was pumped from the reservoir by the pump along the fused silica tubing to generate droplet which were collected in a wide container filled with liquid nitrogen.

Though the addition of a vibrating motor prevented the droplets from growing at the end of the tubing, the diameter of particles measured with different IDs of tubing were very similar, all of which $\sim 40\mu\text{m}$ in diameter.

2.6.3.2 Spraying with water misters and pneumatic sprayer

The second spray application was to use atomiser sprays to generate the droplets. A hand operated sprayer, a compressed cylinder sprayer and an air brush were tested. These were carried out using the destabilised sol in each of the spraying devices.

These devices were deemed unable to deliver the required monodispersity as the spray from each of these was not uniform. A summary of these particles is shown in table 2.6.2

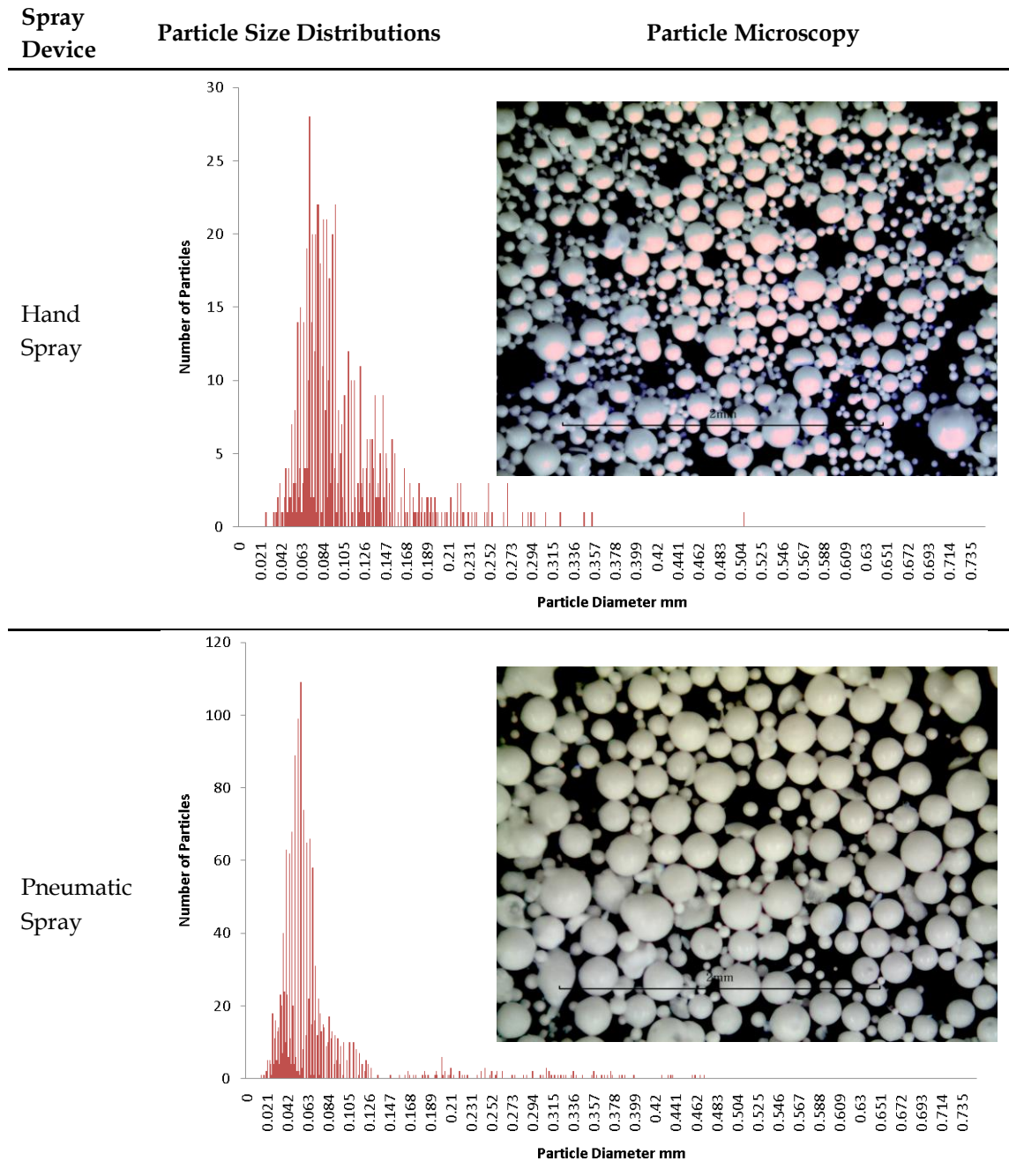


Table 2.6.2. Particles manufactured using the hand spray and pneumatic spray. The particle size distribution was calculated using ImageJ¹⁵ from several optical microscopy images.

Though unsuitable for the application required by DFGF, these materials could perform well in single use applications, such as an alternative to dried blood spotting²⁹. This is due to the fact these particles can be manufactured in a shorter time as the spraying would take less than five minutes including the time to prepare the destabilised sol indicating suitability for mass production.

2.6.3.3 Inkjet and Domino Printer controlled droplet generation

Moving to a more technical approach a 'Domino' industrial inkjet printer³⁰ was utilised to deliver a stable controllable droplet stream. This device features a piezoelectric droplet generator which splits a flow of viscous liquid into a stream of individual droplets. Depending on the solution used, the 'break up' parameter can be altered, as shown in figure 2.6.3, by increasing or lowering the voltage supplied to the piezoelectric valve. These droplets were 80 μ m in diameter which was standard operation for this printer head. These 80 μ m droplets produced particles approximately equal in diameter as the water in the sol expands on freezing, but the particles shrink after calcination. The printer head, figure 2.6.2, works by having a constant stream of droplets spraying from the drop generator. These droplets are recycled into the reservoir by a vacuum collector. Two deflection plates are located parallel to the stream on each side. These are called deflection plates as when an electric field is applied across them they cause an individual droplet to be diverted from the stream and sprayed from the head. Were this ink, this is how an individual pixel of a character would be generated. Such droplets combine over a moving area to make up a character.

In this application, the droplets are simply collected. Two methods of operation were available to enable the collection of these droplets.

The first was to utilise the deflector electrodes. By programming the printer to spray an array of spaced characters, for instance “iiiiiiiiiiiiiiii”, the deflected droplets would be collected. The problem with this was that it relied on the droplets being charged. The ink used in this printer contains a proprietary electrolyte to ensure a charge. Attempts to collect droplets with this method were unsuccessful as the silica sol solution was not observed deflecting in the electric field from the deflector plates.

As a work around, the collection gutter used to recycle to the solution was removed and the constant stream of droplets collected.

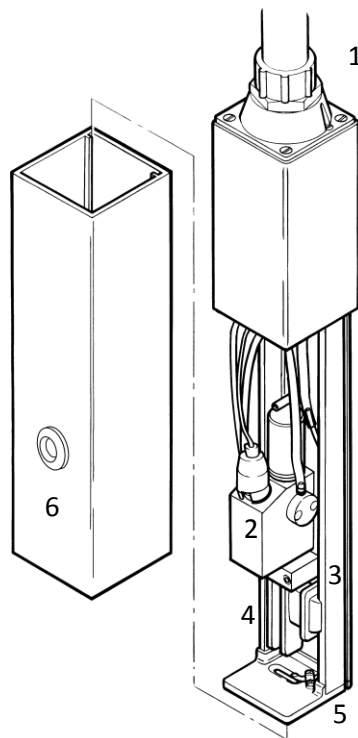


Figure 2.6.2. Printer Head of the Domino printer. 1) Umbilical feeding electrical signal and precursor mixture. 2) Piezoelectric Droplet generator. 3) Charge Electrode. 4) Deflection Electrodes. 5) Gutter collector for recycling unsprayed precursor mixture. 6) Viewing lens with a strobe light ensure correct 'break up' of droplets.³⁰

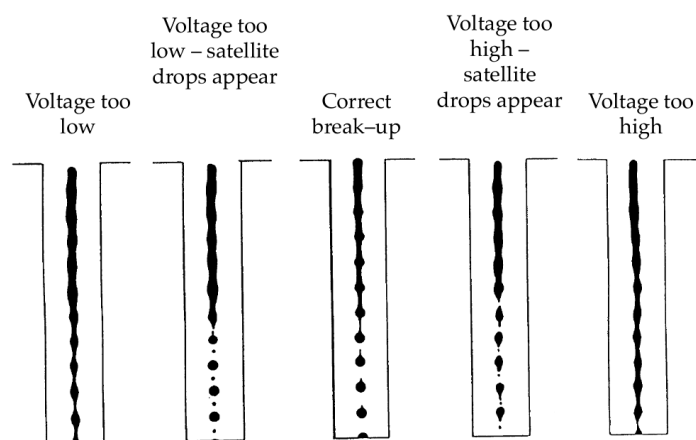


Figure 2.6.3. Adjusting the voltage waveform supplied to the piezoelectric droplet generator determines the 'break up' of droplets leaving the spray head on the Domino printer³⁰.

The spray forms individual droplets at a rate of 128kHz. These were collected for a period no longer than 2mins so as to not cause the collected particles to have sufficient force to coagulate from the pressure formed by layering in the vessel. It was experimentally determined that when using a high power spray of sol from this type printer, if the collection vessel was too close to the nozzle, the particles were smashed when breaking through the surface of the liquid nitrogen. The optimum distance from the spraying head was found to be 50cm. The final setup with the Domino printer is shown in figure 2.6.4. Also shown in the figure 2.6.4, a tall aluminium beaker was used to create a thermal gradient to aid the efficient cooling of the particles.

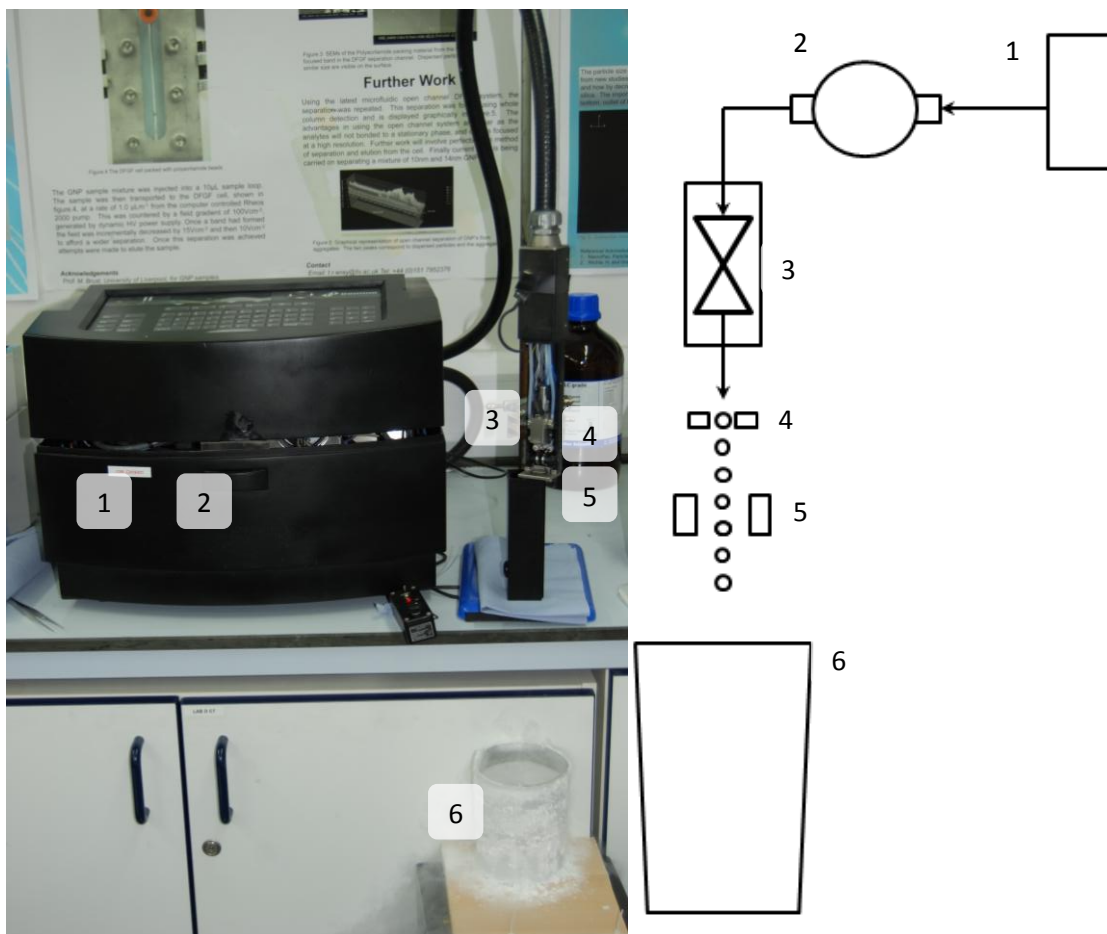


Figure 2.6.4. Spraying monodispersed particles using the modified Domino printer. 1) Silica sol reservoir. 2) Solvent Pump 3) piezoelectric droplet generator in the printer head. 4) Charging electrode. 5) Deflection Electrodes. 6) Collection vessel containing liquid Nitrogen.

These particles were calcined as detailed in the general method and physical characteristics measured. Mercury porosimetry indicated an average pore size of $1\mu\text{m}$, shown by the large peak in figure 2.6.5.

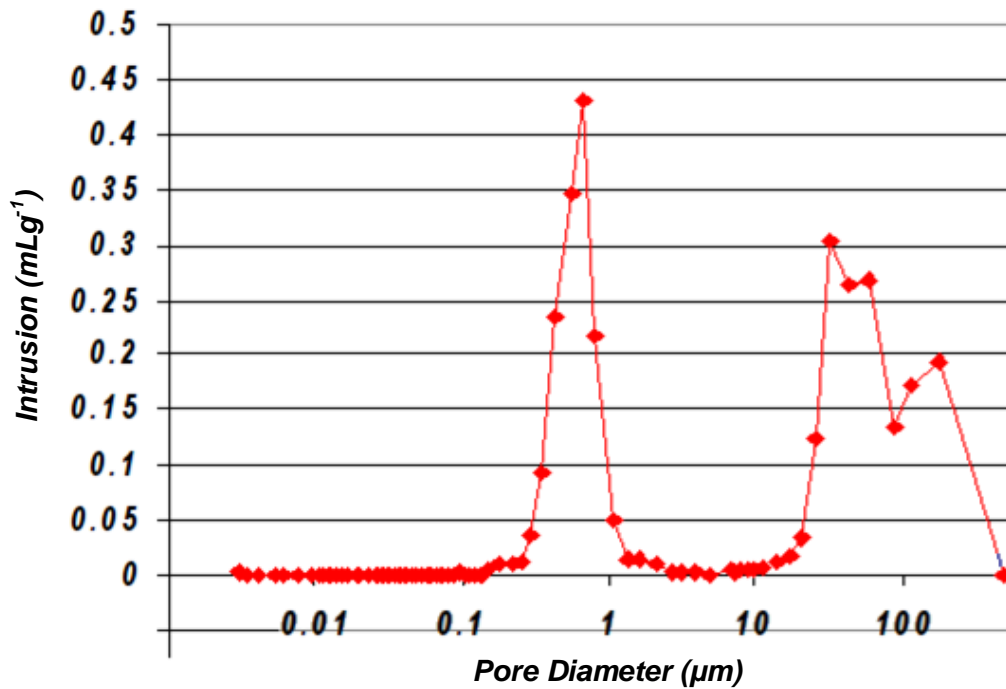


Figure 2.6.5. Mercury Porosimetry of the 80 μm silica particles indicating an average pore size of 1 μm . The peaks around 50 μm to 100 μm correspond to cracks on the surface of the particles or larger surface pores.

The peaks present between 50 μm to 100 μm correspond to cracks on the surface of the particles or larger surface pores. Nitrogen BET surface area analysis provided a value for the surface area to be $\sim 35\text{m}^2\text{g}^{-1}$ which is consistent with a macroporous material. To observe the morphology and surface characteristics Scanning Electron Microscopy (SEM) was carried out on the particles. The SEM images are shown in figure 2.6.6.

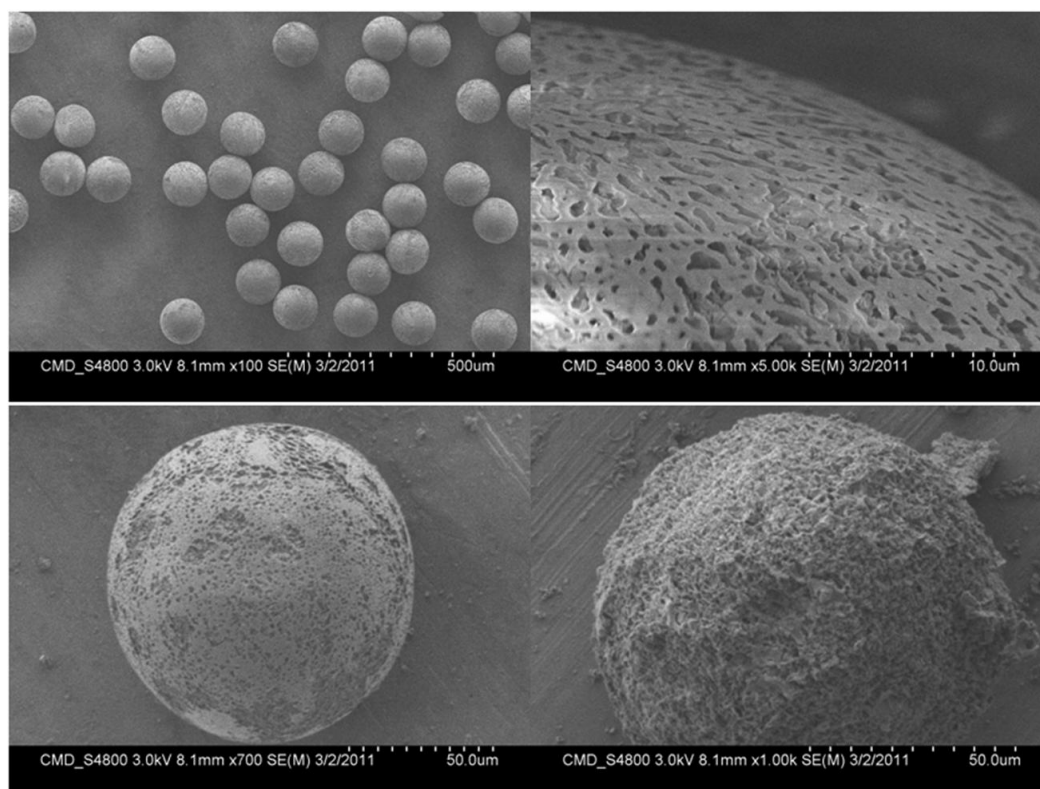


Figure 2.6.6. SEM images of the 80µm diameter silica particles made using the domino printer.

From the SEM images it is observed the particles are indeed monodispersed. The close up of the surface shows the pores of the particles generated by ice formation. Testing this material in another application saw the use of these particles for fully packed column Gas Chromatography.

2.6.4 Testing the particles with Gas Chromatography

1.2m of 500µm ID fused silica tubing was coiled around a GC column cage. The open end of the column was fritted with glass wool. Both ends were then sleeved with PEEK tubing.

These were then fitted with the custom made packing reservoir using standard 1/16" finger tight upchurch fittings. This was then connected to a syringe filled with the packing material dispersed in acetone. Compressed air was then used to push the slurry through the column. During packing the column was submerged in a water trough with a sonic probe. During the packing the slurry was observed moving through the column in a uniform flow. The resulting packed column was analysed under an optical microscope where it was observed that the material had packed into a near perfect hexagonally close packed spiral giving a very uniform distribution of material through the column. This packing is shown in figure 2.6.7.

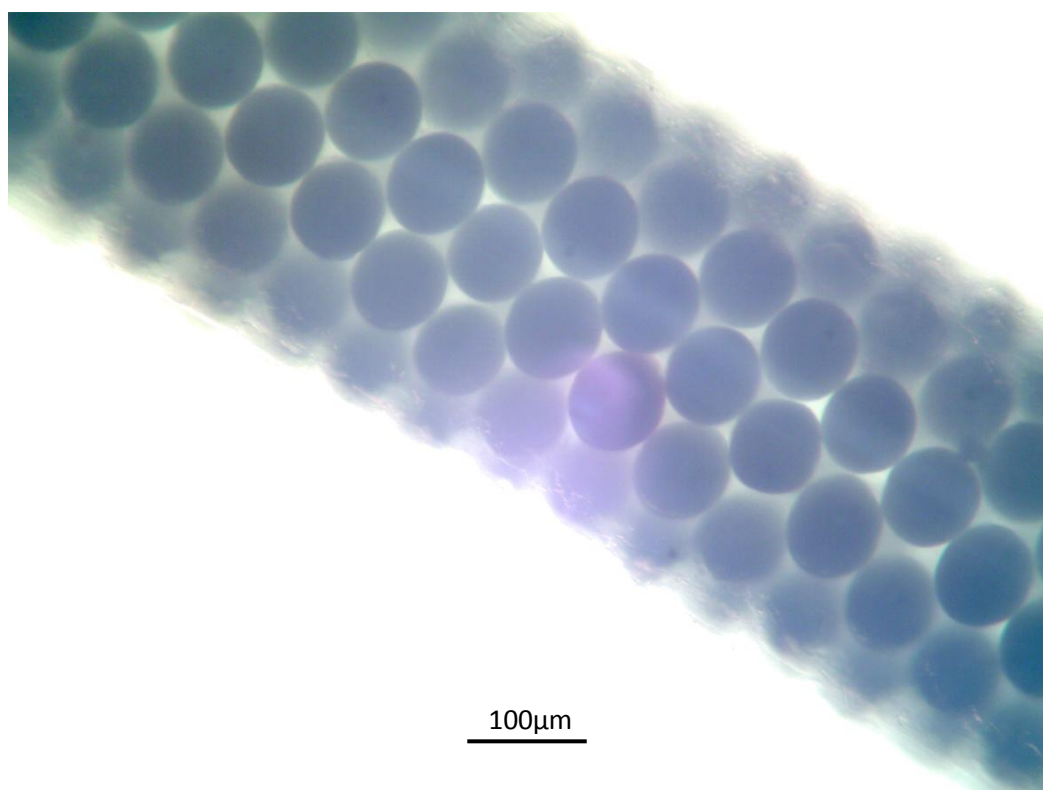


Figure 2.6.7. Optical microscope image of the GC column packed with the 80µm silica particles displaying a near perfect hexagonally close packed spiral.

To this column, a separation of petroleum ether and dichloromethane was performed. The separation was successful with baseline resolution between the peaks in spite of the short column length of only 1.2m compared to that of a +15m column, figure 2.6.8. This shows the high selectivity attained from the increases internal surface area gained by utilising this material in a fully packed column.

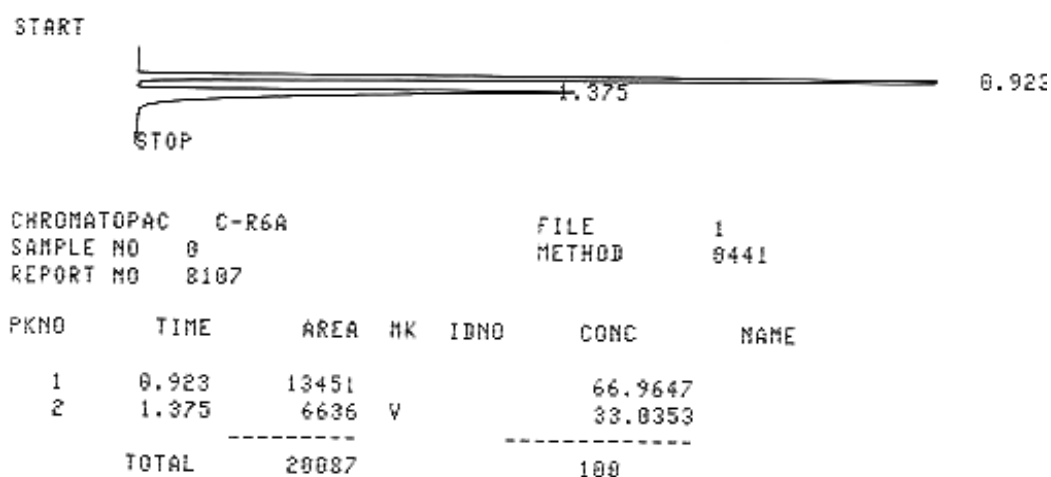


Figure 2.6.8. GC separation of Petroleum Ether and DCM at 60°C using the 1.2m column packed with 80µm silica.

Before these particles were used in the DFGF device they were deactivated. This was done to ensure that there would not be any influence on separation from using these particles. The bare silica surface is polar and would have resulted in chromatographic interactions with the analytes as the hydrodynamic flow moved them along the packed channel. To deactivate the surface of these particles, a sample was heated to 150°C under vacuum for 24hours. These were then calcined a second time at a higher temperature of 1000°C to convert any surface silanols to siloxanes resulting in an inactive non-polar surface.

Fourier Transform Infra Red, FTIR, analysis before and after further calcinations displays the elimination of the Si-OH bond stretch from 2750 to 3750 cm^{-1} , this FTIR trace is shown in figure 2.6.9.

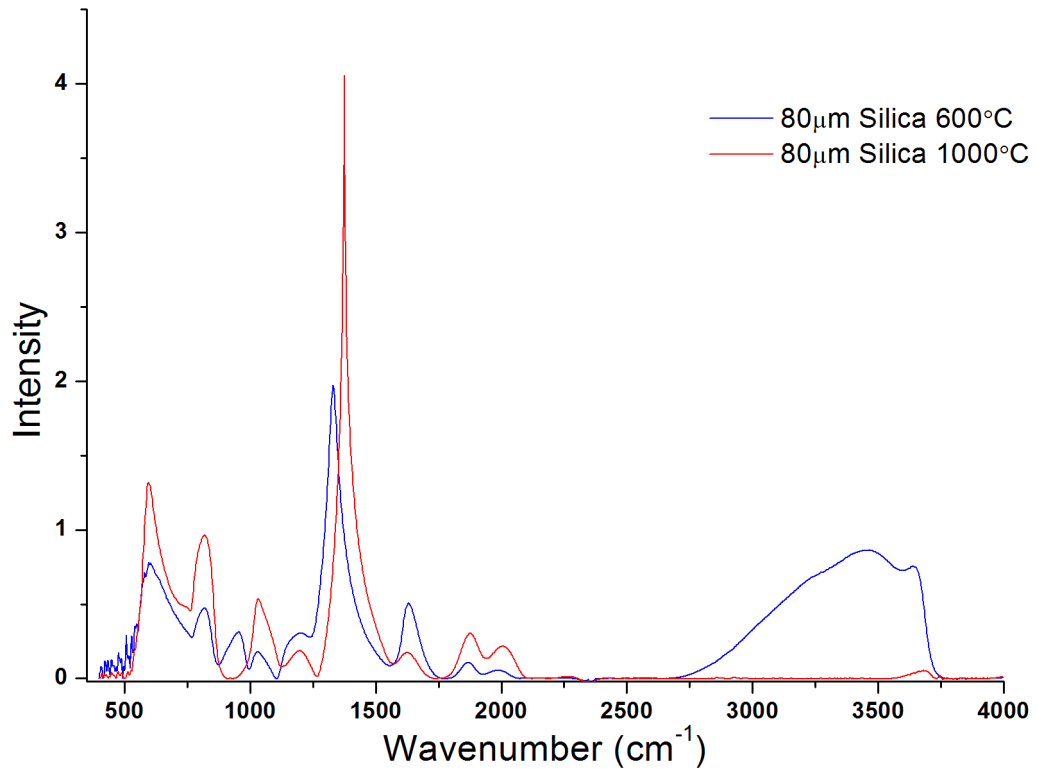


Figure 2.6.9. FTIR analysis of the 80µm particles before and after further calcination at 1000°C.

2.6.5 DFGF experimentation with 80µm Silica particles

2.6.5.1 Packing the DFGF with the 80µm Silica particles

Packing the DFGF with 80µm particles required a slight modification to the inlet of the DFGF device. As the diameter of the particles was only marginally smaller than the width of the inlet port, the inlet was machined to a diameter of 250µm. The packing rig was configured as described above in section 2.2.3.

The first generation DFGF device was prepared with 100MWCO membrane, connected to the packing apparatus and was placed a sonic bath. Having slurried 1g of particles in buffer solution used in the separation channel, the material was packed into the DFGF at 4bar of pressure from compressed air. The presence of a complete bed of material was observed after ~5mins and left to rearrange and settle under a continuous 4bar pressure for 2hours. The observed flow rate of packing solvent was $\sim 100\mu\text{Lmin}^{-1}$. With the separation channel packed the cell was connected to the Rheos pump and left for 24hours to equilibrate at a flow rate of $1\mu\text{Lmin}^{-1}$. The packed DFGF device is shown in figure 2.6.10.

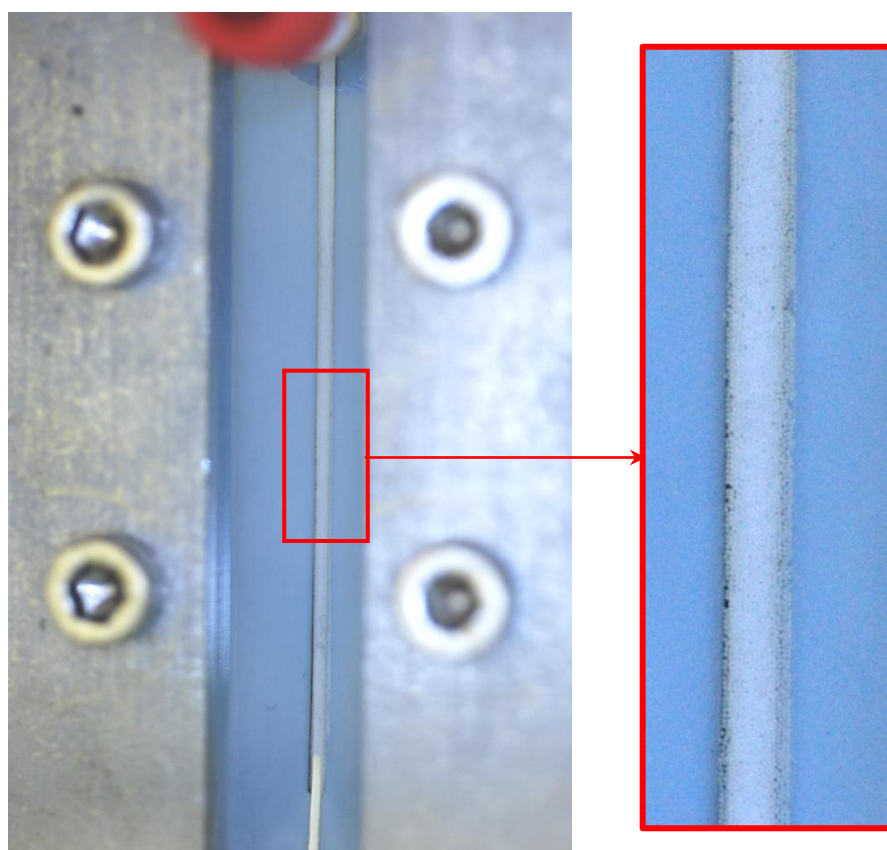
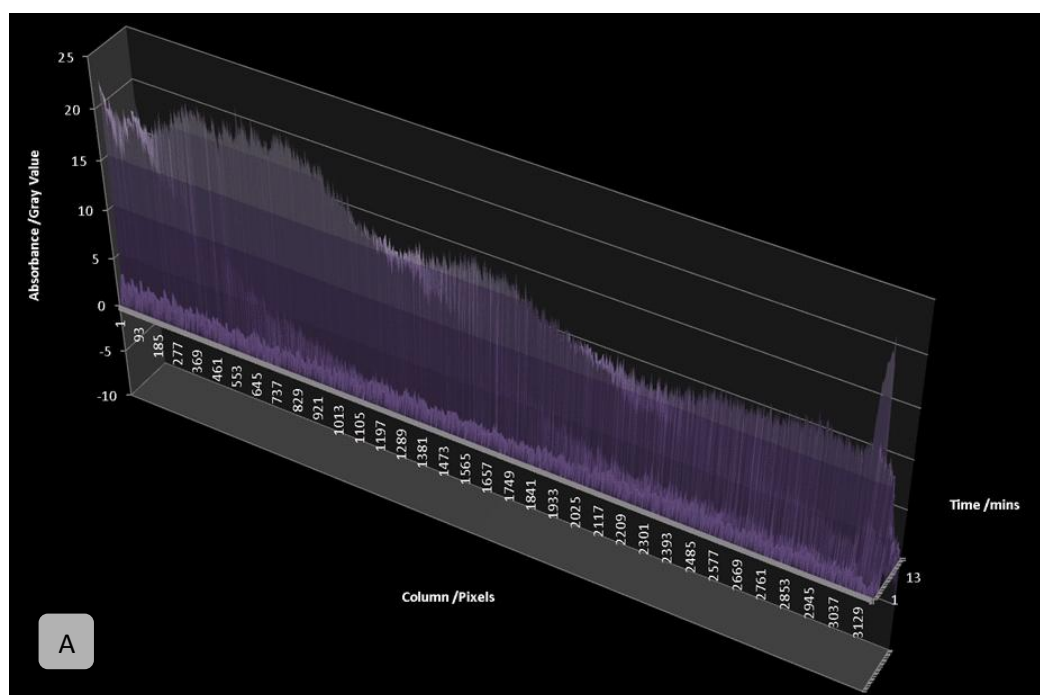


Figure 2.6.10 First Generation DFGF packed with 80µm porous silica particles.

2.6.5.2 DFGF separations with novel packing material

Once the packing had equilibrated a flow through test was carried out to ensure there was no retention by the stationary phase. A 5 μ L injection of 10%v/v BPB AM mixture was made with a flow rate of 1 μ Lmin⁻¹ monitored by the digital camera. The electric field was not used to allow the analyte to pass through the channel. The result of this is shown in figure 2.6.11 where it observed that the sample moved through the device without separation, confirming the inactivity of the packing material.



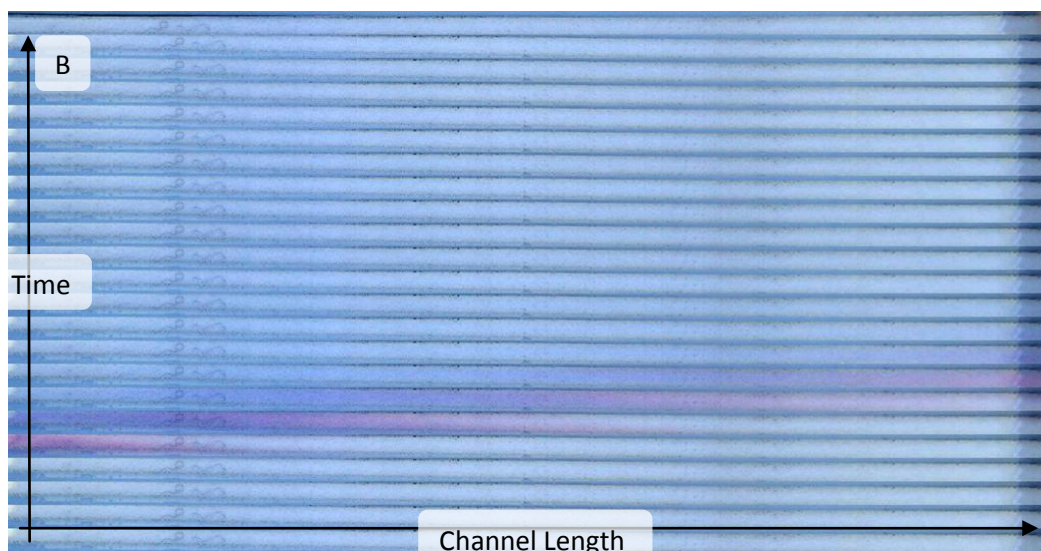


Figure 2.6.11. A) Graphical representation of a flow through of 10% v/v BPB AM mixture at $1\mu\text{Lmin}^{-1}$. B) Montage of images displaying the mixture as purple in colour, showing no derivation of red or blue corresponding to BPB or AM.

Further information provided by the graph in figure 2.6.11 is the illustration of the longitudinal diffusion of the sample. As the sample flows across the column, it is also diffusing causing the intensity to decrease and the width of the peak to increase.

Having confirmed the inactivity of the packing material, a dye test was carried out to assess the impact of these silica particles on separations. A linear EFG was applied to bring the sample into focus. With the more uniform pathway through the monodispersed packing material, it was predicted that the sample would take less time to reach a stationary focal point. The applied voltage profile used to generate the EFG is shown in table 2.6.3. From the graph in figure 2.6.12 showing the focusing of the sample it is apparent that the sample did indeed reach a focal point in less time than using the polyacrylamide packing material indicating an advantage in the monodispersed silica.

The band of analyte was focused and retained giving rise to a prominent peak corresponding to the AM. The peak for the BPB visible in the montage, figure 2.6.12A, is not as clear in the graph as there is less contrast than the red AM.

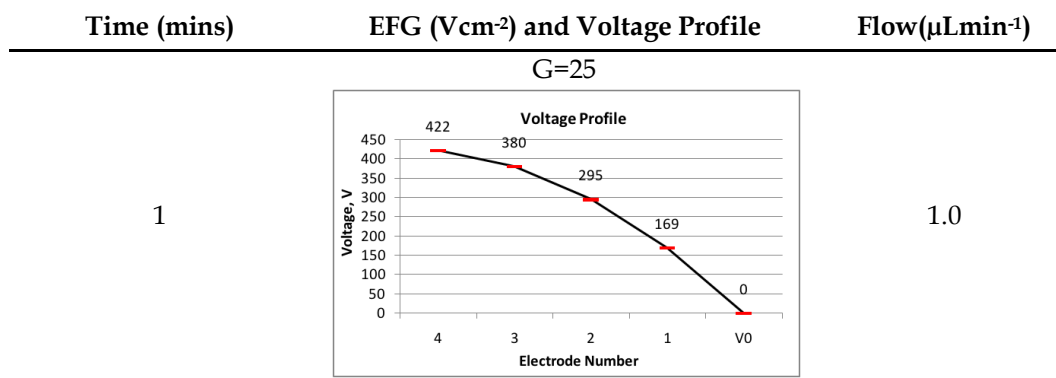
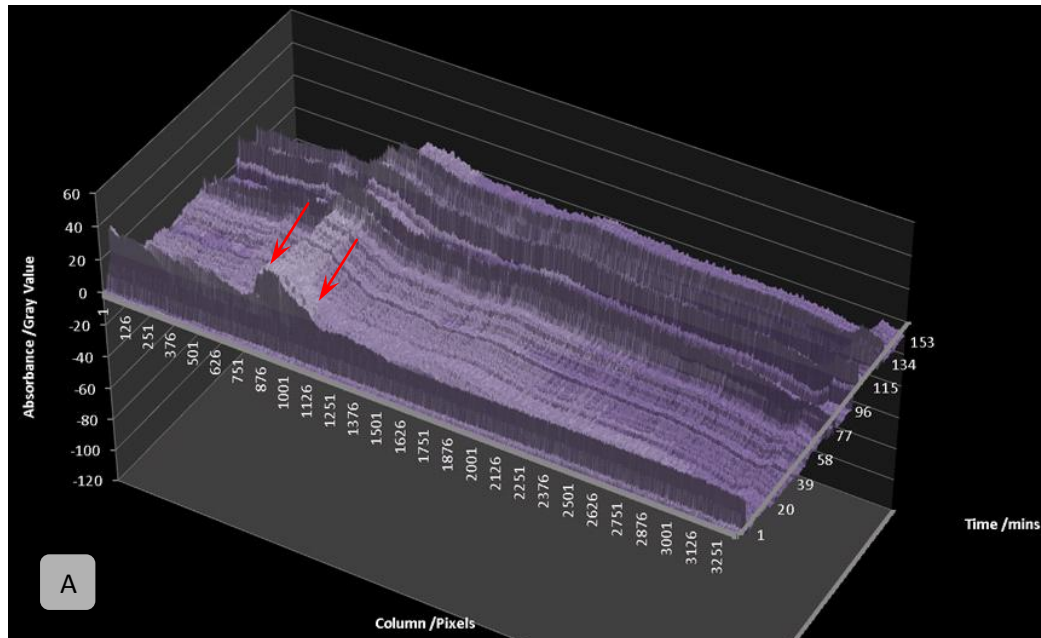


Table 2.6.3 EFG applied to separate the mixture of BPB and AM.



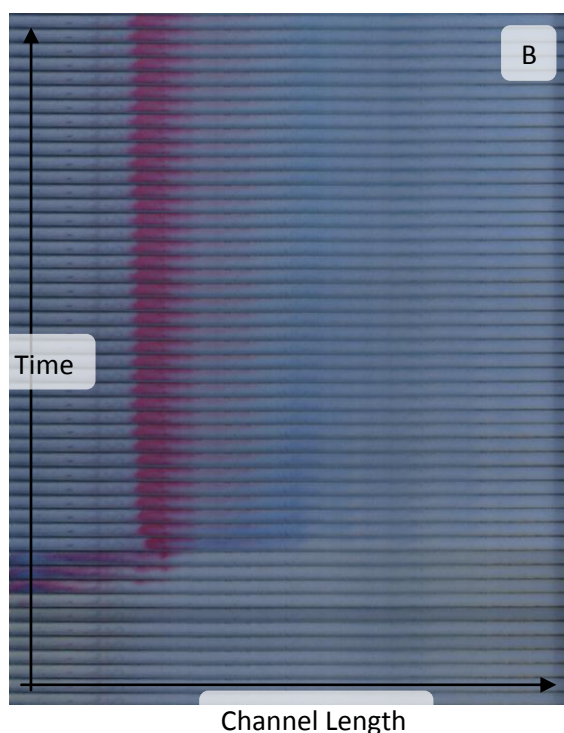


Figure 2.6.12. Separation of BPB and AM in a faster time utilising the larger pore monodispersed packing material. A) Graph of the separation of AM and BPB, analyte peaks marked with red arrows. B) Montage displaying the separation of AM and BPB.

Having shown advantages in speed of focusing smaller species of $\sim 600\text{gmol}^{-1}$ the packing was utilised in a separation of Kaleidoscope mixture, table 2.3.1. As with previous protein separations the running buffer consisted of 50mM Tris, 0.105mM CTAB, 0.035mM SDS to prevent precipitation. The separation demonstrated the rapid focusing of larger species and a separation of the mixture was observed. The conditions of the separation are shown in table 2.6.4 below with a detailed single profile plot to show the achieved plots which are not easily observed from the main graph. The overall separation is shown in figure 2.6.13. The imaging of this protein mixture once again was difficult to attain. As a result, a total of three $5\mu\text{L}$ injections at 2minutes, 47minutes and 88minutes were made to increase the visibility of the proteins.

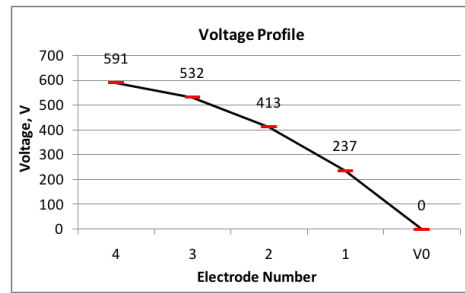
Time (mins)

EFG (Vcm^{-2}) and Voltage Profile

Flow($\mu Lmin^{-1}$)

G=35

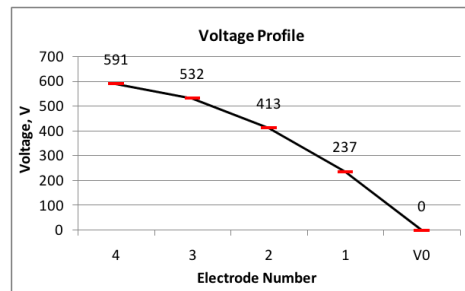
1



5

G=35

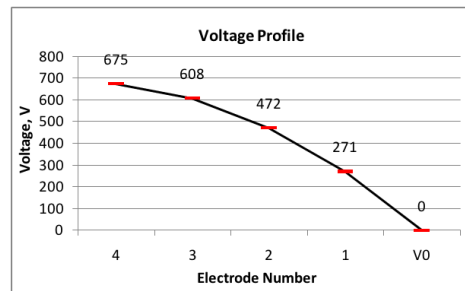
2



1

G=40

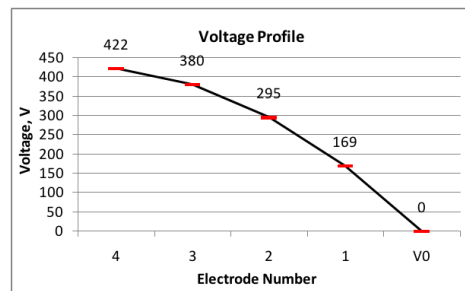
63



1

G=25

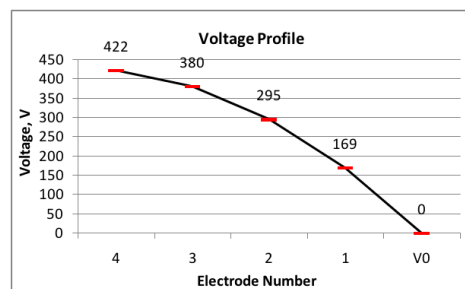
138



1

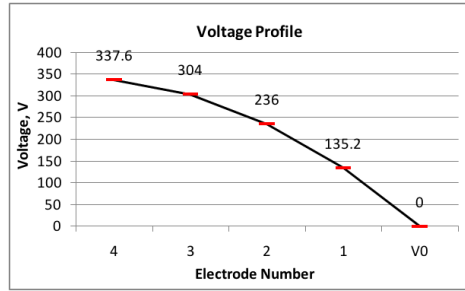
G=25

180



2

G=20



219

1

264

Off

5

Table 2.6.4 Experimental conditions applied to the device to separate the Kaleidoscope test mixture with the monodispersed packing material.

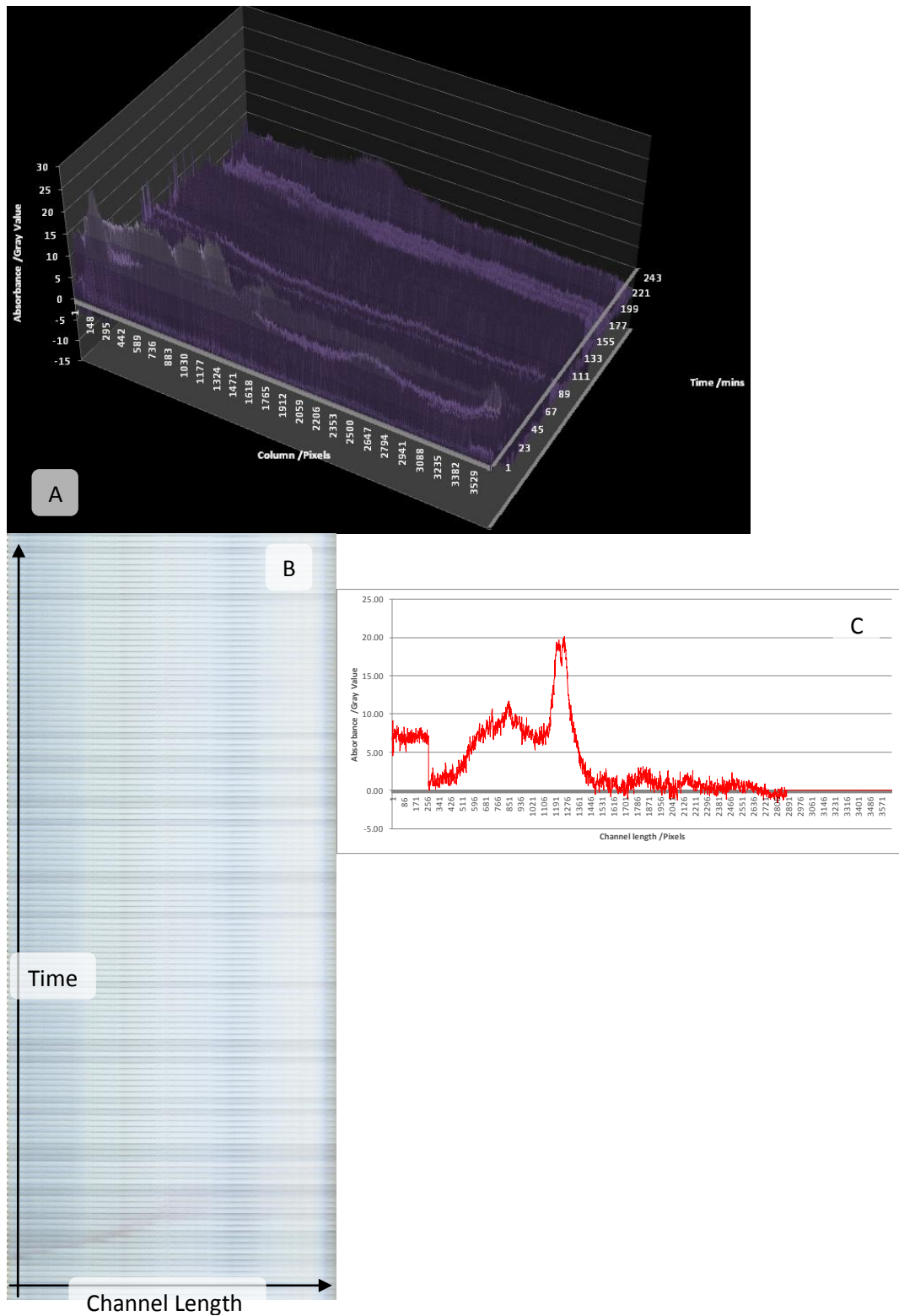


Figure 2.6.13. A) Graph of the separation of the Kaleidoscope test mixture. B) Montage of the Kaleidoscope separation. C) Single plot from 61mins showing an initial separation of 3 components.

From the experimental data presented in figure 2.6.13 the Kaleidoscope test mixture can be observed being focused and manipulated by the applied changes in EFG. Though more difficult to see in this example, the mixture was successfully separated into three individual components. With the improvement of the packing material the bands are more visible and sharper than before. This could be a direct result of the capillaries made by the interstitial space being much more uniform facilitating greater stability of the hydrodynamic flow. Furthermore, from the graph the sample reached an initial focal point in a much short time, again showing an advantage in utilising these wide pore large particles.

Having shown that these particles are suitable for DFGF they could also be used to add another dimension to separation by functionalising the surface.

This dimension would then be utilised by moving the sample back and forth over the stationary phase or even to separate non-charged species from a matrix by them passing through the device but experiencing interaction with the stationary phase, while any charged species are retained and focused.

2.7 Conclusions

Having utilised the Protasis DFGF supporting equipment and software, standard procedures have been developed for the use of the high voltage supply. Implementing the Rheos Flux 2200 pump⁸ has enabled dynamic control over the flow rate of buffer to $\pm 0.1 \mu\text{Lmin}^{-1}$ and therefore the ability to adjust the position of the bands with increased precision.

This is particularly important in this DFGF configuration as in later DFGF devices developed by Ivory *et al.*^{6,31,32}, there are up to 32 individually driven electrodes to provide an electric field with a high resolution across the entire channel compared to only using four electrodes as in this case. However even though only four high voltage supplies were used, effective separations and focusing of samples has been observed with relatively smaller dyes and larger proteins. Controlling these electrodes with the use of the Protasis⁹ Labview Ucontroller software has offered a high level of control over the four electrodes with facile adjustments using the automatically calculated voltages for a specified electric field gradient, and the manual mode enabling independent adjustments to fine tune the dynamic electric field to improve and manipulate individual bands of sample in situ.

Observing the separation and focusing of samples was previously monitored by, and the data interpreted from, manually processing a sequence of more than 200 images. Development detailed above has seen significant improvements in speed of data interpretation from the analysis of images by utilising a series of software tools to automate each step. For the first time an entire DFGF experiment has been plotted on a graph to enable the viewing of the changes in focal point and relative intensity of the bands over the entire separation. In addition, the processed data can also be interpreted further, and individual profile plots from each image are available after analysis without the need for further processing. With the new graphical presentation of the data, the method of which the images were captured was also improved to ensure stability in detection over time. Nevertheless, the reflectance method of data capture has limitations when detecting samples which are less visible against the packing material. Also this detection is only qualitative.

Innovations in previous work saw the addition of a quartz window to the separation channel of a DFGF device which facilitated imaging in the UV end of the spectrum by fluorescence quenching²⁵. This gave advantages in detection by increasing the resolution and enabling the detection of unstained species, however, this technique was limited by image capture. In the devices discussed in this chapter the simple reflectance method was the only method available because of the material used in their construction being opaque to UV light.

The packing method described in this chapter was an improvement on the previous method of solely driving the slurry with compressed air. The addition of the vibrating motor and the sonic probe significantly lowered the number of failed packing attempts.

Further improvements in packing were observed when packing the monodispersed 80 μm particles. The synthesis of this material explored a range of different drop generating techniques.

The most accurate and high turnover droplet generator was the Domino³⁰ industrial printer giving highly accurate well defined droplets at a high velocity and volume.

On the other hand, there were issues with the Domino printer as the narrow tubing and complex components often became blocked by the silica sol. A simple method for drop generation was explored utilising a pneumatic spray bottle, which delivered high volumes of particles, but at the cost of lower monodispersity. Experimentation with the monodispersed particles packed in the first generation device yielded faster and more reliable packing and a more uniform flow profile through the separation channel. This was observed from the improved intensity of focused bands, and the reduction in the time taken for analytes to focus into bands.

Finally, with limitations and issues with both the first generation and Protasis devices being inherently caused by the size and materials they are constructed from, a new approach was needed to solve these limitations. As shown in the theory discussed at the beginning of this chapter, the technique is independent of total column length, therefore, a smaller channel with a length long enough to house the minimum of five electrodes with space between them to form a gradient will be sufficient. This is shown experimentally by the fact that separations have been manipulated to take place in an area ~3-4cm long and as the electric field is dynamic it can be manipulated to a high extent over that small range. Moreover these larger channels require more power, meaning higher voltages, more joule heating, and more supporting equipment. Considering these points, and following on from work done previously by Bartle and Myers²¹, a new approach lends itself to a microfluidic device which will be described in the next chapter. Earlier DFGF devices depended on a packing material or monolith to narrow the diffusion pathway for the flow through the separation channel.

2.8 References

1. W. S. Koegler and C. F. Ivory, *Biotechnology Progress*, 1996, **12**, 822–836.
2. P. H. O'farrell, *Science (New York, N.Y.)*, 1985, **227**, 1586–9.
3. Z. Huang, Washington State University, 2001.
4. W. S. Koegler and C. F. Ivory, *Journal of Chromatography A*, 1996, **726**, 229–236.
5. C. F. IVORY, *Separation Science and Technology*, 2000, **35**, 1777–1793.
6. P. G. Tuñón, Y. Wang, P. Myers, K. D. Bartle, L. Bowhill, C. F. Ivory, and R. J. Ansell, *Electrophoresis*, 2008, **29**, 457–465.
7. J. M. Burke and C. F. Ivory, *Electrophoresis*, 2010, **31**, 893–901.
8. Flux Instruments, http://www.flux.ch/index.php?id=flux_rheos_2200.
9. Protasis Corp, <http://www.protasis.com/>.
10. Nikon, <http://imaging.nikon.com/lineup/dslr/d80/>, Nikon D80 DSLR.
11. Bio-Rad, www.bio-rad.com, 150–4138 Polyacrylamide beads.
12. J. C. LeBlanc, *Review of Scientific Instruments*, 1991, **62**, 1642.
13. UltraVolt, <http://www.ultravolt.com/>.
14. Nikon, http://imaging.nikon.com/lineup/software/control_pro/, Nikon Camera Control Pro.
15. ImageJ, <http://rsbweb.nih.gov/ij/>.
16. Fiji, <http://rsbweb.nih.gov/ij/>.
17. ImageMagik, <http://www.imagemagick.org/script/index.php>.
18. S.-L. Lin, Y. Li, A. T. Woolley, M. L. Lee, H. D. Tolley, and K. F. Warnick, *Electrophoresis*, 2008, **29**, 1058–66.
19. Z. Huang and C. F. Ivory, *Analytical Chemistry*, 1999, **71**, 1628–1632.
20. Bio-Rad, www.bio-rad.com, 161–0324 Kaleidoscope Prestained Standards (broad .
21. P. Myers and K. D. Bartle, *Journal of Chromatography A*, 2004, **1044**, 253–258.
22. R. D. Greenlee and C. F. Ivory, *Biotechnology progress*, 1998, **14**, 300–9.

23. J. M. Burke and C. F. Ivory, *Electrophoresis*, 2008, **29**, 1013–25.
24. U. D. Neue, *Journal of separation science*, 2007, **30**, 1611–27.
25. R. J. Ansell, P. G. Tuñón, Y. Wang, P. Myers, C. F. Ivory, J. N. Keen, and J. B. C. Findlay, *The Analyst*, 2009, **134**, 226–9.
26. J. H. Knox, *Journal of Chromatography A*, 1999, **831**, 3–15.
27. J. J. van Deemter, F. J. Zuiderweg, and A. Klinkenberg, *Chemical Engineering Science*, 1995, **50**, 3869–3882.
28. Kremer, <http://kremerpigments.com/>, Kremer Syton X30.
29. W. Li and F. L. S. Tse, *Biomedical chromatography : BMC*, 2010, **24**, 49–65.
30. Domino, <http://www.domino-printing.com>.
31. N. I. Tracy and C. F. Ivory, *Electrophoresis*, 2008, **29**, 2820–2827.
32. J. M. Burke, Z. Huang, and C. F. Ivory, *Analytical chemistry*, 2009, **81**, 8236–43.

Chapter 3. Microfluidic DFGF

3.1 Microfluidics

Innovations in engineering capabilities to manufacture micro channels in a variety of materials have facilitated the growth of the research area of microfluidics to encompass many fields of science requiring liquid handling and mixing¹. A range of applications have been explored using microfluidic devices across a broad range of analytical applications. These devices offer many advantages including decreased sample sizes, faster separations as well as lower working volumes of reagents². These characteristics make them very attractive for applications including sensors and embedded electronics leading to the prospective future of micro scale analytical devices embedded in everyday devices.

Microfluidics has been implemented in the development of a plethora of bio-orientated separation techniques³ including the electrophoretic focusing techniques discussed in chapter one. In IEF, advancements have been made by utilising microfluidics. These include; improved sample introduction, novel plastic device form factors, novel glass devices, protein separation optimisation, and enhancements to the electric fields⁴⁻⁹. Di-electrophoresis has also seen many advantages in microfluidic approaches to facilitate a range of improved applications including carbon nano tubes, medicinal nano particles and large proteins¹⁰⁻¹⁴. More closely related to DFGF, microfluidic EFGF devices have demonstrated advantages in resolution and speed of separations^{15,16}. These can be attributed to the contribution of cross sectional area of the channel in the equations for band concentration in chapter 2 (equation 2.1.2)¹⁷.

The application of microfluidics for DFGF was first realised by Myers and Bartle¹⁸ in 1996 demonstrating a microfluidic device which was machined from two blocks of Plexiglas. The separation channel was packed with a PolyHipe monolith¹⁸. The two channels were separated by a section of porous glass with 4nm pores in place of cellulose membrane. The results from this work demonstrated the ability of the device to separate and control analytes in the device by successfully resolving the Bio-Rad Kaleidoscope test mixture¹⁹. The main limitations of this first microfluidic device were that the detection method was unable to detect any other wavelengths other than those in the visible.

3.2 The New Microfluidic DFGF

3.2.1 Microfluidic DFGF design

The design of a new microfluidic DFGF device began with the specifications of overcoming the issues with the previous devices. The brief was for a system requiring less power to generate the required electric fields, less supporting equipment, transparency to UV and an innovative design to enable facile assembly and set up of the device with minimal time and complexity.

Specifications for the new microfluidic DFGF were presented to the microfluidics innovation company 'Dolomite'²⁰. Initial designs were proposed, for example figure 3.2.1. However, these had limitations in providing a dynamic research platform, mainly due to only four electrodes being incorporated offering only three positive electrodes to generate the electric field.

Additionally, since these electrodes were fixed there was no scope for changes to be made should an issue arise.

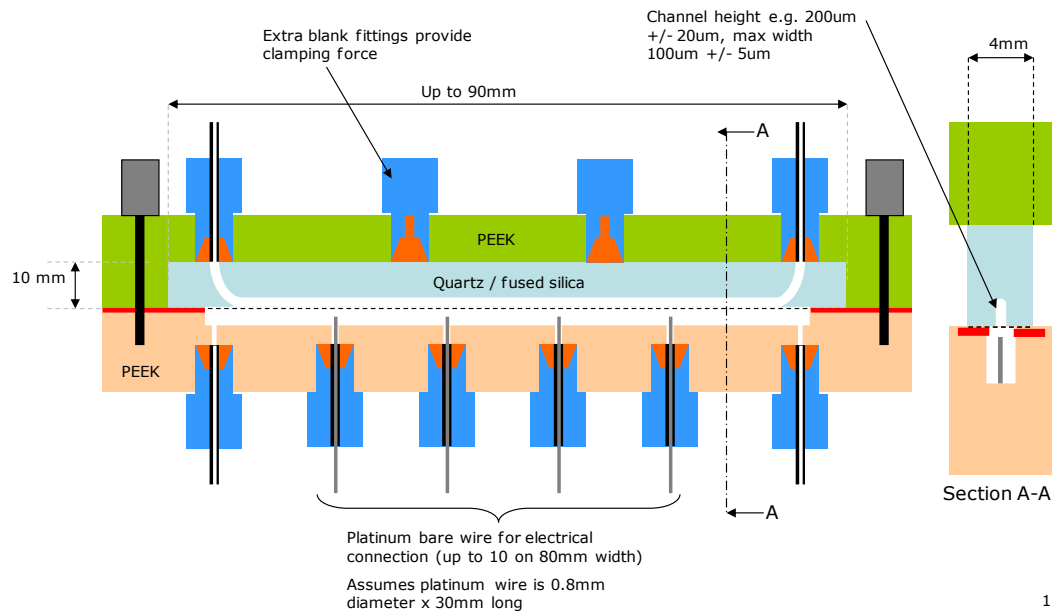


Figure 3.2.1. Initial design of a microfluidic DFGF from Dolomite²⁰.

3.2.2 DFGF Quartz Chip

A final working design was issued featuring a quartz microfluidic chip and glass electrode chip figure 3.2.2. Implementing these chips in a device incorporates design features which meet the specified criteria, eradicating issues with the earlier DFGF devices.

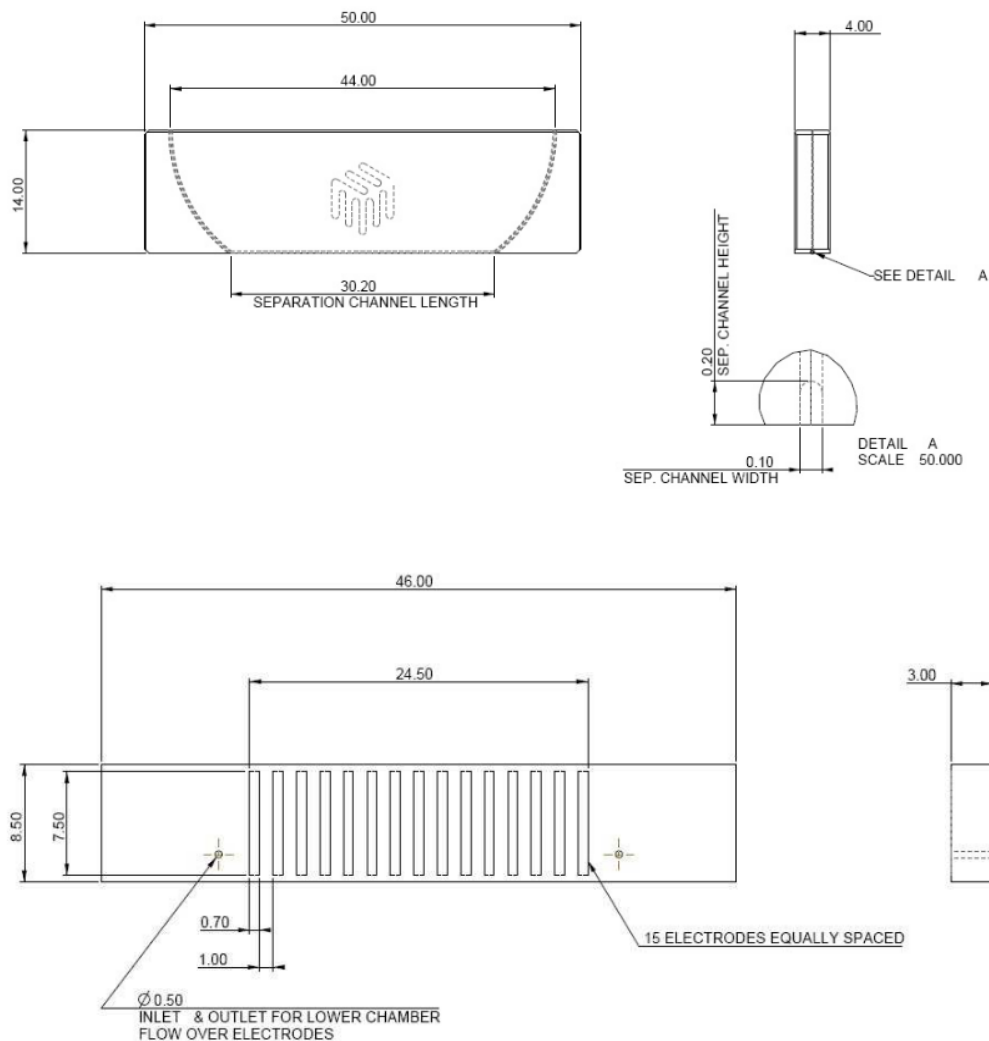


Figure 3.2.2. Design of the Microfluidic DFGF separation channel chip and electrode chip²⁰.

By reducing the channel dimensions down to 100 μ m wide and 200 μ m deep it was possible to run this device without the need of packing material or monolith eliminating all the previously described issues with the packing process and with the use of packed columns. The quartz construction enables detection with UV wavelengths opening the possibility to perform separations on native unstained proteins. In addition, the chip itself is much more resistant to chemical and thermal degradation during operation of the device.

As shown in figure 3.2.2 the separation channel along the base of the chip is fed by two slightly larger channels which flow down through the chip from where the fluid connections are made to the channel itself. The electrode chip supports fifteen individual platinum electrodes which run the full width of the chip to facilitate connection to HV supplies. The electrodes are equally spaced by 1mm across the chip directly beneath the location of the separation channel. Each platinum electrode is 0.7mm wide to provide a high surface area to create a higher current density across the length of the channel. The two holes in the electrode chip are the inlet and outlet for the circulating buffer for the electrode channel. The two glass chips are housed in a single device shown in figure 3.2.3.

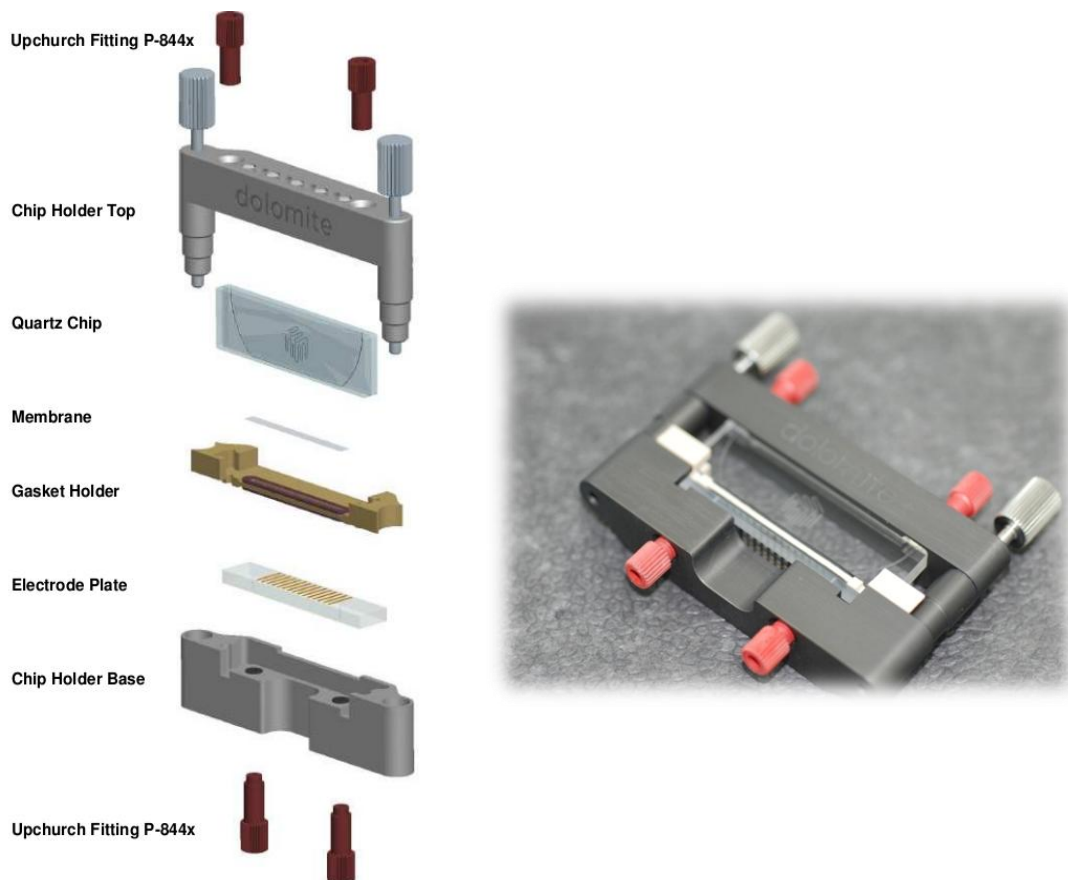


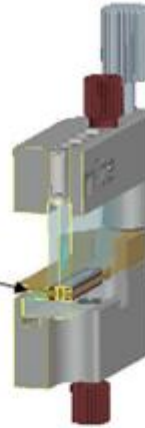
Figure 3.2.3. Microfluidic DFGF device exploded view.

3.2.3 The microfluidic DFGF device design

The design of the device focuses on housing the glass chips, usability, and integration with existing equipment. The following descriptions refer to the list of component parts in figure 3.2.3. Fluid connections are made using standard '1/16" Upchurch P-844x' fittings integrating directly with the current DFGF supporting equipment and other chromatographic platforms. The 'Chip Holder' not only supports the separation channel chip and the electrode chip at a set clamping force, it also features a cut away on the face to allow integration with a Photo Diode Array detector and a recess on the back for electrical connections, detail shown below in figure 3.2.4. The 'Quartz Chip' houses the separation channel described above in figure 3.2.2. As mentioned in the last chapter (figure 2.2.2) the membrane forms the divide between the two channels allowing the electric field to propagate through into the separation channel. To form the electrode channel beneath the membrane the 'Gasket Holder' houses a 1mm wide and 1mm deep channel which is 30mm in length. Also, this component has features, shown in figure 3.2.4, to align the microfluidic chips accordingly. Recessed into the 'Gasket Holder' are two Viton gaskets which seal the fluid connections on the base of the separation channel and the top face of the electrode chip. The electrode chip, as detailed above in figure 3.2.2, was then seated in a recess in the 'Chip Holder Base' which also encompasses two Viton seals that locate over the holes to seal the fluid connections for the flow of the electrode channel buffer solution. These ports continue directly through the component to the bottom of the base where there are two connections for the standard '1/16" Upchurch P-844x' fittings.

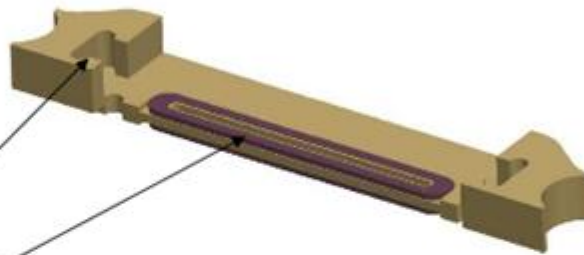
Chip Holder (Cross-section)

- Design allows detector to be positioned flush against glass (43 mm wide cut-away)
- Electrodes extend out from separation channel to allow power supply connection



Gasket Holder

- 2 mm deep slot to create lower chamber
- 0.6 mm thick viton gaskets recessed into top and bottom surfaces
- Features provided for location of quartz chip
- Membrane (2.5 x 32 mm) sits on top surface



Chip Holder Top

- Thumb screws to clamp system together
- Ball spring plungers provide a set clamping force



Chip Holder (Back)

- Slot provided in chip holder base for wires to electrodes
- Gasket holder shields electrode contacts to reduce electric shock risk

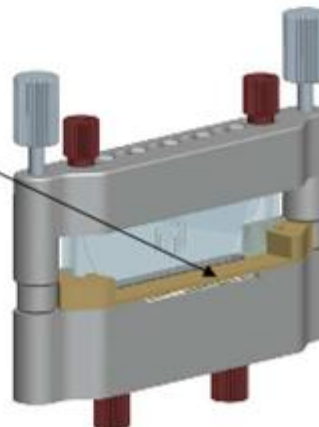


Figure 3.2.4. Microfluidic DFGF device design summary²⁰.

3.3 Experimental

3.3.1 Integration with power supply

Preliminary experimentation with the new device began with the development of an electrical connector to enable the HV supply to be connected to the electrodes. As the Platinum electrodes had been layered onto the glass using a Physical Vapour Deposition (PVD) method, consequently the coverage of platinum was in the order of $\sim 1\text{-}3\mu\text{m}$. Soldering to these electrodes was no longer an option as first discussed in design meetings with Dolomite. A connector utilising small contacts using an IDE cable and IDC connector was constructed, shown in figure 3.3.1.

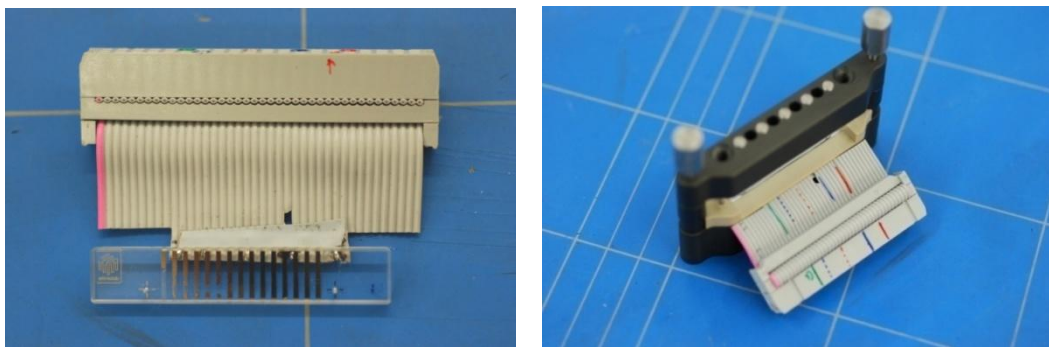


Figure 3.3.1. Prototype Electrode connector made from an IDC connector.

Commissioning of the chip was achieved by applying a signal on the connector cable and measuring the signal on the electrodes. The same principle was then used to construct the electrode connector shown in figure 3.3.2. Made from polypropylene, the connector houses an array of point contacts shaped from electrical solder and an insulation-displacement connector, IDC, at the opposite end held in place with cyanoacrylate. The connector was shaped to the thickness of the recess in the back of the device to enable the connector to be held in place without distorting the gasket holder.

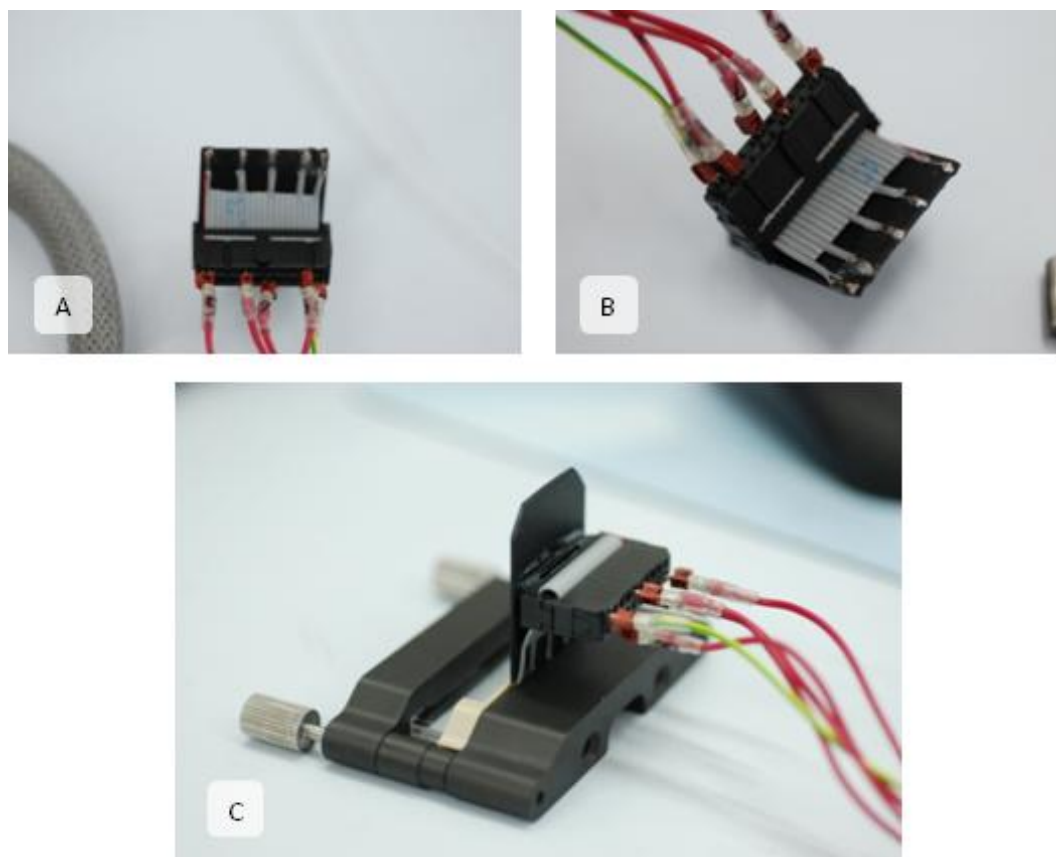


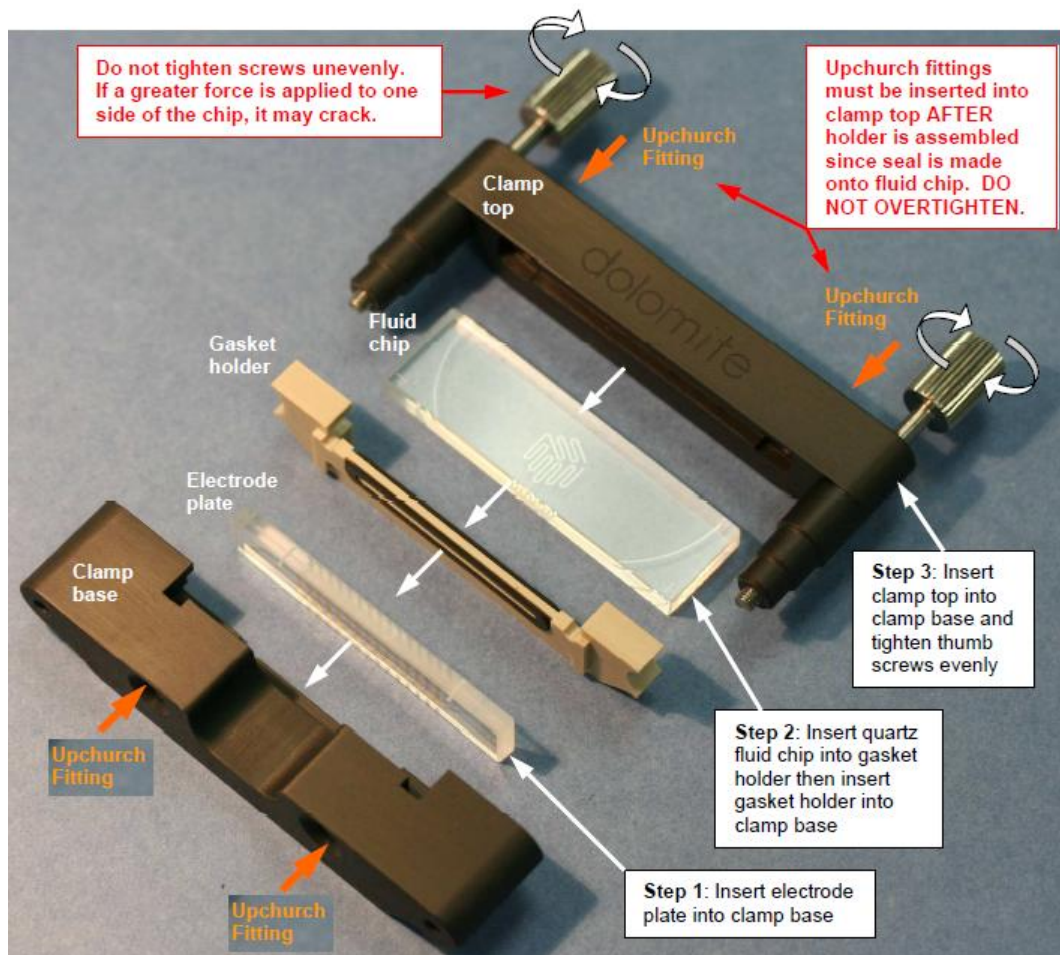
Figure 3.3.2. A) Microfluidic DFGF electrode connector. B) Connector inserted in the recess at the back of the microfluidic DFGF. C) All HV connections in place using IDC connectors.

Having devised a working HV connector, modified HV leads with an insulated 4mm pin terminal connector on one end, (to fit the existing Protasis power supply) and a single IDC pin at the other, (to plug into the device) is shown in figure 3.3.2C. The fluid connection from the sample loop was made to the device using standard 1/32" OD tubing sleeved with Tygon tubing to fit the 1/16" Upchurch fittings. The separation channel output was a 100mm length of 1/16" Tygon tubing. The connections for the electrode channel were also made using Tygon tubing with adapters to the 1/4" rubber tubing required for the peristaltic pump.

The experimental set-up, other than the alterations mentioned, remained the same as the operation for the previous devices describe in section 2.2.3.

3.3.2 Microfluidic DFGF - Instructions for Use

The microfluidic DFGF was set up by following the instructions detailed by Dolomite²⁰ (figure 3.3.3). The device was setup with 100MWCO cellulose membrane cut to the required dimensions of 40mm long 4mm wide. In all of the data presented using the microfluidic device, the fluid connections have been made so that flow is always from left to right.



Check that the 2 circular seals are in the clamp base and that surfaces are clean. Then insert electrode plate into clamp base, with drilled holes towards the front.

Step.2 Check that gaskets are correctly located in the gasket holder. Place membrane carefully onto the top gasket ensuring that it sits in the middle of the gasket. (A seal will not be obtained if the membrane protrudes over the edge of the gasket.) Insert quartz fluid chip into gasket holder, making sure that the chip is the right way up. (If the quartz chip is clamped upside down, then the separation channel will be damaged.) Then insert the gasket holder into the recess in the clamp base.

Step.3 Carefully insert clamp top into clamp base, so that quartz fluid chip is guided into the recess in the clamp top. Tighten thumb screws evenly until the end stop is reached. (Do not tighten one side before the other as this will apply an uneven force to the chip.) The system will now be clamped to a set force provided by ball spring plungers in the clamp top.

Step.4 Screw in Upchurch fittings. Please note that fittings in the clamp top must only be inserted after the chip holder is assembled. (This rule does not apply to fittings in the clamp base.) The fittings in the clamp top seal directly onto the surface of the fluid chip. Tighten only until the tubing is no longer free to move. Do not tighten any further or there is a risk of chip cracking. (The fittings in the clamp base do not seal directly onto the glass, so can be tightened fully.)

Figure 3.3.3. Dolomite User Guide for the microfluidic DFGF.

3.3.3 First Separation using the microfluidic DFGF

The first experiment attempted with the new device was a separation mixture of 10%v/v BPB and AM prepared in 50mM tris HCl buffer solution. The flow rate was set at $1\mu\text{Lmin}^{-1}$ and 10 μL of the test mixture was injected.

Once the sample entered the separation channel, and the two components began to resolve, the analytes came into poorly focused bands near the beginning of the channel, figure 3.3.4. After ~20mins the sample began to migrate further along the channel and eluted from the device with no changes made to the EFG. The conditions applied are shown in table 3.3.1.

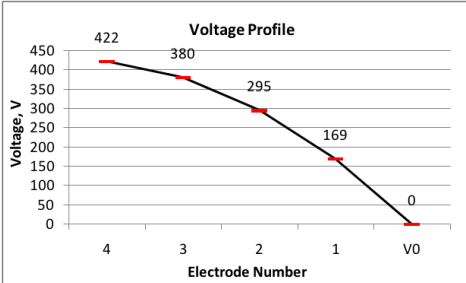
Time (mins)	EFG (Vcm^{-2}) and Voltage Profile	Flow($\mu Lmin^{-1}$)												
1	<p style="text-align: center;">$G=100$</p>  <table border="1"> <caption>Data for Voltage Profile</caption> <thead> <tr> <th>Electrode Number</th> <th>Voltage (V)</th> </tr> </thead> <tbody> <tr> <td>4</td> <td>422</td> </tr> <tr> <td>3</td> <td>380</td> </tr> <tr> <td>2</td> <td>295</td> </tr> <tr> <td>1</td> <td>169</td> </tr> <tr> <td>0 (V0)</td> <td>0</td> </tr> </tbody> </table>	Electrode Number	Voltage (V)	4	422	3	380	2	295	1	169	0 (V0)	0	1.0
Electrode Number	Voltage (V)													
4	422													
3	380													
2	295													
1	169													
0 (V0)	0													

Table 3.3.1. Summary of conditions for a microfluidic DFGF test separation of BPB and AM.

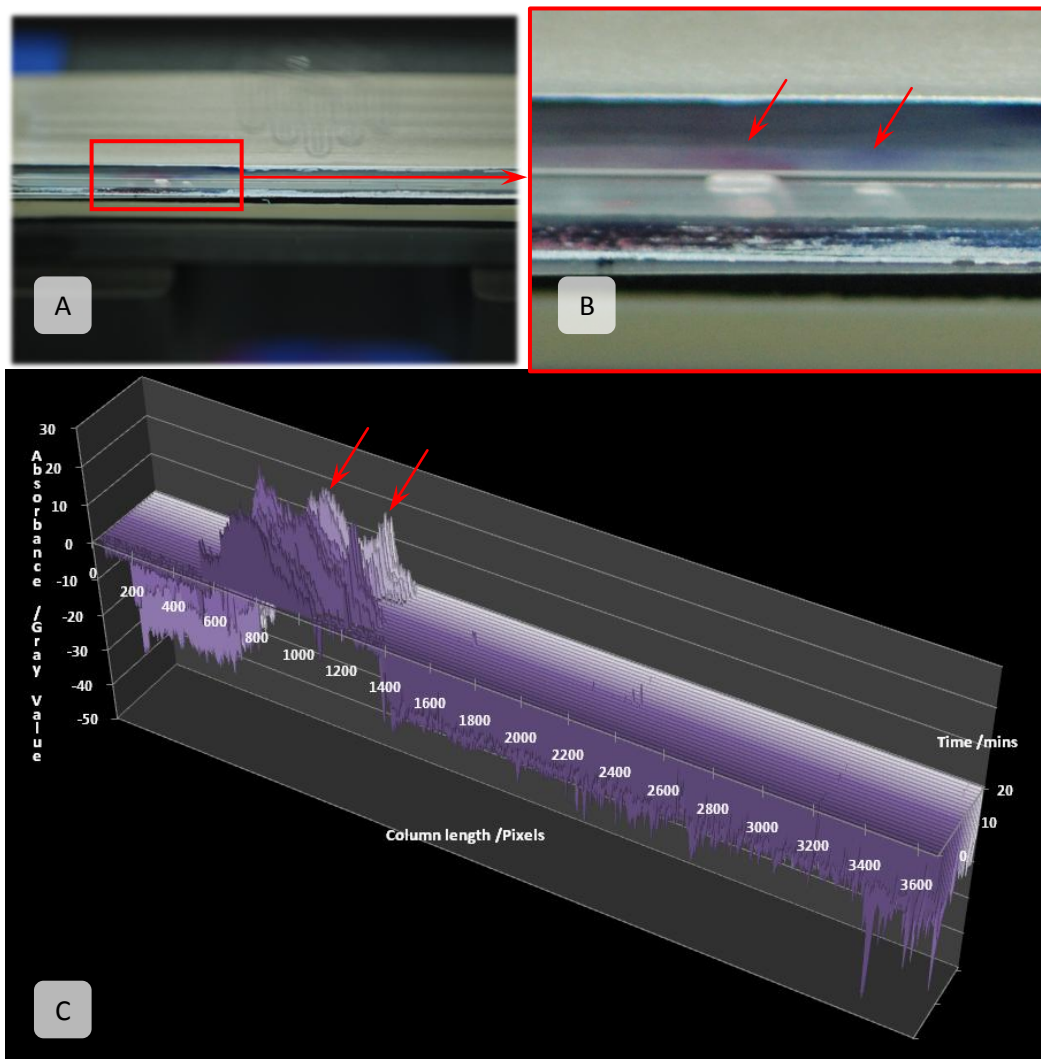


Figure 3.3.4. Initial Separation of BPB and AM. A) Raw image of the separation B) Enlarged view of the separation with focused bands of AM and BPB. C) Graphical representation of the separation. The peaks come into focus before fading as a result of loss of EFG.

3.3.4 Electrode decomposition, New Gold electrodes

Having first ensured there were no issues with the system configuration and the power supply was indeed functioning, the experiment was repeated. The repeat experiment was conducted using the same conditions (table 3.3.1). From the observation of the injected sample passing through the separation channel with no retention or focusing, it was clear there was a serious problem with the device itself. On further examination, it was immediately apparent that the electrode chip was the source of the device failure. The platinum electrodes which had been deposited on the surface had significantly degraded. The degradation occurred as the high current density oxidised the platinum surface removing it from the substrate. The extent of the decomposition is shown in figure 3.3.5.

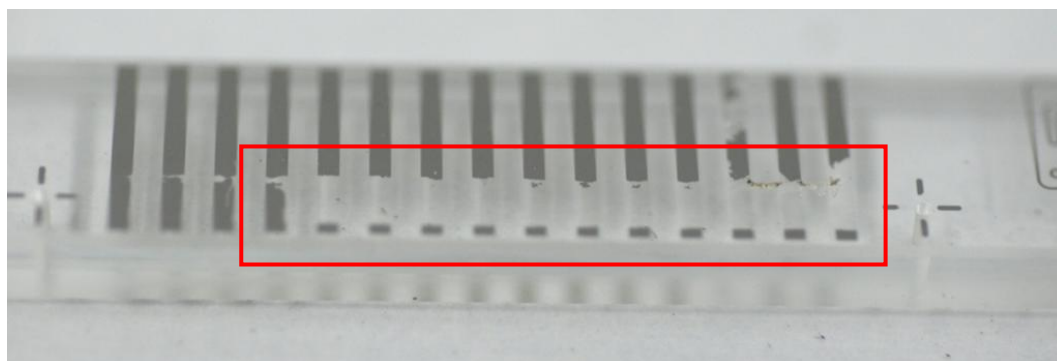


Figure 3.3.5. Severe degradation of the platinum electrodes on the microfluidic DFGF electrode chip. The area highlighted in red displays the degraded electrodes.

To protect the electrodes, and lower the high quantity of electrolysis gasses produced, an electrode plate was coated with a layer of Nafion. The coating was carried out by sequentially dropping 5%v/v Nafion (Sigma Aldrich) suspension onto the surface and evaporating the solvent (water) by heating to 60°C overnight.

Nafion is a fluoropoly-copolymer developed in Germany by DuPont in the 1960's shown in figure 3.3.6²¹. This polymer was considered due to many electrochemical applications in electro-catalysis²² and as membranes in fuel cells²³ as it only facilitates the permeation of small charged ions. With these properties this polymer was also considered as a viable alternative to the cellulose membrane.

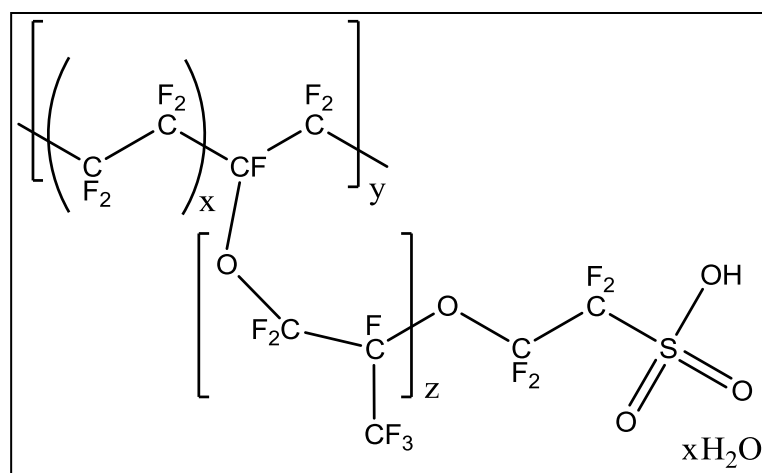


Figure 3.3.6. Molecular structure of Nafion²¹.

Using the conditions in table 3.3.1 a two component test mixture of BPB and AM was injected. The microfluidic DFGF was set up with the same configuration used previously, the only difference being the Nafion Coating over the electrodes. As observed in the initial experiment, the analytes began to focus into bands ~10mm along the separation channel. However, the focused bands faded and eluted from the device. It was later determined that the Nafion coating had deteriorated along with another set of Platinum electrodes the same as in figure 3.3.5. With these results came the realisation that an alternative electrode array was required.

One of the failed electrode chips was taken and five grooves $\sim 350\mu\text{m}$ deep were tooled into the surface equally spaced 5mm apart with the 3rd electrode centred between the two drilled holes in the chip. Inlays of 500 μm diameter gold wire were secured in these grooves using cyanoacrylate. The exposed surface of gold wire was milled down level to the surface of the electrode chip and the whole surface was then polished. The resulting new gold electrode array is shown in figure 3.3.7.

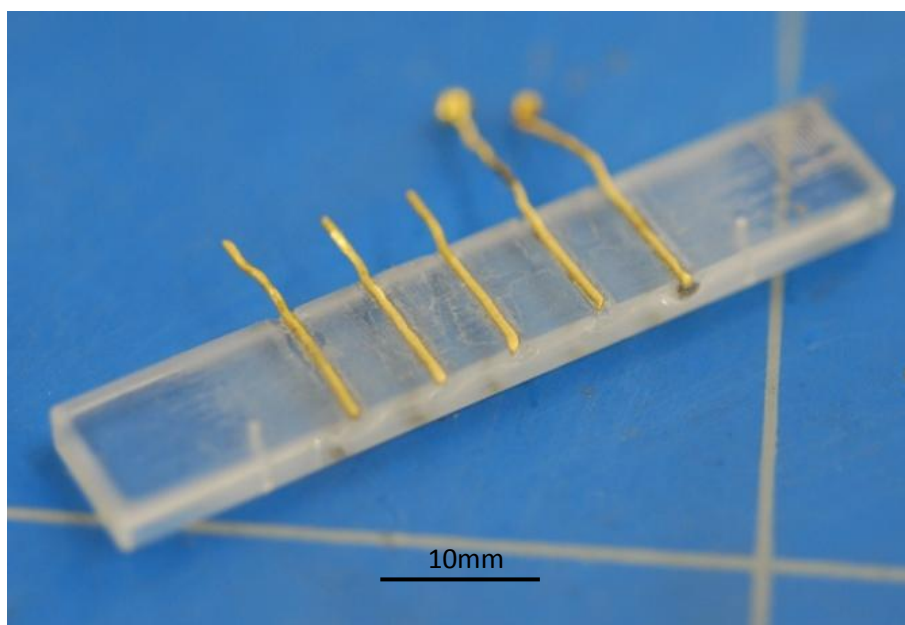


Figure 3.3.7. Gold electrode array on an existing electrode chip.

Integrating this new electrode array into the microfluidic DFGF device involved soldering the electrodes to another IDE cable with an IDC connector. As the soldered joint to these electrodes was brittle the connector was incorporated into the base. As this was a fixed solution, the 'Gasket holder' and electrode channel gasket were set in place and the recess filled with epoxy resin to seal the electrode channel. The completed electrode array and 'Chip Holder Base' are shown in figure 3.3.8.

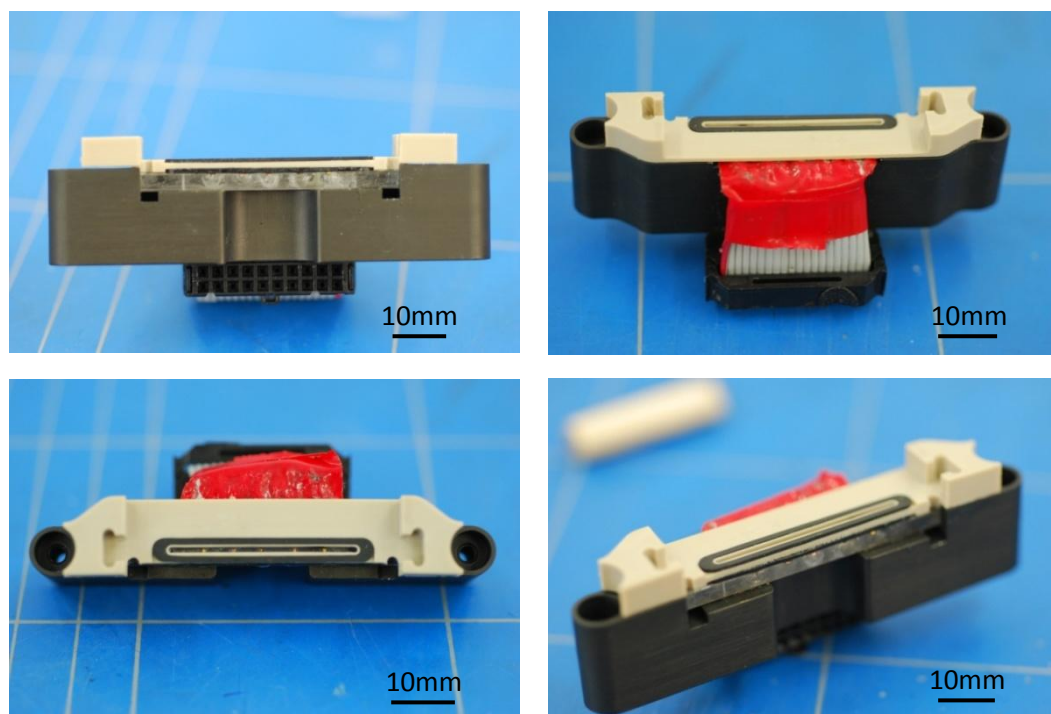


Figure 3.3.8. Different views of the completed gold electrode array and chip holder base with fixed connector.

A new test mixture had been formulated with a third component for these experiments to further demonstrate the degree of the dynamic control over the EFG by identifying changes in the field with an additional focal point. This third component, colloquially known as “Acid Yellow”, was added as it has a different hydrodynamic radius with less net charge than BPB and AM. The molecular structure of Acid Yellow (AY) is shown in figure 3.3.9.

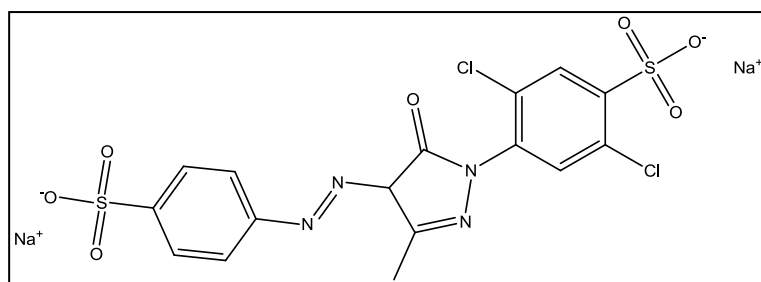


Figure 3.3.9. The molecular structure of Disodium 2,5-dichloro-4-[3-methyl-5-oxo-4-(4-sulfonatophenyl)diazenyl-4H-pyrazol-1-yl]benzenesulfonate (Acid Yellow).

With the new gold electrodes incorporated into the ‘chip holder base’, preparing the device was simplified. The membrane was placed on top of the secured gasket and the separation channel chip inserted into the locating slots before being clamped down over the membrane with the ‘chip holder top’. To complete the setup the two thumb screws were tightened securely.

3.3.5 Separation of a three component test mixture.

At a flow rate of $1\mu\text{Lmin}^{-1}$, 50mM tris HCl was pumped through the separation channel while circulating 10mM tris HCl was pumped at $\sim 1\text{mLmin}^{-1}$. A linear EFG of 400Vcm^{-2} was applied and subsequently adjusted according to the profiles shown in table 3.3.2. Reflectance measurements were taken at 2 minute intervals using the detection method described in chapter 2 (figure 2.2.1).

Time (mins)	EFG (Vcm ⁻²) and Voltage Profile	Flow(μLmin ⁻¹)
000	G=000	1.0
	G=400	
9		1.0
20		1.0
26		0.5
	G=300	
33		0.5
45	Off	1.0

Table 3.3.2. Conditions for the separation of BPB, AM and AY in figure 3.3.10.

The change in voltage profile at 40mins saw the analytes migrate and separate into focused bands at 50mins, this can be seen in the graph in figure 3.3.10.

As the bands of analytes were located 20mm along the channel, the flow was reduced to $0.5\mu\text{Lmin}^{-1}$. It was expected that with a high electric field gradient the sample would be retained at around 10mm along the channel. Moreover, a faint colouration of eluting buffer was observed which indicated that some of the injected sample had not been retained. The reduction in flow rate ensured that the remaining analytes were retained and focused. At 60mins the analytes were observed slightly further back down the channel. Increasing the flow and dropping the electric field brought the analytes into focus 25mm along the channel. A decrease in EFG at 90mins allowed them to elute as a focused band from the device.

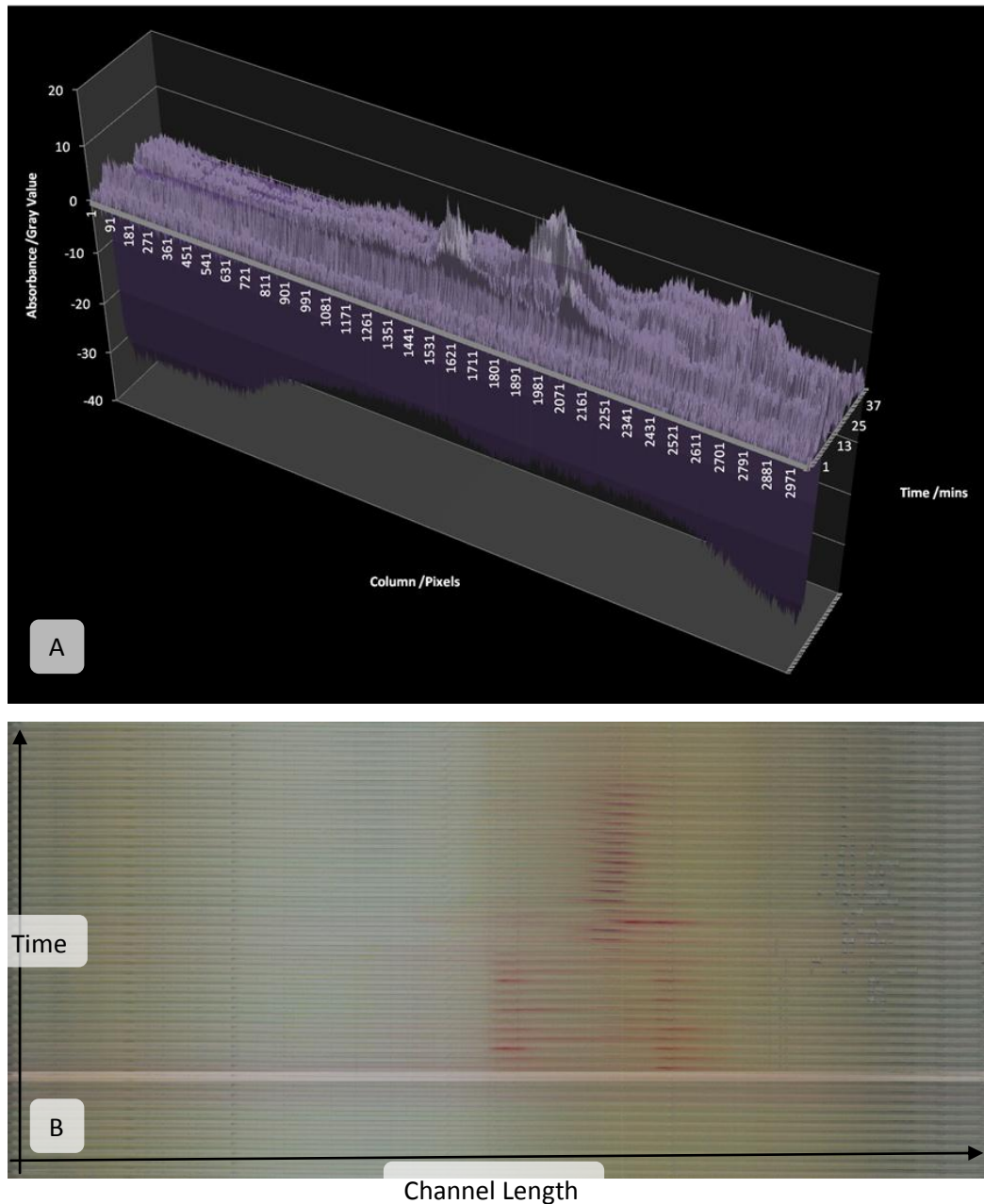


Figure 3.3.10. Separation and focusing of BPB, AM and AY. A) Graph of the separation. B) Montage of the separation. The separation can be observed in the graphical representation and the individual components identified from the coloured bands visible in the montage.

The successful focusing of this mixture was a preliminary indication of the functionality of the microfluidic device, however the voltages used (table 3.3.2) shows that the full 1000V was used to retain the sample.

As the specifications for the new device stated (detailed earlier in this chapter section 3.2) the microfluidic device should be capable of performing separations while operating with lower voltages. A key milestone in the development of this miniaturised device was to be able to use voltages no larger than 600V per electrode. This is because miniaturising this type of device also means developing improved supporting hardware and once the required voltage is below this figure existing, miniature, and cheaper electronic components can be used to generate the high voltage.

3.3.6 Separation using lower voltages

A separation was carried out with the aim of repeating the focused analytes seen previous but only using an EFG generated using maximum voltages of 600V. A linear EFG of 250Vcm^{-2} was applied and the three component test mixture injected at a flow rate of $3.0\mu\text{Lmin}^{-1}$. After an initial 3mins the flow rate was reduced to the standard $1\mu\text{Lmin}^{-1}$. The reason for this initial increased flow rate was to reduce the loading time. The sample came into focus $\sim 15\text{mm}$ along the separation channel. The gradient was reduced to provide the required difference in field for the sample to begin to separate into individual focused bands. A summary of the conditions applied during this separation is shown in table 3.3.3. Only a small separation was observed as the detection was mostly saturated by the red AM band.

A graph of the separation displays a single peak coming into focus and then decreasing in intensity as the individual components begin to separate (figure 3.3.11). The analytes were held for 20mins to focus further, however no further focusing was observed.

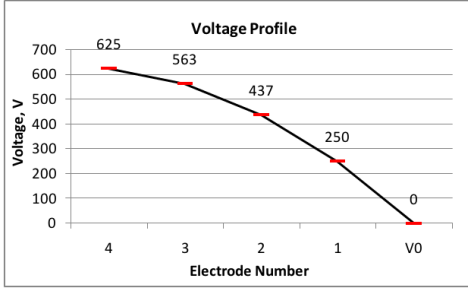
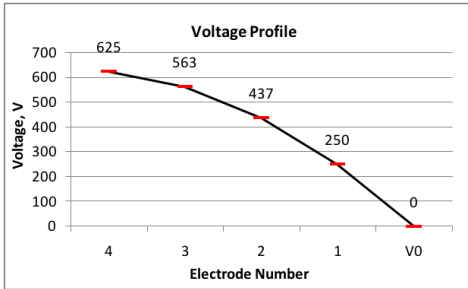
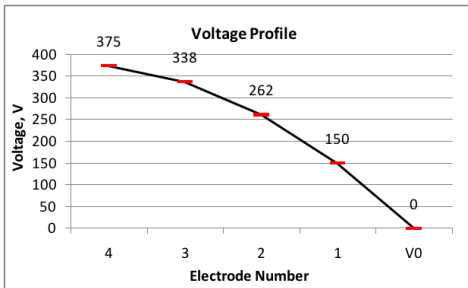
Time (mins)	EFG (Vcm ⁻²) and Voltage Profile	Flow(μLmin ⁻¹)
000	0	3.0
	250	
3		1.0
	250	
11		0.5
	150	
42		0.5
53	Off	1.0

Table 3.3.3. Conditions used to result in the focusing of the 3 component mixture of AM and BPB and Acid Yellow.

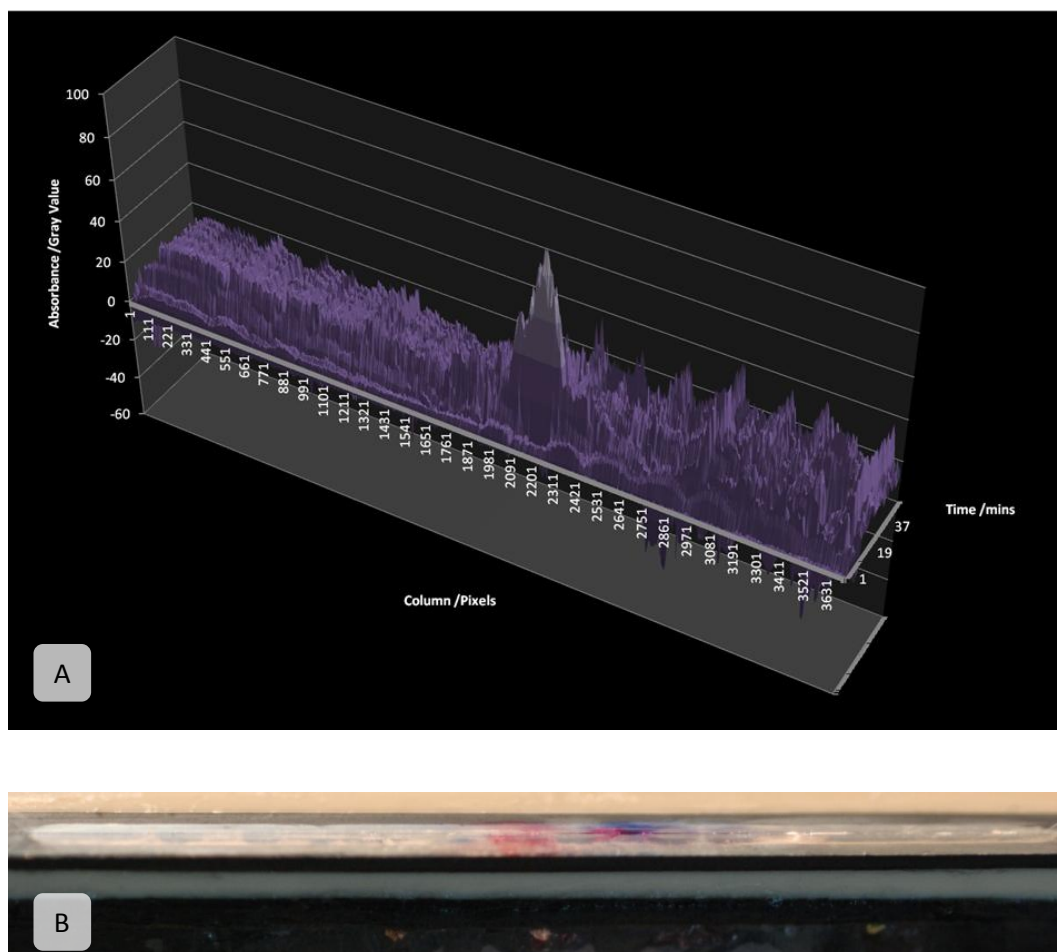
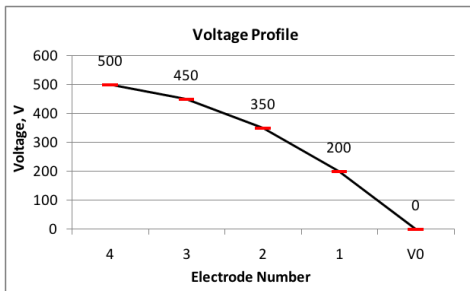
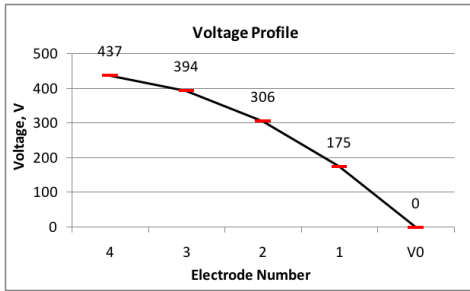
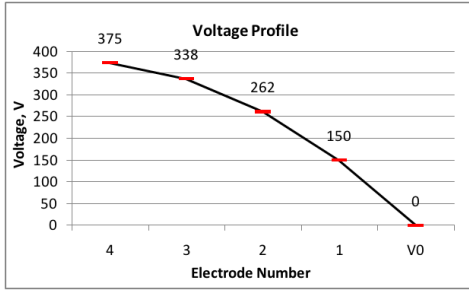


Figure 3.3.11. A) Graphical representation of the focusing of the 3 component mixture of AM and BPB and Acid Yellow. B) Image of the separation channel of the focused band where it is apparent that some of the sample has leaked from the separation channel.

From this experiment a key observation was made. In figure 3.3.11B the analytes can be seen outside the boundary of the separation channel, clearly presenting a serious issue with sample recovery from the device. The 10 μ L sample loop was reduced to 5 μ L for subsequent injections having speculated the leakage was caused by sample overload.

3.3.7 Sample leakage issues

To test this theory the microfluidic device was set up and the initial hydrodynamic flow set at $1\mu\text{Lmin}^{-1}$. A $5\mu\text{L}$ injection of the previously used three-component test mixture was made. A linear EFG was applied at 200Vcm^{-2} to retain the analytes. A lower EFG was used than in earlier experiments as it was shown (table 3.3.3) that a linear EFG of 150Vcm^{-2} was capable of retention. Following the conditions for this experiment through table 3.3.4, the resulting separation is shown in figure 3.3.12.

Time (mins)	EFG (Vcm^{-2}) and Voltage Profile	Flow(μLmin^{-1})
1	<p style="text-align: center;">$G=200$</p> 	1.0
20	<p style="text-align: center;">$G=175$</p> 	1.0
34	<p style="text-align: center;">$G=150$</p> 	1.0

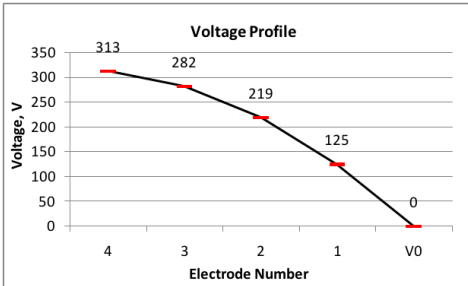
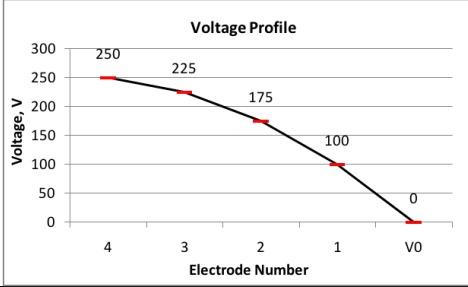
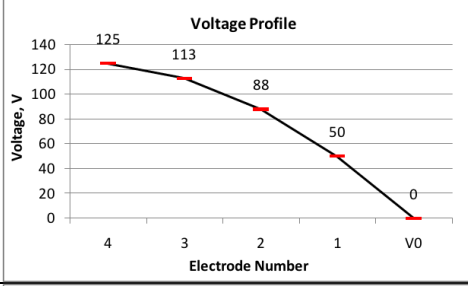
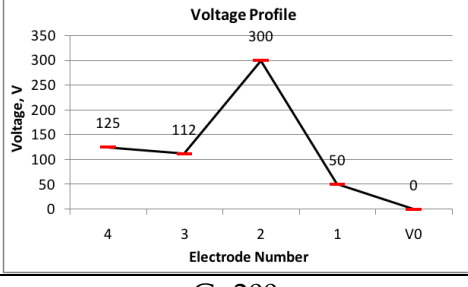
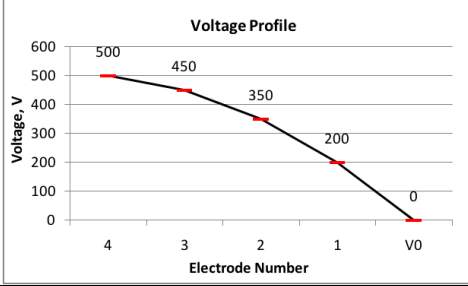
53	<p style="text-align: center;">G=125</p>  <p style="text-align: center;">Voltage Profile</p> <p>Voltage, V</p> <p>Electrode Number</p> <table border="1"> <thead> <tr> <th>Electrode Number</th> <th>Voltage, V</th> </tr> </thead> <tbody> <tr> <td>4</td> <td>313</td> </tr> <tr> <td>3</td> <td>282</td> </tr> <tr> <td>2</td> <td>219</td> </tr> <tr> <td>1</td> <td>125</td> </tr> <tr> <td>V0</td> <td>0</td> </tr> </tbody> </table>	Electrode Number	Voltage, V	4	313	3	282	2	219	1	125	V0	0	1.0
Electrode Number	Voltage, V													
4	313													
3	282													
2	219													
1	125													
V0	0													
57	<p style="text-align: center;">G=100</p>  <p style="text-align: center;">Voltage Profile</p> <p>Voltage, V</p> <p>Electrode Number</p> <table border="1"> <thead> <tr> <th>Electrode Number</th> <th>Voltage, V</th> </tr> </thead> <tbody> <tr> <td>4</td> <td>250</td> </tr> <tr> <td>3</td> <td>225</td> </tr> <tr> <td>2</td> <td>175</td> </tr> <tr> <td>1</td> <td>100</td> </tr> <tr> <td>V0</td> <td>0</td> </tr> </tbody> </table>	Electrode Number	Voltage, V	4	250	3	225	2	175	1	100	V0	0	0.5
Electrode Number	Voltage, V													
4	250													
3	225													
2	175													
1	100													
V0	0													
63	<p style="text-align: center;">G=50</p>  <p style="text-align: center;">Voltage Profile</p> <p>Voltage, V</p> <p>Electrode Number</p> <table border="1"> <thead> <tr> <th>Electrode Number</th> <th>Voltage, V</th> </tr> </thead> <tbody> <tr> <td>4</td> <td>125</td> </tr> <tr> <td>3</td> <td>113</td> </tr> <tr> <td>2</td> <td>88</td> </tr> <tr> <td>1</td> <td>50</td> </tr> <tr> <td>V0</td> <td>0</td> </tr> </tbody> </table>	Electrode Number	Voltage, V	4	125	3	113	2	88	1	50	V0	0	0.5
Electrode Number	Voltage, V													
4	125													
3	113													
2	88													
1	50													
V0	0													
74	<p style="text-align: center;">Voltage Profile</p>  <p>Voltage, V</p> <p>Electrode Number</p> <table border="1"> <thead> <tr> <th>Electrode Number</th> <th>Voltage, V</th> </tr> </thead> <tbody> <tr> <td>4</td> <td>125</td> </tr> <tr> <td>3</td> <td>112</td> </tr> <tr> <td>2</td> <td>300</td> </tr> <tr> <td>1</td> <td>50</td> </tr> <tr> <td>V0</td> <td>0</td> </tr> </tbody> </table>	Electrode Number	Voltage, V	4	125	3	112	2	300	1	50	V0	0	0.5
Electrode Number	Voltage, V													
4	125													
3	112													
2	300													
1	50													
V0	0													
80	<p style="text-align: center;">G=200</p>  <p style="text-align: center;">Voltage Profile</p> <p>Voltage, V</p> <p>Electrode Number</p> <table border="1"> <thead> <tr> <th>Electrode Number</th> <th>Voltage, V</th> </tr> </thead> <tbody> <tr> <td>4</td> <td>500</td> </tr> <tr> <td>3</td> <td>450</td> </tr> <tr> <td>2</td> <td>350</td> </tr> <tr> <td>1</td> <td>200</td> </tr> <tr> <td>V0</td> <td>0</td> </tr> </tbody> </table>	Electrode Number	Voltage, V	4	500	3	450	2	350	1	200	V0	0	1.0
Electrode Number	Voltage, V													
4	500													
3	450													
2	350													
1	200													
V0	0													
94	Off	3.0												

Table 3.3.4. Experimental parameters for the separation of 5 μ L of 10%v/v BPB AM and AY test mixture.

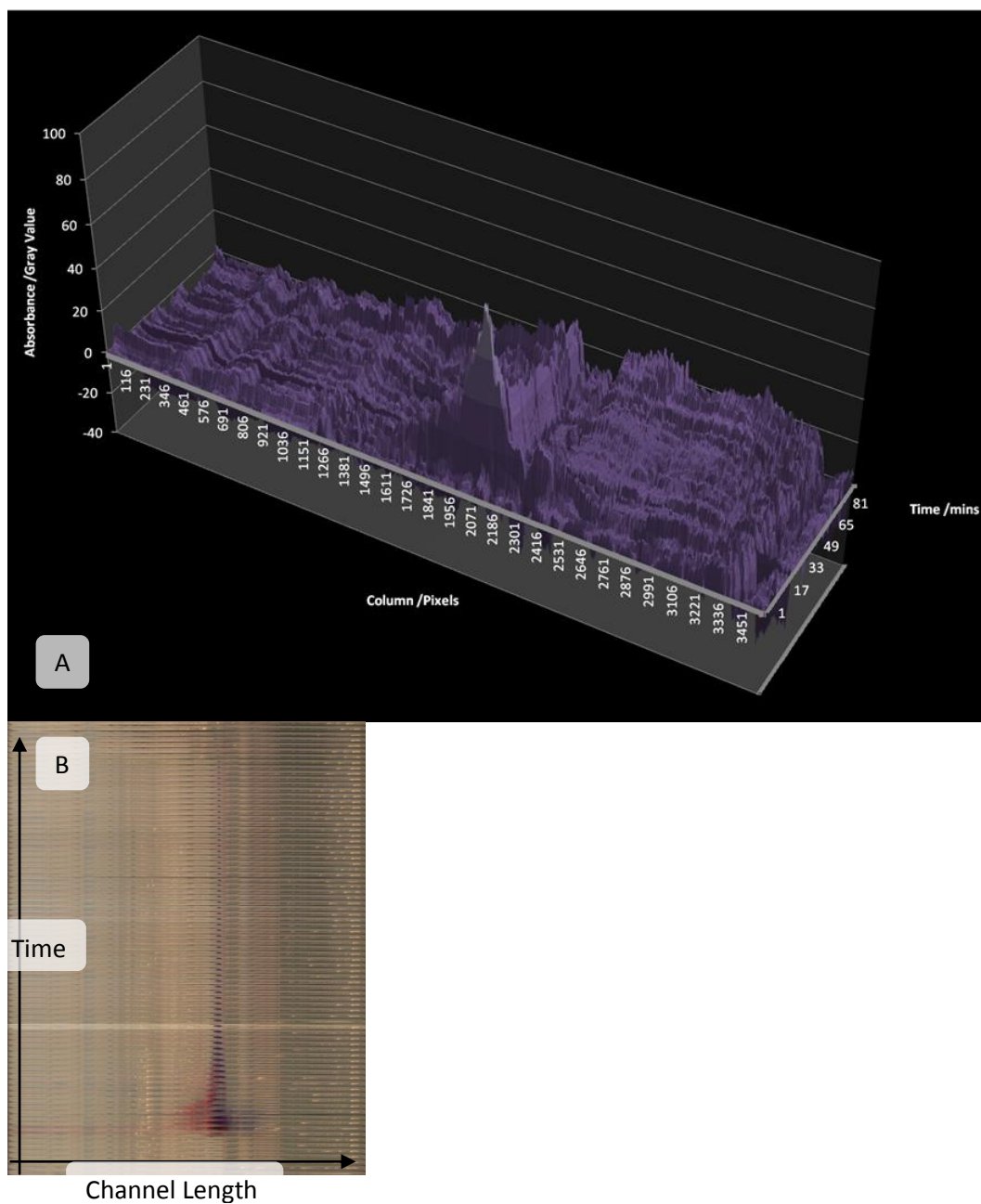


Figure 3.3.12. Graph showing the separation and focusing of a 5µL injection of the BPB AM and AY. After 120mins there are three areas visible across the channel corresponding to the three components.

Reducing the injection volume had decreased the extent of analytes leaking outside the separation channel but did not prevent the issue. In order to study the position of the sample in relation to the separation channel the device was carefully dismantled and the membrane removed.

The positions of the electrodes along the length of the membrane were noted and images collected. Figure 3.3.13 displays the membrane, after the separation, where the analytes have escaped from the separation channel. The red spots in figure 3.3.13, ~15mm along the channel between electrode 1 and 2, are concentrated; this implies that the electric field has caused the sample to migrate out of the separation channel and focused according to the shape of the electric field. In contrast, the other components of the test mixture appear to have flowed out under capillary action. However, considering the affect of the electric field, it is likely that the sample focused into a band which was then forced out of the join between the membrane and the separation channel chip (refer to figure 3.2.3).

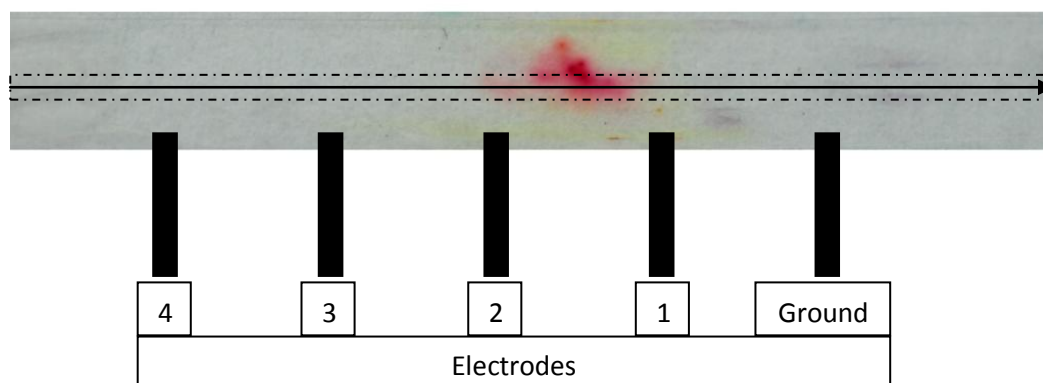


Figure 3.3.13. Membrane from experiment in figure 3.3.11. The electrode positions are shown by the black rectangles labelled 1-4 and ground. The Dash-dotted line displays the position of the electrode channel and solid line the position of the separation channel. The concentrated red dots of AM show that the field has pulled the sample onto the membrane, in contrast to the BPB over the ground electrode appears to have flowed out under capillary action.

The cause of this leakage was determined to be in the construction of the 'Gasket holder'. As the electrode channel was designed and constructed with a channel 1mm wide compared to the 100 μ m separation channel, the electric field was present either side of the separation channel. Moreover, the use of gaskets has worsened the problem as this resulted in an area of the membrane either side of the electrode channel which was not held under the controlled pressure required to maintain the integrity of the device. The cross section in figure 3.3.14 shows this issue where the membrane can be seen having an area 500 μ m wide on both sides of the channel which is not supported. This may have caused the membrane to sag from the force of the hydrodynamic flow, resulting in the separation channel becoming as wide as the distance between the inner edges of Viton gasket. This also has negative implications on the propagation of the electric field. As the membrane was forced down it resulted in the buffer from the electrode channel meeting the membrane all the way across the separation channel chip, which, as observed in figure 3.3.14, caused the sample to reach focal points outside the channel.

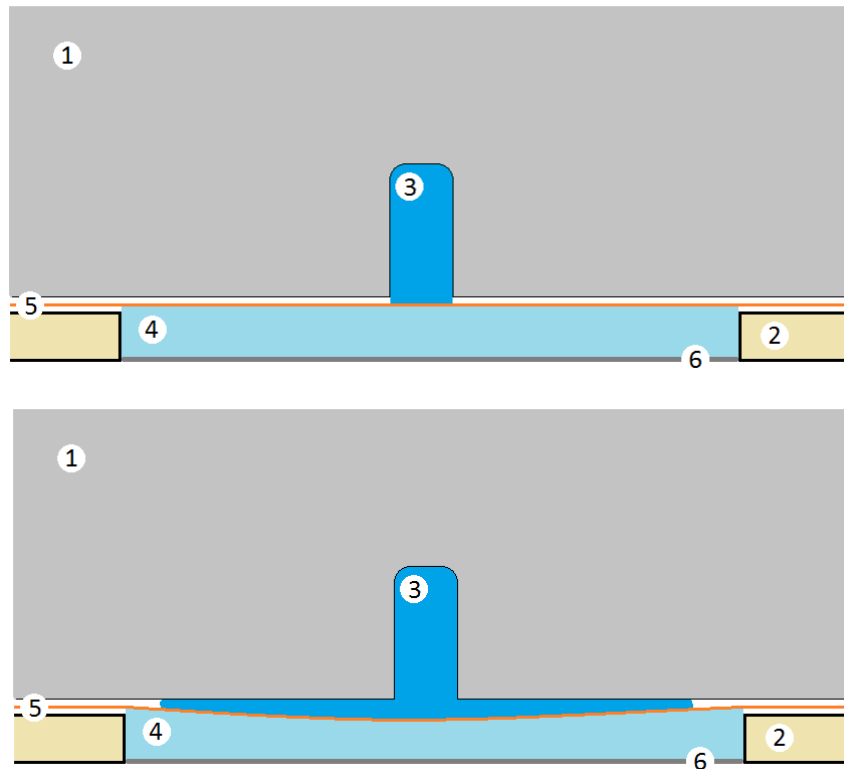


Figure 3.3.14. Enlarged cross section of the microfluidic DFGF detailing the issue with the channel dimensions and leakage. 1) Separation channel chip. 2) ‘Gasket Holder’ housing the electrode channel. 3) Separation channel buffer solution. 4) Electrode channel buffer solution. 5) Cellulose dialysis membrane. 6) Electrodes. Top image represent how the setup was designed to work. Bottom image displays a possible cause of the sample leakage issue caused by buffer from the separation channel being forced out between the chip and the membrane.

A prototype replacement electrode channel was designed having identified the possible cause of the issues to be the design of the ‘gasket holder’. The prototype was constructed using one of the existing ‘gasket holders’. The guide ring around the immediate edge of the electrode channel was trimmed away to leave a flat surface with the 1mm channel below. Using a computer controlled milling machine, Roland Modella MDX-20²⁴, a Teflon sheet was machined to the dimensions of the top recessed surface of the ‘Gasket holder’ and a 100 μ m channel (the length of the separation channel) machined down the centre.

This was then inserted into the 'Gasket holder'. The design of this Teflon insert was to resolve the issue by providing further support for the membrane while reducing the dimensions of the electrode channel at the connection to the separation channel.

The Teflon insert and assembly is shown in figure 3.3.15.

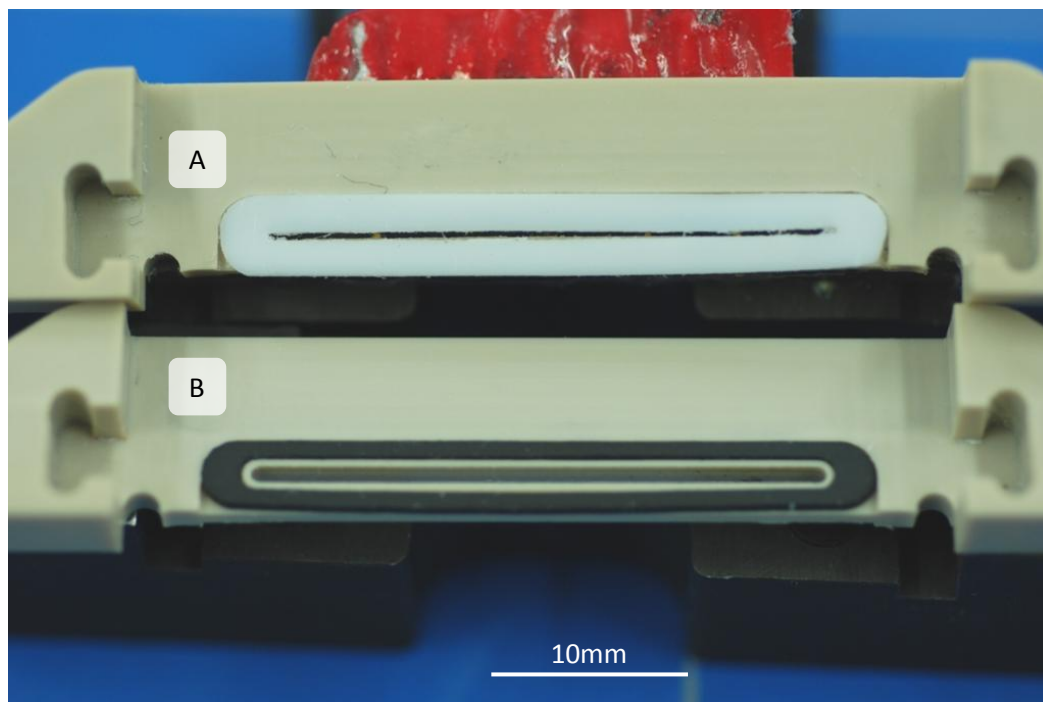


Figure 3.3.15. A) Prototype Teflon insert to provide a narrower electrode channel and better support for the membrane in comparison to; B) The original PEEK electrode channel and gasket.

Initial testing with the Teflon insert began using the gold array described earlier figure 3.3.8. Unfortunately, the gold electrode array was damaged as buffer from the electrode channel leaked onto the back of the electrodes causing them to short circuit resulting in severe heating which degraded the connections. As a result a more reliable electrode replacement was required. The design and manufacture of a prototype platinum array was completed. As discussed in the design of the microfluidic DFGF, it was not possible to solder onto the existing platinum electrodes as the coverage was in the order a few microns. Moving to using platinum foil, the connecting electronics were soldered directly onto the electrodes. These electrodes were then bonded to a plastic chip to fit directly into the 'chip holder bottom' of the device. The platinum electrode prototype array is shown in figure 3.3.16.

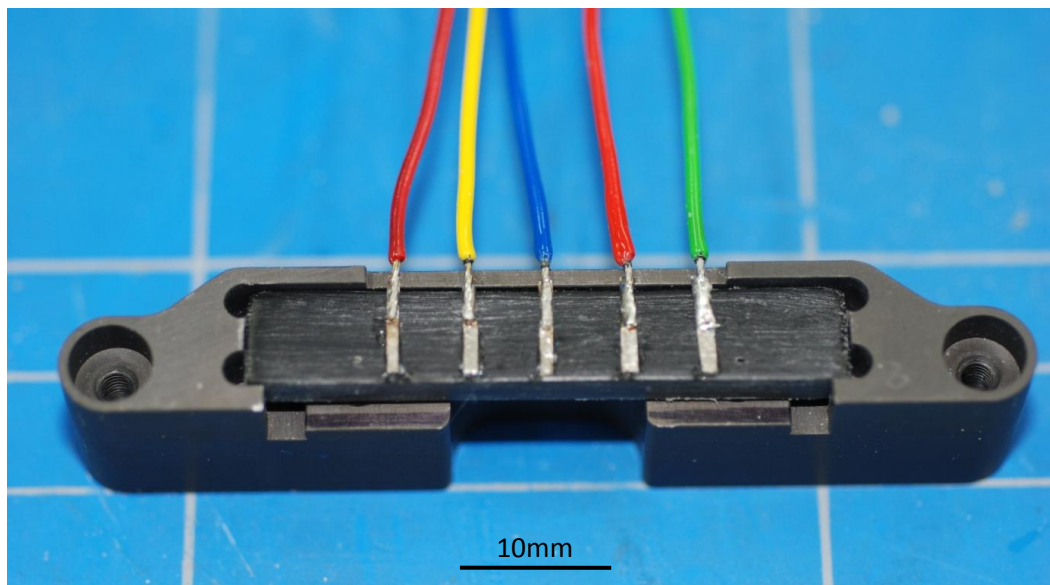


Figure 3.3.16. Prototype Platinum Electrodes on a plastic chip with holes drilled for the flow of electrode channel buffer and an IDC connector to interface with the Protasis Power Supply.

Assembling the microfluidic DFGF device involved precision positioning of the Teflon insert over the existing electrode channel to align the separation channel to the channel in the insert. A strip of 100MWCO cellulose membrane was positioned on top of the Teflon insert and the devices assembled. The device was configured with the supporting equipment and testing with improved channel and electrodes commenced. Positive results with a simple test to focus the three component dye mixture showed further reduction in the leakage of samples from the channel. With the device operational a separation of the Bio-Rad Kaleidoscope test mixture¹⁹ was conducted.

At a flow rate of $1\mu\text{Lmin}^{-1}$ $5\mu\text{L}$ of 10%v/v Kaleidoscope test mixture was injected. A linear EFG was applied at 200Vcm^{-2} . The sample was observed to be focused into a plug 5mm along the channel. After 20mins the field was dropped to a lower linear EFG of 150Vcm^{-2} , to enable the analytes move further along the channel and separate, (summarised in table 3.3.5). Observing figure 3.3.17B, though a little difficult to see from the graph, the individual plot shows the separation of three components from the mixture. The analytes were held for 15mins before an increase in the EFG to 200Vcm^{-2} to ensure that sample movement under the unbalanced forces in favour of electrophoretic over hydrodynamic force maintained the sample in the boundaries of the separation channel. From the images captured the sample was successfully held in the separation channel.

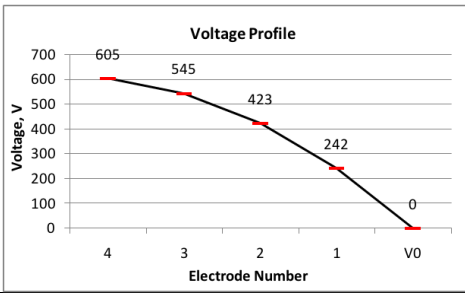
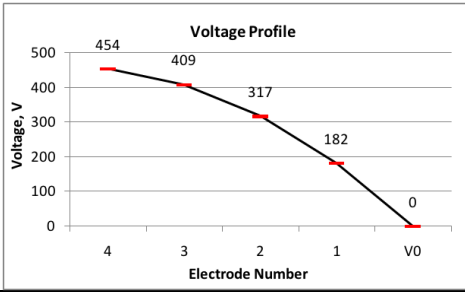
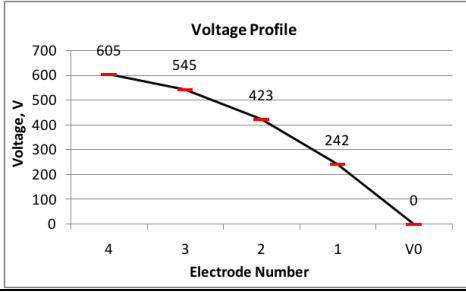
Time (mins)	EFG (Vcm ⁻²) and Voltage Profile	Flow(μLmin ⁻¹)
1	<p style="text-align: center;">G=200</p> 	1.0
11	<p style="text-align: center;">G=150</p> 	1.0
17	<p style="text-align: center;">G=200</p> 	1.0

Table 3.3.5. Conditions for the separation of the 'Bio-Rad Kaleidoscope Pre-stain Standards¹⁹' in figure 3.3.17.

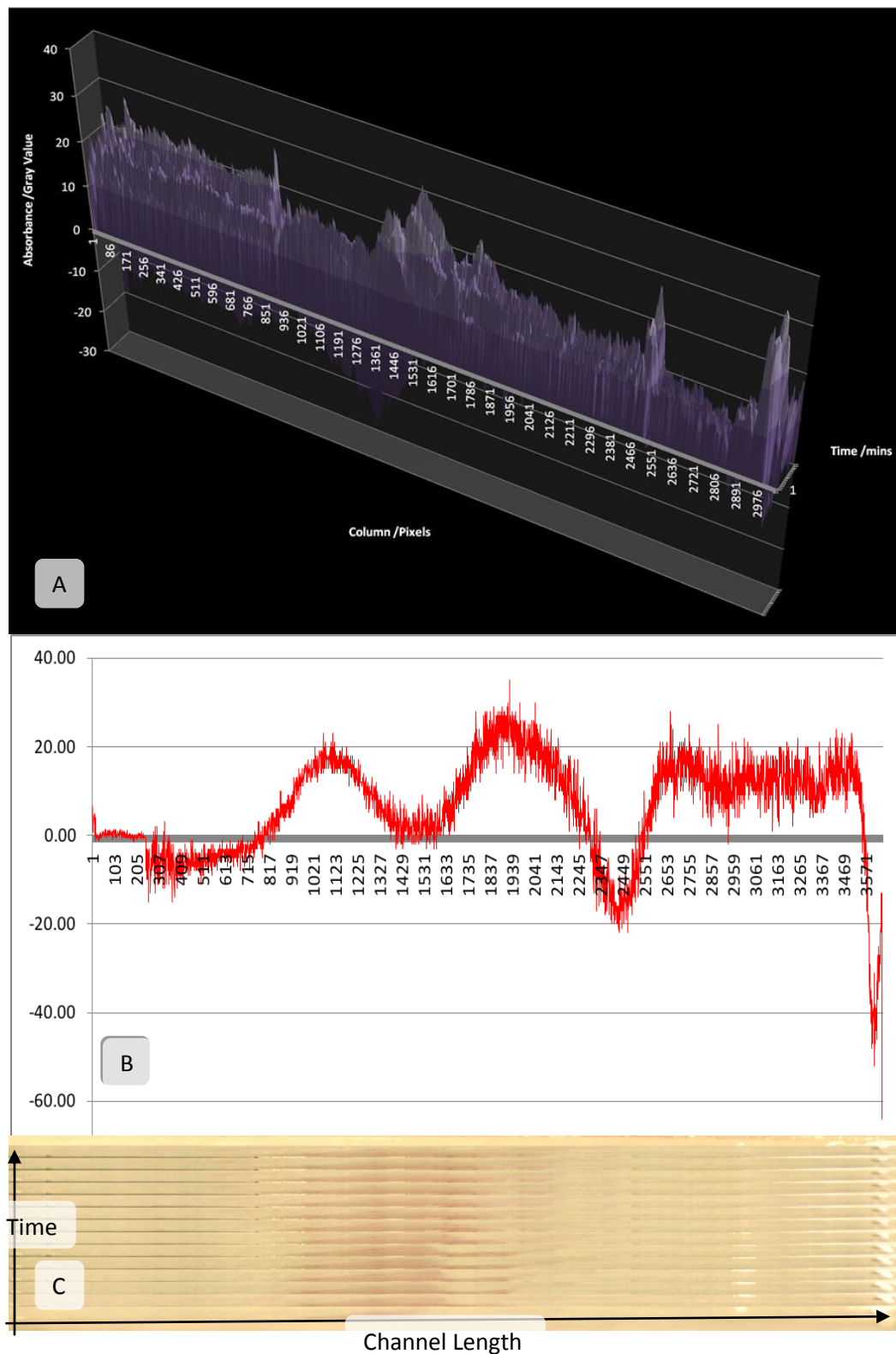


Figure 3.3.17. A) Graph of the separation and focusing of the 'Bio-Rad Kaleidoscope Pre-stain Standards' in the microfluidic DFGF using the prototype platinum electrode array and prototype Teflon electrode channel. B) Single Plot of Separation at 24mins. C) Montage showing the sample retained in the channel.

Repeating the previous experiment reinforced that reducing the electrode channel width and using reliable electrodes had improved the issue of the sample escaping the separation channel. With these developments tested, collaboration with the University Of Liverpool Department Of Engineering led to the design of several pilot components using a new innovation in Rapid Prototyping.

3.3.8 Rapid Prototyping (RP)

Rapid prototyping (RP) is a process developed in the 1980's as a means of producing prototypes or models²⁵. As the technology has progressed RP has become the link between designs and the real world. A design drawn using Computer Aided Design (CAD) software can be interpreted into a series of layers which are then grown or sculpted to give a product, the prototype. The first rapid prototypers were simple free form cutting machines programmed by basic CAD software. There are many different types of RP devices which have been devised since then, including the Roland MDX-20²⁴ used earlier to manufacture the Teflon prototype. One of these more advanced techniques is Stereolithography Rapid Prototyping which has been utilised for this work.

3.3.9 Stereolithography Rapid Prototyping

Stereolithography, derived from the Greek 'to write with light', is a process where a material in a liquid state is photopolymerised yielding a solid²⁶. Shapes are generated by a series of light manipulating devices projecting a two dimensional image onto a bed of liquid, causing selective polymerisation of the area illumined.

As these 2D images cause polymerisation the newly formed solid is lifted from the bed, these layers build up the three dimensional structure which emerges from the liquid, figure 3.3.18.

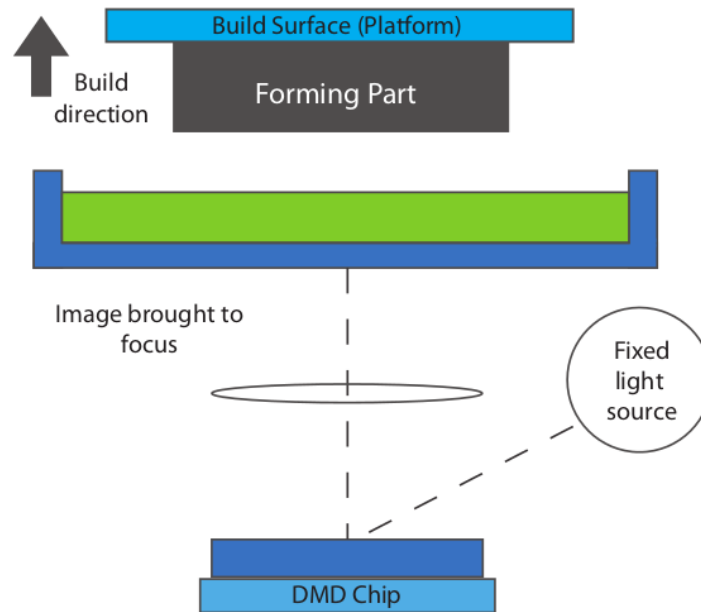


Figure 3.3.18. Schematic displaying the process of Stereolithography Apparatus.

The development of a high resolution Stereolithography RP device at the University Of Liverpool Department Of Engineering has been undertaken by Jetinder Singh²⁷. This system was capable of producing components with features accurate down to just $\pm 6\mu\text{m}$. This was achieved by using state-of-the-art software, laser control and stepper motor control refinements to the 'Envisiontec Perfactoy'²⁸. This refined Stereolithography RP machine provides the capability of forming complex microfluidic devices in a fraction of the time it would have normally taken going through a classical machining route with a significant reduction in cost.

The photopolymer used to form these prototypes was an acrylic resin Pentaerythritotritetraacrylate (CAS 4986-89-4) mixed with 1,1,1-Trihydroxymethylpropyltriacylate (CAS 15625-89-5, 3524-68-3), known by the acronym 'PMMA' and was supplied by Envisiontec²⁸.

The free radical polymerisation was initiated by the photodecomposition of the initiator species present in the mixture. The decomposition results in an electron pair from the initiator attacking a monomer to form the reactive radical. With further exposure to the light source, generated by an incandescent bulb and filtered to ~550nm (exact wavelength is proprietary), propagation of the polymer occurs as the radical reacts with more monomers adding to the chain while sustaining the reactive radical species. Termination occurs by two reactive radical chains coupling, or by a chain bonding becoming a branch of another polymer chain.

Having polymerised a two dimensional layer, the stepper motor control moves the build platform away once the required 'curing' time has been left and the next image is projected to form the next layer of the component. This process is completed for each layer to build up the structure until it is complete.

3.3.10 RP Mask for Electrode Manufacture

The first application of Stereolithography RP for the microfluidic DFGF was to design and build a mask for the manufacture of a new electrode array by physical vapour deposition, PVD. As shown in figure 3.3.5 the supplied dolomite electrodes were also made using PVD.

In this case the aim was to attempt to manufacture a reliable electrode array by depositing a greater thickness of Platinum to enable a soldered connection and operation of the electrodes under the conditions in the microfluidic device. Using RP a design was drawn in CAD software and is shown in figure 3.3.19.

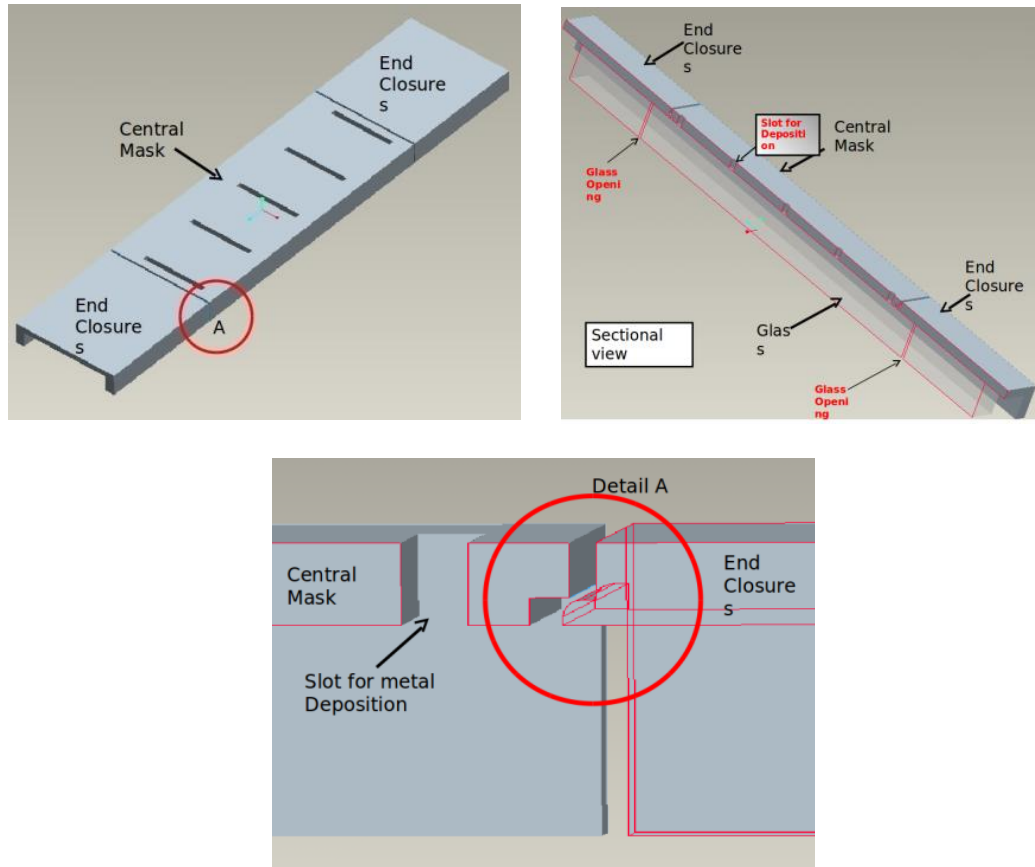


Figure 3.3.19. Electrode chip mask design drawn in CAD software.

The manufacture of the electrode mask was undertaken and completed in less than 12 hours. PVD was implemented and successfully deposited $\sim 10\mu\text{m}$ coverage of platinum using an Edwards sputter coater. A flow of plasma in a vacuum vaporises the metal, in this case platinum, and deposits it onto the target material.

The thickness of the coating depends on the energy of the plasma and the duration of the deposition. The finished electrodes and mask are shown in figure 3.3.20.

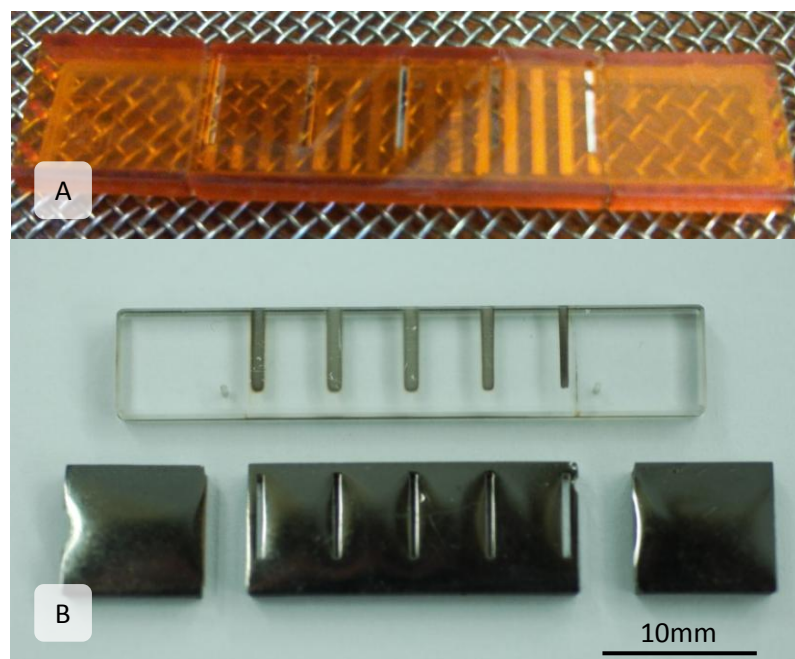


Figure 3.3.20. PVD Platinum electrode plate and the RP mask. A) The mask positioned over the electrode chip. B) The mask after sputtering with the newly formed electrodes on the chip.

With the PVD platinum electrode chip installed in the microfluidic DFGF device a test experiment was undertaken to verify the functionality of these electrodes. With a linear EFG of 200Vcm^{-2} applied and the flow rate at $1\mu\text{Lmin}^{-1}$ an injection of the three component dye mixture was made. After 5mins the sample began to focus, however after leaving the sample to initially focus for 20mins before adjusting the electric field, the sample eluted from the device. On further inspection the electrodes had degraded as with previous platinum electrodes despite having a more substantial coverage of platinum. Therefore, electrodes manufactured by this method are not suitable as electrodes in this application.

The electrode chip is shown in figure 3.3.21 displaying evidence of the degradation. From this it was determined that electrodes used in the device must either be wire or a thin sheet of the chosen metal.

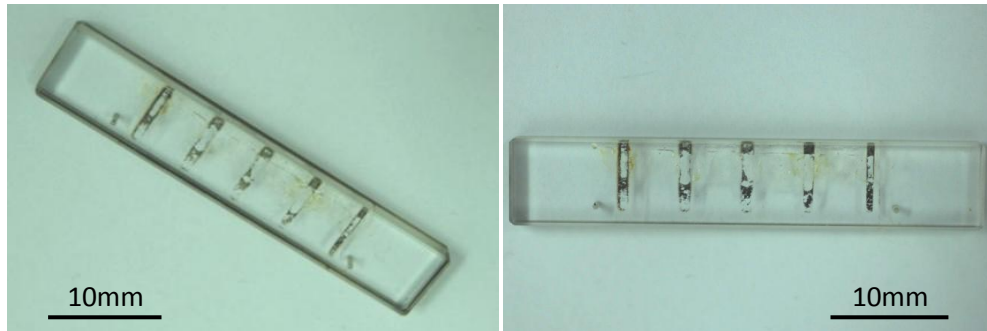


Figure 3.3.21. Two angles of the decomposed PVD electrodes after 20mins at 200Vcm^{-2} .

With the failure of the PVD electrode and the positive results obtained for the platinum foil electrode, a final electrode array was manufactured utilising an existing electrode chip in combination with the platinum electrodes and IDC connector. This final electrode chip is shown in figure 3.3.22. This chip was made utilising an expired electrode chip and hand tooling the channels for the electrodes and bonding them in place with resin.

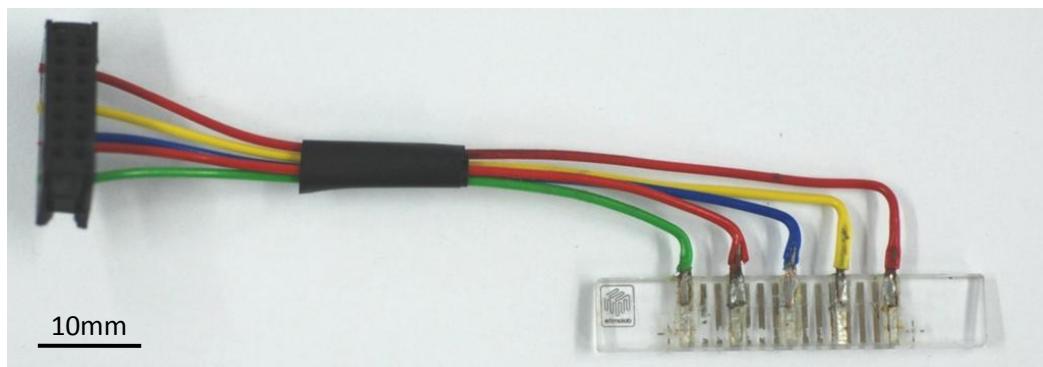


Figure 3.3.22. Final electrode chip. This accommodates five platinum electrodes on a glass chip with an IDC connector.

3.3.11 RP Modified Electrode channels

The primary work done using Stereolithography RP to further the development of the microfluidic DFGF was the development of the replacement 'Gasket Holder' component. Before designing and testing replacement components the original 'Gasket Holder' was replicated to ensure the suitability of components in this material and manufacture by SLA RP. The duplicate 'Gasket holder' CAD model is shown in figure 3.3.23. The component is shown during manufacture below in figure 3.3.23D. The manufacture of the component was completed after 12hours.

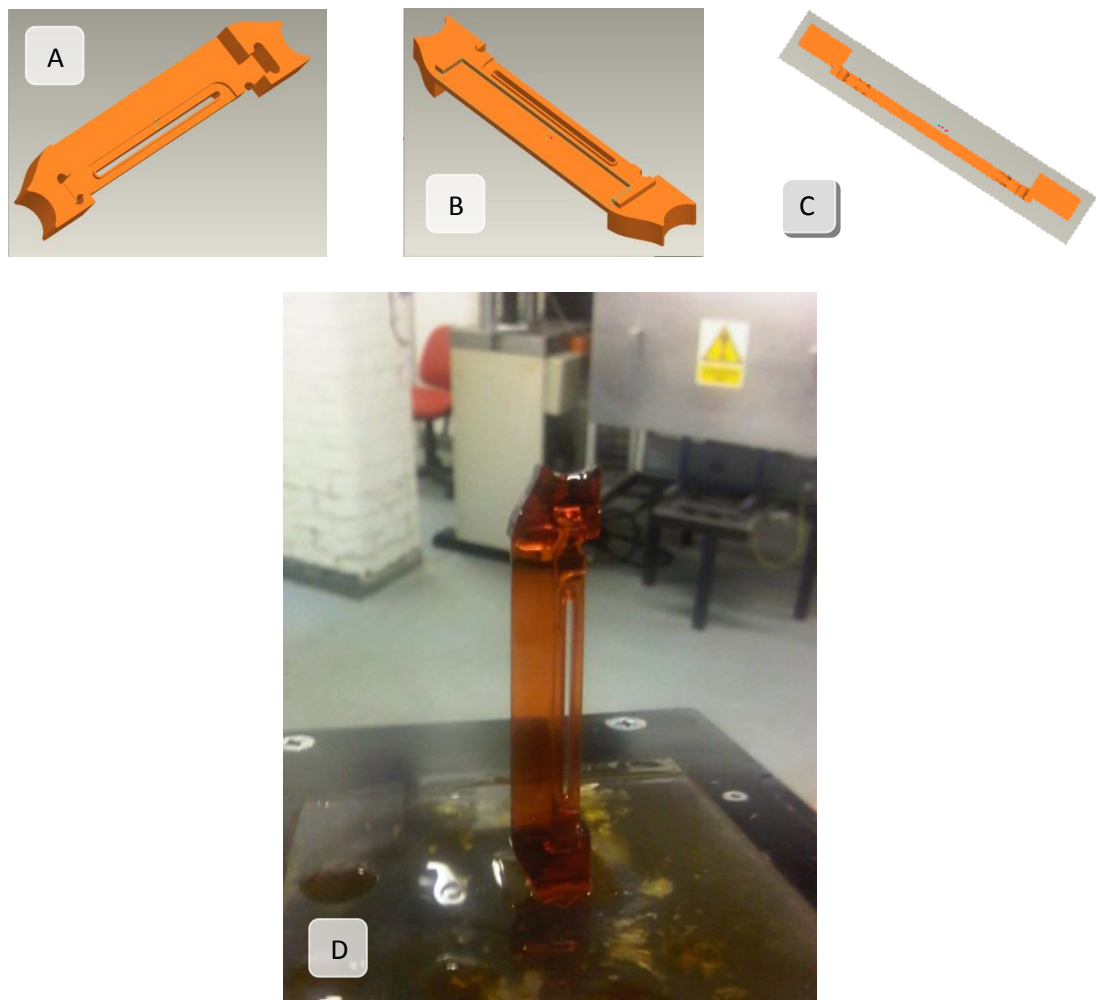


Figure 3.3.23. A, B & C) 'Gasket Holder' drawn in CAD ready for SLA manufacture. Top, Base, and Front elevations respectively. D) Manufacture of 'Gasket Holder' using SLA RP displaying the new component rising from the liquid precursor.

The finished 'Gasket Holder' is shown in figure 3.3.24 alongside the original for comparison. A set back arose from vibrations of the stepper motor causing inaccuracies across the length of the component. However, having adjusted the CAD to include some side supports to be removed post fabrication, the problem was solved.

The microfluidic DFGF was assembled using the SLA 'Gasket Holder' in place of the original supplied by Dolomite also using the Viton gaskets. The device was tested for leaks using flow rates greater than those used experimentally to rule out defects. The SLA 'Gasket Holder' performed well without any leaks observed. With the success of the proof of concept component, the CAD model was modified to incorporate the desired channel width of 100 μ m. As many components can be fabricated with only small changes to the design, for comparison a second design with 200 μ m channel width was also manufactured. Schematics and the modified CAD of these are shown in figure 3.3.24.

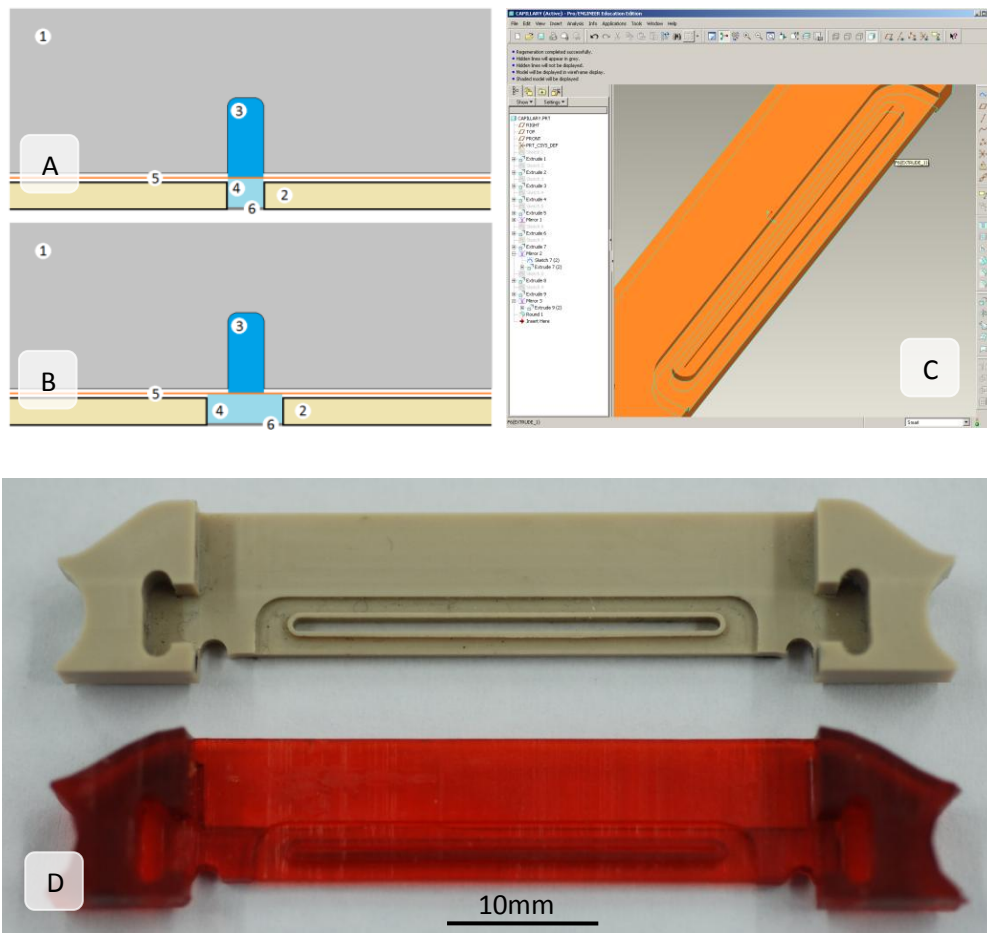


Figure 3.3.24. A) and B) Cross section schematics of the 'Gasket Holder' with channel widths of 100µm and 200µm respectively (key as in figure 3.3.14). C) Modified CAD drawing for the 100µm channel D) 100µm manufactured component (orange) compared to standard gasket holder.

With the completion of the SLA RP process the operation of these components was investigated. Changes to the imaging were made following observations from the initial experimentation with the microfluidic DFGF device. These were that the analytes responded to changes in the electric field in less time, ~5min in an open channel, as opposed to ~30mins in the previous DFGF devices using packed channels. Collecting an image every 2mins was therefore determined to be giving poor resolution in terms of tracking the movement of the species in the separation channel. The solution was to collect reflectance measurements every minute.

Examples of this can be seen by comparing the time which is required for an initial focused mixture to appear in first generation device in chapter 2 (figure 2.3.4) taking ~50mins and figure 3.3.25, taking only 16mins. Additionally, the quartz construction of the separation channel was found to be the cause of the high noise level in the baseline of the graphs while imaging. Improving the clarity of images required a reduction in glare. Therefore, the whole chip was coated with black acrylic paint except for the area over the serration channel.

Another imaging issue was observed from the numerous graphical separation data discussed in this chapter, figure 3.3.11A in particular. Towards the ground electrode on the right of the separation channel, correlating to the far right of the x-axis, there appears to be ranges of smaller peaks or noise. These peaks are not generated by the presence of an analyte, but by the gaseous electrolysis products. Though these are not permeating the membrane, or affecting the analytes, they are visible and alter the 'background' of the image therefore appear as peaks on the graph. As these gasses evolve and rise, becoming visible on the membrane, a simple response was to configure the microfluidic DFGF to run upside-down to eradicate the interference in detection due to the reflection of the bubbles.

The advantages of these imaging improvements are shown in the baselines of subsequent plots, for example figure 3.3.11A, compared to those that follow, e.g. figure 3.3.27. As the profiles for these graphs calculate the peaks as a factor of grey value, the more stable the baseline the greater the difference between the average baseline and that of peak from the presence of a band of analyte.

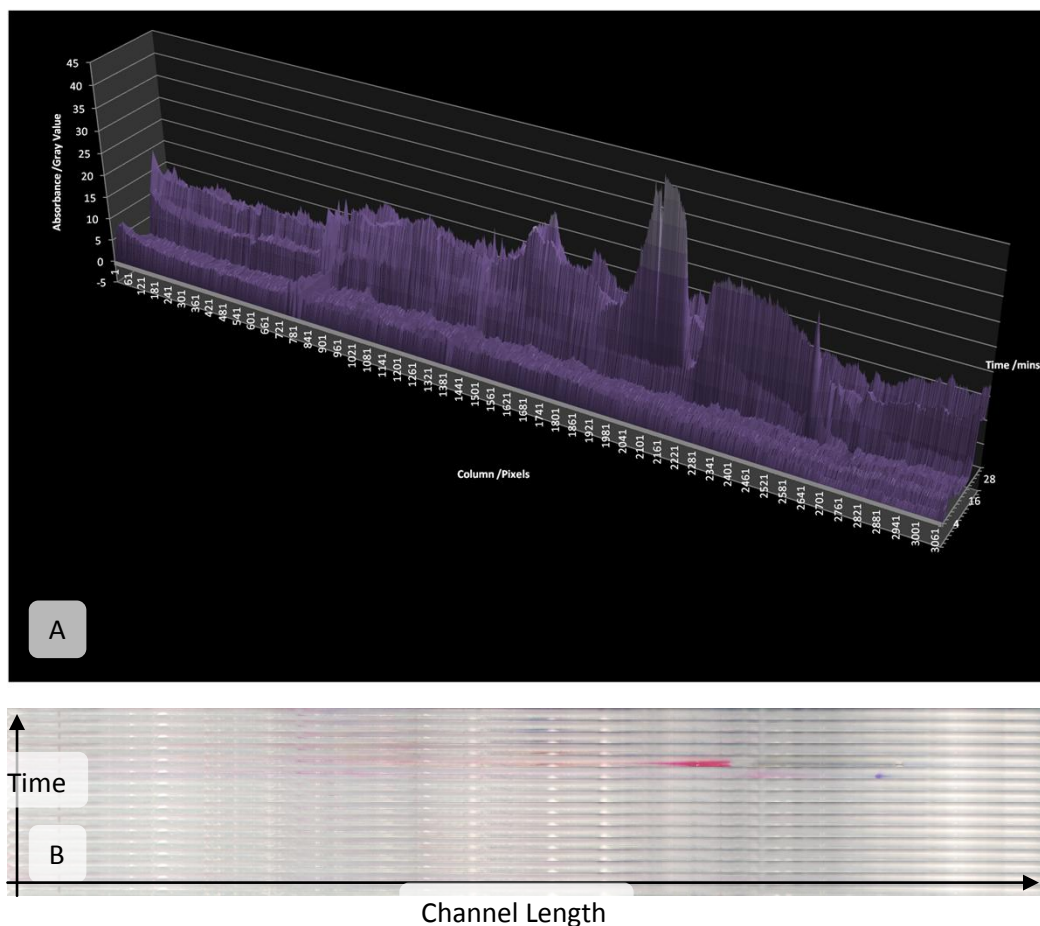


Figure 3.3.25. A) This graph displays the need to collect images at a shorter time intervals as the bands of analyte comes into focus, seemingly instantaneously, where this effect in actual is a gradual phenomenon. B) The montage also displays this as the AM and BPB are observed.

3.3.12 Testing with the 100 μ m Electrode Channel

Moving forward with the imaging system optimised, the 100 μ m electrode channel was incorporated in the microfluidic DFGF. This was assembled following the original instructions, with the addition of the application of a very thin bead of vacuum grease around the electrode channel, to aid forming a tight seal. The membrane used was 100MWCO cellulose dialysis membrane. The aim was to eradicate the sample leakage issue and improve the propagation of the field.

A 5 μ L sample of 10%v/v AM and BPB was injected at a flow rate of 1 μ Lmin⁻¹. With the utilisation of the narrower channel, the current density appears to have increased as the electrophoretic force (at a linear EFG of 125Vcm⁻²) retained the sample at the beginning of the channel. This can be observed in figure 3.3.26 by the peak at ~124pixels. After 72mins the EFG was lowered to 30Vcm⁻² and some separation is observed. However, such a reduction in the EFG should have enabled the sample to migrate further along the channel. From the graph in figure 3.3.26 the focused analyte can be observed in a similar position to the initial focusing. This indicated that some of the sample had been trapped outside of the separation channel and the rest of the sample had focused briefly around 3322pixels before eluting from the device.

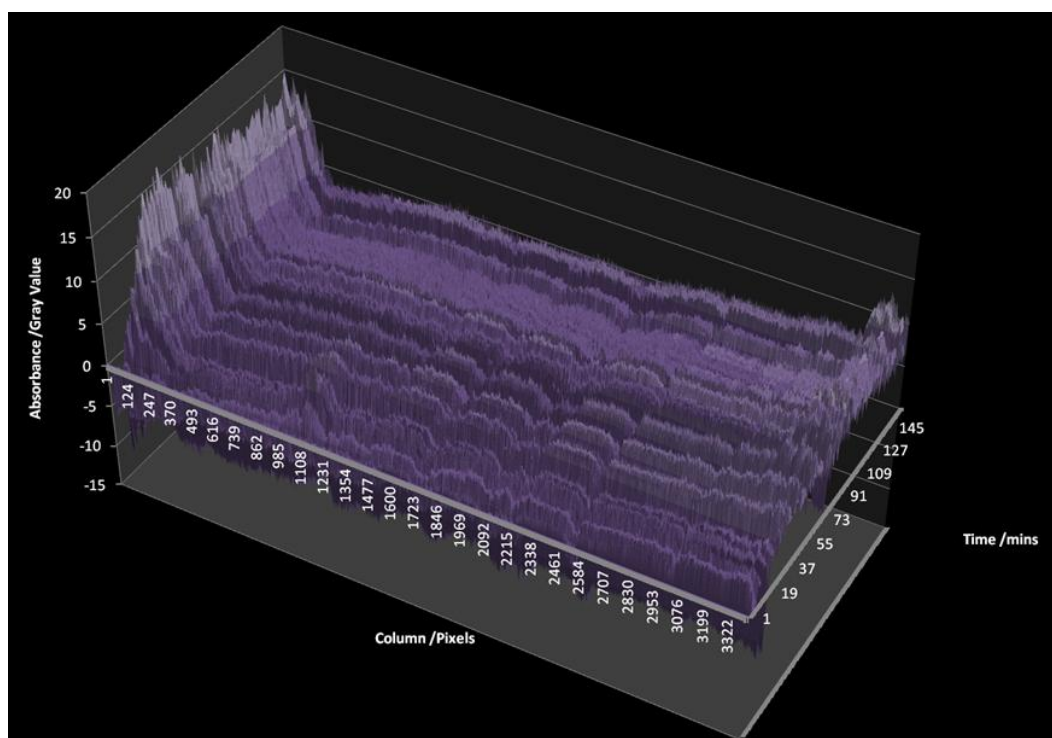


Figure 3.3.26. Separation of BPB and AM using 100 μ m electrode channel. Observing the sharp band forming from 19-70mins indicates a high current density. On changing the electric field after 70mins, the single peak splits into two close bands.

Additional experimentation using the 100 μm electrode channel often led to leakage of buffer solution, even at flow rates as low as 0.5mLmin⁻¹ to reduce the back pressure. The issues can be directly attributed to the width of channel and accuracy of the application of sealant. The underlying issue was that any sealant which was present in the channel caused blockages and in some cases was observed to be preventing the electric field from being generated.

Theoretically, this channel should have prevented the sample leakage issues. However, the feasibility of the use of this component prevented the device from functioning effectively with few benefits observed. The main improvement this component made was the extra support for the membrane, though as discussed, the electrode channel itself would fail.

3.3.13 Testing with the 200 μm Electrode Channel

Experimentation using the 200 μm electrode channel was performed using the same setup as previously described for the 100 μm electrode channel. The circulating electrode buffer was pumped at 1.5mLmin⁻¹, this was higher than that used for the 100 μm component as a larger channel width was observed to be less susceptible to failure by leakages.

A buffer solution, of 50mM tris HCl, was pumped through the separation channel at 1 μLmin^{-1} and 5 μL of 10%v/v BPB and AM mixture injected. Successively decreasing voltages were used to ascertain the functionality of the electric field across the length of the device. These conditions are shown in table 3.3.6 and the separation presented graphically in figure 3.3.27.

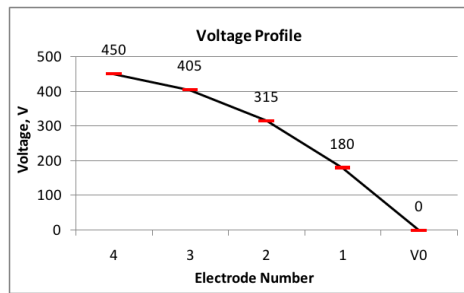
Time (mins)

EFG (Vcm⁻²) and Voltage Profile

Flow(μLmin⁻¹)

G=125

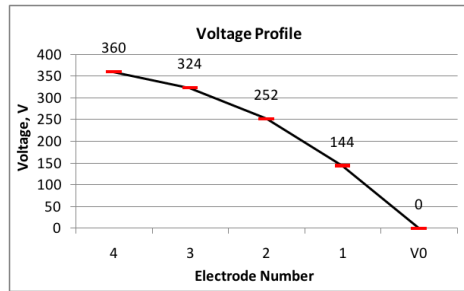
1



1.0

G=100

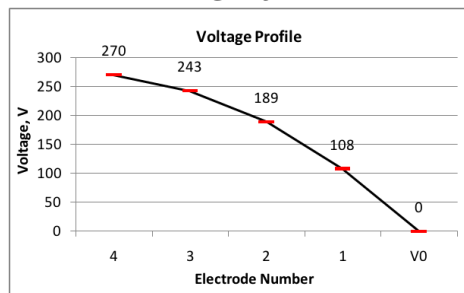
60



1.0

G=75

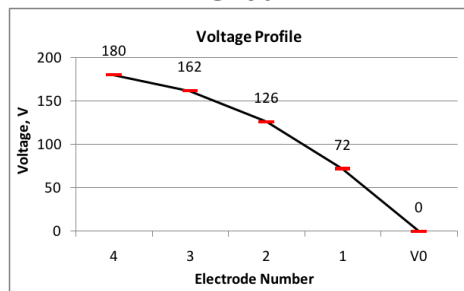
85



1.0

G=50

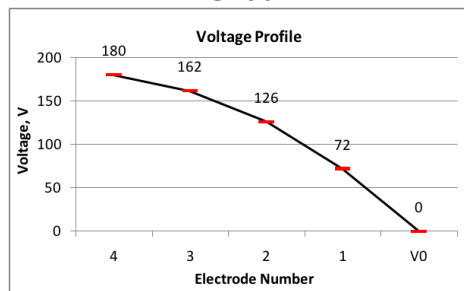
105



1.0

G=50

117



1.5

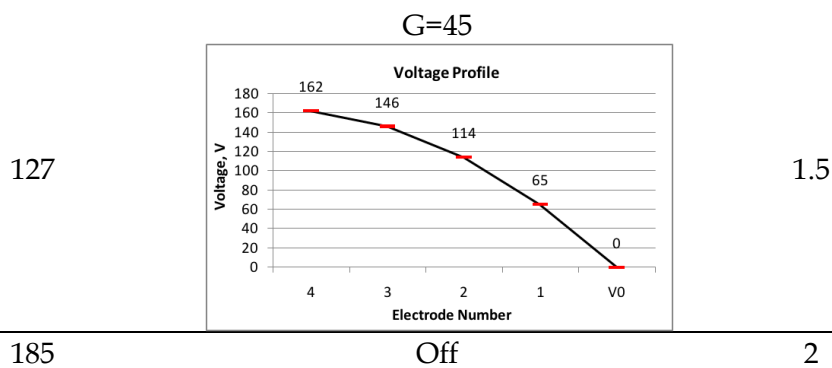


Table 3.3.6. Conditions used to separate AM and BPB testing the 200 μ m electrode channel.

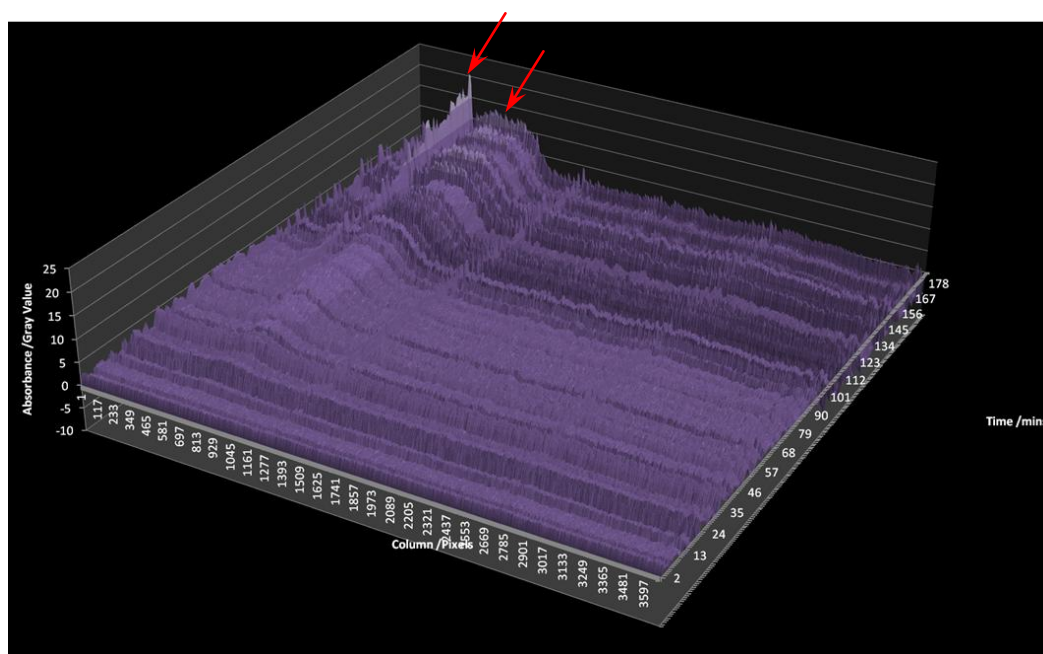


Figure 3.3.27. Graph of separation using the 200 μ m electrode channel. Observe the smaller sharp peak around 600pixels move further along the column over time as the EFG is lowered. This is also noted by the broader peak of analyte coming into sharper focus over time.

Comparing the performance of the device using the new 200 μ m electrode channel to the original 1mm electrode channel, it was exhibited that the sample leakage had been greatly reduced and peaks could be seen to be focusing into more concentrated bands. When the 100 μ m channel was used, the channel became blocked with very small amounts of sealant.

Another feasibility issue observed was that the circulation of the buffer through the electrode channel required lower flow rates, due to the decreased channel cross section, which did not effectively remove gaseous species. This resulted in a poor stability of the electric field.

The optimisation of the microfluidic DFGF device described through this chapter has yielded the system used in the separation in figure 3.3.27. Improvements have been made in the operation of the device and the detection of analytes. A summary of the optimised system is shown in table 3.3.7. Following the separations of dyes performed with this system, a separation of proteins was undertaken.




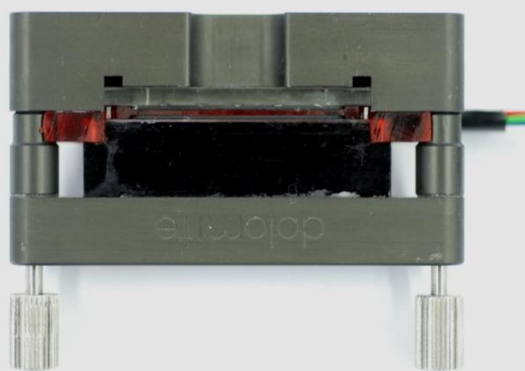
Component	Description
Platinum Electrodes 	Platinum Electrodes 1mm wide spaced equally 0.6mm apart. Offer a high current density and provide a stable reliable EFG, without degradation.
200µm Electrode Channel 	The 200µm electrode channel provides a better support for the membrane while being more resistant to failure from leakages and blockage from sealant. Reduces sample loss from the separation channel.
Blacked out separation channel chip 	Blacked out separation channel chip reduces the fluctuations in surrounding light and therefore improves the baseline of graphical representations of plots improving sensitivity of detection. This chip is mandatory when using the PDA as this detection system requires a much more stable light source.
Device Rotated 180° 	Running the device upside down causes any gaseous by-products from field generation to rise out of the electrode channel, preventing these from giving rise to response from the detector by causing shadows of reflections in the separation channel.
Imaging Technique (timing)	Increasing the frequency of image sample collection from 2minutes to one every minute has enabled a clearer view of separations as focusing occurs.
Light sources	Moving away from only ambient light to illuminate the device and providing a stable light source with minimal interference has enabled more sensitive data collection.

Table 3.3.7. Optimised Microfluidic DFGF device.

The Kaleidoscope test mixture¹⁹ was successfully separated into five bands using the optimised microfluidic DFGF (table 3.3.7). This followed changes to the electric field gradient and voltage profile shown in table 3.3.8. with the result in figure 3.3.28. The experiment was also repeated to improve the visibility of the separation as shown in table 3.3.9 and figure 3.3.29.

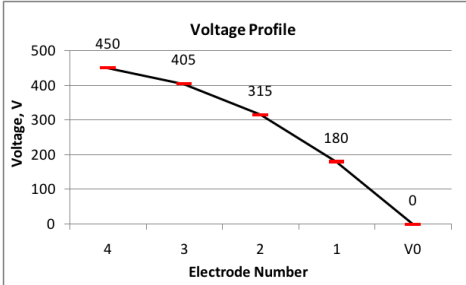
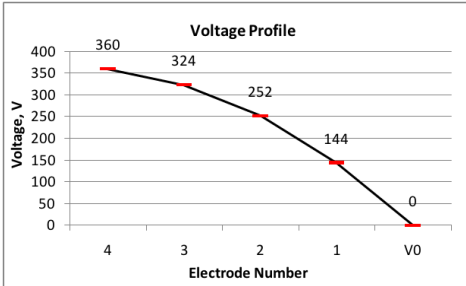
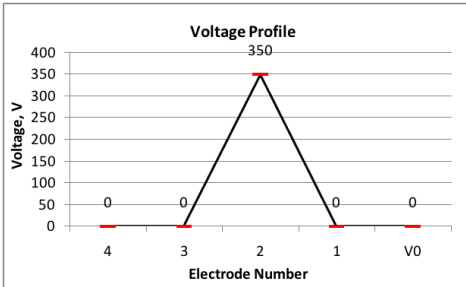
Time (mins)	EFG (Vcm ⁻²) and Voltage Profile	Flow(μLmin ⁻¹)
1	<p style="text-align: center;">G=125</p> 	1.0
40	<p style="text-align: center;">G=100</p> 	1.0
60	<p style="text-align: center;">0.0.0.350.</p> 	1.0
105	0	2

Table 3.3.8. Conditions the separation of Kaleidoscope Proteins in figure 3.3.28.

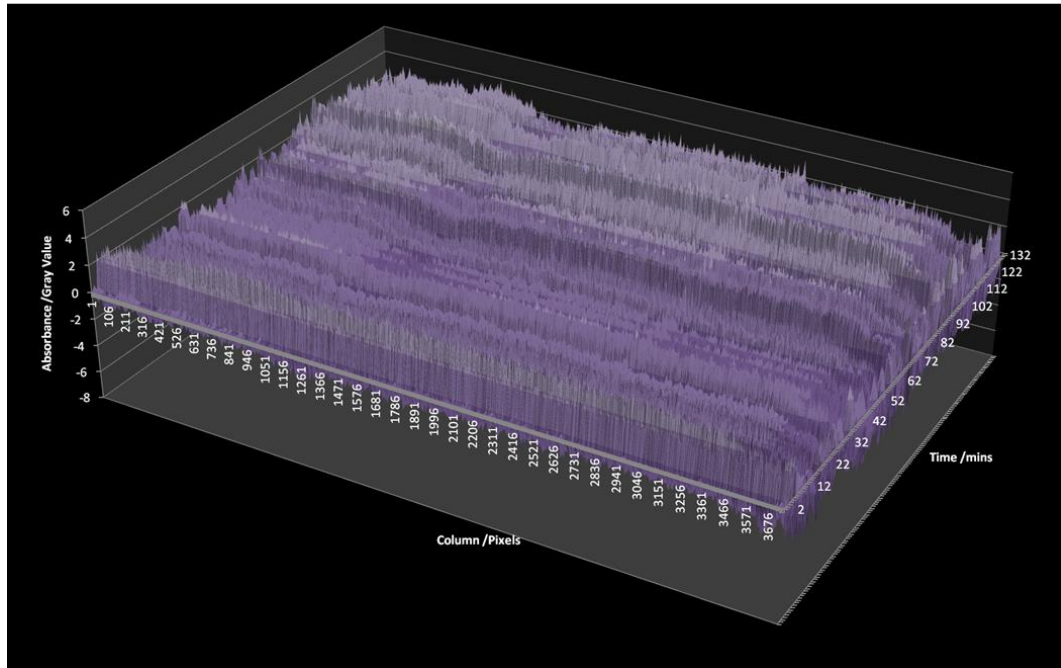
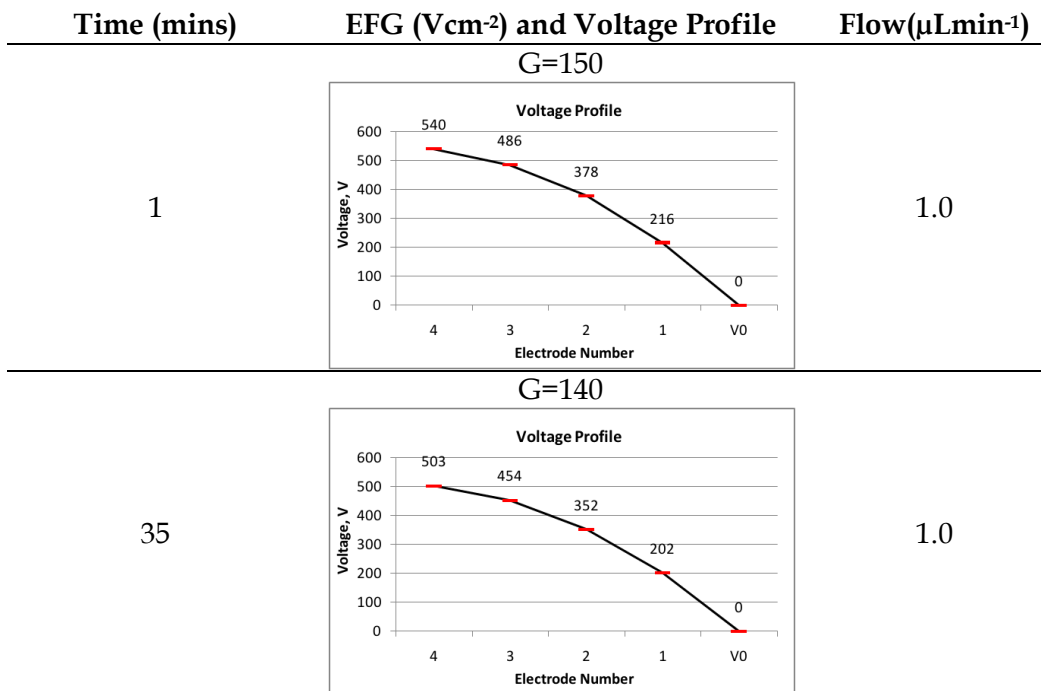
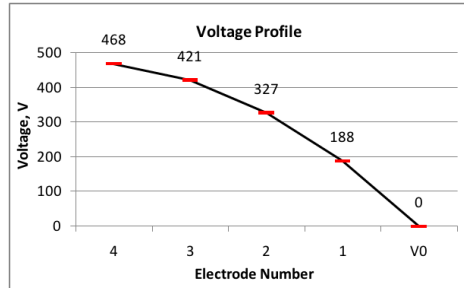


Figure 3.3.28. Separation of Kaleidoscope test mixture displaying a region of focused proteins around 5mm along the separation channel (~650px) after 92mins. A sharp band is also visible at around 20mm (2600px) from 52mins.



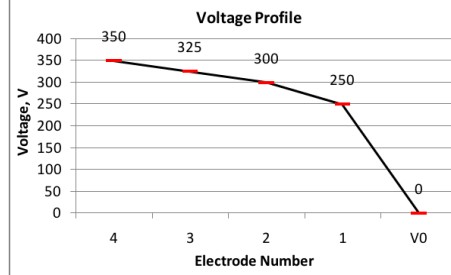
G=130

65



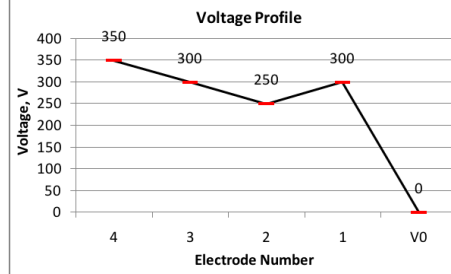
1.0

85



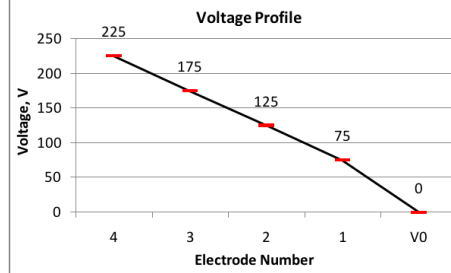
1.0

90



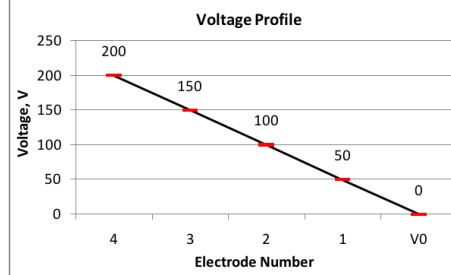
1.0

125



1.0

135



1.0

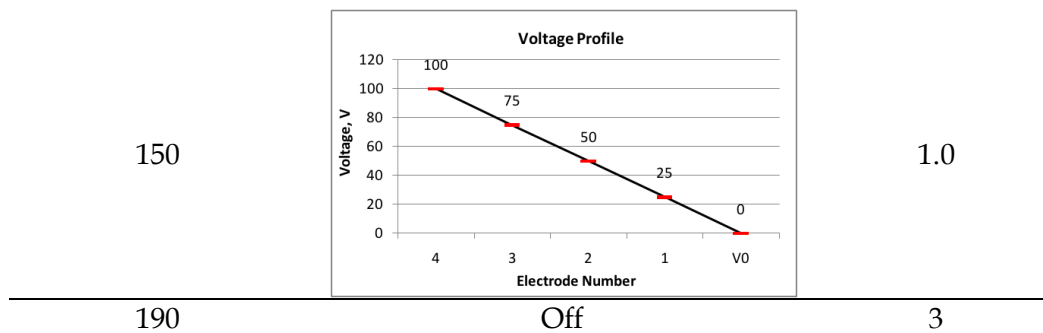


Table 3.3.9. Table of voltage profiles and flow rates for the repeat separation of the kaleidoscope test mixture using the optimised microfluidic DFGF.

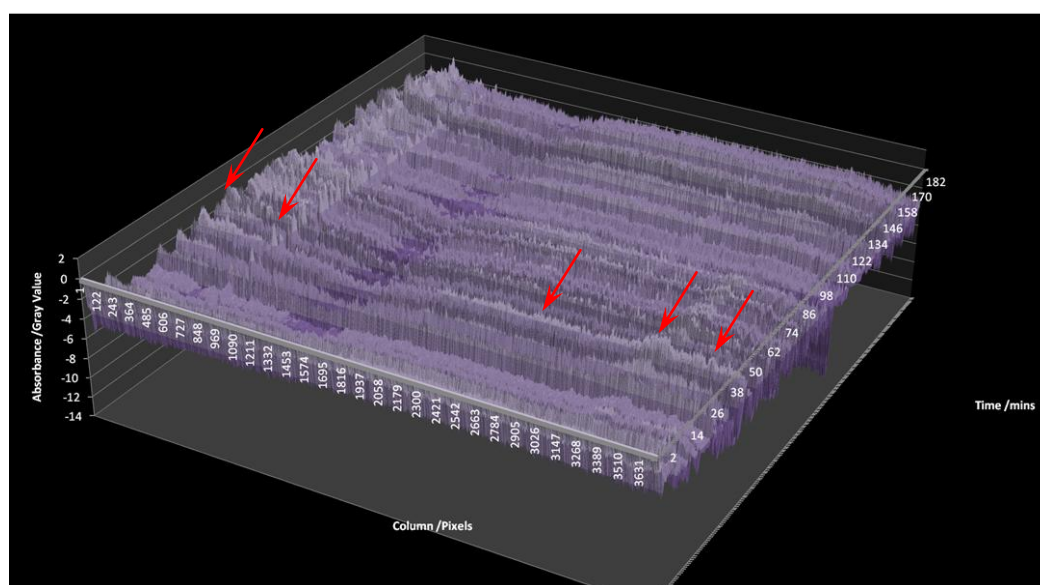


Figure 3.3.29. Separation of the kaleidoscope test mixture using the optimised microfluidic DFGF with enhanced imaging. Five bands are visible on the graph which indicated a partial separation of the protein mixture.

Despite the significant improvements to the imaging across the separation channel by reflectance there were still major issues. Aside from being limited to samples which absorb light in the visible range of the spectrum the reliability and reproducibility of the detector were often the root cause of imaging issues as interference can be caused by any small fluctuation of light level in the vicinity of the device.

The poor resolution in the detection of the bands of analyte in figure 3.3.28 was attributed to the rising base line in the time axis (z-axis). This increase was caused by an unstable light source. The repeat of the experiment did not show this baseline interference and displayed faint peaks where the components of the kaleidoscope mixture were partially separated and focused. However, the sensitivity of reflectance detection is fundamentally limited by the small size of the channel and the extreme difficulty in configuring the system to capture clear images. Also referring back to the specifications of the microfluidic DFGF device, a recess was left on the face of the device for a Photo Diode Array (PDA) detector to be utilised.

3.3.14 PDA Detection

Whole on column UV Detection has been studied previously with the Ivory DFGF device²⁹. In this case the packing material was manufactured to absorb and emit light from the source. Detection of analytes was achieved by fluorescence quenching. A digital camera was used to collect the images and the data collected from these images using ImageJ as in figure 2.2.10 in Chapter 2. Moving away from using data from exposures captured by a digital camera, a Toshiba TC101 PDA detector, figure 3.3.30, was implemented to acquire data from separations. This also involved the implementation of bespoke software to run the PDA and controller board.

The software written in C#, figure 3.3.31, gave the user full control over the detector using the parameters shown in table 3.3.10.

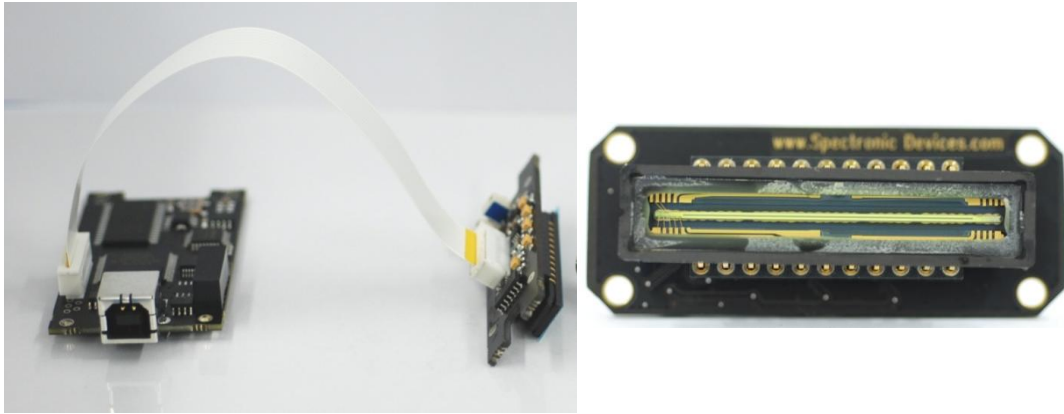


Figure 3.3.30. Toshiba TC101 PDA Detector.

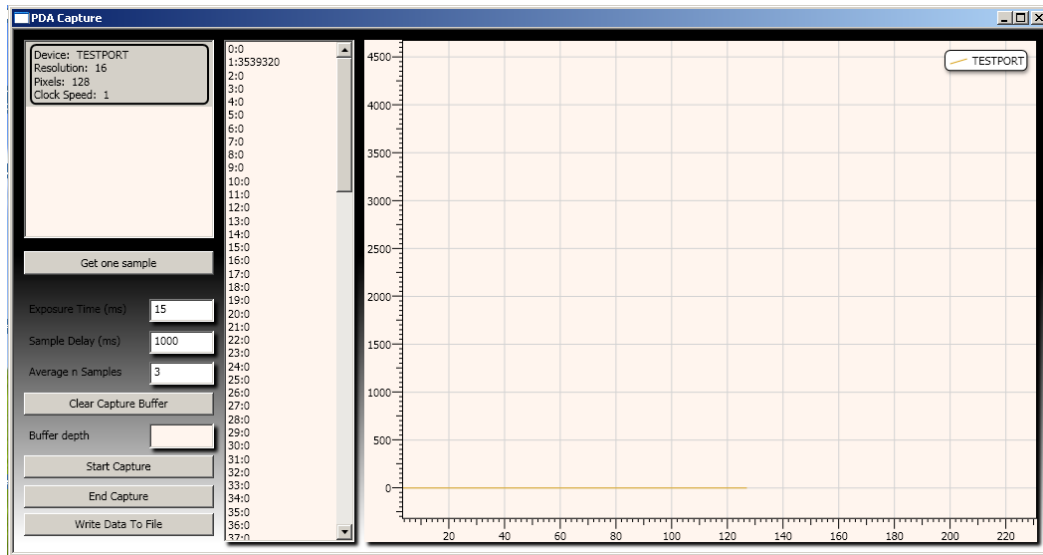


Figure 3.3.31. PDA software user interface with option to collect single samples or collect a sequence which are stored in the capture buffer before writing to a *.CSV file.

Parameter	Description
Exposure time	The exposure time in milliseconds is the time for which measurements from the diodes will be recorded in the memory of the device.
Sample Delay	Sample delay, also in milliseconds, is the time between the sample of measurements taken from the PDA device.
Average samples (n)	Average samples is the number of measures which will be recorded before being averaged to give a sample.
Save	Saves the multiple samples stored in the memory buffer as a *.CSV file to be interpreted by data handling software.

Table 3.3.10. Summary of controlling parameters and features available in data acquisition from the PDA using the bespoke software.

With the capability to acquire the data from the PDA, and adjust the data capture method, the PDA detector was configured with the DFGF as shown in figure 3.3.32.

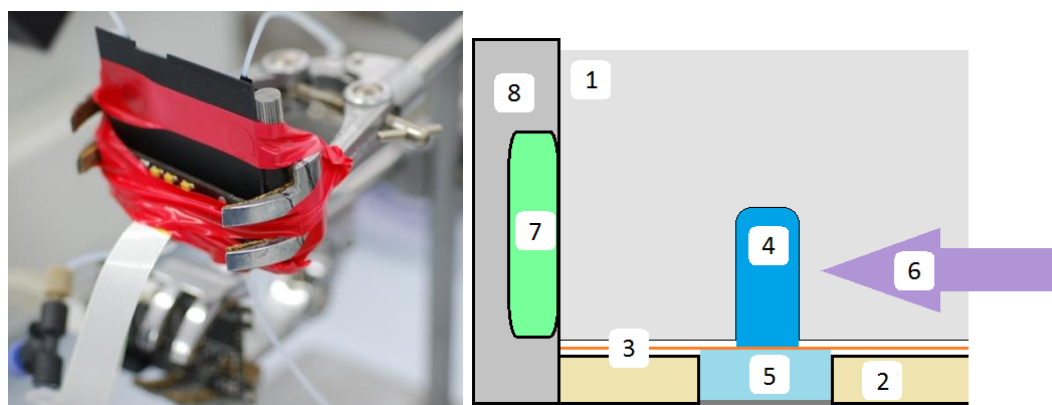


Figure 3.3.32. PDA DFGF configuration using ambient light. Left: Image illustrates the setup. Right: Cross section of the chip and the PDA. 1) Separation channel chip 2) Gasket Holder 3) Membrane 4) Separation Channel 5) Electrode Channel 6) Incident Light from source 7) Photo Diode Array. 8) Detector Housing.

In order to obtain the greatest signal from the detector the light source was required to almost saturate the detector. Therefore, when a sample absorbs light there will be a range of absorbance over the full range of the detector.

A limiting factor of this detection method is the narrow path length of the light before it reaches the detector. In this case the cell width is defined as the width of the separation channel at only 100 μm . This issue is overcome by taking a high number of readings and taking the average, resulting in a higher signal to noise ratio. Plotting the data collected from the PDA was done using the same Microsoft Excel system used to plot the data interpreted from images.

As detailed above in table 3.3.9 the PDA software exports an array of acquired data in comma spaced variable (*.csv) file format.

The data from these *.csv files was plotted to give the same type of graphs obtained from reflectance measurements. A notable difference is that using the PDA detector provides a more stable plot over the z-axis of time as interference is reduced by detecting more uniform light in exactly the same position. The first graph from the PDA detector was a sequence of data collected of the separation channel while empty. Then, the capture paused for three markers to be added to the channel, and the data acquisition was started again. This produced the graph in figure 3.3.33.

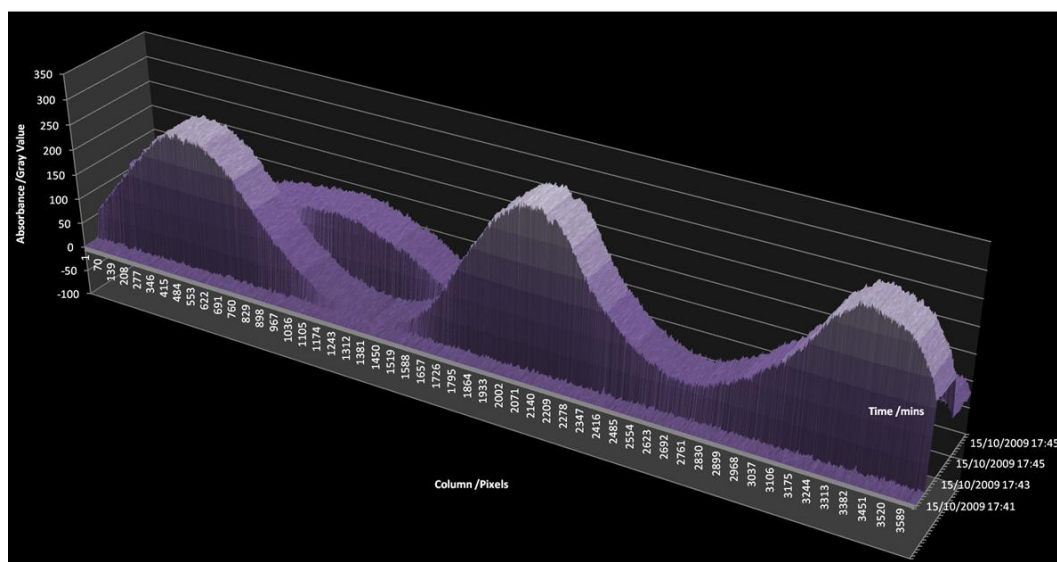
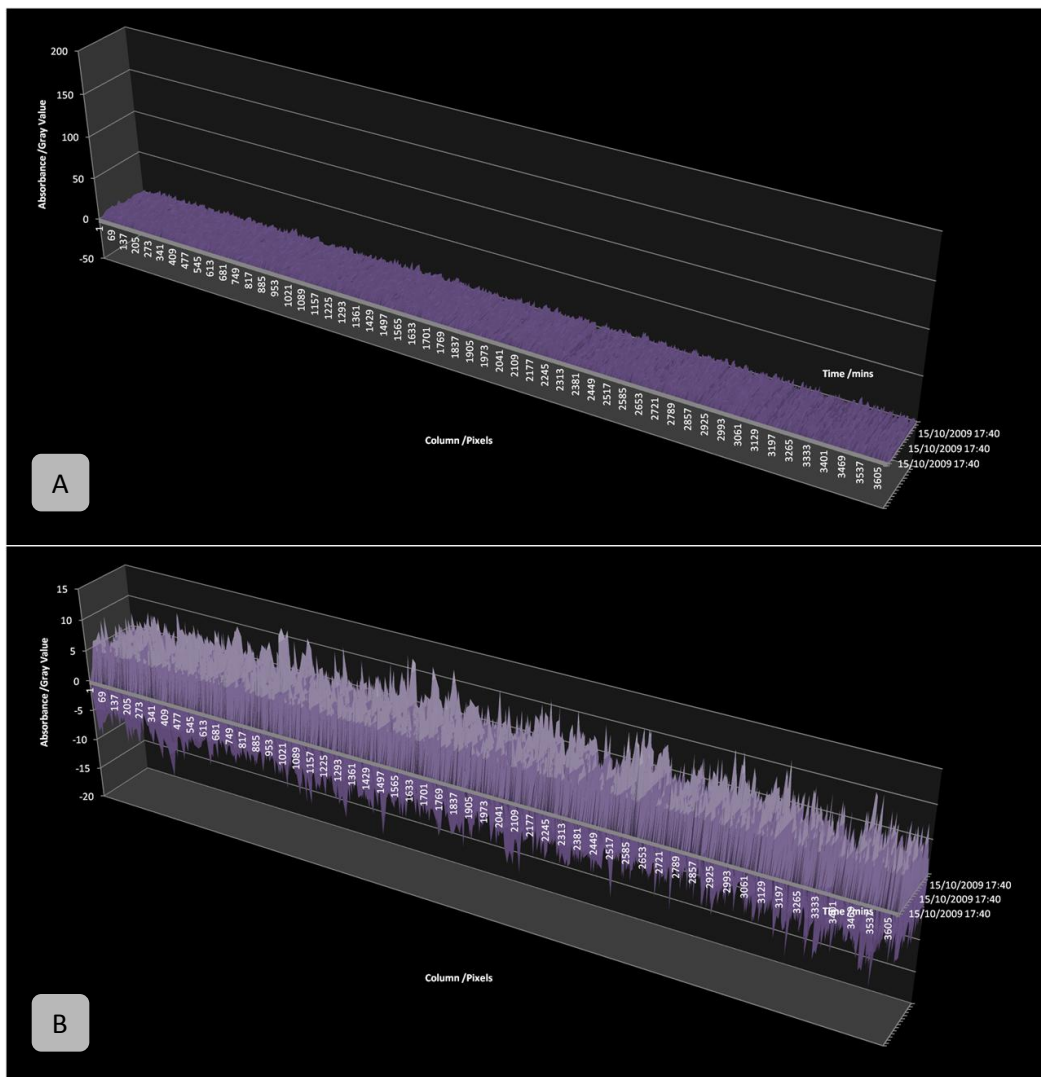


Figure 3.3.33. PDA detector graph showing three peaks corresponding to the three markers on the separation channel.

This preliminary test indicated that the detector had detected the three marks made on the separation channel corresponding to the three 'peaks' displayed on the graph in figure 3.3.33. Using ambient light was satisfactory to assess the functionality of data capture. However, for accurate and reproducible detection of analytes, a stable light source was sought.

Some initial ideas included the use of: 1) a laser line light source; 2) a bar code scanner; and 3) a liquid crystal display (LCD) backlight. The standard set up for these experiments was to have the system contained in a dark box to eradicate any interference from other light sources. The detector was configured with each of the light sources. With each one, samples were taken every second for 1min, yielding the data plotted in figure 3.3.34. What is expected is a flat uniform baseline along both the x-axis and z-axis. From the graphs in figure 3.3.34 it is clear that the backlight from an LCD was the most stable.



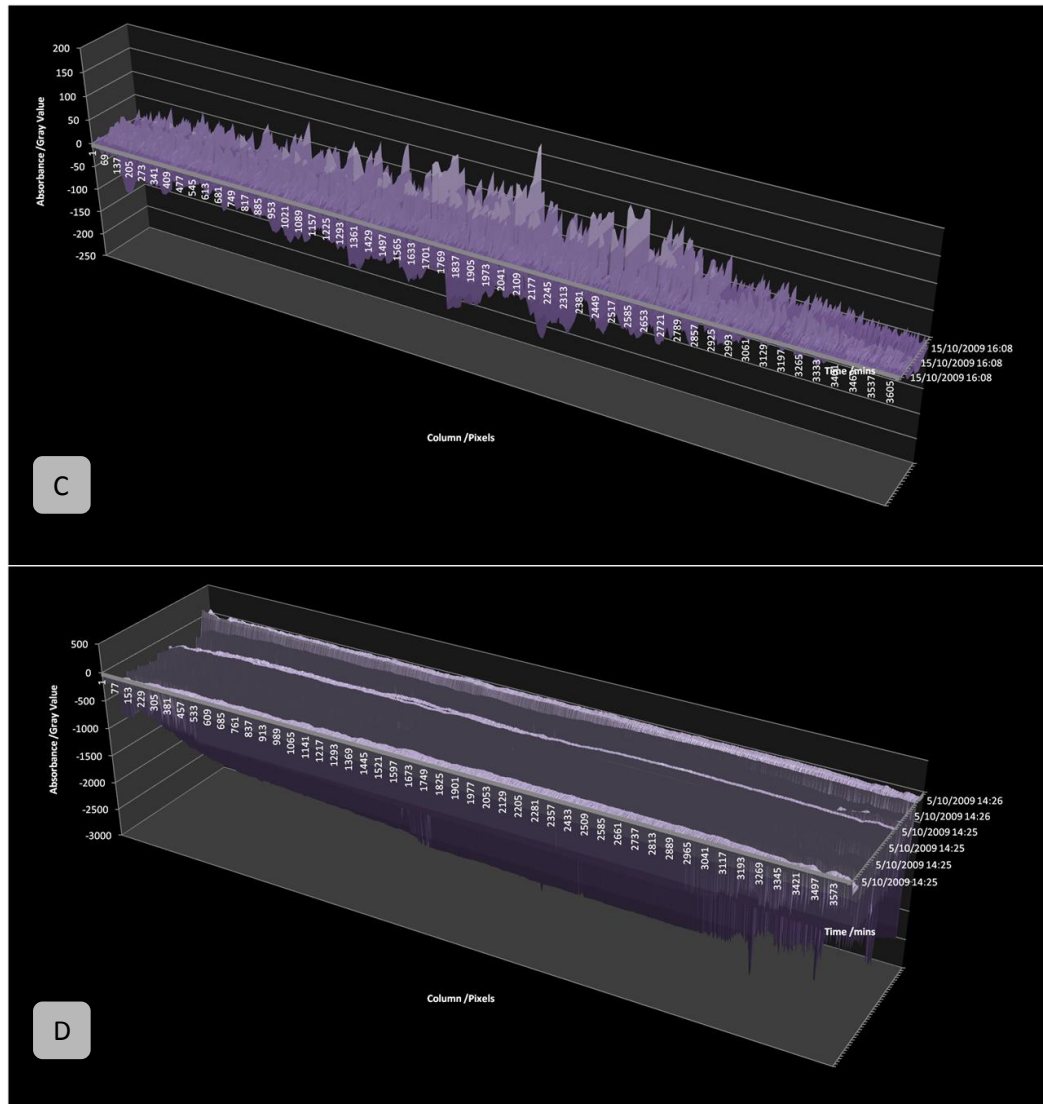


Figure 3.3.34. PDA Light sources A) LCD Backlight (y axis adjusted for comparison) B) LCD Backlight. C) Laser line source D) Barcode scanner

Initial separations monitored with the PDA in a visible mode were carried out using the LCD back light. Continuing with the aim of separating the Kaleidoscope test mixture, the following experiment shows the results of monitoring the separation of the Kaleidoscope test mixture using the PDA and PDA software.

The PDA detector settings were set as shown in table 3.3.11. The microfluidic DFGF device was setup with 500MWCO membrane and the 200 μ m electrode channel sealed with vacuum grease and automotive instant gasket. During this experiment the electrode channel was set to a flow rate of $\sim 2\text{mlmin}^{-1}$. The conditions applied to the separation channel are shown in table 3.3.12. This separation of the Kaleidoscope test mixture is presented in figure 3.3.35.

Parameter	Setting
Exposure time	125ms
Sample Delay	60000ms
Average samples (n)	20

Table 3.3.11. Optimum PDA Detection parameter using the LCD backlight.

Time (mins)	EFG (Vcm^{-2}) and Voltage Profile	Flow(μLmin^{-1})												
1	<p style="text-align: center;">G=150</p> <table border="1"> <caption>Voltage Profile Data (1 min)</caption> <thead> <tr> <th>Electrode Number</th> <th>Voltage, V</th> </tr> </thead> <tbody> <tr> <td>4</td> <td>540</td> </tr> <tr> <td>3</td> <td>486</td> </tr> <tr> <td>2</td> <td>378</td> </tr> <tr> <td>1</td> <td>216</td> </tr> <tr> <td>V0</td> <td>0</td> </tr> </tbody> </table>	Electrode Number	Voltage, V	4	540	3	486	2	378	1	216	V0	0	1.0
Electrode Number	Voltage, V													
4	540													
3	486													
2	378													
1	216													
V0	0													
30	<table border="1"> <caption>Voltage Profile Data (30 min)</caption> <thead> <tr> <th>Electrode Number</th> <th>Voltage, V</th> </tr> </thead> <tbody> <tr> <td>4</td> <td>350</td> </tr> <tr> <td>3</td> <td>325</td> </tr> <tr> <td>2</td> <td>300</td> </tr> <tr> <td>1</td> <td>275</td> </tr> <tr> <td>V0</td> <td>0</td> </tr> </tbody> </table>	Electrode Number	Voltage, V	4	350	3	325	2	300	1	275	V0	0	1.0
Electrode Number	Voltage, V													
4	350													
3	325													
2	300													
1	275													
V0	0													

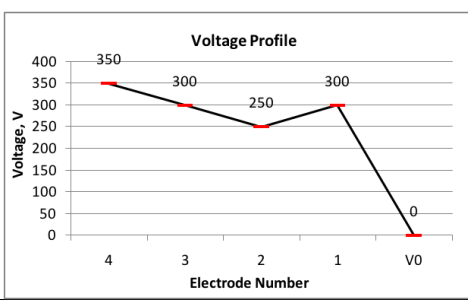
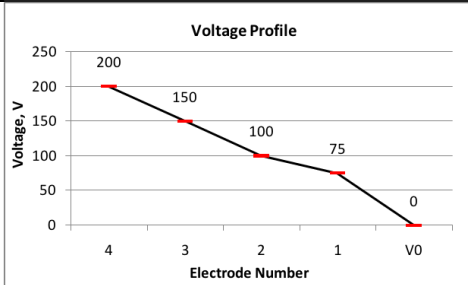
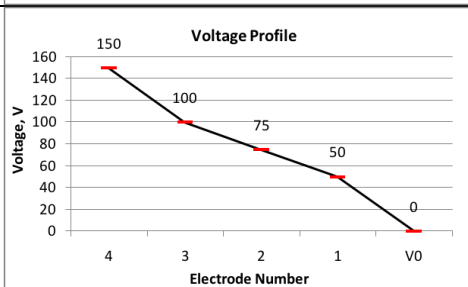
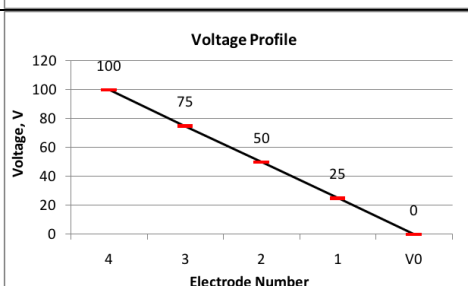
50		1.0
70		1.0
90		1.0
100		1.0
130	Off	3

Table 3.3.12. Separation of the kaleidoscope mixture detected with the PDA detector in figure 3.3.35.

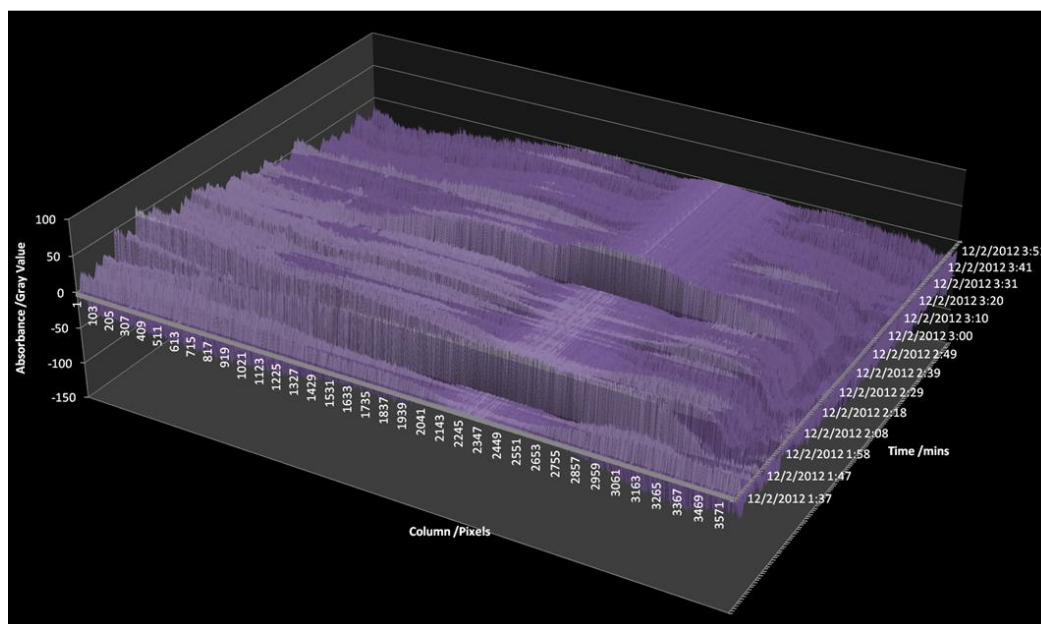


Figure 3.3.35. Separation attempt of the Kaleidoscope protein mixture using the conditions in table 3.3.12. Faint areas of protein are observed with a stable baseline.

Having monitored separations of stained protein mixtures using light in the visible range, a UV source was required to facilitate the detection of samples transparent to visible light. A 254nm UV mercury light source was extracted from a Waters 440 absorbance detector. This was mounted on an optics rail and focused into a beam to illuminate an area 2mm x 30mm across the back of the separation channel. The setup was enclosed in a dark box and the data acquisition, DAQ, for the PDA detector was run for 10minutes. A standard HPLC test mixture, which contained a mixture of UV absorbers, was injected directly into the channel. Data collection from the PDA detector was continued for an addition 10minutes. The data collected was then plotted showing the results in figure 3.3.36.

From this graph it observed that the detector has indeed detected the injection and diffusion of the test mixture using the 254nm source.

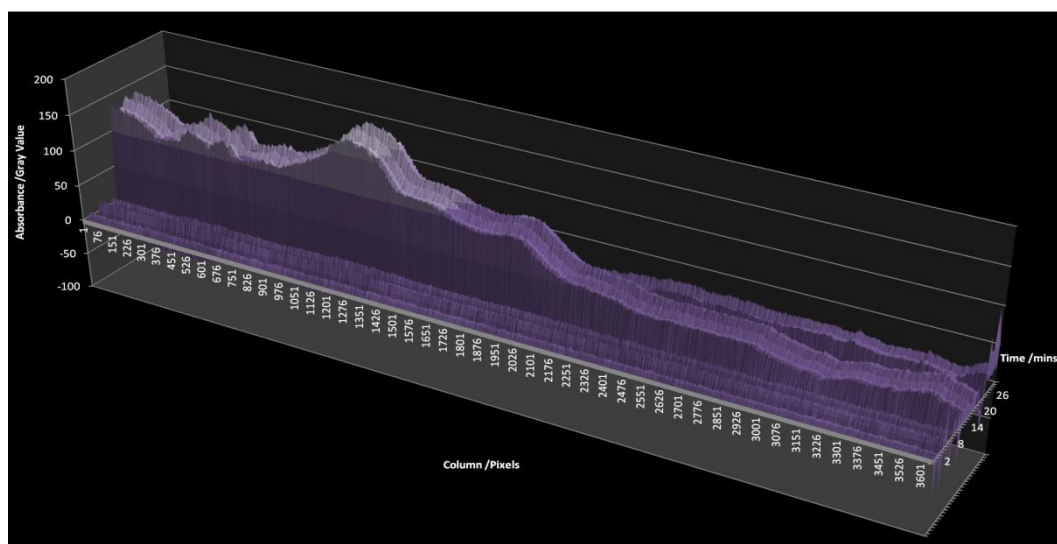


Figure 3.3.36. Test displaying the introduction of a Test mixture into the separation channel. The gradual decrease in the response was caused by the diffusion of the mixture along the channel.

After this initial experiment the mercury UV light source was used to illuminate the device with the buffer solution flowing through. The measurements from the PDA detector were not consistent, indicating a problem. The configuration of the PDA software was altered in an attempt to minimise the affect of fluctuation in the light source. The configurations used and results of these changes are presented in table 3.3.13. However the light source had become too unstable to use in detection.

This could have been caused by either the power supply or the deterioration of the mercury lamp itself. Modern detection systems incorporate a variety of stability hardware to counteract shock noise and other fluctuations in the power supply and output wavelength.

**PDA
Sampling
Parameters** **Setting** **Graph of baseline**

Exposure time	30	
Sample Delay	60000	
Average samples (n)	20	
Exposure time	60	
Sample Delay	60000	
Average samples (n)	40	
Exposure time	1	
Sample Delay	60000	
Average samples (n)	1	
Exposure time	125	
Sample Delay	60000	
Average samples (n)	20	

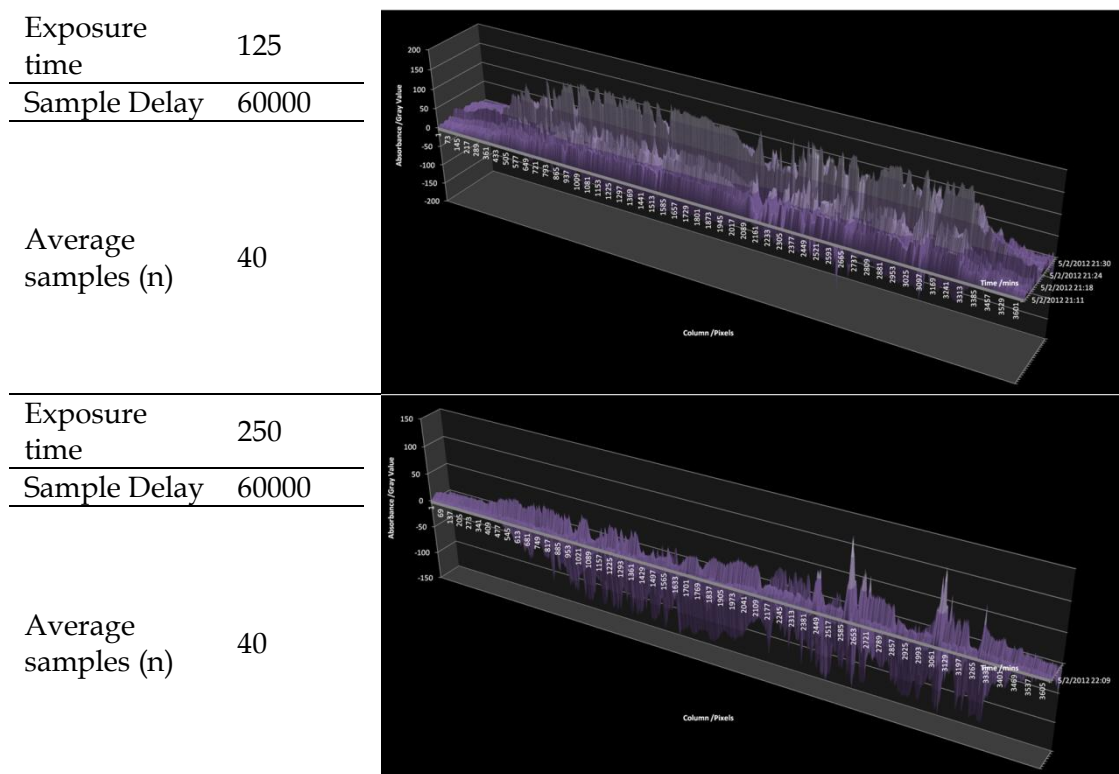


Table 3.3.13. Samples taken with the UV light source. Detection settings were altered to stabilise the baseline. However, stability issues were observed indicating power supply or bulb flaws.

3.4 Conclusions

Advances have been made in the functionality, control and feedback from the microfluidic DFGF. Initial testing with the mixture of BPB and AM identified faults with the design most notably the failure of the electrodes and the sample leakage issues. Despite these problems the initial testing of the device saw a successful separation of a two component test mixture with whole column detection without the need for a packing material or monolith. This preliminary testing clearly proved the design as a successful microfluidic device for DFGF.

The development of hardware which integrated the microfluidic DFGF device with the existing Protasis DFGF supporting equipment were successful and continued to be reliable throughout the experiments in this chapter.

The innovative design ensured that fluid connections were made with appropriate standard Upchurch fittings requiring only the implementation of a sleeve connection the DFGF to the 6-port injection valve. Utilising the approach from the first generation Ivory device, all the electrode connectors used IDC connectors to enable ease of connection to the Protasis power supply, using hardware already available. As the electrode connection developed, the need for a separate connector was made redundant by the final Platinum foil electrodes with the connector integrated as into a single component. The electrodes themselves advanced with the working gold electrodes performing a separation of a three component test mixture before expiring, leading to further development. Utilising the RP approach to build a sputtering mask enabled the conclusive testing of a second attempt at platinum electrodes manufactured by PVD. However, with the complications in the connection of these electrodes and the poor resistance to failure, the conclusion was that electrodes made using PVD were not at all suited to applications in DFGF. This led to the production of the final electrode array featuring platinum foil electrodes inlaid in the glass electrode chip. These electrodes performed the later separations with the Kaleidoscope protein test mixture and various dye mixtures.

Following on the employment of RP for the PVD mask, the sample leakage issues were addressed. With a simple narrow, RP, Teflon, channel prototype fully integrated, replacement components for the 'Gasket Holder' were put into operation. This led to the experimental determination of a suitable electrode channel width of 200 μ m, as the issue was still observed to a greater extent with wider channels. With the narrower 100 μ m electrode channel further issues with forming a reliable seal and the channel becoming blocked were observed.

While developing the optimised system the improvements made to the detection method in this chapter saw the improvement of reflectance measurements by innovations in light sources and modification of the microfluidic DFGF itself. Refined imaging with the digital camera by using a diffuse light source, the 'black-out' chip and rotating the device to run in an inverted position enabled further advancement in detection by implementing the whole-on-column PDA detector. This detector monitored the separation of the two component system test of BPB and AM and the partial separation of the Kaleidoscope test mixture. From achieving this working detection the utilisation of the custom built UV light source has produced results from the first UV whole on column detection data with DFGF. It is unfortunate that the stability of the UV light source suffered resulting in instability. Further work with this system would enable the correlation of fluctuations in light levels with the detector to enable a calibrated detector with a higher sensitivity.

These developments have moved the technology towards a stable platform for a new commercial instrumentation in chromatography. With the use of RP and outside collaborations the finalised new chip has enabled research in applications of the system.

3.5 References

1. G. Velve-Casquillas, M. Le Berre, M. Piel, and P. T. Tran, *Nano today*, 2010, **5**, 28–47.
2. G. M. Whitesides, *Nature*, 2006, **442**, 368–73.
3. N. T. Tran, I. Ayed, A. Pallandre, and M. Taverna, *Electrophoresis*, 2010, **31**, 147–73.
4. Y. Li, D. L. DeVoe, and C. S. Lee, *Electrophoresis*, 2003, **24**, 193–9.
5. C. Das and Z. H. Fan, *Electrophoresis*, 2006, **27**, 3619–26.
6. J. Wen, E. W. Wilker, M. B. Yaffe, and K. F. Jensen, *Analytical chemistry*, 2010, **82**, 1253–60.
7. K. S. Yang, P. Clementz, T. J. Park, S. J. S. Y. Lee, J. P. Park, and D. H. Kim, *Current Applied Physics*, 2009, **9**, e66–e70.
8. Y. Cong, Y. Liang, L. Zhang, W. Zhang, and Y. Zhang, *Journal of separation science*, 2009, **32**, 462–5.
9. D. Kohlheyer, G. A. J. Besselink, S. Schlautmann, and R. B. M. Schasfoort, *Lab on a chip*, 2006, **6**, 374–80.
10. L. Wang, L. A. Flanagan, E. Monuki, N. L. Jeon, and A. P. Lee, *Lab on a chip*, 2007, **7**, 1114–20.
11. J. Zhu, T.-R. J. Tzeng, and X. Xuan, *Electrophoresis*, 2010, **31**, 1382–8.
12. K. Khoshmanesh, C. Zhang, S. Nahavandi, S. Baratchi, A. Mitchell, and K. Kalantar-zadeh, *Electrophoresis*, 2010, **31**, 3380–90.
13. C. Iliescu, L. Yu, G. Xu, and F. E. H. Tay, *Journal of Microelectromechanical Systems*, 2006, **15**, 1506–1513.
14. F. Du, M. Baune, a. Kück, J. Thöming, A. Kuck, and J. Thoming, *Separation Science and Technology*, 2008, **43**, 3842–3855.
15. J. Liu, X. Sun, P. B. Farnsworth, and M. L. Lee, *Analytical Chemistry*, 2006, **78**, 4654–4662.
16. R. K. Anand, E. Sheridan, D. Hlushkou, U. Tallarek, and R. M. Crooks, *Lab on a chip*, 2011, **11**, 518–27.
17. Z. Huang, Washington State University, 2001.
18. P. Myers and K. D. Bartle, *Journal of Chromatography A*, 2004, **1044**, 253–258.

19. Bio-Rad, *www.bio-rad.com*, 161-0324 Kaleidoscope Prestained Standards (broad .
20. Dolomite, *http://www.dolomite-microfluidics.com/*, Dolomite Microfluidics.
21. L. K. Blair and W. G. Grot, 1969.
22. S. Chabi and M. Kheirmand, *Applied Surface Science*, 2011, **257**, 10408-10413.
23. Pine Research Instrumentation, *Technical Note*, 2005, **1**, 1-5.
24. Roland, *http://www.rolanddg.com/product/3d/3d/mdx-20_15/mdx-20_15.html*, Roland Modella MDX-20.
25. C. W. Hull, 1986, 4,575,330.
26. F. P. W. Melchels, J. Feijen, and D. W. Grijpma, *Biomaterials*, 2010, **31**, 6121-30.
27. P. R. Chalker, K. M. Berggreen, J. Singh, A. T. Clare, and C. J. Sutcliffe, *Solid State Phenomena*, 2009, **154**, 1-7.
28. Envisiontec-R05, *http://www.envisiontec.de/index.php?id=54*.
29. R. J. Ansell, P. G. Tuñón, Y. Wang, P. Myers, C. F. Ivory, J. N. Keen, and J. B. C. Findlay, *The Analyst*, 2009, **134**, 226-9.

Chapter 4. Applications using the microfluidic DFGF

4.1 DFGF Applications

Demonstrations of successful focusing and indeed separations of samples with the optimised microfluidic DFGF, indicated the system was operating effectively and with sufficient stability to experiment with novel applications of the device in both samples and integration with existing analytical equipment. One of these novel separations was that of a mixture of functionalised Gold Nanoparticles. Integration of the microfluidic DFGF with contactless conductivity detection and post column UV detection gave preliminary results which provide the factors for consideration to facilitate integration with a range of post device detection systems. Following this the microfluidic DFGF device was configured with a Thermo Fisher Scientific two dimensional High Performance Liquid Chromatography and Mass Spectrometry system.

4.2 Functionalised Gold Nano Particle Separation

Being a fundamental element, gold, known for being an unreactive metal and found naturally occurring in pure elemental form, has been used in medicinal practice for centuries. Gold nano particles, though known before this, were first reported in scientific literature by Michael Faraday in 1857. Faraday described “Fine Particles” which were synthesised by aqueous reduction of gold chloride with phosphorus in the presence of stabilising agent carbon disulfide yielding a “Ruby Red Fluid”¹.

Research with gold nano particles has continued throughout history. However, it is only in the last decade, with the advancements in electronics and medical technologies, that the unique electronic and cellular interactive properties of these macromolecular structures have been realised. Current research focuses on the application of GNPs with drug delivery and targeted cancer treatments². With utilising these particles for specific tasks functionalisation of the surface is required. The sample of functionalised gold nano particles donated by the M. Brust group were synthesised for the application of cell uptake using the Turkevich-Frenz procedure and stabilised with trisodium citrate³. The particle size distribution of these particles was determined by analytical centrifugation (CPS). The CPS data for the supplied sample shows that the particles have a size distribution centring at 12nm and 17nm, with some larger particulates from the distribution shown in figure 4.2.1

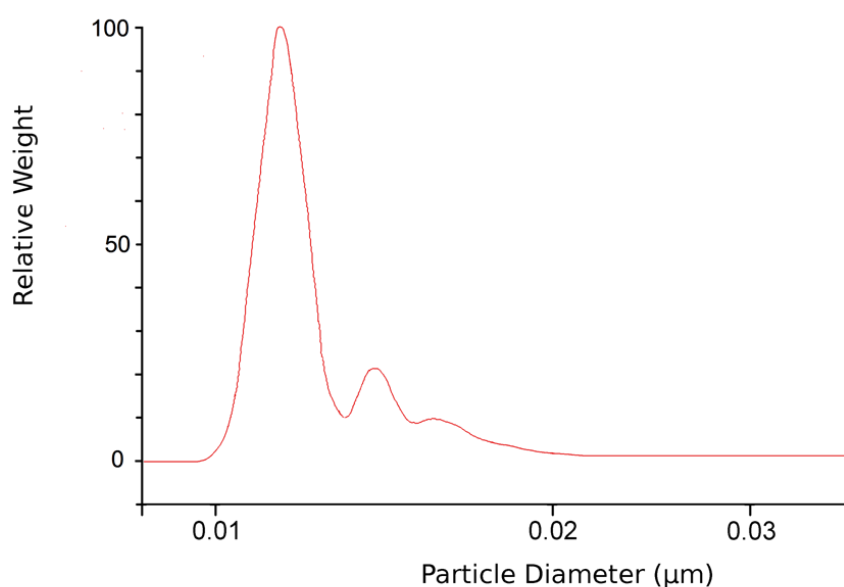


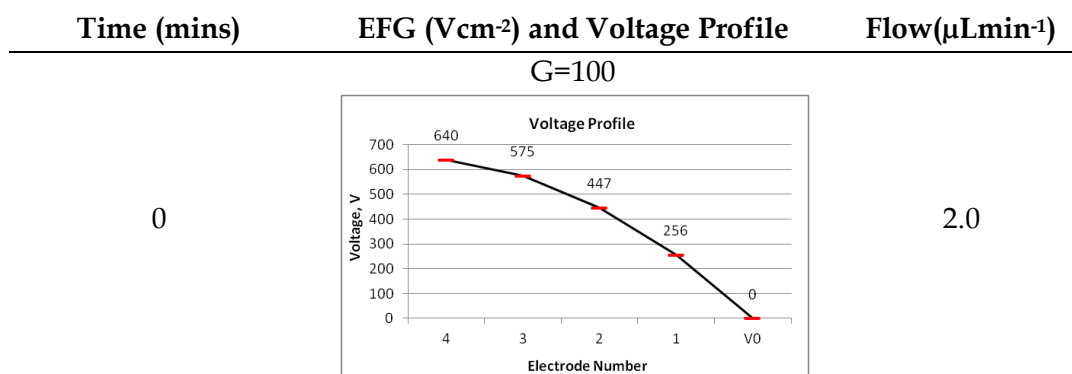
Figure 4.2.1. Analytical centrifugation of the functionalised gold nano particles.

Though these applications for uses of GNP have developed, there are limitations associated with the separation and purification of these macro molecular structures, especially when the surface has been functionalised⁴.

As these GNPs are charged and have a particle size distribution larger than the pore diameter of the membrane these species can be separated using DFGF. Recent publications show that nano particulates can be separated by CE⁵ which confirms that an electrophoretic technique is suitable for the separation of these GNPs.

4.2.1 Gold Nano Particle separation in a packed column using the first generation DFGF

Initially the first generation DFGF device was used to separate the mixture of GNPs. The device was packed as described in section 2.2.2 using the Bio-Rad polyacrylamide packing material⁶. The electrode spacing was set at 0.8cm and the applied voltages are shown in table 4.2.1. The results from this separation are shown in figure 4.2.2.



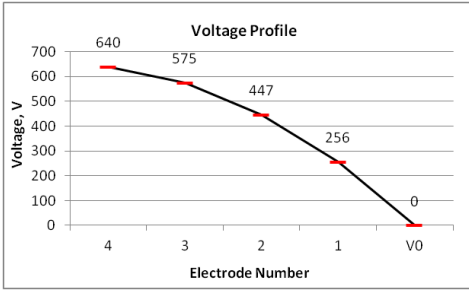
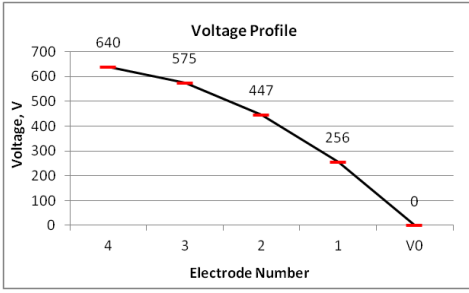
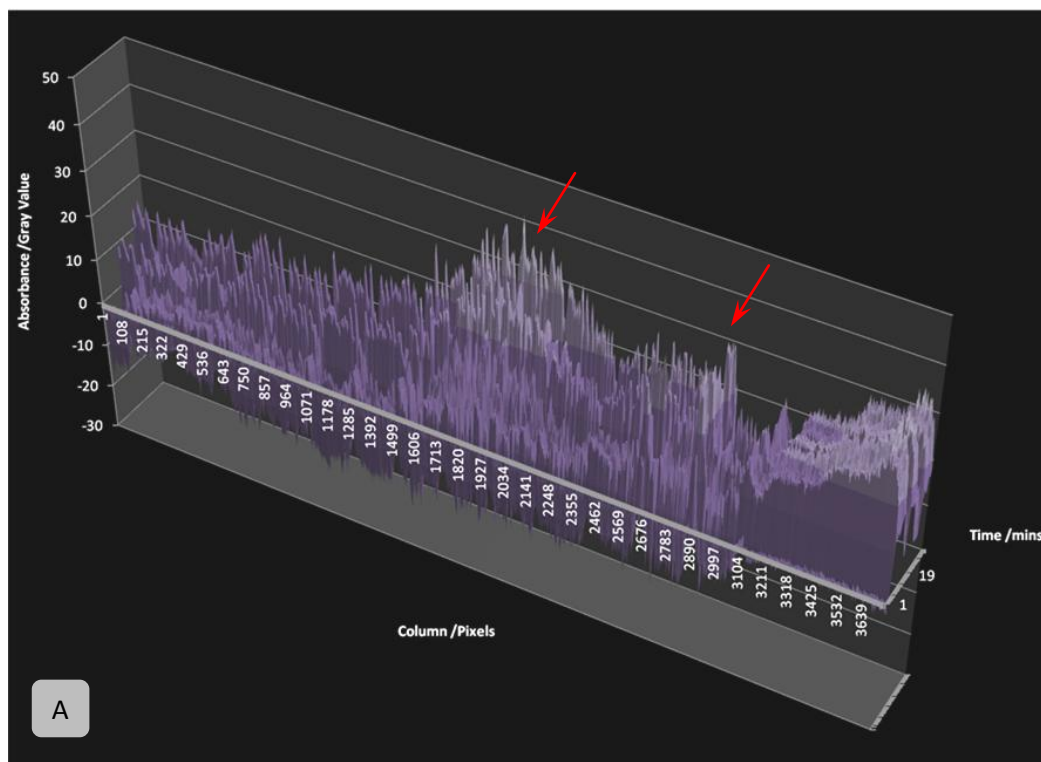
8	G=100 Voltage Profile 	1.0
16	G=100 Voltage Profile 	3.0
22	Off	5.0
45	Off	10

Table 4.2.1. Voltage profiles and flow rates applied to separate the functionalised GNPs.



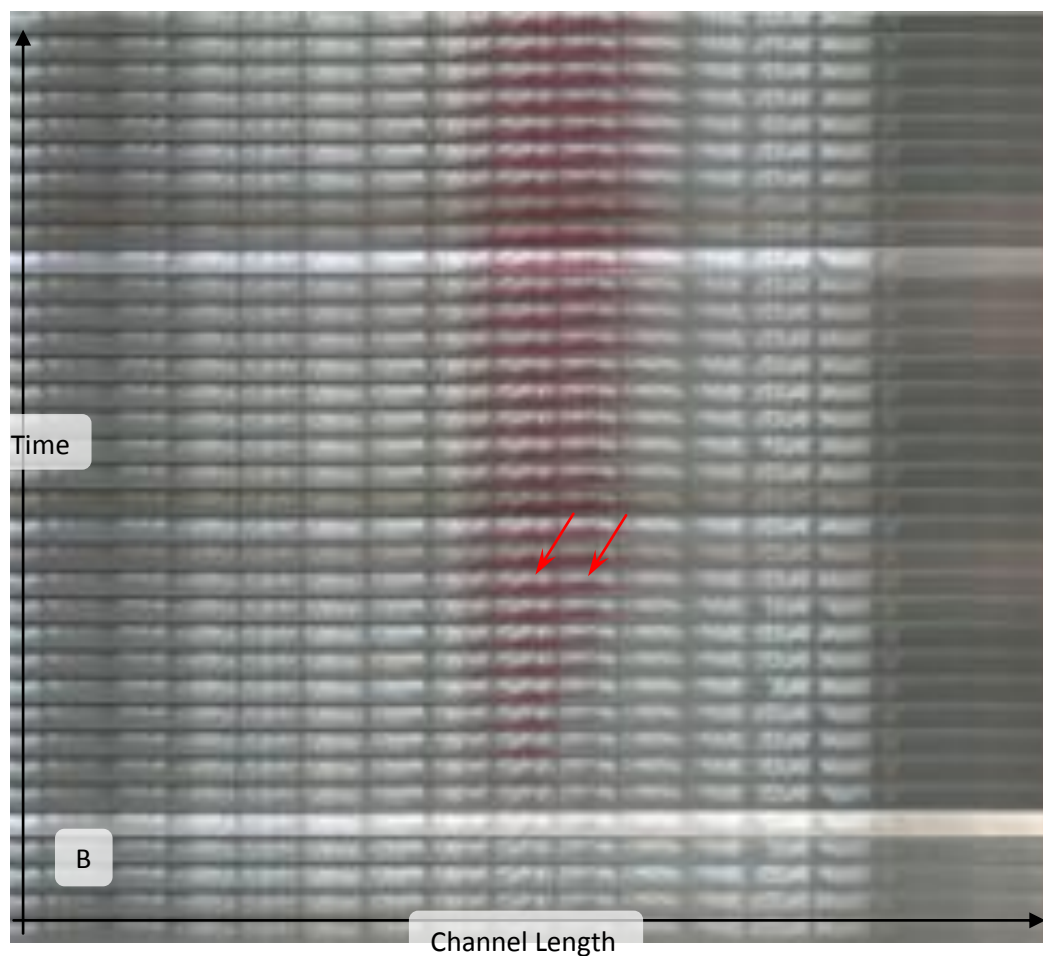


Figure 4.2.2. A) Graphical representation of the separation of the functionalised GNPs in the first generation DFGF device. B) Montage of the separation, two slightly more concentrated bands are visible in the larger band.

After 22mins the EFG was switched off and the flow rate was increased to the working maximum $10\mu\text{Lmin}^{-1}$ with a packed channel in an attempt to elute the GNPs from the device. Observing the graph in figure 4.2.2, the characteristic fading of the peaks and elution profile is not present. This is due to the GNPs attraction to the polyacrylamide. SEM of the packing material post separation shows the GNP's had bonded to the surface of the polyacrylamide spheres.

This analysis also gave a qualitative determination of the outcome of the separation determining that the two peaks corresponded to free nano particles and aggregates. As aggregated particles have less charge over the surface and have a higher hydrodynamic radius they migrated further along the separation channel. With a lower charge the retention of the EFG is less than that of single particles and with the higher hydrodynamic radius the hydrodynamic flow forces the aggregates further still along the column. The SEM results for the first and second peaks are shown in figure 4.2.3 for the first peak, and figure 4.2.4 for the second peak, corresponding to the dispersed GNPs and aggregates respectively.

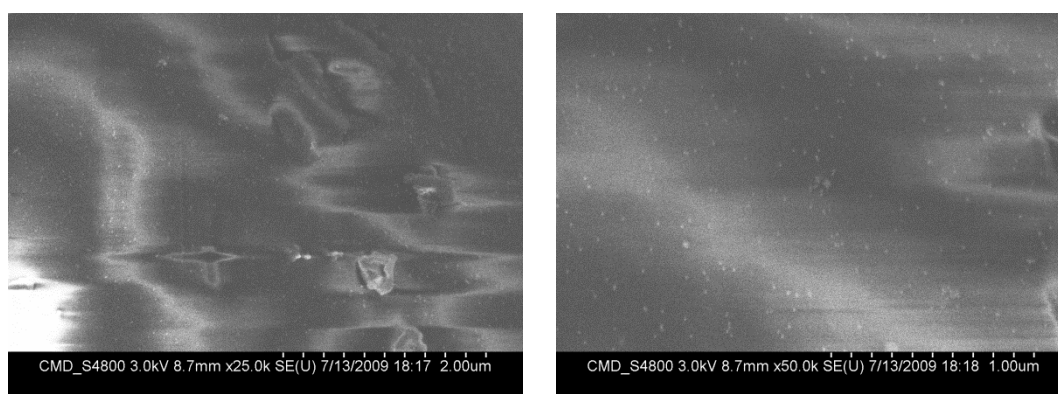


Figure 4.2.3. SEM of the packing material from the band 40mm along the channel displaying singular GNPs on the surface of the polyacrylamide spheres.

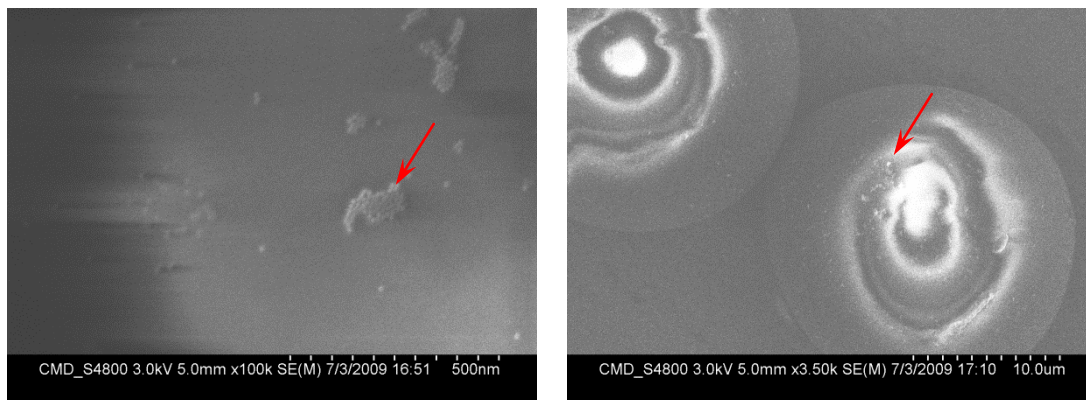


Figure 4.2.4. SEM of the packing material from the band 55mm along the channel displaying aggregates of the GNPs on the surface of the polyacrylamide spheres.

With approximate sizing from the SEM images it was clear that a degree of separation had been achieved. To perform the separation and successfully elute the GNPs, the microfluidic DFGF device was used as the main issue in the previous experiment was caused by the packing material.

4.2.2. Microfluidic DFGF GNP Separation.

The microfluidic DFGF was prepared following the method in section 3.3.3. using the 100MWCO membrane. The device was part way through the optimisation of the device hence the device is in the original orientation and the original PEEK 1mm electrode channel was used. Table 4.2.2 below details the voltage profiles and flow rates applied to the device.

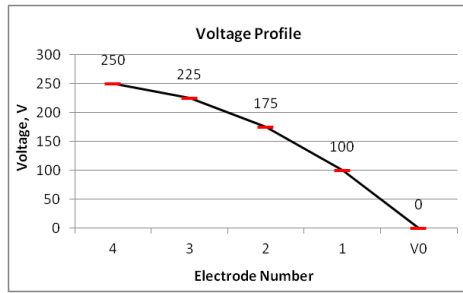
Time (mins)

EFG (Vcm^{-2}) and Voltage Profile

Flow($\mu Lmin^{-1}$)

G=100

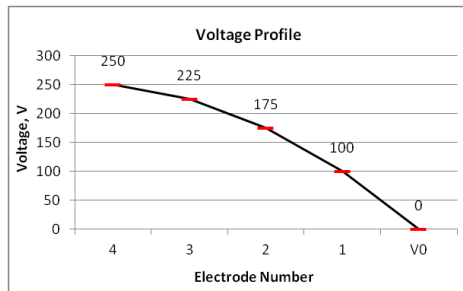
0



0.5

G=100

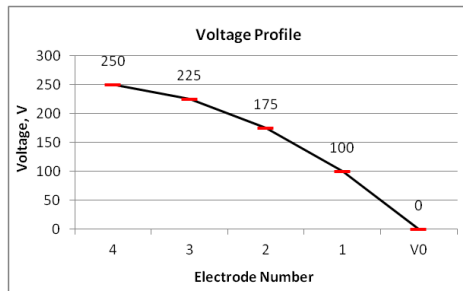
5



2.0

G=100

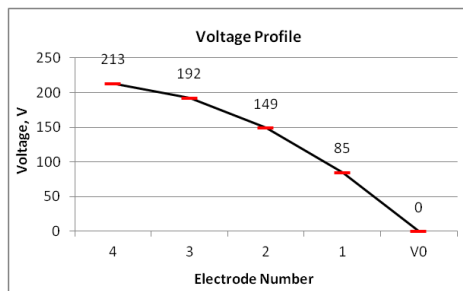
22



1.0

G=85

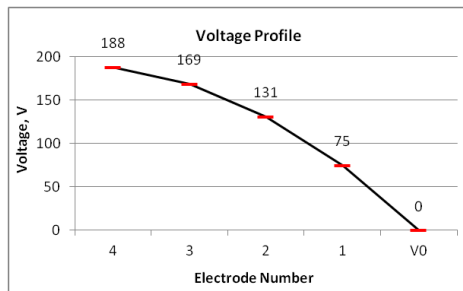
28



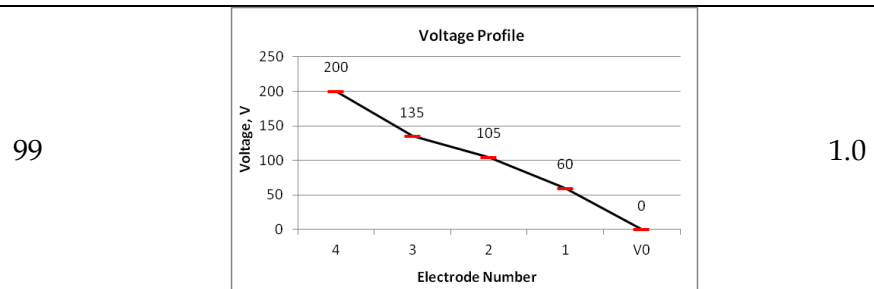
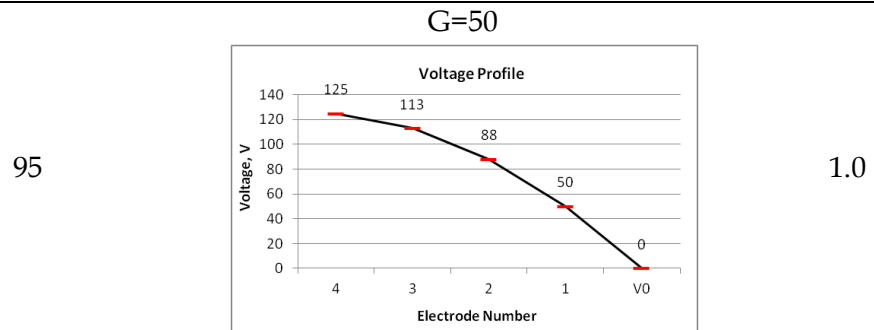
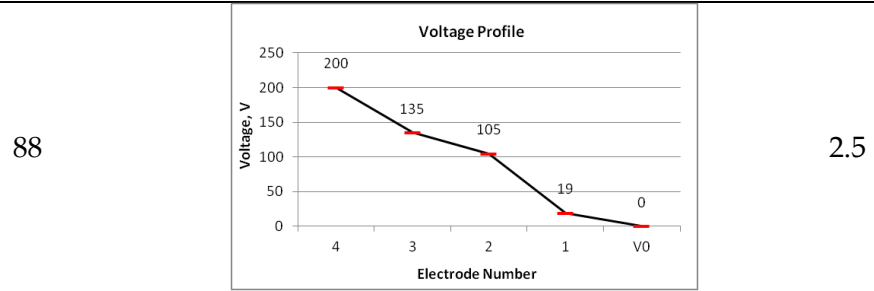
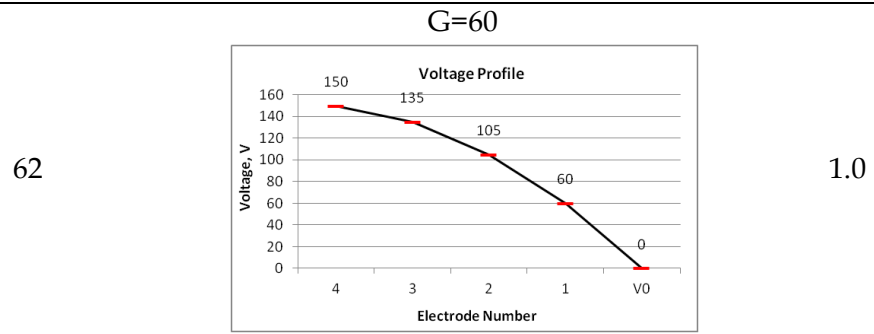
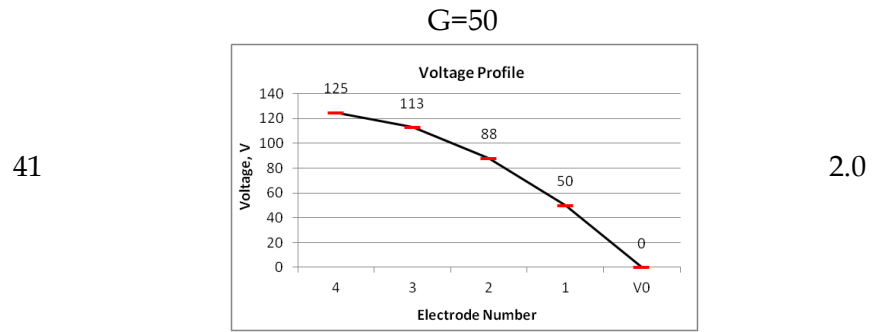
1.0

G=75

35



1.25



120		1.5
127		1.5
133	Off	2.0

Table 4.2.2. Parameters used in separating the GNPs in the microfluidic DFGF.

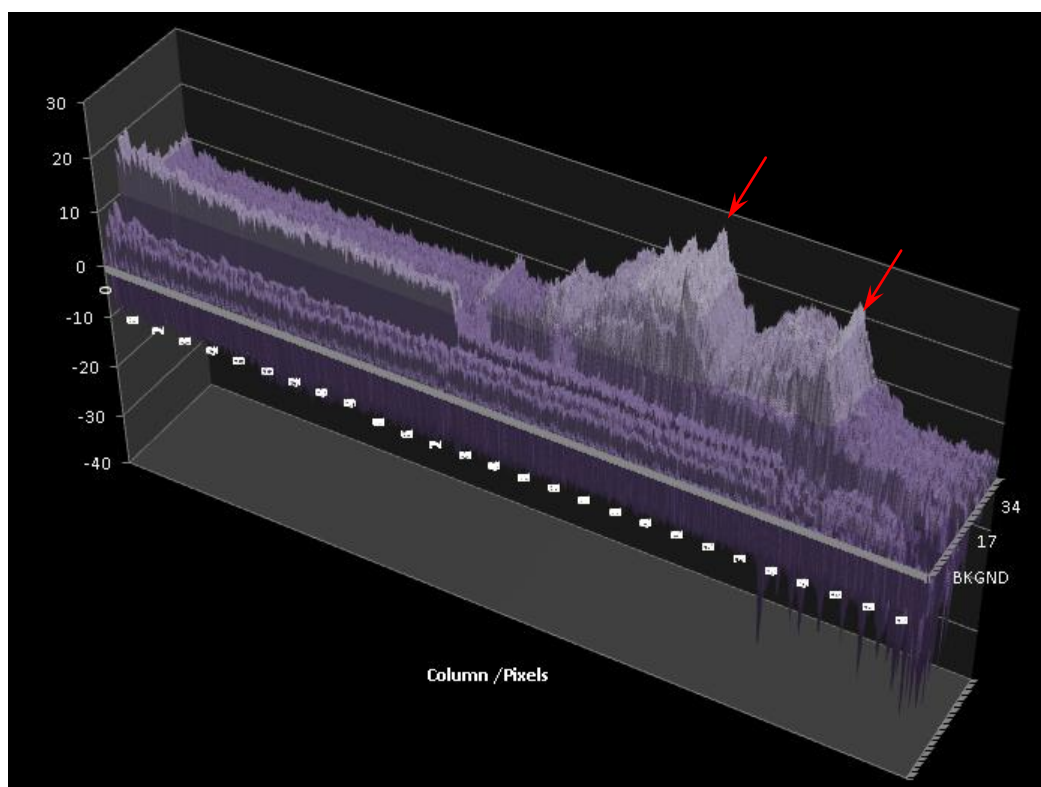


Figure 4.2.5. Open channel microfluidic DFGF separation of the GNPs. Two peaks (red arrows) corresponding to two bands of analyte which are the singular GNPs and aggregates respectively.

After the time points 25mins and 35mins, the EFG was lowered to enable to the sample to migrate further along the length of the channel with the aim of greater separation. This effect can be seen in the graphical representation of the separation in figure 4.2.5 at the respective time points. Once the separation had occurred resulting in two focused bands after 104mins, the voltage profile was applied to reduce the electric field at the end of the channel, allowing the aggregate band to elute from the device. However after a prolonged period inside the separation channel it was apparent that, despite alterations to the applied voltages, the focused bands had become immobilised. Alterations to the voltage profile resulted in the bands slightly changing shape, as in the tail would increase or decrease in the direction of lesser force. Even after switching off the power supplies and increasing the flow rate to $2.0\mu\text{Lmin}^{-1}$, the bands remained in the separation channel. Figure 4.2.6 shows the two focused bands with sample leaked outside of the confines of the separation channel. This observation further exemplifies the issues discussed with the wider electrode channel in section 3.3.7. The immobilisation of the sample was caused by some of the particles being pulled onto the membrane by the applied EFG. Furthermore, the sample which had been pulled from the separation channel was then trapped between the bottom edge of the chip and the membrane, making it impossible to elute from the device.



Figure 4.2.6. Image of the separation channel with the bands of GNP's and the aggregates. It is clear that the bands have flowed out of the separation channel.

Unfortunately, having dissected the membrane after the experiment it was not possible to characterise the GNPs on the membrane. The desired procedure was to take a sample of a section of the membrane and disperse some of the particles into a solution to analyse the particle size distribution by Dynamic Light Scattering. The result of this separation confirms that DFGF can indeed be utilised for the separation of nano scale samples. Though the sample was not successfully eluted it was separated efficiently and retained with the electric field. On the other hand, it is possible that some of the sample was eluted during the experiment further reinforcing the requirement of post column detection when testing the microfluidic DFGF.

4.3 Post column Detection

Having devised a detector to monitor the whole column of the microfluidic DFGF device under UV, it was necessary to analyse focused bands of analyte as they eluted from the device. Observing how well the sample elutes was the first step for integration with existing analytical technology, which has long been a suggested application for DFGF⁷. Additionally, as described above in section 4.2.2, when carrying out novel separations with the device, it is of great importance to monitor the buffer solution flowing out of the device to confirm retention and elution of analytes.

4.3.1 Capacitively Coupled Contactless Conductivity Detection (C⁴D)

Capacitively Coupled Contactless Conductivity Detection (CCCCD or C⁴D) is a form of detection utilising the electrical interference caused by a change in the media that the signal is traversing⁸. This is achieved by transmitting a high frequency, high amplitude AC signal from a source electrode which then traverses the sampling region where it is detected by a receiving electrode. As the signal passes through the sampling region small changes in the conductivity result in gain or loss of amplitude of the signal. These changes can then be observed as fluctuations in amplitude, which can then be interpreted by deconvolution giving rise to peaks corresponding to changes in voltage. Due to the principle of operation utilising an electromagnetic signal, this detection method is most sensitive to small ions. Since being identified as an alternative detection method for CE in 1998 C⁴D has become widely used in applications for a range of chromatographic techniques including HPLC and Ion chromatography⁸. As with CE, DFGF performs separations of charged species, ideal for detection by C⁴D. A C⁴D detection device was sourced from eDAQ⁹, a commercial manufacturer of conductivity detection devices. The “ET121” device was selected as it is designed for applications with microfluidic chips giving the versatility for eventual on chip detection as well as working post device with fused silica capillary tubing.

4.3.2 Microfluidic DFGF post column detection

Preliminary work with the C⁴D detector was conducted post column using the setup in figure 4.3.1.

The addition of a Waters 486 tuneable UV detector enabled to the detection of the test species to provide confirmation of the operation of the C⁴D and provide data on the performance of the UV detector as a secondary detector.

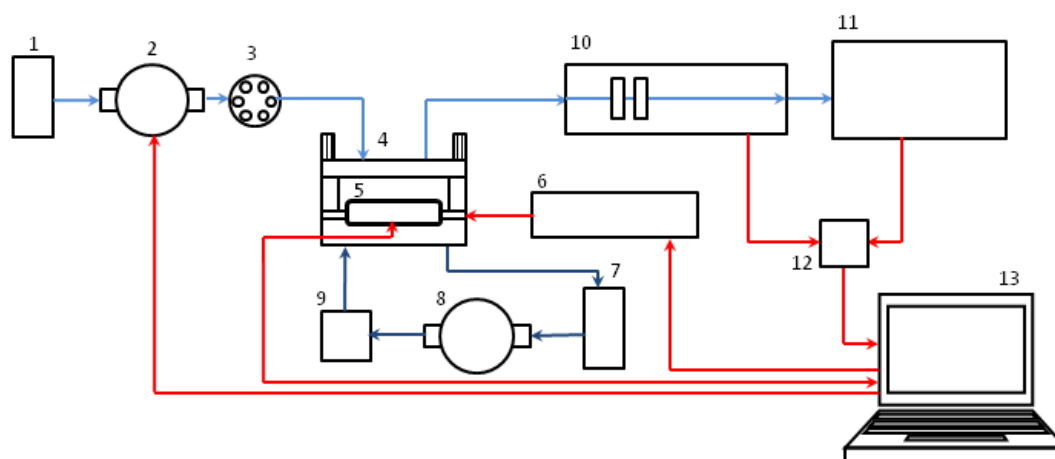


Figure 4.3.1. Microfluidic DFGF with UV and C⁴D configuration, with electrical connections in red, separation channel fluid flow in light blue and electrode channel fluid flow in dark blue. 1) Separation Channel buffer reservoir. 2) Computer controlled Rheos Flux Pump. 3) 6-Port switching valve with Injection port. 4) DFGF device. 5) PDA Detector 6) Computer controlled High Voltage Supply. 7) Electrode channel buffer reservoir with cooler. 8) Peristaltic pump. 9) De-gasser 10) C⁴D Detector. 11) UV detector 12) NI USB DAQmx interface. 13) Computer.

Having configured the C⁴D and UV detectors the control software from eDAQ⁹ was used to establish the correct conditions to facilitate the best detection performance from the C⁴D device. The operating parameters of the C⁴D device are; the frequency, amplitude, offset, and gain with head stage gain on or off. This is done by first injecting a 1%v/v mixture of the analyte with mobile and running the 'Profile' function in the software which systematically adjusts the C⁴D detection parameters one at a time, a reading is taken for each configuration and the response is plotted on a graph. This is then repeated having flushed the tubing with pure mobile phase.

The software then overlays the two graphs to enable the user to find the optimum configuration. These graphs are shown in figure 4.3.2 for BPB.

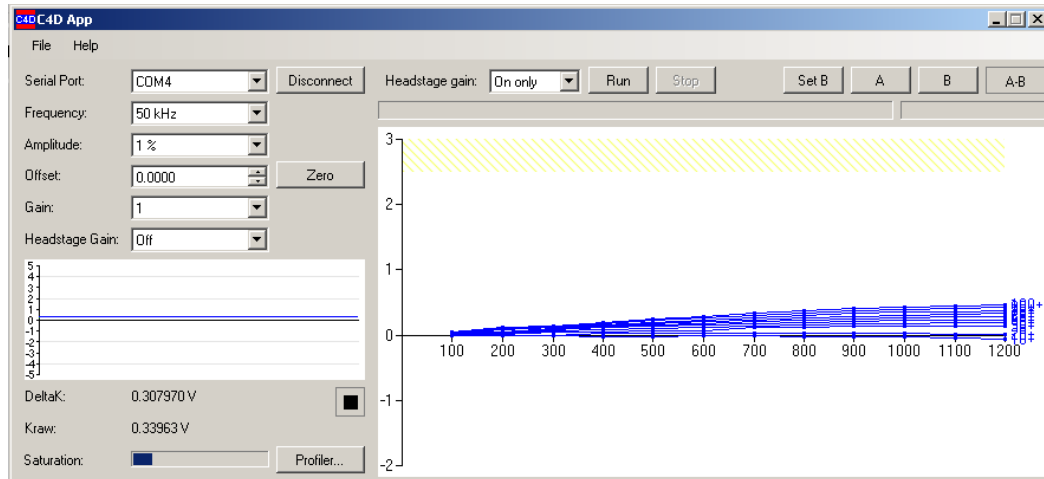


Figure 4.3.2. Profile of condition for C⁴D detection of BPB.

Parameter	Setting
Frequency	1200kHz
Amplitude	100%
Head stage Gain	ON
Gain	100

Table 4.3.1 Optimal conditions for detection by C⁴D from the profiling for BPB.

Once the required parameters were determined (table 3.4.1) a viable method for data capture was required for both the C⁴D and UV detector. A simple Data Acquisition (DAQ) system was written in LabView to record the voltage outputs from both devices. Using the LabView USB DAQmx interface¹⁰ the C⁴D and UV detectors were wired to individual analogue inputs. The LabView software is shown in figure 4.3.3.

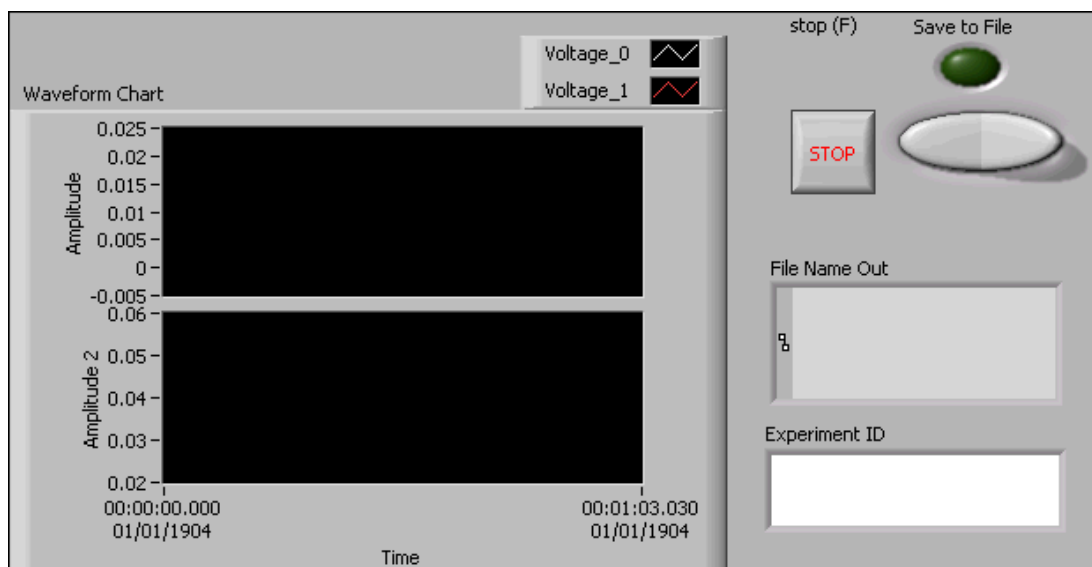


Figure 4.3.3. Labview DAQ System for C⁴D and UV detectors. “Voltage_0” displays the signal from the UV detector while “Voltage_1” displays the signal from the C⁴D detector.

This Labview DAQ system (appendix F) was able to record data from the devices simultaneously at 1kHz and record this data in the proprietary National Instruments binary file format, *.tdm extension. The software also provided the user with an automatically updating scrolling view of the live data from both devices. The saved data files for each experiment were plotted using the data analysis software (Originlab’s Origin)¹¹.

Whilst running the post-DFGF detection array in parallel with reflectance or PDA detection, a number of separations were carried out. These probed the viability of the additional detectors as well providing key observations as to the performance of this microfluidic DFGF device.

4.3.3 Results with all detection

Initially the Labview DAQ system was tested by powering up the C⁴D and UV detectors and setting the software to acquire for over 5mins. The software correctly collected and recorded data from both detectors. This test run data is shown below in figure 4.3.4.

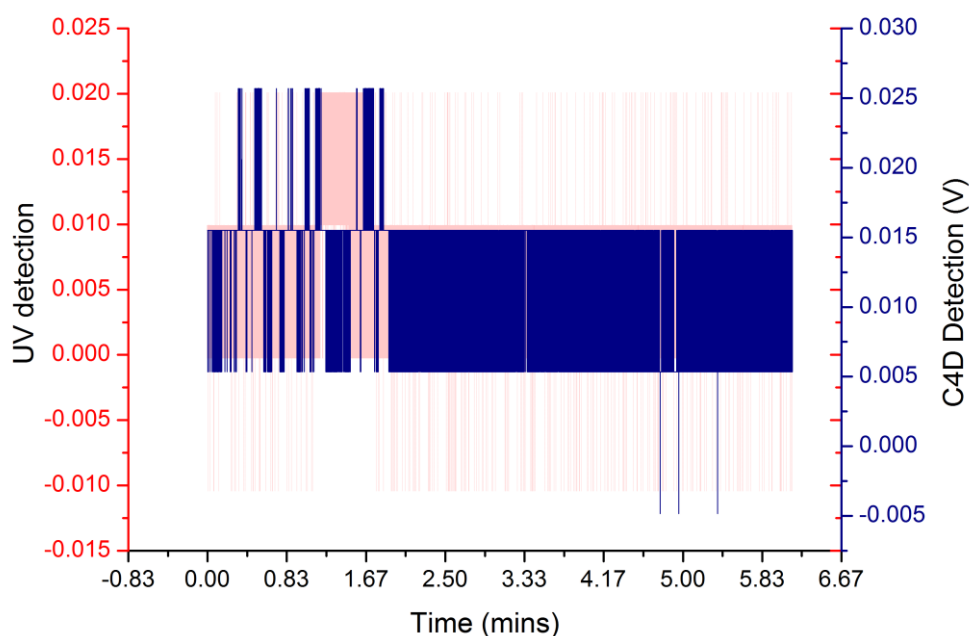
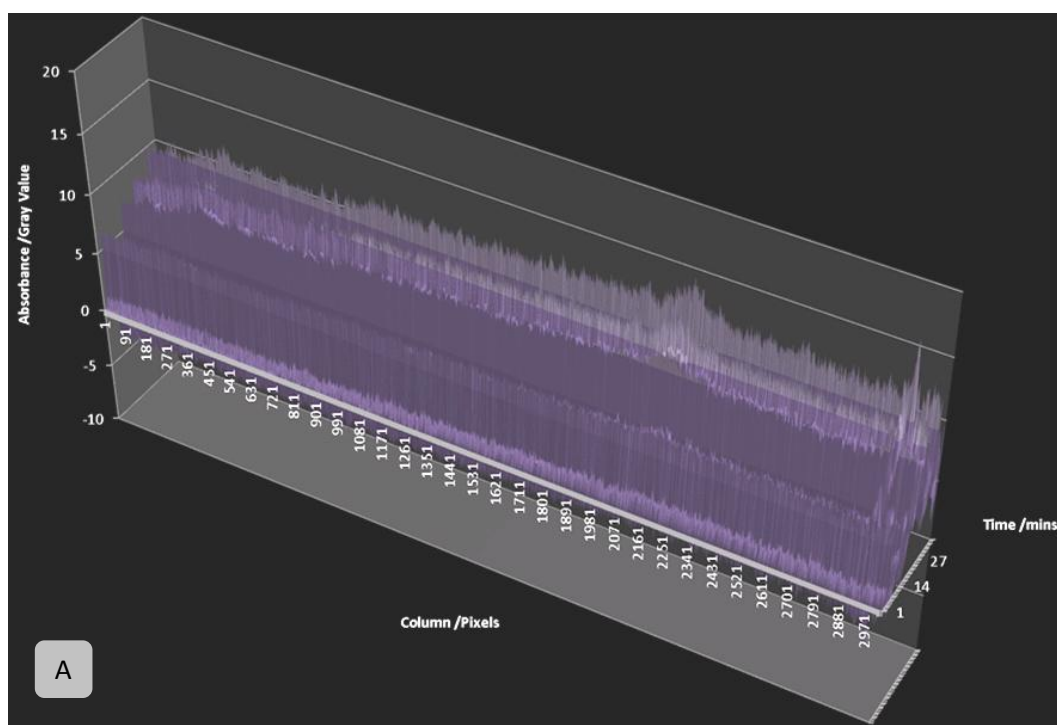


Figure 4.3.4 The first data successfully collected from the DAQ system showing a flat base line for each detector (UV in red and C⁴D in blue).

Having observed a stable baseline and successful data recording, the detection system was tested with a single analyte. A 10%v/v mixture of BPB was injected and at flow rate of $1\mu\text{Lmin}^{-1}$, was pumped through the microfluidic DFGF device, and the sample observed by reflectance measurements and the post column detectors.

The BPB eluted from the device after 7mins, and was observed by the UV detector after a further 12mins. The graphical whole-on-column detection and the C⁴D-UV data are shown in figure 4.3.5 for the BPB passing directly through the system. Note that the time for a given analyte to flow through the microfluidic DFGF, with no retention, and be detected is 7mins for the C⁴D and 19mins for the UV detector.



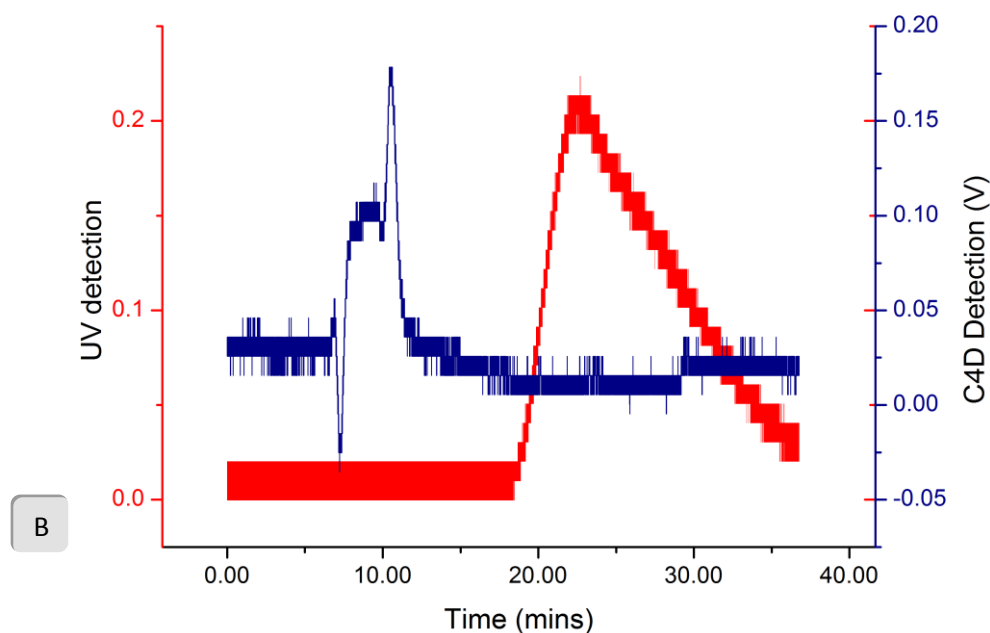


Figure 4.3.5. A) Graphical representation of the whole column reflectance data displaying the BPB moving through the microfluidic DFGF. B) The first test was to inject a sample and allow it flow directly through the device and through the detectors. These reading from the C⁴D and the UV detector show BPB passing straight through.

Repeating the injection of BPB, a linear EFG was applied to retain the analyte, again following this with reflectance measurements and the post column detection devices. The graph in figure 4.3.6 shows the species eluting from the device around the same time as if there was no retention from the electric field. However, on closer analysis, the area under the peak is smaller and the reflectance data does indeed show retention of the BPB. The explanation for the eluted peak is that the microfluidic DFGF must have been overloaded with sample and the majority of the injected sample has passed directly through the device.

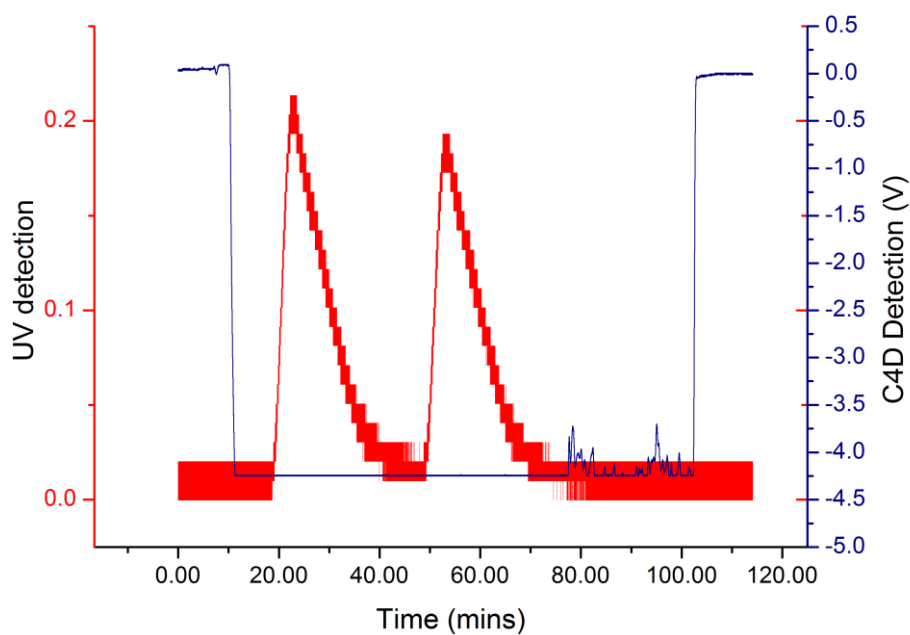


Figure 4.3.6. UV and C⁴D data for the elution of BPB which was injected and attempted to be focused, but a peak was detected eluting from the device at 20mins, the same as in figure 4.3.5 where there was no EFG. The second peak in the UV trace corresponds to the elution of a second injection. The C⁴D trace has not detected the analyte.

Following a separation of AM and BPB again, a peak eluted, indicating that some of the sample was not retained. However, after the EFG was lowered a second larger peak was detected by the C⁴D detector, figure 4.3.7. The delay of this second peak shows that some of the sample is indeed being retained and separated.

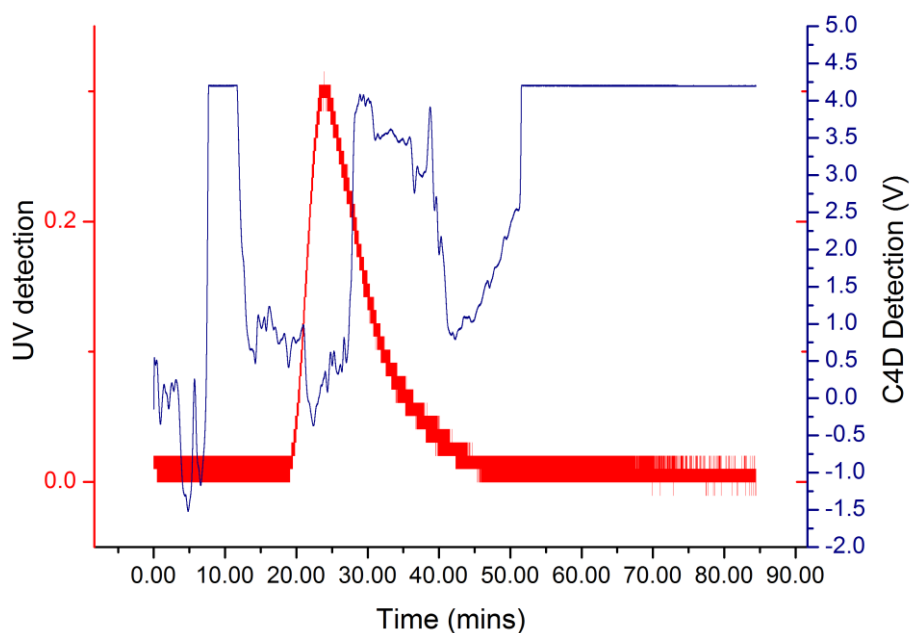


Figure 4.3.7. UV and C⁴D data for the elution of AM and BPB having been injected and not retained by an EFG of 100Vcm⁻². The C⁴D trace has detected the analyte at 10mins, though the peak has flat topped having reached the limit of detection.

Furthermore from figure 4.3.7 there are a number of interesting responses from the C⁴D detector which seem to be fluctuations in the signal, coinciding with the changes in the EFG. This is further exemplified in figure 4.3.8. The changes in EFG, shown in table 4.3.2, cause a change in the concentration of ions in the buffer solution leaving the device. These changes in ion concentration are observed in the C⁴D trace as the signal incrementally steps up because of changes in conductivity of the solution.

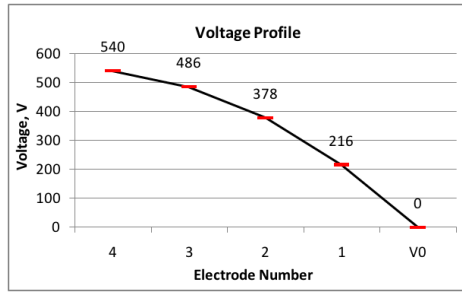
Time (mins)

EFG (Vcm^{-2}) and Voltage Profile

Flow($\mu Lmin^{-1}$)

G=150

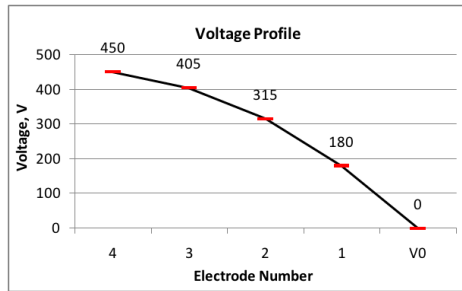
1



1.0

G=125

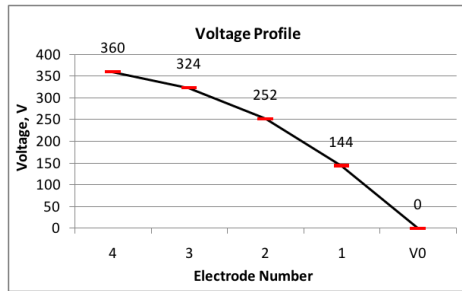
25



1.0

G=100

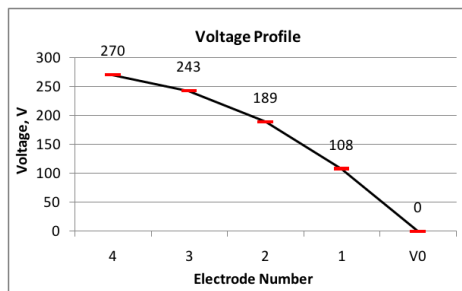
35



1.0

G=75

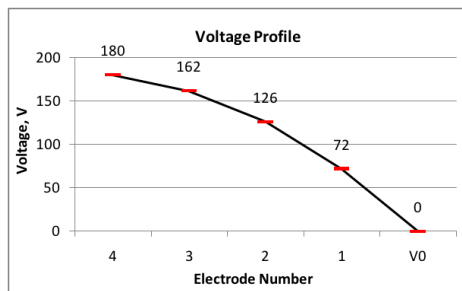
45



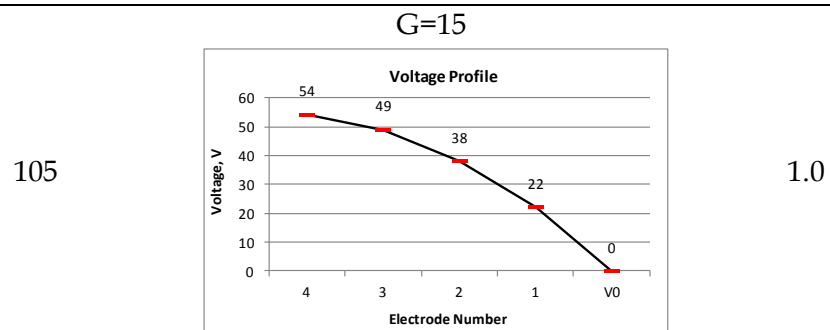
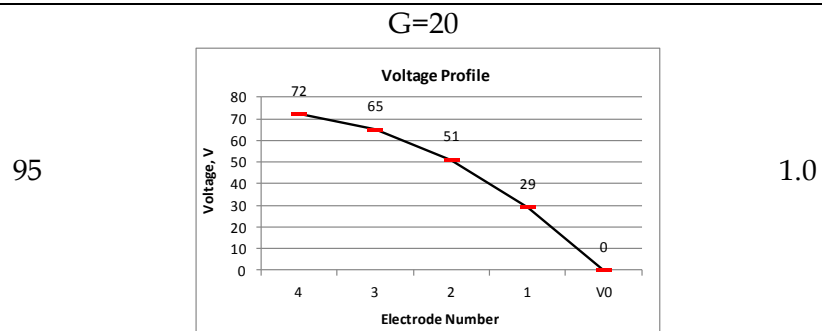
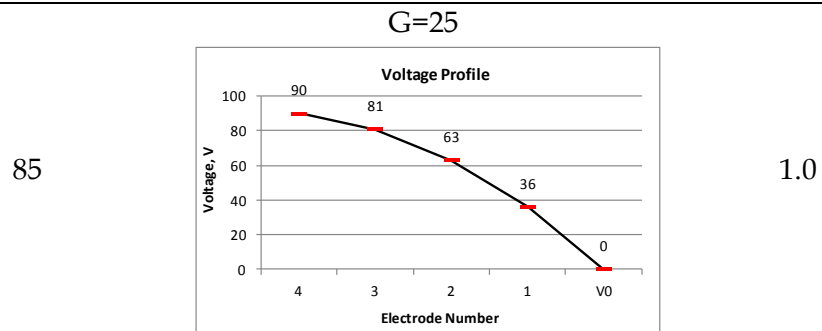
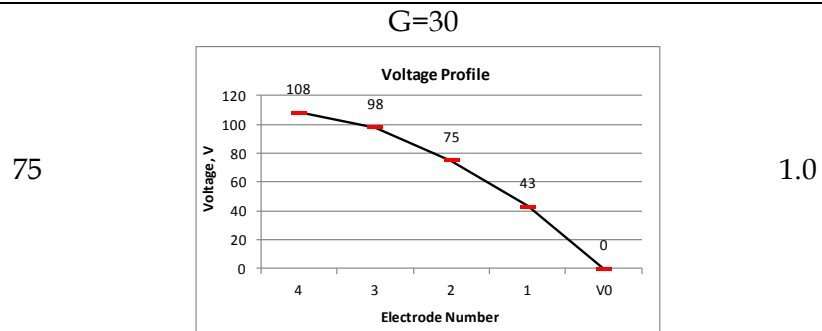
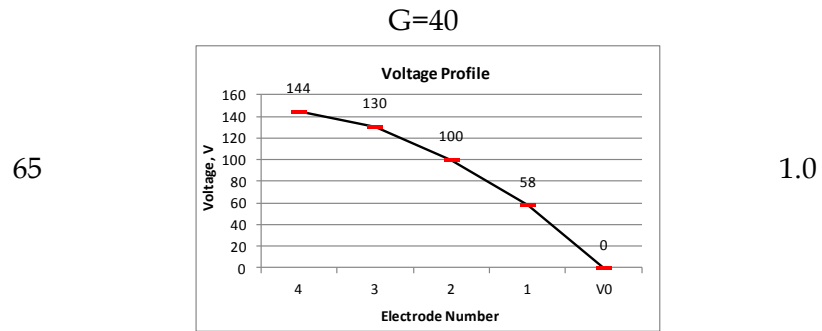
1.0

G=50

55



1.0



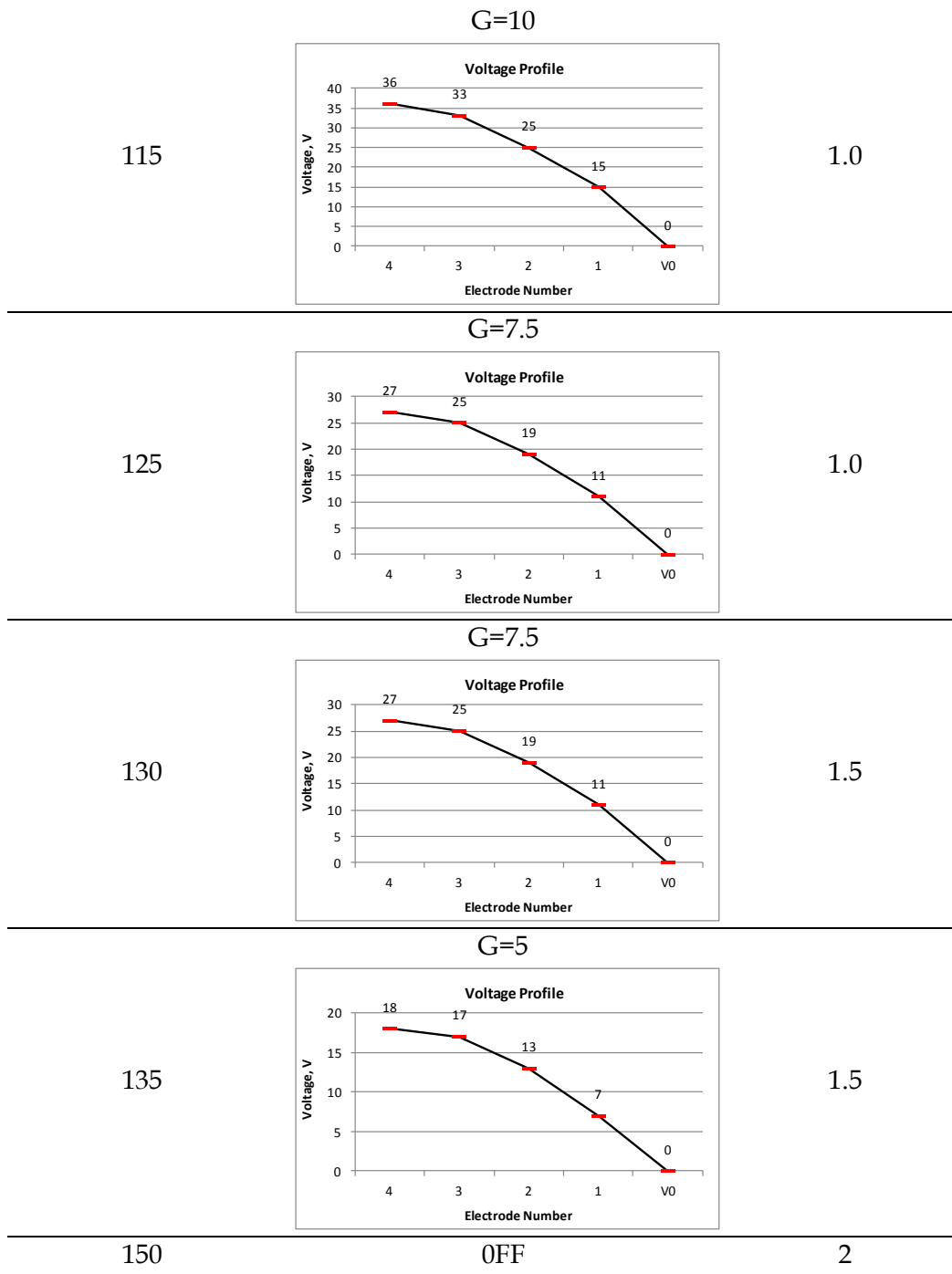


Table 4.3.2. Changes in EFG for the separation of AM and BPB in figure 4.3.8.

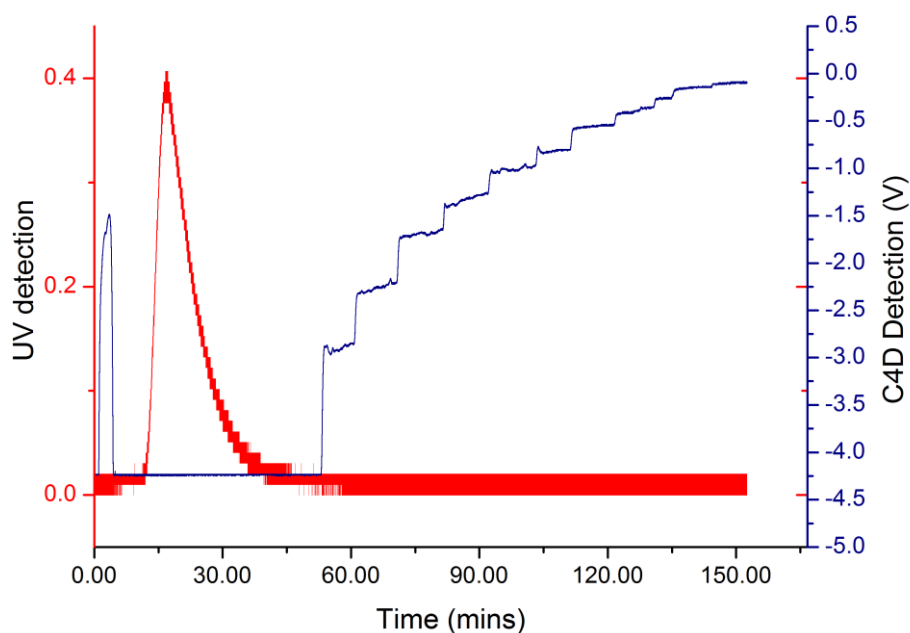


Figure 4.3.8. UV and C⁴D traces following an injection of BPB and AM. The analytes have eluted without being retained by the EFG. This is shown by the large peaks at 7min with C⁴D and 19mins with UV. The stepped rises in the C⁴D detection correspond to changes in the EFG detailed in table 4.3.2.

Where multiple injections are used in an attempt to build up the concentration of a sample to aid the detection by reflectance or PDA, detection of the subsequent injections can also be seen eluting from the device with very little retention. Figure 4.3.9 below shows that three injections of the AM and BPB test mixture were detected by the C⁴D at 5, 20, and 33minutes. The changes in EFG are shown in table 4.3.3.

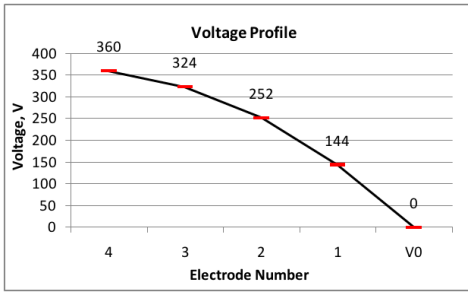
Time (mins)	EFG (Vcm ⁻²) and Voltage Profile	Flow(μLmin ⁻¹)
	G=100	
1		1.0
90	Off	1.0

Table 4.3.3. Conditions for the separation of AM and BPB monitored by C⁴D and UV. The detection data is shown in figure 4.3.9. After the initial injection at 0mins, two further injections were made at 10mins and 25mins.

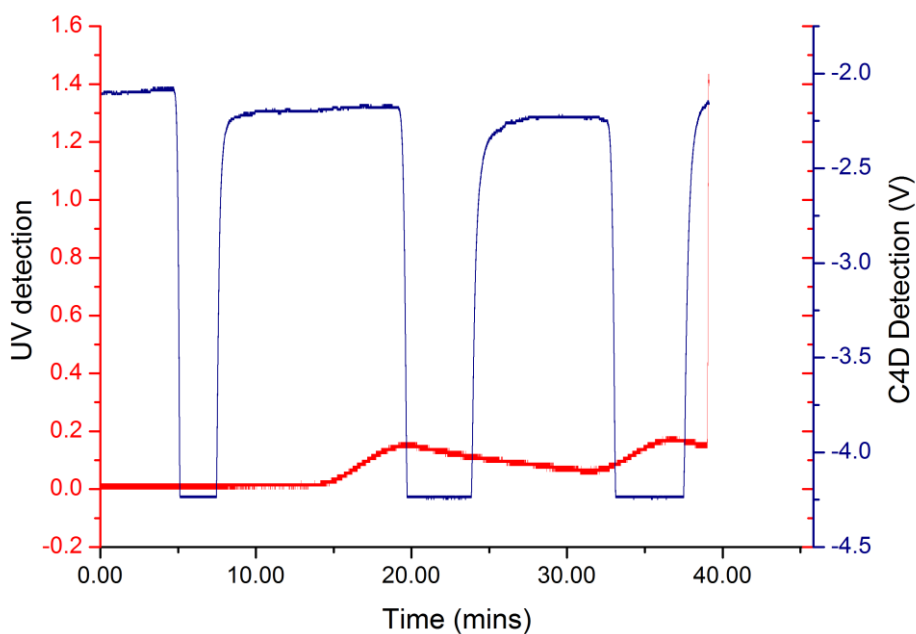


Figure 4.3.9. Three injections correlate to the C⁴D responses observed at 5, 20, and 33minutes, all of which eluting ~5mins after injection. The C⁴D peak are negative which could be due to the detection beginning with a lower EFG. However, from the reflectance data some of the sample was still retained and focused.

Previously in chapter three several separations of the kaleidoscope test mixture were undertaken.

During these separations the post column detectors were running. The following three separations of the Kaleidoscope test mixture gave an interesting array of results.

Firstly, the separation in figure 4.3.10 shows the characteristic overload elution profile with some peaks in the C⁴D detection correlating with changes in the electric field. The conditions used and the whole-on-column detection are presented in chapter three in table 3.3.9 and figure 3.3.28 respectively. The presence of peaks in the UV trace and the C⁴D signal show that most of the sample eluted. From the C⁴D trace between 75minutes and 150minutes there are a series of increases in the signal. These may be due to the separated proteins, however the changes in EFG which followed had an effect reading making this inconclusive.

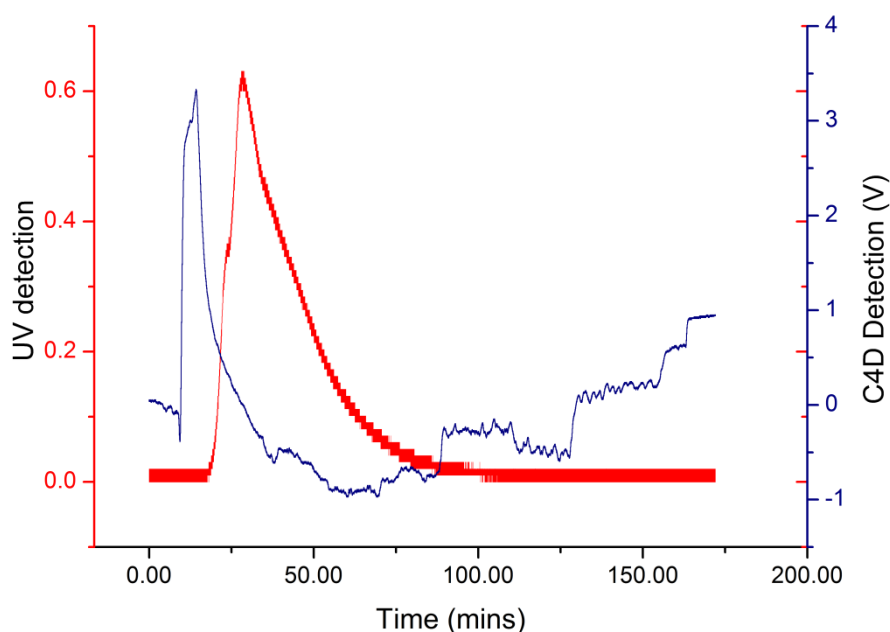


Figure 4.3.10. Post separation channel detection for the separation of kaleidoscope test mixture in chapter three, figure 3.3.28. The signal displays sample overload on injection and perhaps the C⁴D responding to the changes in EFG.

With a repeat run of the kaleidoscope test mixture, the C⁴D detector was zeroed having equilibrated the system with the initial EFG giving less baseline fluctuation during the experiment. The C⁴D trace and the UV detection for the separation of the kaleidoscope test mixture is shown in figure 4.3.11B. The whole-on-column PDA detection observed a region of focused bands of proteins, figure 4.3.11A. When the EFG was lowered to an elution profile, these bands eluted and were detected in the C⁴D. The conditions for this experiment are shown in table 4.3.4. Four peaks are visible in the C⁴D signal at 35mins, concordant with the detection delay of ~7minutes after the field was adjusted at 30mins.

Time (mins)	EFG (Vcm ⁻²) and Voltage Profile	Flow(μLmin ⁻¹)												
	G=150													
1	<table border="1"> <caption>Voltage Profile Data for 1 min</caption> <thead> <tr> <th>Electrode Number</th> <th>Voltage, V</th> </tr> </thead> <tbody> <tr><td>4</td><td>540</td></tr> <tr><td>3</td><td>486</td></tr> <tr><td>2</td><td>377</td></tr> <tr><td>1</td><td>216</td></tr> <tr><td>V0</td><td>0</td></tr> </tbody> </table>	Electrode Number	Voltage, V	4	540	3	486	2	377	1	216	V0	0	1.0
Electrode Number	Voltage, V													
4	540													
3	486													
2	377													
1	216													
V0	0													
30	<table border="1"> <caption>Voltage Profile Data for 30 min</caption> <thead> <tr> <th>Electrode Number</th> <th>Voltage, V</th> </tr> </thead> <tbody> <tr><td>4</td><td>350</td></tr> <tr><td>3</td><td>325</td></tr> <tr><td>2</td><td>300</td></tr> <tr><td>1</td><td>250</td></tr> <tr><td>V0</td><td>0</td></tr> </tbody> </table>	Electrode Number	Voltage, V	4	350	3	325	2	300	1	250	V0	0	1.0
Electrode Number	Voltage, V													
4	350													
3	325													
2	300													
1	250													
V0	0													
40	<table border="1"> <caption>Voltage Profile Data for 40 min</caption> <thead> <tr> <th>Electrode Number</th> <th>Voltage, V</th> </tr> </thead> <tbody> <tr><td>4</td><td>350</td></tr> <tr><td>3</td><td>300</td></tr> <tr><td>2</td><td>250</td></tr> <tr><td>1</td><td>300</td></tr> <tr><td>V0</td><td>0</td></tr> </tbody> </table>	Electrode Number	Voltage, V	4	350	3	300	2	250	1	300	V0	0	1.0
Electrode Number	Voltage, V													
4	350													
3	300													
2	250													
1	300													
V0	0													
53	Off	1.0												

Table 4.3.4. Conditions for repeat separation of the Kaleidoscope proteins in figure 4.3.11.

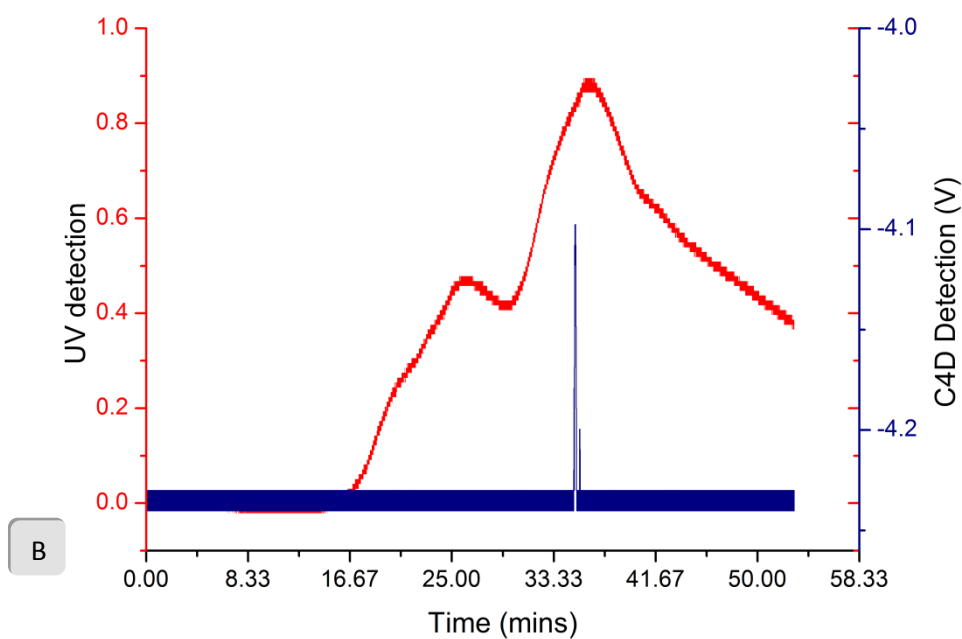
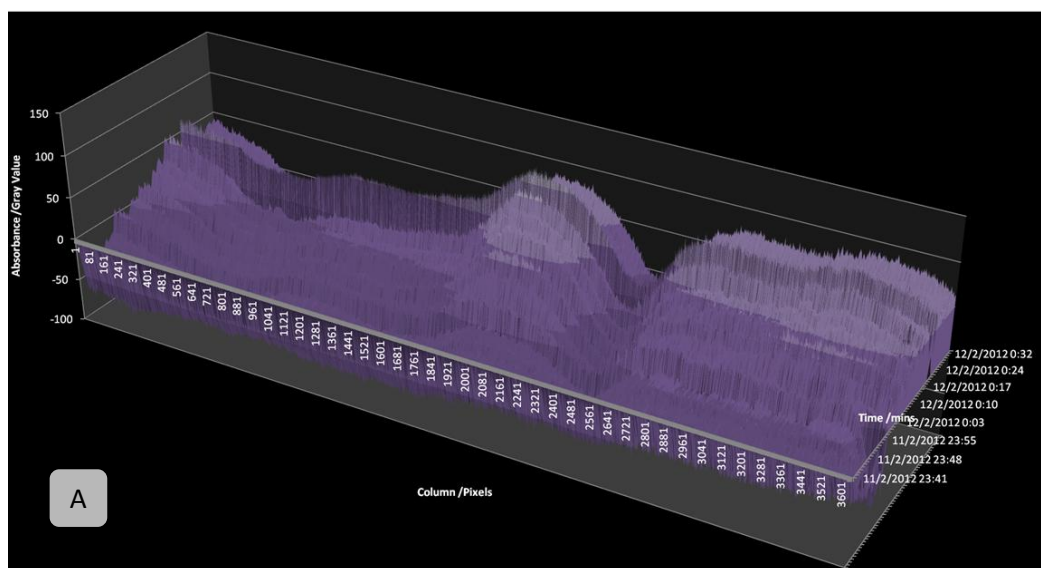


Figure 4.3.11. A) Graph displaying the PDA data for the separation attempt of the kaleidoscope test mixture. B) C⁴D and UV detection following the separation, the C⁴D peaks at 36mins correspond to elution as the EFG was changed. The UV is displaying the overload and continuing to rise causing low sensitivity to further detection.

This result forms a comprehensive detection technique for the microfluidic DFGF, with the whole-on-column PDA enabling real time adjustments to focusing and the post column C⁴D and UV detectors showing the peak shapes attainable when focused bands elute from the device.

Post column detection highlighted an issue with the maximum moles of a compound which can be retained by the electric field in the microfluidic DFGF when using voltages capped at 600V. To calculate an appropriate concentration for sample injection, a plot with both the initial excess sample and a peak corresponding to the retained sample was required. The UV trace in figure 4.3.12 clearly displays a large broad peak eluting at around 20mins, corresponding to excess sample, and a smaller peak at 135minutes corresponding to the retained sample eluting after the electric field being switched off. The conditions for this separation and PDA detection are presented in chapter 3 in table 3.3.12 and figure 3.3.34. Integration of this pair of peaks can be used to calculate a percentage of the injected sample which was retained, therefore a known quantity of retained sample can be calculated.

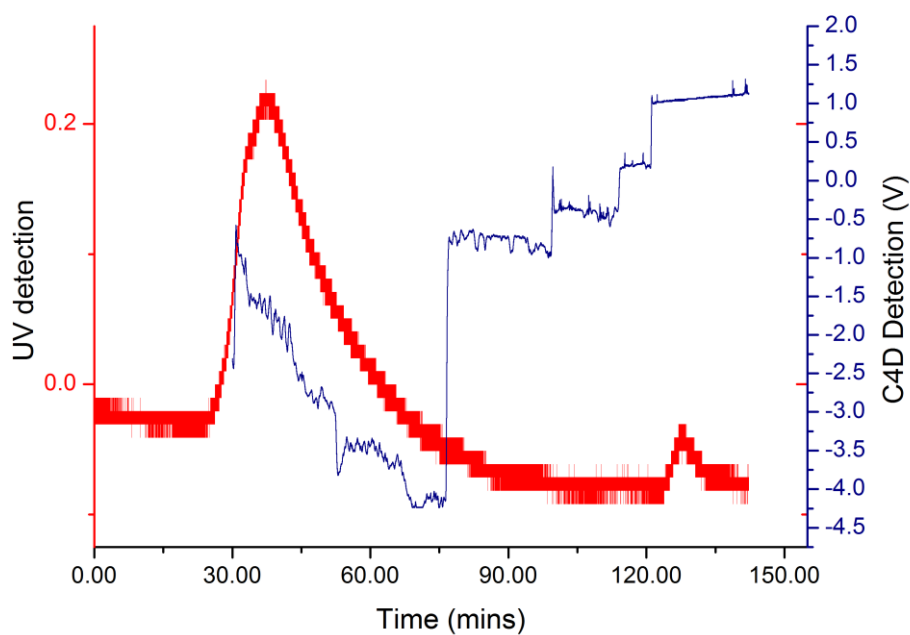


Figure 4.3.12. Post separation channel detection for the separation of the Kaleidoscope test mixture described in chapter three figure 3.3.34. The UV data enabled the calculation of loading capacity and the C⁴D correlates to the changes in EFG.

The maximum sample loading volume for the microfluidic DFGF was determined to be only 5% of the volume injected. This was determined by integration of the UV data in figure 4.3.12. Until the implementation of the PDA detector an excess of sample was required to improve the visibility of a focused band of analyte to aid in the reflectance detection. Having progressed with this detection, the correct working volume of sample can be used.

4.4 Applications with Analytical Instrumentation

4.4.1. 2D-HPLC

The utilisation of High Performance Liquid Chromatography for the analysis of proteins, peptides, and metabolites has become more and more favourable, moving away from simple gel electrophoresis¹². A driving factor for this change has been the advancement of two dimensional HPLC. With the addition of a second dimension these separations provide greater resolution and selectivity. Typically, a strong cation exchange (SCX) column is used in the first dimension and a Reverse Phase (RP) column in the second dimension¹³. Using two dimensions, results in the separated sample components from the first dimension then being sequentially passed through the second dimension, which are then separated further by a different mechanism. This results in a chromatogram of each peak within the chromatogram for the first dimension.

Though 2D-HPLC has many advantages, the fact that the sample in the mobile phase through two columns and extra tubing results in a detrimental contribution from the B term (longitudinal diffusion) of the Van Deemter equation¹⁴. This is where the sample is constantly diffusing into the surrounding mobile phase within the column and any tubing.

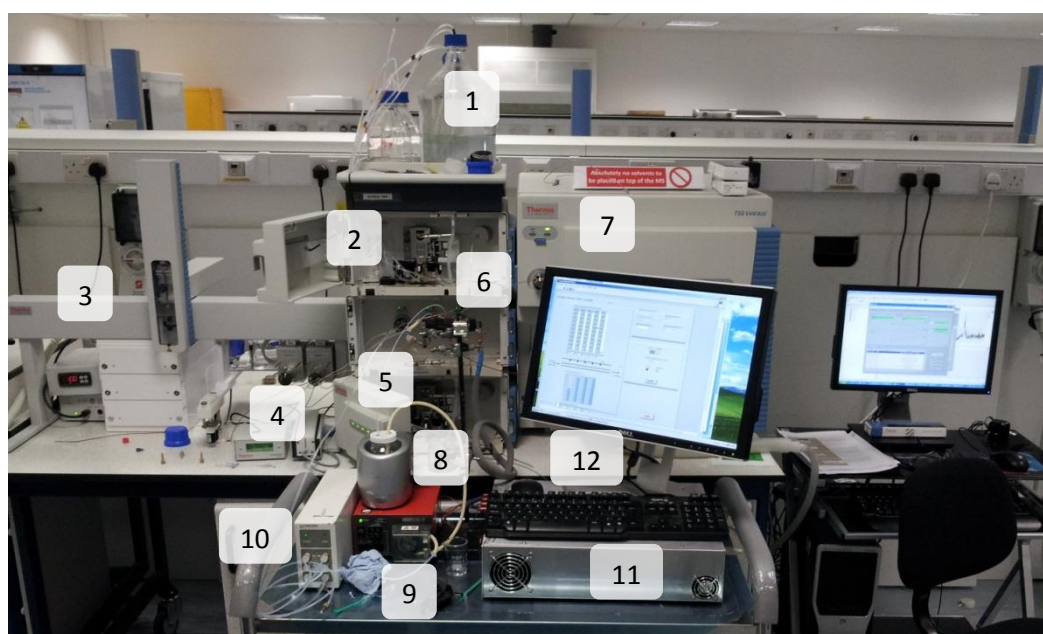
As previously demonstrated, proteins and other similar biological samples are charged, enabling the utilisation of DFGF. In this case, instead of using DFGF as the main separation technique, the DFGF device will be used in the same way as a valve or switch, using the electric field to hold back a sample, and then release it to reach a detector.

Referring to fundamentals of DFGF in section 2.1, when a sample is retained by the EFG the sample is also concentrated.

It is the effect of re-concentrating the sample having been in free solution which will improve the resolution of a 2D HPLC separation by “pre concentrating” the sample before passing it through the second dimension.

4.4.2 HPLC-DFGF-MS: Single Valve Work

Initial experimentation utilising the microfluidic DFGF as an electrophoretic switch was carried out by configuring the DFGF post column with minimal dead volume between the outlet of the DFGF device and inlet of the MS. In this configuration, shown in figure 4.4.1, the existing HPLC methods were used. The aim of this series of experiments was to demonstrate the ability of the DFGF to retain a sample before allowing it to pass into the MS.



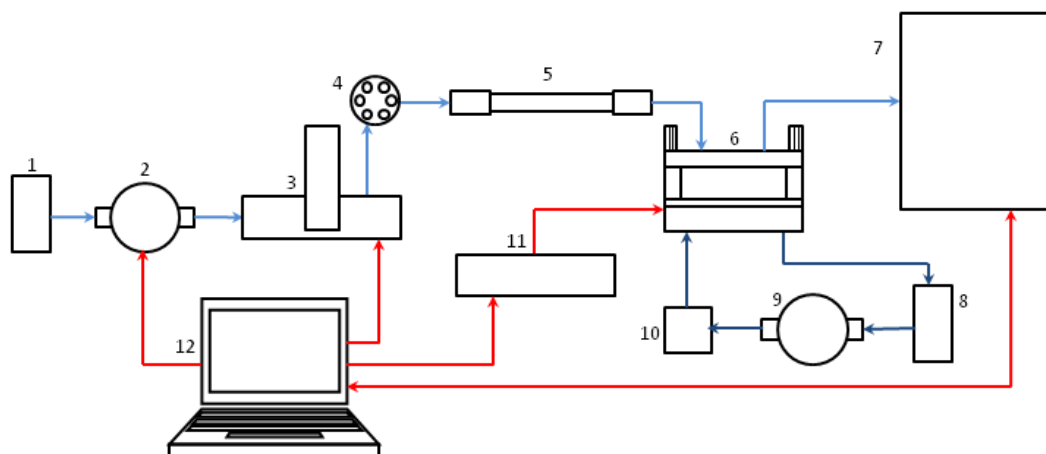


Figure 4.4.1. HPLC-DFGF-MS Set up with electrical connections in red, separation channel fluid flow in light blue and electrode channel fluid flow in dark blue. 1) Mobile Phase Reservoir. 2) uHPLC pump. 3) CTC auto sampler. 4) Injection Valve with 10 μ L sample loop. 5) Thermo Accucore column. 6) Microfluidic DFGF device. 7) Thermo TSQ Mass Spectrometer. 8) Electrode channel buffer solution reservoir. 9) Peristaltic pump. 10) De-gasser. 11) Protasis HV power supply. 12) Control Computer.

Initial testing highlighted key issues with this configuration. Firstly, the flow rates in operation were too high for the EFG to retain the sample against. Using the model for the hydrodynamic flow and electric field as opposing forces, with a flow rate as high as 200 μ Lmin⁻¹ the sample was simply pumped straight through the column and onto the MS. Lowering the flow rate to only 100 μ Lmin⁻¹ saw the issue decrease, however the EFG was not able to fully retain a sample before releasing it to the MS. With a Thermo Fisher reverse phase column and a mobile phase of 60:40 methanol:water 0.1%v/v formic acid, an injection of 0.1mgmL⁻¹ Insulin was injected. The mass spectrometer was configured for the specified mass range for 4+ fragment, 1434Da¹⁵. At a flow rate of 100 μ Lmin⁻¹ the sample was pumped through the column, through the microfluidic DFGF and onto the mass spectrometer without the use of the EFG.

The chromatogram obtained is shown in figure 4.4.2; note the peak width, height, and retention time. On a repeat injection, with an EFG generated with 1kV on each of the four electrodes, the sample passed through onto the MS. The chromatogram with an EFG applied is shown in figure 4.4.3. The EFG was applied from 1minute and switched off after 6.5minutes. Comparing these two chromatograms, figure 4.4.4, indications of retention of the sample by the electric field are observed. The EFG resulted in a large increase, fivefold, in peak height. The retention time has been extended slightly, by 0.3mins, as result of the further retention by the EFG.

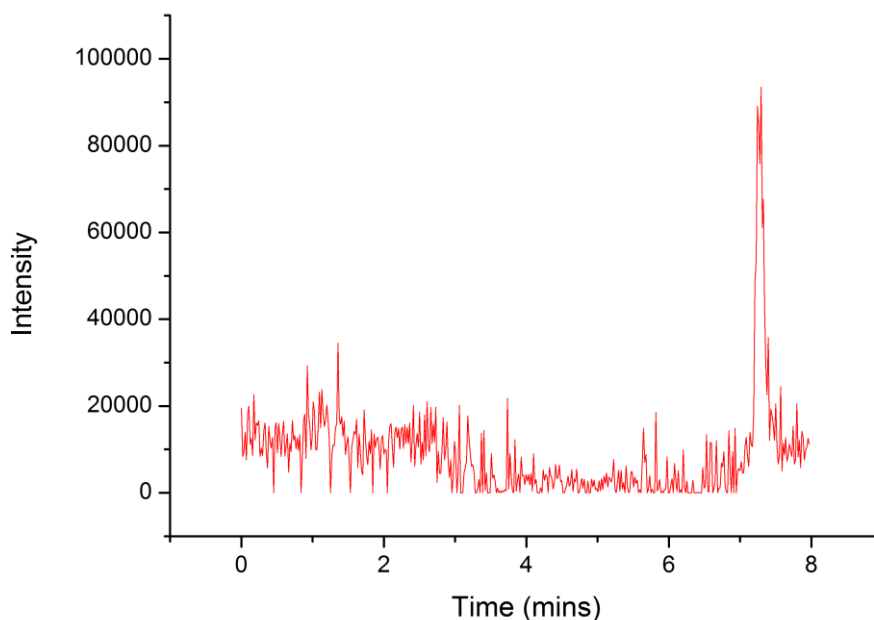


Figure 4.4.2. Total ion count (TIC) from MS of an injection of insulin pumped at $100\mu\text{Lmin}^{-1}$ through column1 and the microfluidic DFGF without an applied electric field.

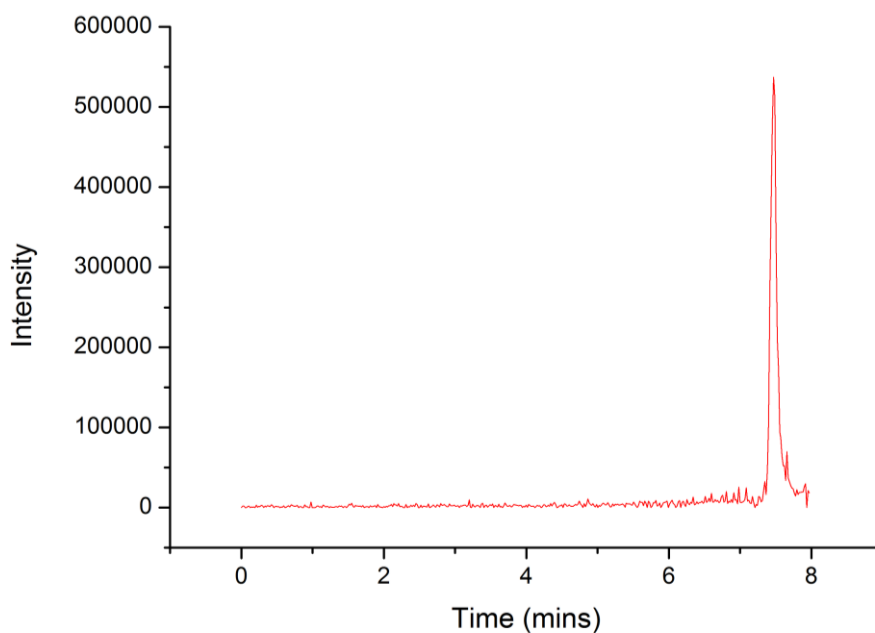


Figure 4.4.3. TIC from MS of an injection of insulin pumped at $100\mu\text{Lmin}^{-1}$ with the electric field applied between 1min and 6.5min with 1000V on each electrode. The peak height has been significantly increased and the retention time slightly extended by 0.5min.

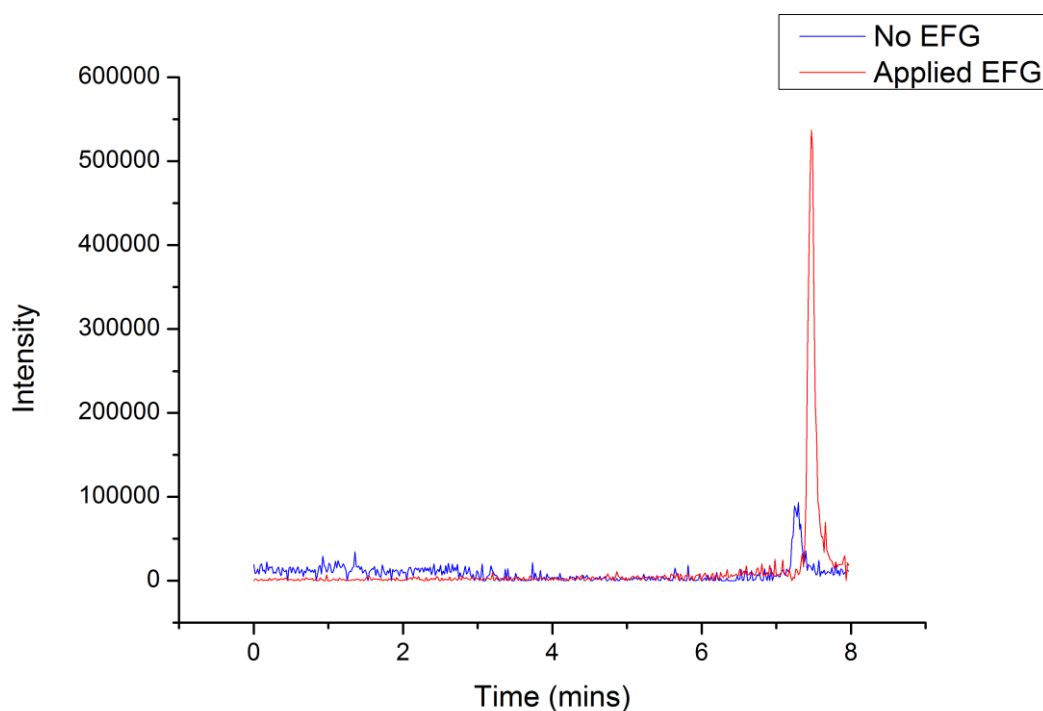


Figure 4.4.4. Overlaid chromatograms (from figures 4.4.2 & 4.4.3) from the test injection of insulin with and without the use of the electric field.

Having observed some change in retention of the sample directly caused by the DFGF device, it was determined necessary to establish the extent to which a sample could be retained. Using a single component for testing, and with the low flow rates used, the column was removed and the sample injected directly onto the DFGF. The Rheos Flux pump¹⁶ was used to generate the required lower flow rates. The reduction of the flow rate meant the operating conditions of the mass spectrometer needed to be altered. The spray tip was moved further forward and sheath gas flow rate increased to generate the correct electro spray. With the mobile phase running at $5\mu\text{Lmin}^{-1}$, there was a little retention, however the difference in retention time between a sample injected with and without an EFG was still not significant. The mobile phase was changed to 60:40 MeOH:H₂O with 50mM Ammonium Acetate (~pH7). This was done to increase the ionic strength of the mobile phase to increase the propagation of the electric field and ultimately increase the retention of sample in the device. After further reduction of the flow rate to $2\mu\text{Lmin}^{-1}$, there was a difference of ~2minutes in retention time and the peak shape had been broadened. With the EFG having some effect on the sample, the peak width was reduced and the peak height increased corresponding in an increase in the concentration of the sample reaching the mass spectrometer. Figure 4.4.5 displays the chromatogram without an EFG applied and figure 4.4.6 shows the chromatogram where an EFG has caused an increase in the concentration of the sample in free solution before detection. Plotting these chromatograms together in figure 4.4.7.

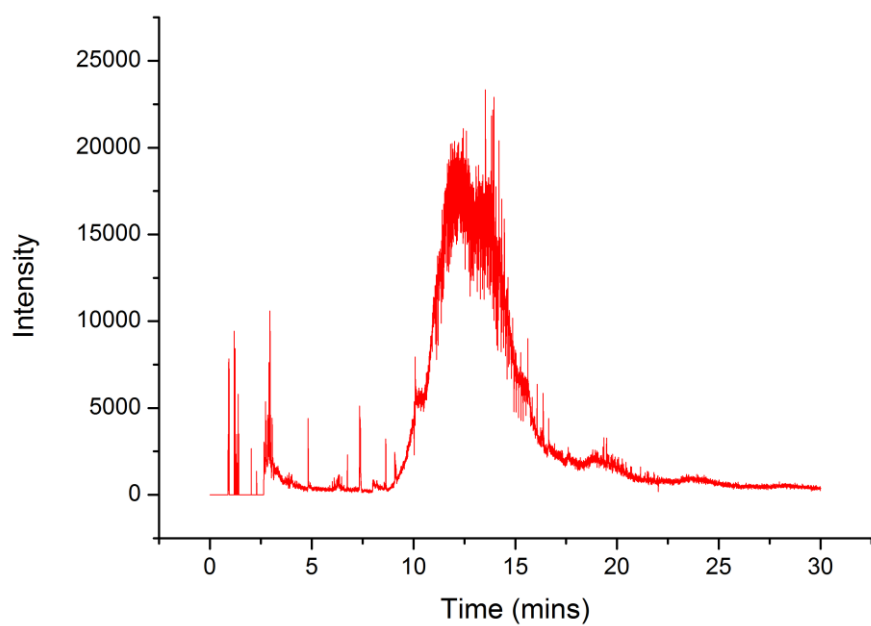


Figure 4.4.5. TIC from MS of an injection and flow through of the sample without a column at $2\mu\text{Lm}^{-1}$ with no electric field applied.

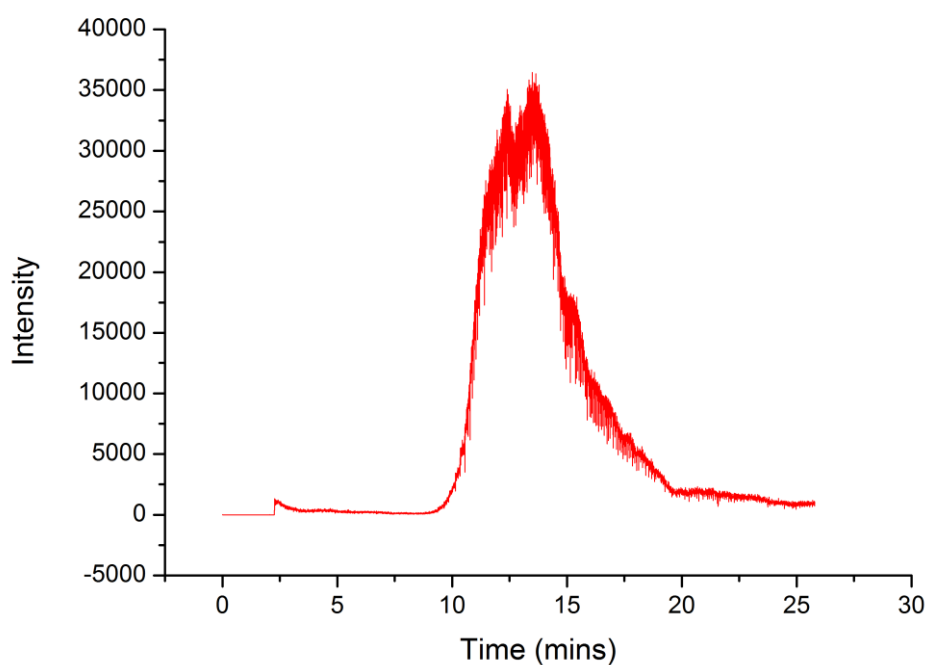


Figure 4.4.6. TIC from MS of an injection and flow through of the sample without a column at $2\mu\text{Lm}^{-1}$ with an electric field applied from 0mins until the end of the run.

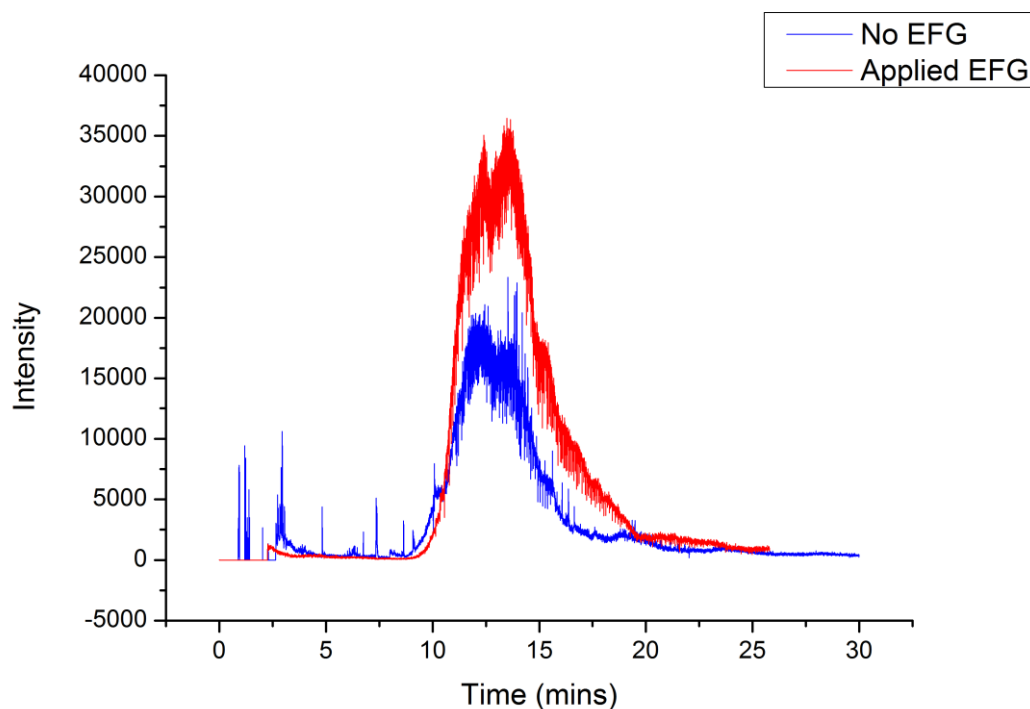


Figure 4.4.7. Overlaid chromatograms (from figures 4.4.5 & 4.4.6) comparing the retention and peak shape with and without an applied EFG where there was no column in place.

This slight change in retention time and peak shape at a flow rate within normal operation of the DFGF device shows that the field was not strong enough to fully hold back a sample. Having already reduced the flow rate the next step was to increase the strength of the EFG. This was achieved by utilising an additional 30kV power supply configured in parallel with the Protasis power supplies. Furthermore to increase the EFG the powers supplies were all connected to a single electrode directly adjacent to the ground electrode resulting in the highest possible current density and strongest electric field gradient.

4.4.2 2D-HPLC: Dual Valve Set Up

With the ability of DFGF to focus and concentrate a sample simultaneously the system can be used as a switch for 2D HPLC by pre concentrating a sample before passing through into the second dimension.

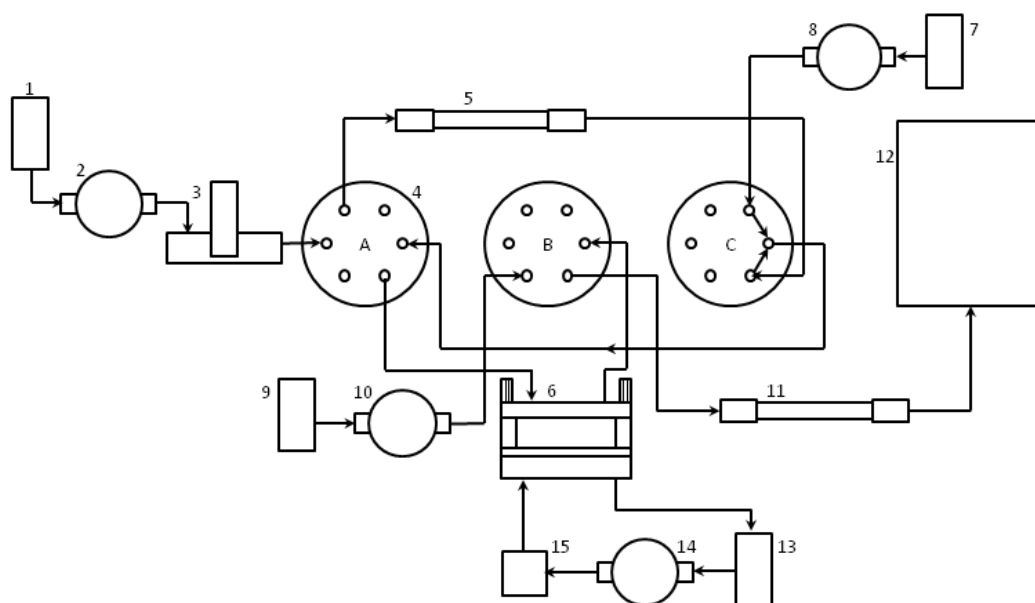
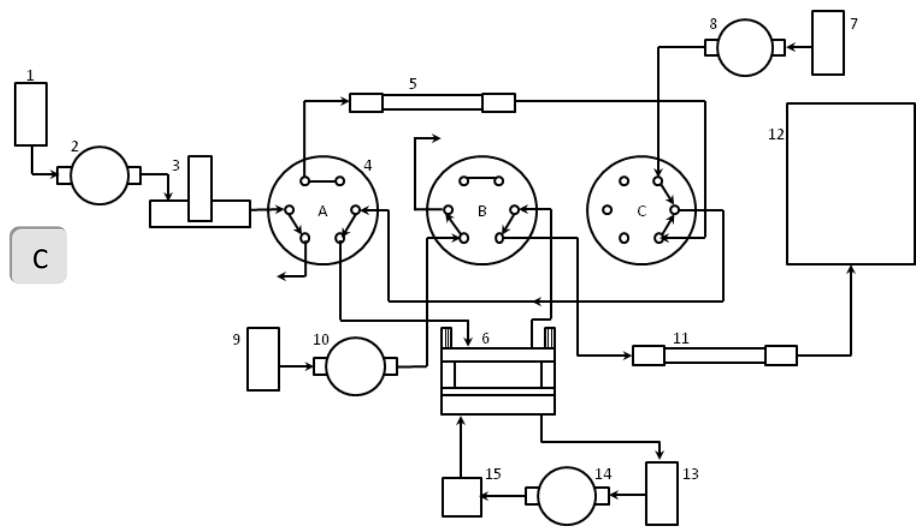
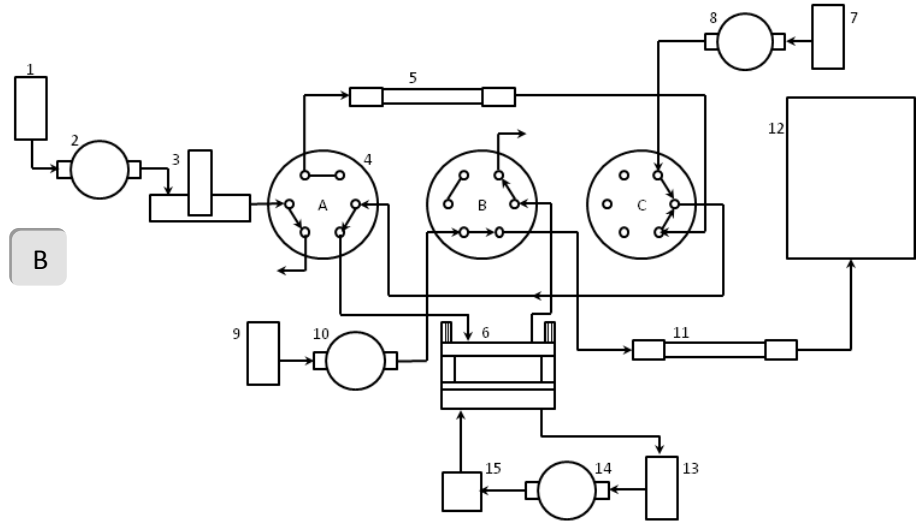
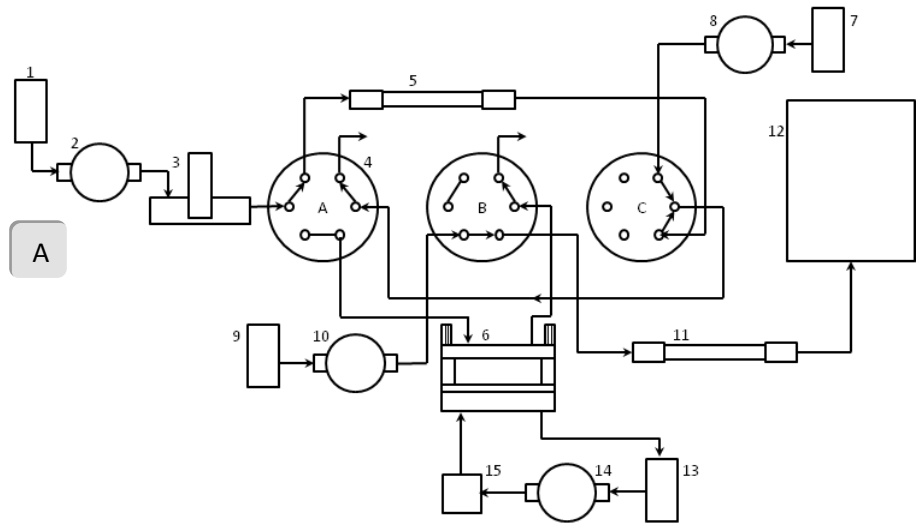


Figure 4.4.8. Integration of the microfluidic DFGF with a 2D HPLC valve switching array. 1) Mobile Phase Reservoir for Column1. 2) uHPLC pump1. 3) CTC auto sampler with injection valve and 10 μ L sample loop. 4) Switching Valves A, B and C. 5)Thermo Accucore column1. 6) Microfluidic DFGF device. 7) Mobile Phase Reservoir for DFGF. 8) Rheos Flux DFGF pump[pump3] 9) Mobile Phase Reservoir for Column2. 10) uHPLC pump2. 11) Thermo Accucore column2. 12) Thermo TSQ Mass Spectrometer. 13) Electrode channel buffer solution reservoir. 14) Peristaltic pump. 15) De-gasser.

The microfluidic DFGF device was integrated into a customised two dimensional configuration as shown in figure 4.4.8 enabling an analyte eluting from the first dimension to be concentrated before being released onto the second dimension. An injected sample was pumped from the sample loop to column one using pump1 with valves A and B both in position 1, figure 4.4.9A.

Meanwhile constant mobile phase for the second column was pumped directly through column2 for equilibration on to the TSQ mass spec. After 30s of running column 1 at 400 μ Lmin⁻¹, valve A was switched to introduce the first cut into the DFGF, figure 4.4.9B. This was done by pump 3 at 5 μ Lmin⁻¹. Having eluted from the first dimension into the DFGF an electric field of 1kV was applied and the flow of pump 3 reduced to 1 μ Lmin⁻¹. This was held for 5mins to ensure concentration of the sample. The electric field was reduced to 200V and pump 3 increased to 5 μ Lmin⁻¹ and valve B switch to position2, figure 4.4.9C. This loaded the concentrated sample onto column2. After 3mins of loading, valve B was returned to position1 and the sample pumped through the second dimension, figure 4.4.9D. Simultaneously, valve A which had been switched back to position1, figure 4.4.9E, and run for an additional 30s was then switched to position2 to load and concentrate the next segment for the second dimension. This sequence was repeated four times to give a 2minute run on column1 and four runs on column2 with detection on the TSQ MS. The HPLC method for column1, the first dimension, was isocratic at 60:40 MeOH:H₂O with 50mM ammonium acetate buffer, while the method for the second dimension was a gradient run moving from 90% v/v MeOH to 0% v/v after 20seconds. The positions of the switching valves and routes of flow of solvent from the three pumps for this method are shown in figure 4.4.9.



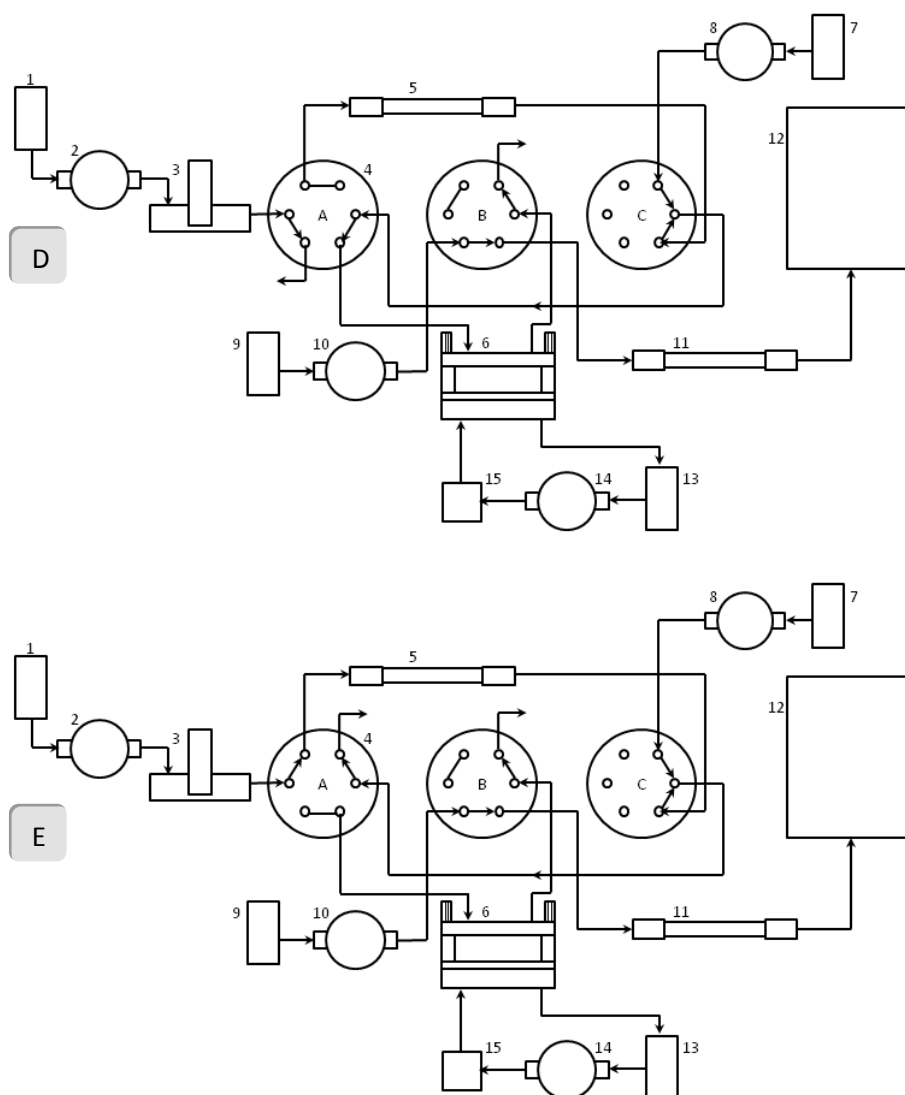


Figure 4.4.9. Switching valve positions and flow of sample for the DFGF assisted 2D HPLC procedure. A) Running of the first dimension and loading a segment to the DFGF. B) Pausing the first dimension and concentrating the segment. C) Loading of the concentrated segment onto the second dimension. D) Gradient run on second dimension. E) Return to initial position and the process repeated with the running of the first dimension. (Refer to Figure 4.4.8 for label key)

A test mixture of Bovine Serum Albumin (BSA) was injected and the separation procedure run without the EFG being applied so there was no pre focusing of sample from the DFGF. The chromatogram from this run is shown in figure 4.4.10.

The four regions of detection are caused by the divert valve on the mass spectrometer only allowing the flow of analyte during analysis when the sample was eluting from column2.

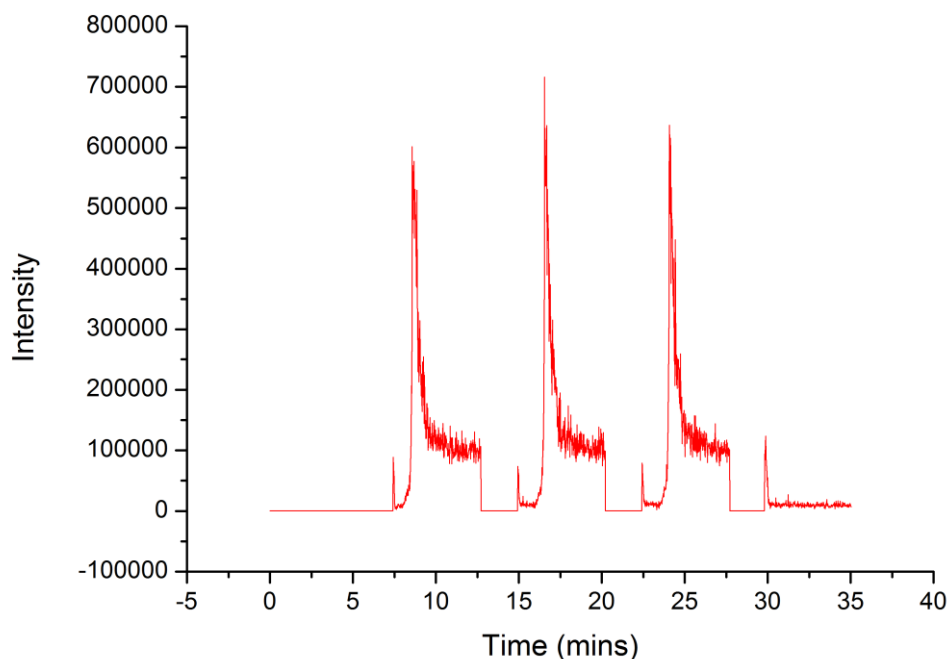


Figure 4.4.10. TIC chromatogram from an injection of BSA using the DFGF assisted 2D HPLC procedure. This data was collected running without the use of the EFG for comparison. The three peaks correspond to the elution from the second dimension.

Observing the chromatogram from figure 4.4.10 the peaks display slight tailing. The procedure was run again utilising the electric field by applying an EFG with the timings as shown in table 4.4.1. This gave the sample time to be focused before the electric field was dropped and the sample loaded onto the second column resulting in a less diffuse peak detected by the mass spectrometer. The electric field was applied to the electrode closest to the ground electrode.

The voltages used were 1kV from each of the four Ultra Volt power supplies and an additional 1.5kV from the extra 30kV power supply all connected to a common ground rail on the same electrode. Figure 4.4.11 displays the chromatogram for the DFGF assisted 2D HPLC separation.

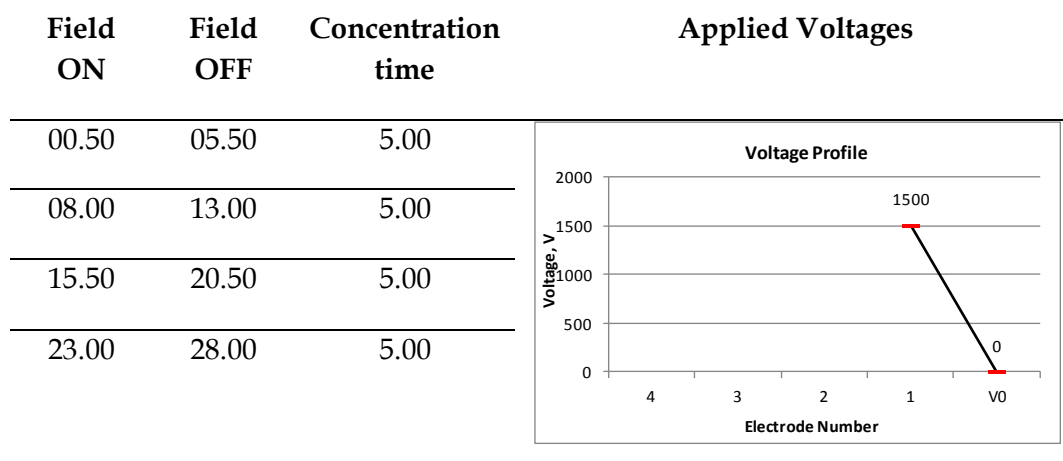


Table 4.4.1 Timings for the application of the EFG in the microfluidic device during 2D method.

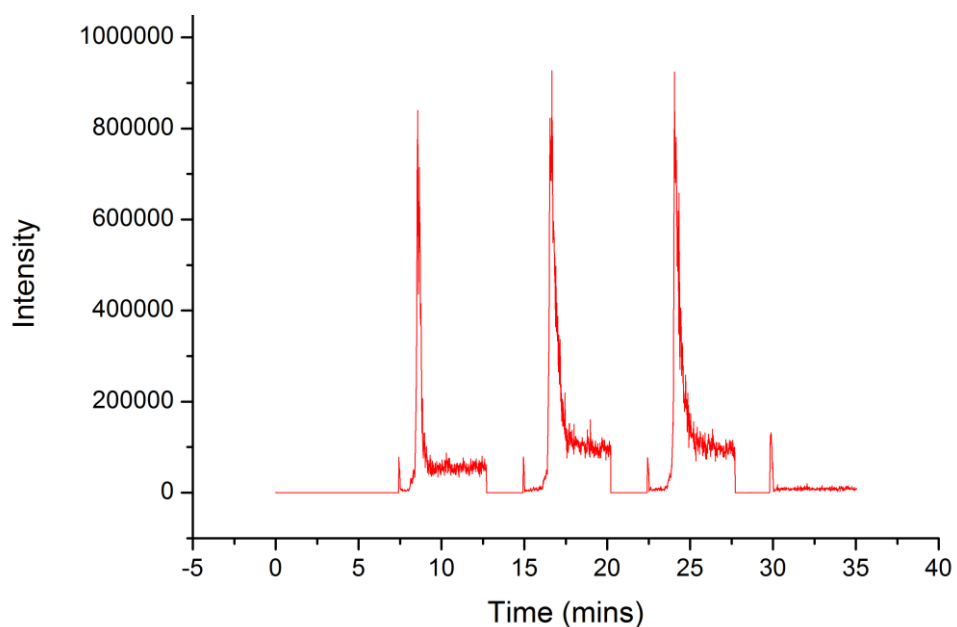


Figure 4.4.11. Chromatogram from the DFGF assisted 2D HPLC separation with the EFG in operation.

Comparing the chromatograms in figure 4.4.10 and figure 4.4.11, the electric field has given rise to an increase in the concentration of the analyte entering the second dimension hence the higher concentration reaching MS, and therefore the sharper the peaks in the chromatogram. This was displayed by the increase in intensity and improvement in peak shape, most notably the first peak. Further comparison of the two chromatograms is displayed in figure 4.4.12 where the two chromatograms overlaid emphasises the difference in the intensity and improvement of the peak shape in the first segment.

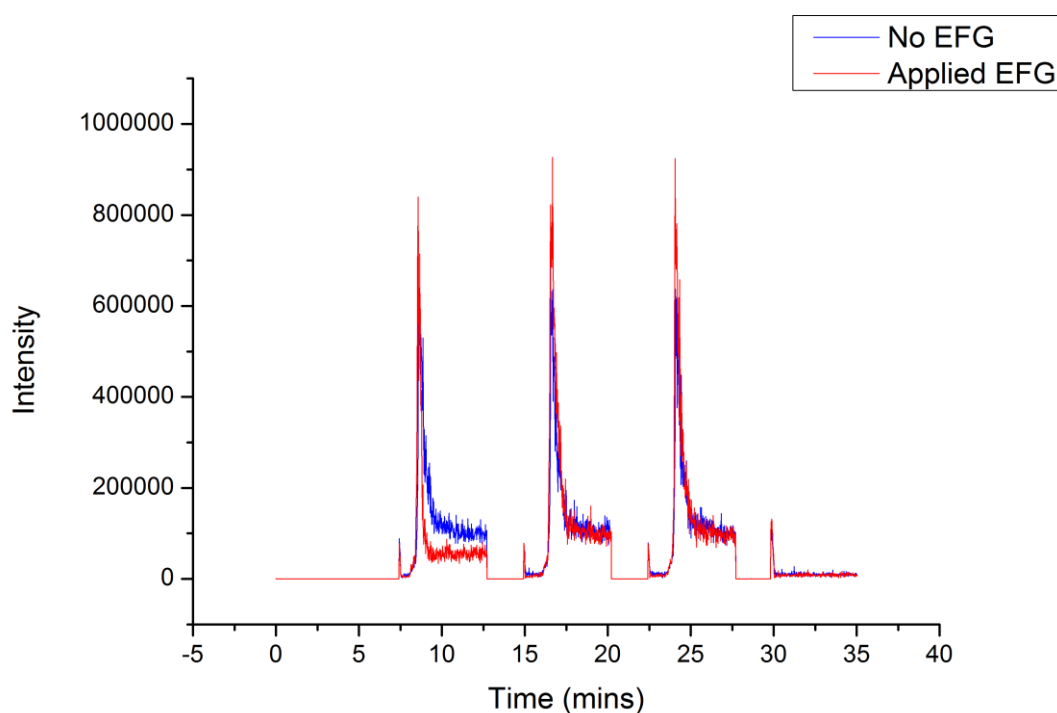


Figure 4.4.12. Overlaid chromatograms (from figures 4.4.11 & 4.4.12) from the DFGF assisted 2D HPLC separations with and without the pre-concentration of the electric field.

4.5 Conclusions

From the data presented in this chapter the microfluidic DFGF has been utilised in applications which have shown the scope of future uses for this technique and indeed highlighted areas where improvements need to be made in further developing a microfluidic DFGF device.

As seen above the separation of a mixture of functionalised GNP's was demonstrated, confirming the suitability of DFGF for separation and purification of these macromolecular structures of future medical importance². The microfluidic DFGF was able to focus the GNP's into two bands consisting of the individual particles and aggregates of these particles. Two defined bands were formed using voltage profiles with no more than the 600V mentioned, enabling potential downsizing of the power supply unit. With the use of the microfluidic DFGF it is noted that the separation of the GNPs was performed in an open channel which was a clear advantage. Having moved away from the use of the packing material as the polyacrylamide beads resulted in the sample becoming bonded to the surface. Though the separation was successful and very clear peaks were observed in the whole-on-column detection, the sample itself further demonstrated the issue with the leakage of the sample from the separation channel when being focused in the DFGF device. Additionally, the sample of GNPs failed to elute from the device as a result of trapping in the membrane and also the fact that a large proportion of the sample had in fact been trapped in the device between the membrane and the separation channel chip. Future work with the applications of the DFGF would aim to see the sample collected from the device having been separated.

This could be achieved by reducing the total amount of time spent in the column, reducing the amount of sample being pulled into the membrane by the high current density of the EFG. Despite not collecting the sample of the GNPs an open channel separation was observed having been recorded utilising the whole column reflectance method. This proof of concept work indicates that DFGF is possibly well suited for this application and that further advancement in this area is necessary in the future.

Having determined that samples injected onto the DFGF device were not being completely retained or correctly eluting from the device, the need for post column detection was realised. The microfluidic DFGF device was configured with C⁴D and UV detection. A bespoke Data acquisition system was devised and shown to work well giving the user data on-the-fly as well as recording the entire separation to a data file. The separations undertaken with the post column detection indicated that for a given injection only ~5% of that sample was retained by the EFG while the rest of the sample passed straight through the separation channel. This is clearly the most severe of the issues encountered with this microfluidic DFGF device. Though the loading of the sample can be reduced to prevent this effect, the stacking of samples in this device becomes impossible as when more of the sample is introduced it would simply flow through the separation channel unretained. Successful elution of retained sample gave a UV trace which enabled the comparison of the sample which passed through and that which had been retained. A seemingly small design oversight may be the cause of this issue. The separation channel in the first generation device for example was shallow and wide in respect of a perpendicular cross-section.

Also the design of the Protasis device saw the separation channel cross-section wide and shallow, the same as the first generation device. The reason for this shape of the channel cross-section is that the propagation of the electric field decreases as the distance from the electrodes increase. Therefore a channel which is wide and shallow is favoured; where in the case of the microfluidic DFGF the manufacturing procedure was less complex to have the separation channel thin and tall, resulting in ineffective electric field propagation and even turbulent flow of the sample in the open channel.

Aside from the issue with the volume of sample retained, a separation of the Kaleidoscope test mixture¹⁷ resulted in a C⁴D trace with 4-5 very sharp peaks detected as the field was lowered to an elution profile. In this instance the UV data also displayed a response. However, this was a broad peak determining that either the UV detector could not correctly distinguish the samples, or the post separation channel dead volume between the C⁴D and the UV detectors allowed the sample to significantly diffuse causing the broad UV peaks.

Further integration of the microfluidic DFGF with existing chromatographic technology saw the device utilised as a sample “pre concentrator” for 2D HPLC and HPLC-MS. Preliminary results with the microfluidic DFGF configured with a single column saw the pre concentration of insulin. This concentrating of the sample saw a large increase in the peak height and a decrease in peak width. This was a clear demonstration of the device functioning as an effective addition to this setup. The enhancement of peaks in this way enables a heightened resolution of complex samples by the decrease in the peak width translating to increased baseline resolution between peaks.

A more complex integration saw the device perform this pre concentration between the dimensions of a two dimensional separation. With the segment eluting from the first dimension, the microfluidic DFGF was then used to concentrate the sample before loading onto the second dimension. Comparison between chromatograms with and without the electric field displayed an improvement in the chromatography by the increased peak height and the improvement of the peak shape. This increase in peak height enables improvement in the sensitivity of the MS by higher concentrations of the sample injected to facilitate an increased response.

The successful improvements to the separations and MS detection indicated that the microfluidic DFGF device had worked well as a valuable addition to the analytical tools available for larger charged species. However, the initial aim was for the device to fully hold back a sample before loading onto the MS. Also with the 2D HPLC application it was postulated that the device would be able to fully retain a given analyte to counteract the longitudinal diffusion before further separation of the second dimension. Though this was observed, improvements to the device as discussed above in changing the shape of the separation channel would see the expectation of a functional electrophoretic switch realised. Having an operational switch would be favoured as the sample could be held and stacked before loading onto the MS.

Finally, the microfluidic DFGF has advanced from the separations of simple test mixture to applications with biomacromolecules and nanoparticulates as demonstrated in this chapter. Having been tested and successfully performing separations as a standalone device, the DFGF has also been successfully integrated with current technologies offering improvements in resolution in two dimension High Performance Liquid Chromatography.

4.6 References

1. M. Faraday, *Philosophical Transactions of the Royal Society of London*, 1857, **147**, 145-181.
2. E. C. Dreaden, A. M. Alkilany, X. Huang, C. J. Murphy, and M. a El-Sayed, *Chemical Society reviews*, 2011.
3. Ž. Krpetić, P. Nativo, I. a Prior, and M. Brust, *Small (Weinheim an der Bergstrasse, Germany)*, 2011, **7**, 1982-6.
4. M. M. Meighan, S. J. R. Staton, and M. A. Hayes, *Electrophoresis*, 2009, **30**, 852-865.
5. M. a. Rodriguez and D. W. Armstrong, *Journal of Chromatography B*, 2004, **800**, 7-25.
6. Bio-Rad, *www.bio-rad.com*, 150-4138 Polyacrylamide beads.
7. Z. Huang, Washington State University, 2001.
8. P. Kubán and P. C. Hauser, *Analytica chimica acta*, 2008, **607**, 15-29.
9. eDAQ, *www.eDAQ.com*.
10. NI-USB-6008, <http://sine.ni.com/psp/app/doc/p/id/psp-117/lang/e>.
11. OriginLab, <http://www.originlab.com/>, Origin 8.5.
12. J. Tang, M. Gao, C. Deng, and X. Zhang, *Journal of chromatography. B, Analytical technologies in the biomedical and life sciences*, 2008, **866**, 123-32.
13. H. Wang and S. Hanash, *Journal of Chromatography B*, 2003, **787**, 11-18.
14. J. J. van Deemter, F. J. Zuiderweg, and A. Klinkenberg, *Chemical Engineering Science*, 1995, **50**, 3869-3882.
15. S. M. Darby, M. L. Miller, R. O. Allen, and M. LeBeau, *Journal of analytical toxicology*, 2001, **25**, 8-14.
16. Flux Instruments, http://www.flux.ch/index.php?id=flux_rheos_2200.
17. Bio-Rad, *www.bio-rad.com*, 161-0324 Kaleidoscope Prestained Standards (broad .

Chapter 5. Final Conclusions

5.1 Conclusions

Following the progression of work through this project, progress towards new steps forward in the evolution of DFGF have been observed. With the initial experimentation carried out on the first generation Ivory device¹, refinements were made to this device including the addition of a Teflon membrane support. This replaced the earlier configuration using a ceramic support. The use of this Teflon membrane support simplified assembly of the device with no differences in operation. The first generation device provided an existing working platform for this project to embark from. Working with this device saw successful focusing and separations of two component dye mixtures utilising the Protasis² power supply and other DFGF supporting equipment including the Flux Instruments Rheos 2200³ pump. Advancement through this initial work saw the optimisation of the packing method. Preceding packing methods for these devices would often result in failure or a suboptimal packed bed. The addition of the vibrating motor to the packing reservoir and submerging the entire device in a sonic bath resulted in a higher success rate and the packed bed itself required less time to equilibrate on the system, in some cases the packing was equilibrated after only 3hours.

During the operation of this device the imaging process was improved to enable plots of the whole DFGF separation to be presented displaying the positions and concentrations of samples across the whole channel. With this system the imaging process was more sensitive to less visible bands in the separation channel.

Moreover, the image interpretation process was applicable to all forms of whole column detection throughout the project, including all three DFGF devices and both the reflectance detection and with PDA detection.

While the first generation device was used to assess the dimensions for the microfluidic device, the new Protais² DFGF device was successful in handling larger injection volumes of sample. In experiments shown in chapter two, the device demonstrated the retention and focusing of 40 μ L of the Kaleidoscope protein mixture.

Refining both of these devices saw the production of an innovative new packing material. The 80 μ m spherical silica particles further improved the success rate of packing the channels as well as providing a more uniform flow through the separation channel. These particles were also packed into a GC column which displayed near perfect hexagonal close packing of these particles. This GC column demonstrated a separation of a two component mixture while only being 1.2m in length compared to a typical open channel GC column at 15m. Results from these particles when packed in the DFGF device saw a reduction in time for injected analytes to reach initial focal points in the device, and the time for bands to migrate to new focal points in response to changes in the EFG.

Having identified key issues with the size and construction of the larger scale DFGF devices the design and production of the microfluidic DFGF device was carried out yielding a device, which was successfully integrated with existing DFGF equipment, while providing a system which was able to be modified and developed further to result in a working microfluidic system.

Through chapter three key areas of development were the integration of the microfluidic DFGF with supporting equipment, electrode improvement, imaging optimisation, electrode channel enhancement, and finally the utilisation of a PDA detector.

Through the development of the electrodes, the design flaws with the original electrode chips were identified, confirmed and the degradation issues solved by utilising platinum foil electrodes. With the utilisation of RP, the sample leakage issue was reduced by implementing a 200 μ m electrode channel chip. The RP process has proved a useful tool in the development of analytical platforms^{4,5}. With the fluidics and electronics working correctly, the enhancement of the imaging process led to separation channel chip being coated to eliminate interference from stray light. In addition the microfluidic device was operated running upside down to eliminate the detection of gaseous species evolving from the electrolysis in the separation channel. These enhancements provided increased stability and sensitivity in the reflectance and PDA detection. Moving forward with detection, the incorporation of the PDA detector demonstrated the ability to determine the position and intensity of analytes in the separation channel. Additional bespoke software was utilised demonstrating full control over the PDA detector. A simple UV light source was introduced and the first whole-on-column UV detection was observed for a microfluidic DFGF device. Though this detection proved the concept further work is required in fully utilising this method and are discussed in section 5.2. The result of each of these refinements yielded the optimised microfluidic DFGF device which was observed to be suitable for the separation of proteins by partially resolving five components of the Kaleidoscope test mixture⁶.

Comparing this to the performance of the microfluidic DFGF by Myers and Bartle⁷ it is apparent that the earlier device was able to resolve six of the seven components. This can be attributed to the additional electrode in the Myers and Bartle device giving an additional gradient to resolve the sixth component. Despite the deficiency in separating all seven species the microfluidic DFGF device has achieved these separations in an open channel without the need for a packing material or monolith which is advantageous in facile setup and longevity of operation.

Having shown stable operation the microfluidic DFGF device was implemented in a series of applications as described through chapter four. The first of these was the work on GNPs. This separation found a mixture of GNPs could be separated by size and charge in the microfluidic DFGF device. Though the GNPs were not efficiently recovered from the device, the concept of separating these macromolecular structures using DFGF is certainly a feasible technique, adding to the existing methods using di-electrophoresis⁸. Further work in improving this separation would see the utilisation of the 80µm silica particles with a diol bonded surface⁹ packed into the Protasis² device where the sample would have no interaction with the silica surface and, with the larger volumes capable of the Protasis device, the sample could be separated in larger batches and using the stacking of sample a particular size could be selectively retained and collected.

The detection of samples eluting from the DFGF devices was deemed necessary to determine the extent of which samples were retained and indeed how concentrated these bands were on elution. With the DFGF exclusively separating charged species, C⁴D was identified as the most suitable detection method as it is most sensitive to charged species. To facilitate the validation of the C⁴D detector a secondary detection method, a Waters tuneable UV detector, was integrated.

As mentioned in chapter four data from these detectors was collected using a simple DAQ system written in LabView which successfully collected and stored data enabling interpretation in Origin. Observing the data from the post column detection, sharp concentrated peaks were seen eluting from the device. In some cases broad peaks were observed in the UV detection caused by the time in free solution before reaching the detector. The successful detection of species with the C⁴D detector¹⁰ confirm that integrating this detection system into the next microfluidic design would enable the production of a traditional chromatogram from the DFGF device while providing a trigger of the eluted species to initiate an automated fraction collector, switching valve or further analytical detection system.

With the demonstration of samples eluting from the microfluidic DFGF device, applications with existing HPLC technology were carried out. Initially the aim was to retain the sample from the single column before releasing the analyte on to the Mass Spectrometer. However with the observations in attempting this and the work with the C⁴D detector, the analytes were not fully retained. The second approach saw the application of the electric field to simply counteract the longitudinal diffusion. Preliminary data from this approach saw the pre-concentration of an injection of insulin. Pre-concentration of these species improves the detection of the samples where only small amounts are available. Introducing a second column involved a tailored configuration utilising three six port switching valves to enable the concentration of the sample between dimensions. The switching valve array would not be required if the electric field gradient in this device was capable of fully retaining the sample. In contrast, the configuration described in chapter four can be used to change the solvent system between dimensions.

Directly comparing two runs with and without the use of the electric field displayed increased peak heights when the sample reached the mass spectrometer. As a proof of concept this has shown with the utilisation of an applied electric field gradient, a segment from the first dimension can be re-concentrated inline before being loaded onto the second dimension. The advantages of this are clear in instances where a sample containing many components can more effectively resolve these components as a result of the peak height increase resulting in narrower peaks increasing the baseline between peaks that many have previously co-eluted. The effect of sharpened peaks have been described in a similar work where a wide bore electrophoresis system was placed after the second dimension ¹¹. With this proof of concept a device specifically designed to operate a switching valve could be used. For example, the microfluidic electrokinetic valve described by Ivory *et al.*¹² could be further developed to perform in this application.

5.2 Further work

With the manufacture of the 80µm silica particles for DFGF, preliminary experiments using the Protasis system for CE were explored. There were significant failings in sample mobility in attempting CE caused by poor field propagation through the organic mobile phase. In order to increase the versatility of the Protasis device, when packed with functionalised 80µm particles, the system could be used for HPLC, CE and DFGF by only changing the mobile phase. This would be advantageous in providing a versatile device capable of a range of separation techniques in a single instrument.

Additional work with first generation and Protasis devices would be to integrate these with the post column detection system using the C⁴D and UV detectors to fully assess the retention and peak elution profiles from these systems.

From the data collected monitoring the mobile phase leaving the microfluidic DFGF it was observed that after injections only 5%v/v of the sample was held by the EFG. This can be attributed to a number of factors including; the shape of the separation channel, the flexibility of the membrane, and the higher volume of solution in the open channel (at any given point) compared to a packed channel.

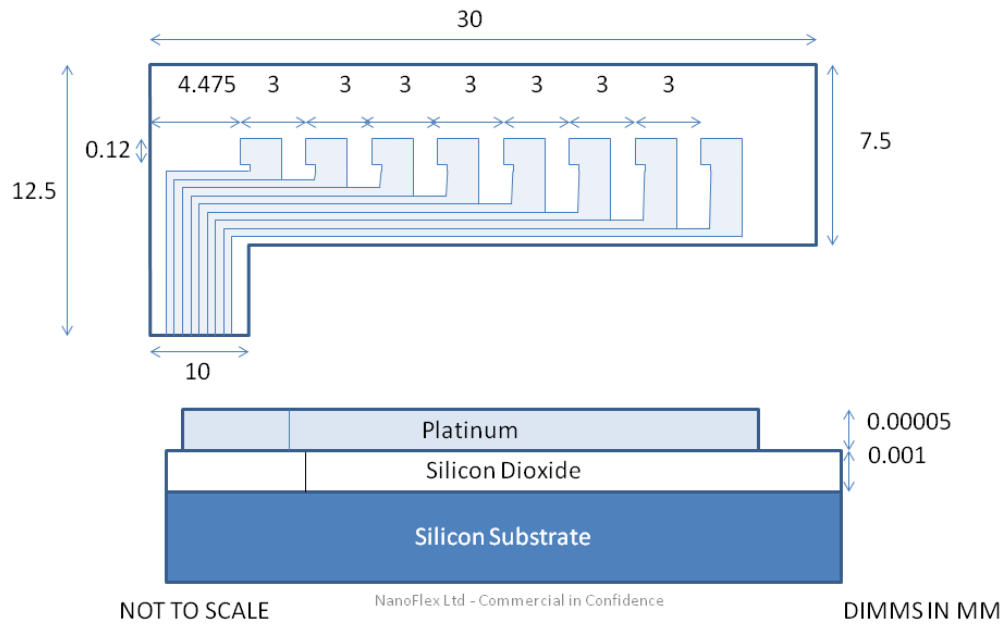
The membrane was identified as a weak link in the technique from the outset of this project. An experimental solution discussed by Ivory¹³ details a membrane-less DFGF system based on the large Ivory device. This design is not easily scalable down to a microfluidic device. Further development of DFGF would be to work towards a microfluidic membrane-less DFGF. This could be achieved using oil boundary electrodes as in work by Thwar¹⁴ or by utilising a permanent porous material as with the porous glass used by Myers and Bartle⁷.

The membrane also caused serious issues in the microfluidic DFGF being the source of the sample leakage issue. As the membrane is a flexible material, it can stretch and becomes distorted when the force of the hydrodynamic flow is applied. This issue was reduced with the 200µm wide electrode channel. However, the issue was still observed. Further work with the current microfluidic device would see a complete replacement structure for all components including the membrane. This could for instance, all be a singular sealed component housing the electrodes, electrode channel, and interfaces to the supporting equipment.

The best possible way to achieve this would be to integrate the electrodes onto a PCB and also house the PDA detector and even electrodes for C⁴D detection all on the same board further simplifying the system. Further work on the electrodes would contribute to the aim of a membrane-less system with the use of an emerging electrode technology from NanoFlex Ltd¹⁵.

These new nano electrodes are composed of a layer of conductive electrode material between insulating layers. The result of this nano electrode configuration is that gaseous electrolysis products do not form bubbles in the solution and pH changes are confined to small zones around the electrodes. A design for these electrodes for application in the microfluidic DFGF is shown in figure 5.2.1. The chip is the same dimensions as specified in the dolomite design with a 5mm edge connector for integrating with the power supplies. There are eight 50nm nanoband electrodes each one 100µm wide. The band electrodes are normal to the surface 500nm within a trench which is ~1000nm deep.

Platinum Layer



Insulating Layer

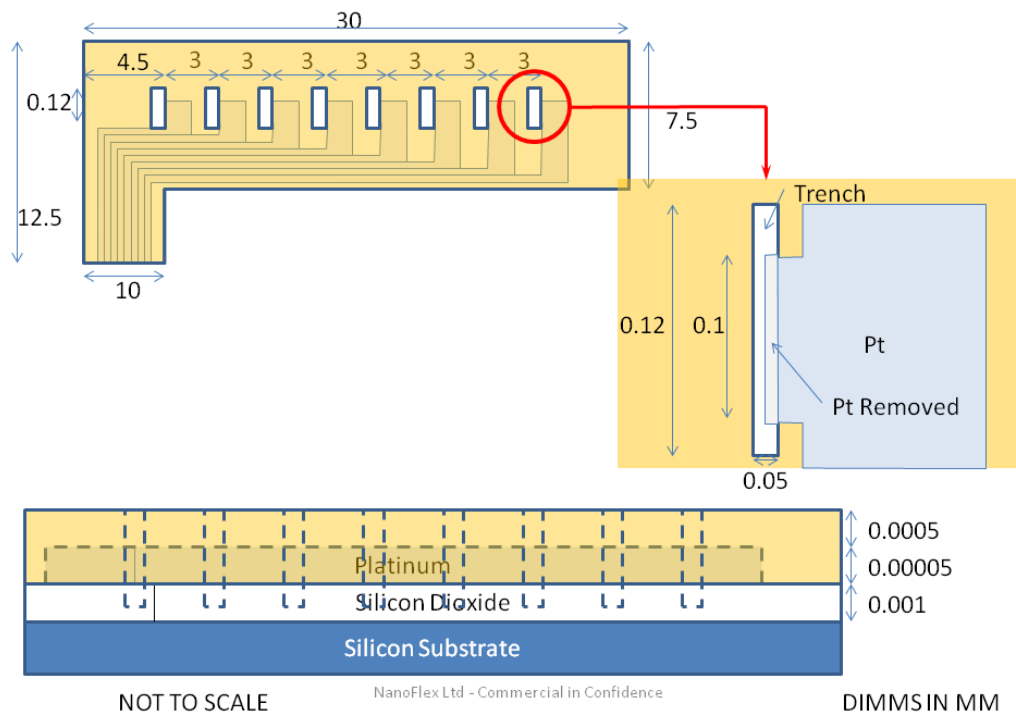


Figure 5.2.1. NanoFlex¹⁵ Electrode chip design. The nanoband electrodes are located between a layer of silicon dioxide and an insulating top layer. Only the sides of the electrodes exposed in the trench make contact with the solution over a controlled uniform surface.

With these electrodes, investigations into shaping the electric field with the aim of concentrating the electric field accurately over the separation channel could be undertaken. This could be done by exposing the electrodes in specific points along the trenches. Moreover, the nano sized electrode width has an advantage in that any gaseous species formed by electrolysis are in bubbles which are so small that they dissolve into the solution. The effect could be a key feature in the elimination of the membrane. An alternative method of eliminating gas evolution would be to use Ruthenium Oxide electrodes which do not catalyse the splitting of water¹⁶.

The chip designed by NanoFlex houses eight electrodes though the Protasis power supply only has four. The presence of the eight electrodes would be to facilitate the use of a multiplexer. A multiplexer is a device which would enable the use of a single HV supply to generate an electric field gradient. This is achieved by 'flashing' the correct voltage across each of the electrodes sequentially. This enables the miniaturisation of the HV power supply leading to a reduced laboratory footprint.

To resolve the key issue with the microfluidic DFGF, the sample leakage issue, the separation channel itself should be replaced with a channel with the same proportions as those used by Ivory^{17,18} and Myers^{7,19}. In these devices the separation channel is wide and shallow in the plane parallel to the electrode channel. The separation channel in the microfluidic DFGF is narrow and deep. This affects the propagation as shown by computer modelling of the electric field degradation by Ivory²⁰ which shows that the further away from the electrodes the field must propagate, the weaker the electric field. As the strength of the field is highest closer to the electrode the separation channel should be 100-200 μm wide and 50-100 μm deep to most efficiently utilise the electric field.

Furthermore, with this change in channel shape the surface area of membrane forming the base of the separation channel would be larger, reducing the pressure. This would, therefore, reduce the force causing the stretching and flexing of the membrane, and ultimately prevent the sample leaking out of the separation channel. With a reliable system, further application in medicinal pharmaceutical and biological areas would be possible. Even larger species such as particles and even whole cells could be mobilised in the device similar to existing work on electric field induced locomotion²¹.

With the advances made throughout this project, DFGF has been moved closer to becoming a technique which could be widely used to improve research across multiple disciplines of science.

5.3 References

1. R. D. Greenlee and C. F. Ivory, *Biotechnology progress*, 1998, **14**, 300-9.
2. Protasis Corp, <http://www.protasis.com/>.
3. Flux Instruments, http://www.flux.ch/index.php?id=flux_rheos_2200.
4. T. Wray and P. Myers, *Chromatography Today*, 2011, 34-36.
5. B. Brkić, N. France, A. T. Clare, C. J. Sutcliffe, P. R. Chalker, and S. Taylor, *J. Am. Soc. Mass Spectrom.*, 2009, **20**, 1359-1365.
6. Bio-Rad, 161-0324 *Kaleidoscope Prestained Standards (broad range)*.
7. P. Myers and K. D. Bartle, *Journal of Chromatography A*, 2004, **1044**, 253-258.
8. F. Du, M. Baune, a. Kück, J. Thöming, A. Kuck, and J. Thoming, *Separation Science and Technology*, 2008, **43**, 3842-3855.
9. Z. Huang, Washington State University, 2001.
10. eDAQ, www.eDAQ.com.
11. Y. Li, X. Fang, S. Zhao, T. Zhai, X. Sun, and J. J. Bao, *Chemistry Letters*, 2010, **39**, 983-985.
12. H. Cui, Z. Huang, P. Dutta, and C. F. Ivory, *Analytical chemistry*, 2007, **79**, 1456-65.
13. J. M. Burke, C. D. Smith, and C. F. Ivory, *Electrophoresis*, 2010, **31**, 902-9.
14. P. K. Thwar, J. J. Linderman, and M. a Burns, *Electrophoresis*, 2007, **28**, 4572-81.
15. NanoFlex Ltd, www.nanoflex.com.
16. D. Pletcher, in *Industrial Electrochemistry*, 1990, pp. 90-95.

17. Z. Huang and C. F. Ivory, *Analytical Chemistry*, 1999, **71**, 1628-1632.
18. J. M. Burke, Z. Huang, and C. F. Ivory, *Analytical chemistry*, 2009, **81**, 8236-43.
19. P. G. Tuñón, Y. Wang, P. Myers, K. D. Bartle, L. Bowhill, C. F. Ivory, and R. J. Ansell, *Electrophoresis*, 2008, **29**, 457-465.
20. J. M. Burke and C. F. Ivory, *Electrophoresis*, 2008, **29**, 1013-25.
21. G. Loget and A. Kuhn, *Nature communications*, 2011, **2**, 535.

Appendix

Appendix A. List of Abbreviations

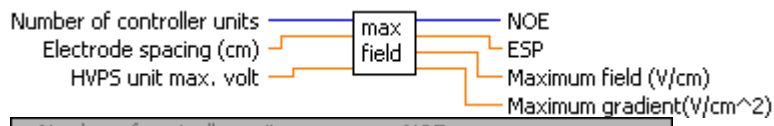
*.CSV	Comma Separated Values
2-DGE	Two Dimensional Gel Electrophoresis
2-DGE/MS	Two Dimensional Gel Electrophoresis with Mass Spectrometry
2D-HPLC	Two Dimensional High Performance Liquid Chromatography
AC	Affinity Chromatography
AC	Alternating Current
AM	Amaranth
AY	Acid Yellow
BET	Brunauer, Emmett, and Teller isotherm
BPB	Bromophenol Blue
BSA	Bovine Serum Albumin
C⁴D	Capacitively Coupled Contactless Conductivity Detection
CACE	Counteracting Chromatographic Electrophoresis
CAD	Computer Aided Design
CAS	Chemical Abstracts Service
CE	Capillary Electrophoresis
CE/MS	Capillary Electrophoresis with Mass Spectrometry
CEC	Capillary Electrokinetic Chromatography
CPS	Centrifugal Particle Size analysis
CTAB	Cetyl trimethylammonium bromide
DAQ	Data Acquisition
DCM	Dichloromethane
DFGF	Dynamic Field Gradient Focusing

DSLR	Digital Single Lens Refraction camera
EC	Electro-Chromatography
EFG	Electric Field Gradient
EFGF	Electric Field Gradient Focusing
FCCE	Flow Counterbalanced Capillary Electrophoresis
FTIR	Fourier Transform Infrared Spectroscopy
GC	Gas Chromatography
GC/MS	Gas Chromatography with Mass Spectrometry
GE	Gel Electrophoresis
GE/MS	Gel Electrophoresis with Mass Spectrometry
GIMP	Gnu Image Manipulation Program
GNP	Gold Nanoparticles
HPLC	High Performance Liquid Chromatography
HV	High Voltage
ID	Internal Diameter
IDC	Insulation-Displacement Connector
IDE	Integrated Drive Electronics
IEF	Isoelectric Focusing
ITP	Isotachopheresis
LC	Liquid Chromatography
LC/MS	Liquid Chromatography with Mass Spectrometry
LCD	Liquid Crystal Display
LED	Light Emitting Diode
MS	Mass Spectrometry
MWCO	Molecular Weight Cut Off (Daltons)
NI	National Instruments
OD	Outer Diameter

PCB	Printed Circuit Board
PDA	Photo Diode Array
PEEK	Polyether ether ketone
PVD	Physical Vapour Deposition
RP	Rapid Prototyping
RP-HPLC	Reverse Phase High Performance Liquid Chromatography
SCX	strong cat-ion exchange
SDS	Sodium dodecyl sulfate
SEM	Scanning Electron Microscopy
SLA	Stereolithography
SLA RP	Stereolithography Rapid Prototyping
SLR	Single Lens Reflex
TIC	Total Ion Count
TSQ MS	Triple Stage Quadrupole Mass Spectrometer
USB	Universal Serial Bus
UV	Ultra Violet light
VBA	Visual Basic for Applications

Appendix B. Protasis voltage array and control software

maximumfield.vi



Number of controller units	NOE
<input type="text" value="4"/>	<input type="text" value="4"/>
Electrode spacing (cm)	ESP
<input type="text" value="0.50"/>	<input type="text" value="0.50"/>
	Maximum field (V/cm)
	<input type="text" value="800.00"/>
HVPS unit max. volt	Maximum gradient(V/cm ²)
<input type="text" value="1000.00"/>	<input type="text" value="400.00"/>

DBL HVPS unit max. volt

I32 Number of controller units

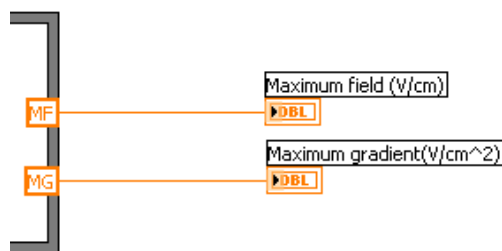
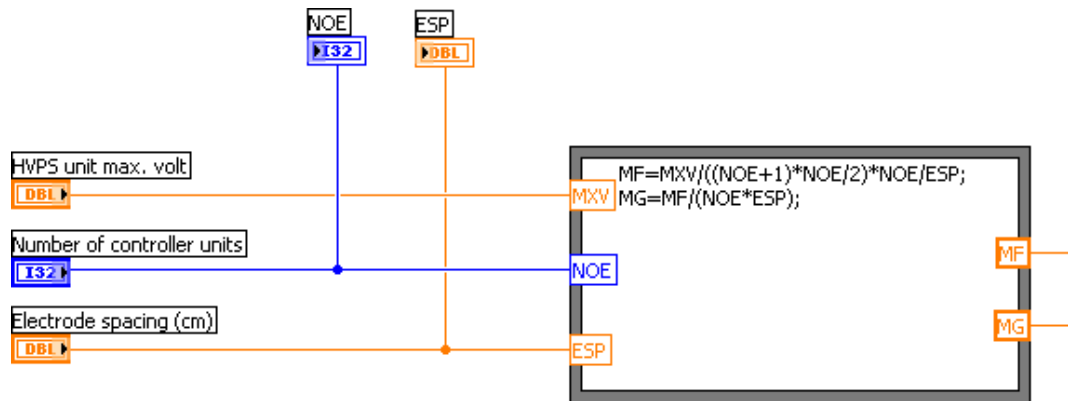
DBL Electrode spacing (cm)

DBL Maximum gradient(V/cm²)

DBL Maximum field (V/cm)

I32 NOE

DBL ESP



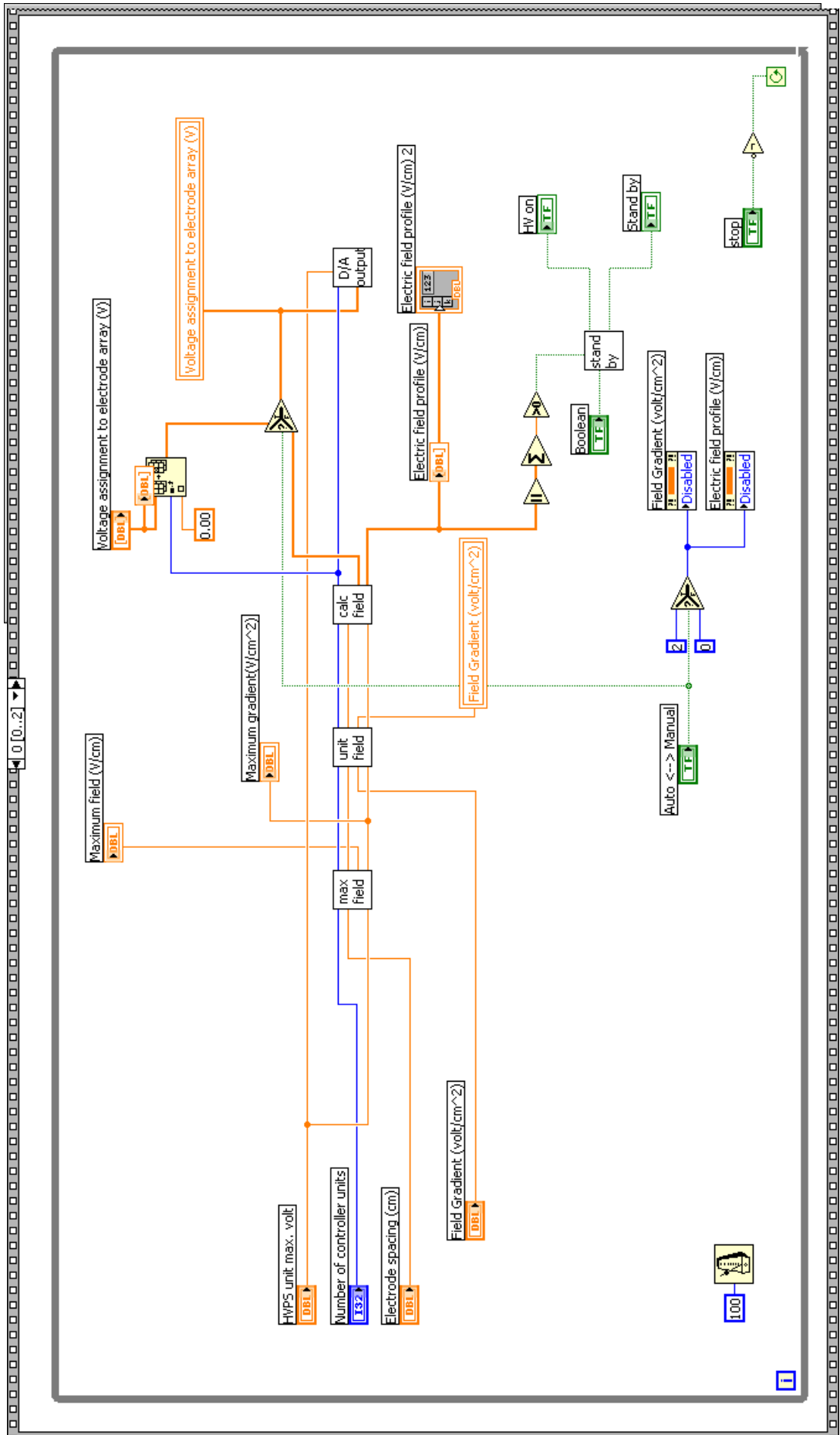
"maximumfield.vi History"
Current Revision: 2

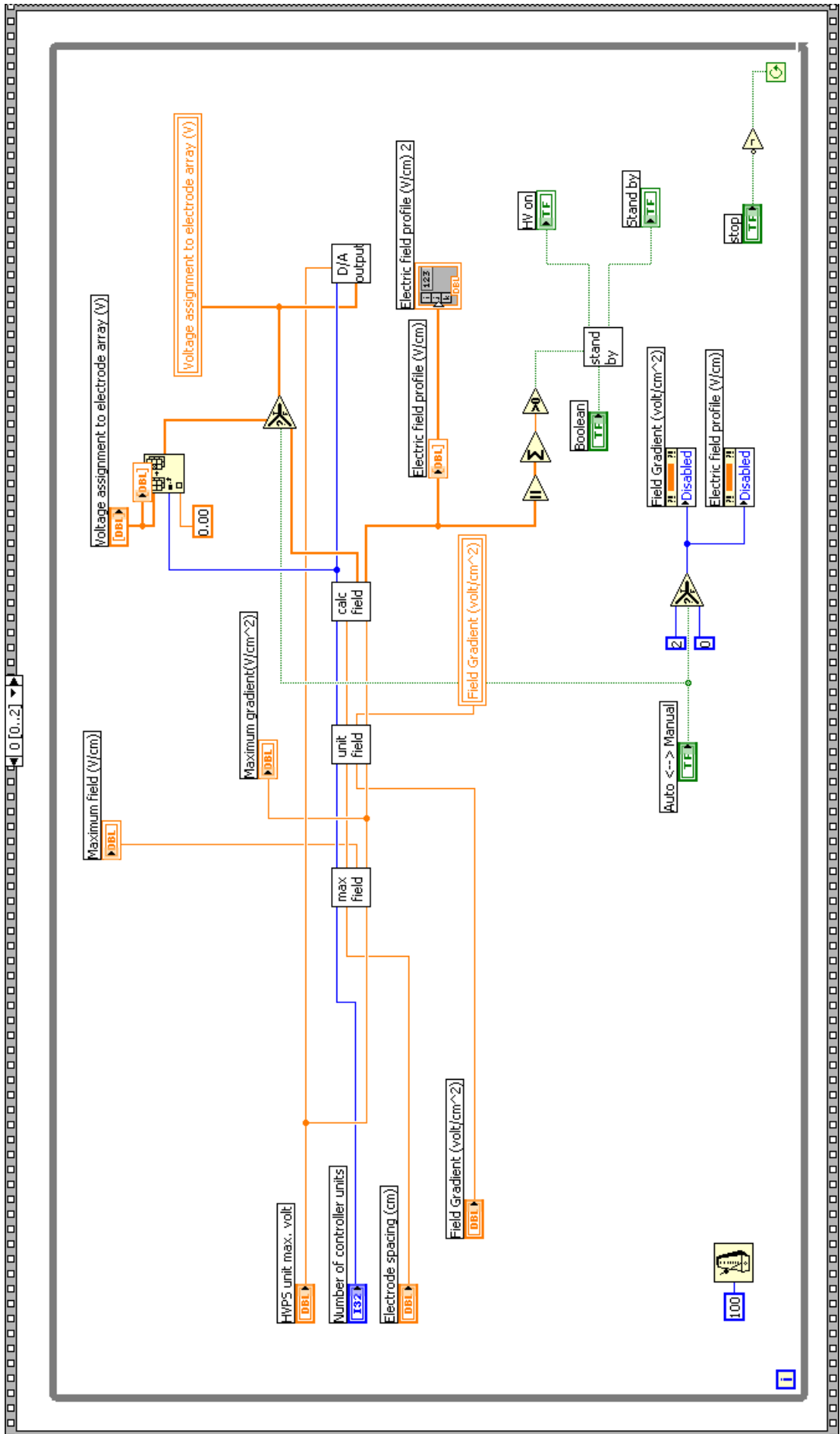
Position in Hierarchy

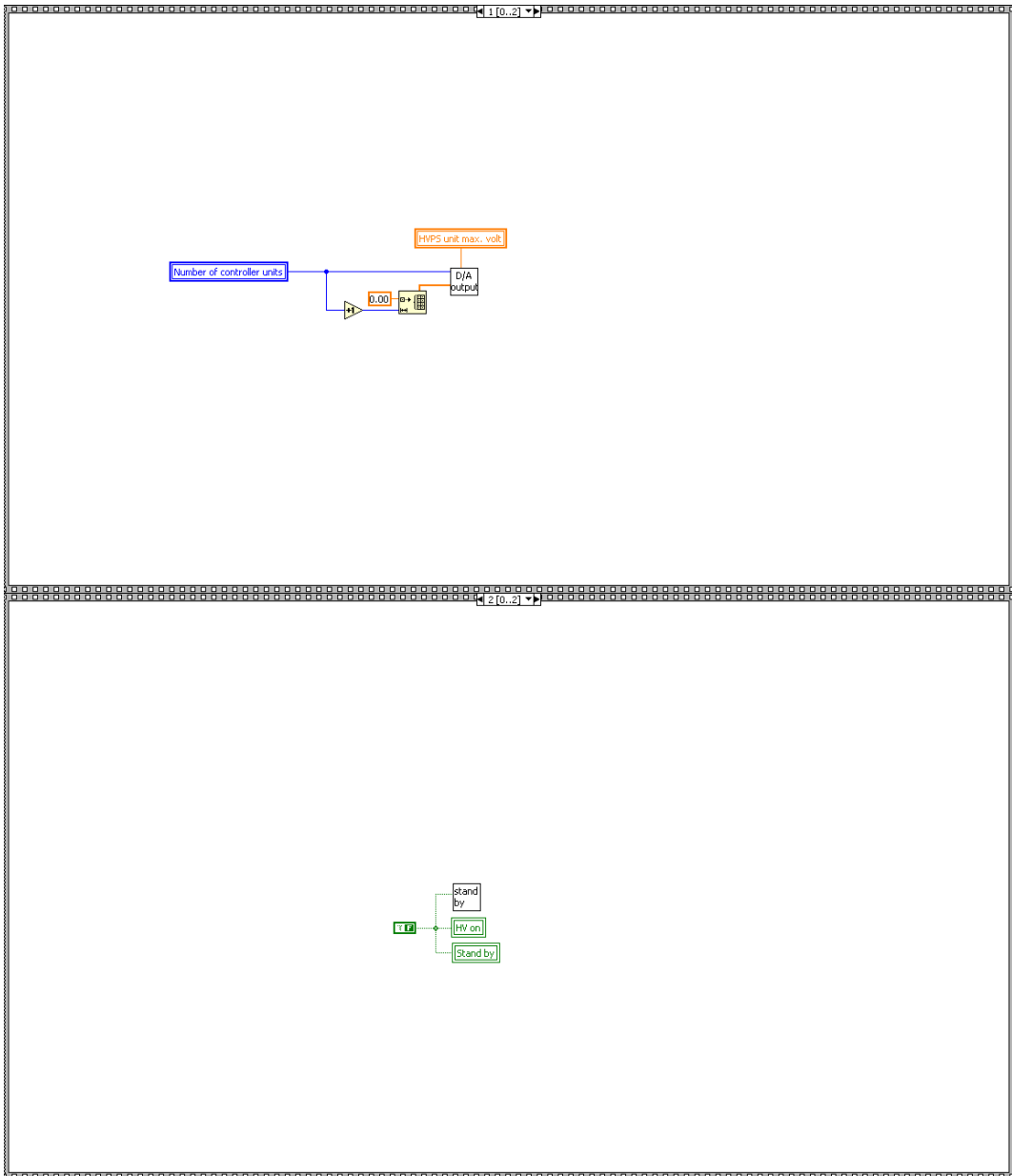


UcontrollerREVISED.vi









max
field

maximumfield.vi

C:\Documents and Settings\Lab Pc\Desktop\DfGF controller V2\Ucontroller.llb\maximumfield.vi

unit
field

unitfield.vi

C:\Documents and Settings\Lab Pc\Desktop\DfGF controller V2\Ucontroller.llb\unitfield.vi

calc
field

calcfield.vi

C:\Documents and Settings\Lab Pc\Desktop\DfGF controller V2\Ucontroller.llb\calcfield.vi

D/A
output

CMDout.vi

C:\Documents and Settings\Lab Pc\Desktop\DfGF controller V2\Ucontroller.llb\CMDout.vi

stand
by

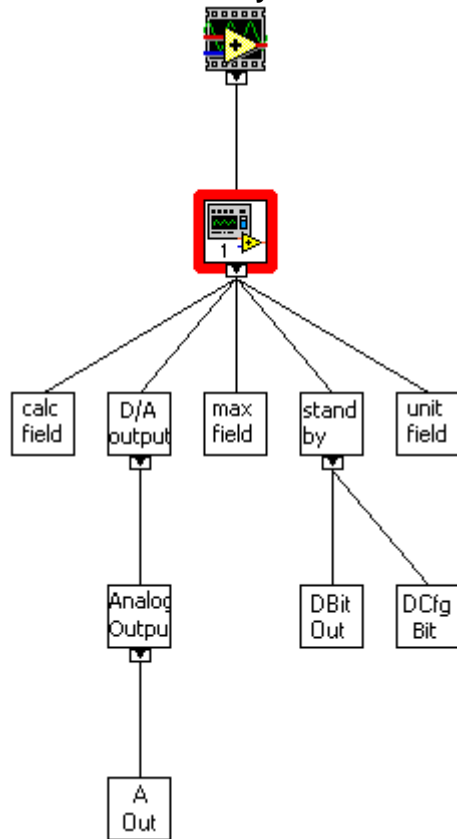
Standby.vi

C:\Documents and Settings\Lab Pc\Desktop\DfGF controller V2\Ucontroller.llb\Standby.vi

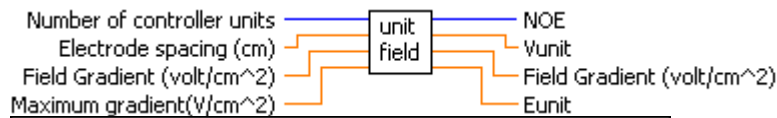
"UcontrollerREVISED.vi History"

Current Revision: 17

Position in Hierarchy



unitfield.vi



Number of controller units	NOE
<input type="text" value="4"/>	<input type="text" value="4"/>
Electrode spacing (cm)	Vunit
<input type="text" value="0.50"/>	<input type="text" value="100.00"/>
Field Gradient (volt/cm ²)	Field Gradient (volt/cm ²)
<input type="text" value="400.00"/>	<input type="text" value="400.00"/>
Maximum gradient(V/cm ²)	Eunit
<input type="text" value="400.00"/>	<input type="text" value="200.00"/>




DBL Electrode spacing (cm)

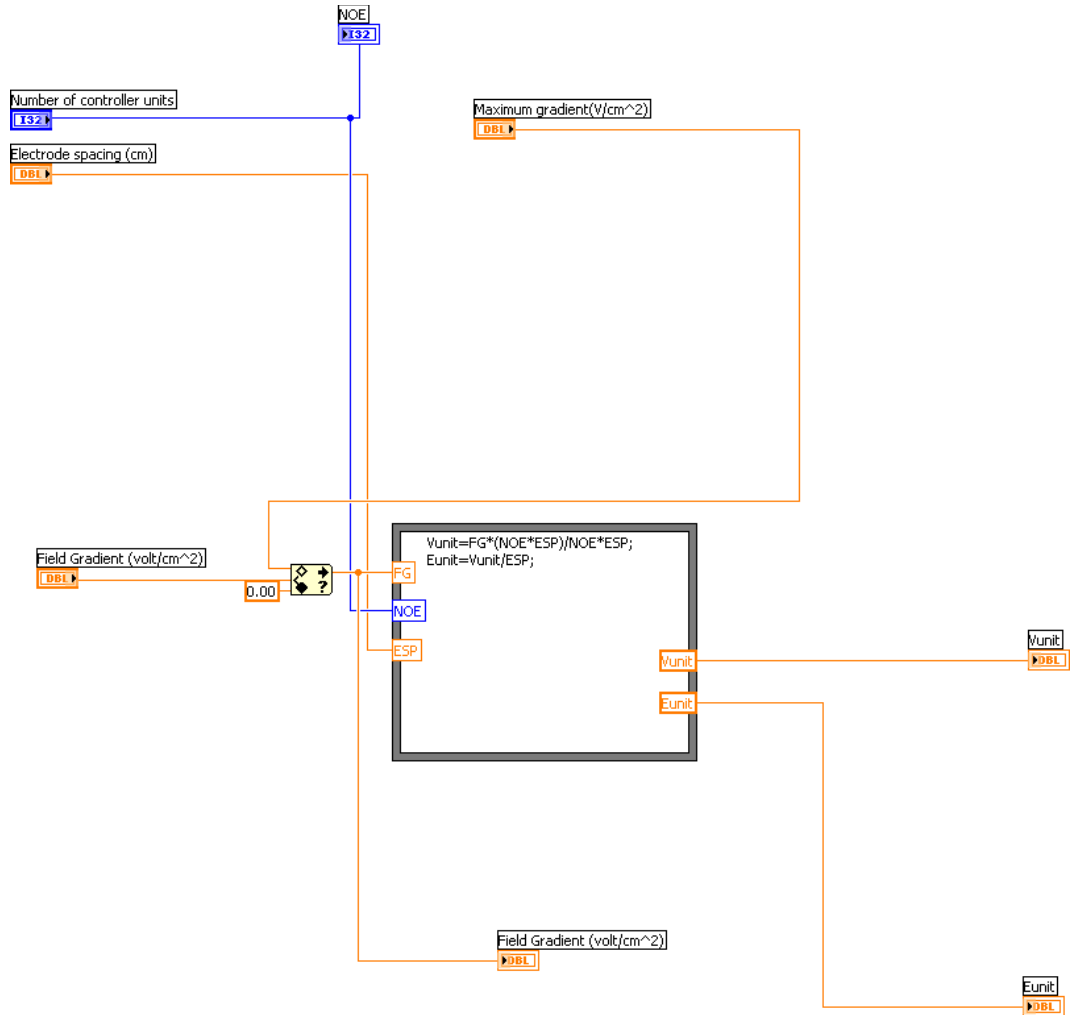
I32 Number of controller units

DBL Maximum gradient(V/cm²)

DBL Field Gradient (volt/cm²)

DBL Vunit

-  Eunit
-  Field Gradient (volt/cm^2)
-  NOE

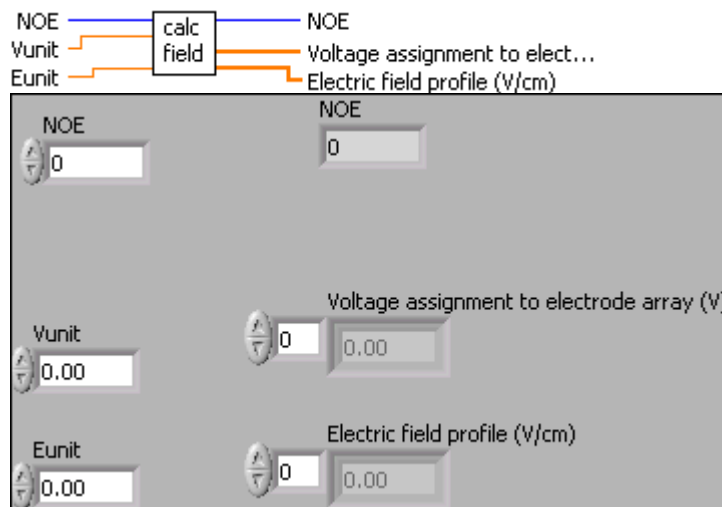


"unitfield.vi History"
Current Revision: 1

Position in Hierarchy



calcfld.vi



DBL Vunit

DBL Eunit

I32 NOE

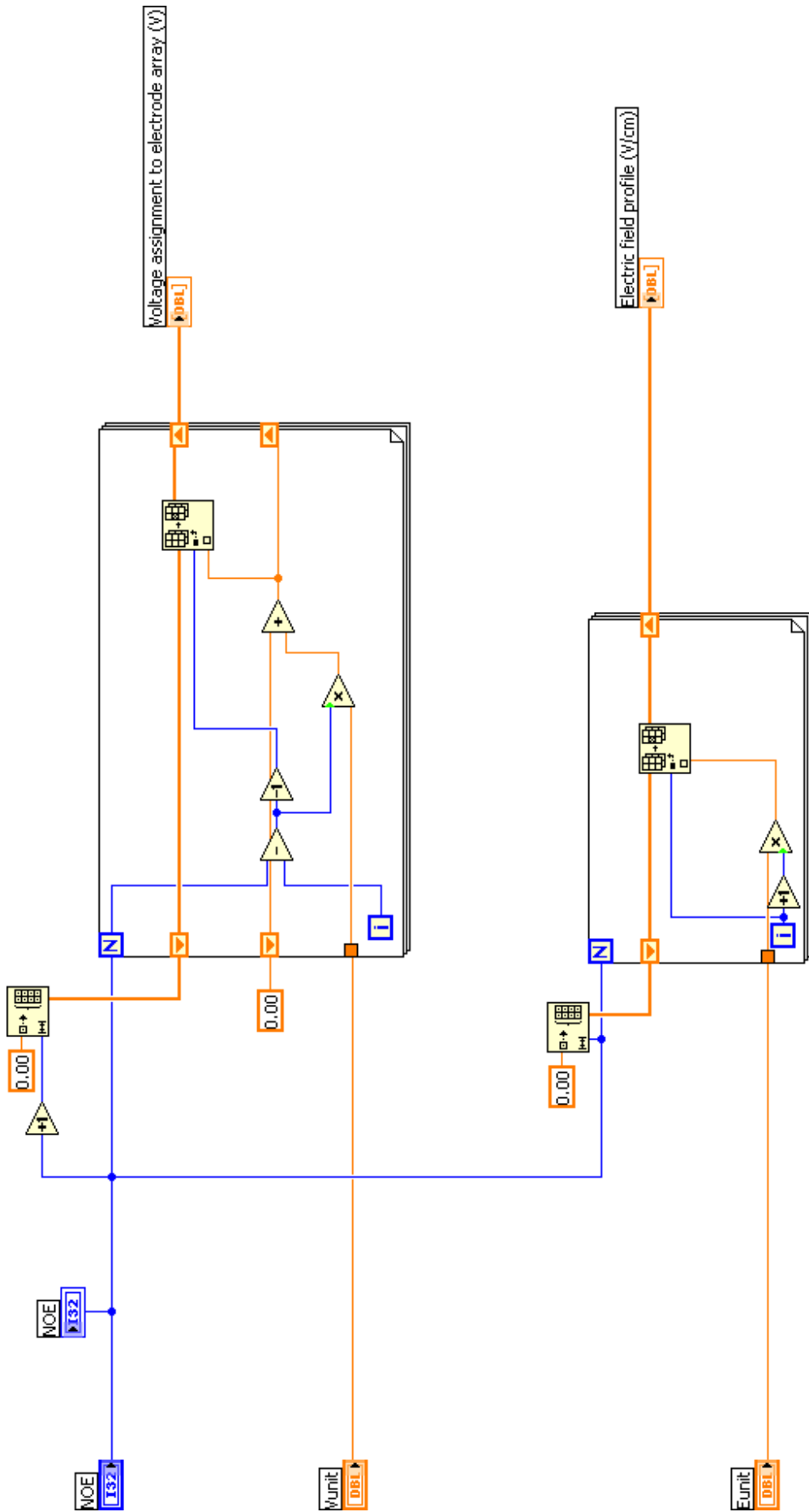
DBL Electric field profile (V/cm)

DBL Slide

DBL Voltage assignment to electrode array (V)

DBL ch1

I32 NOE

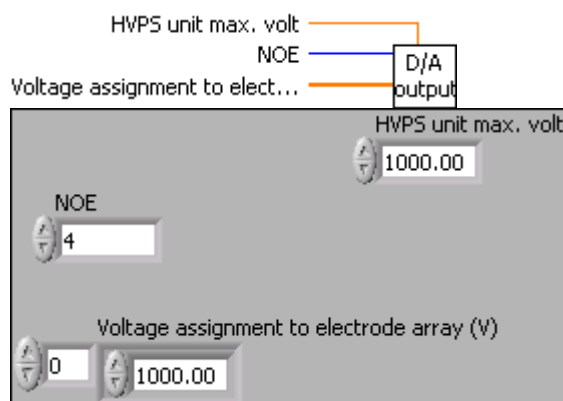


"calfield.vi History"
Current Revision: 1

Position in Hierarchy



CMDout.vi

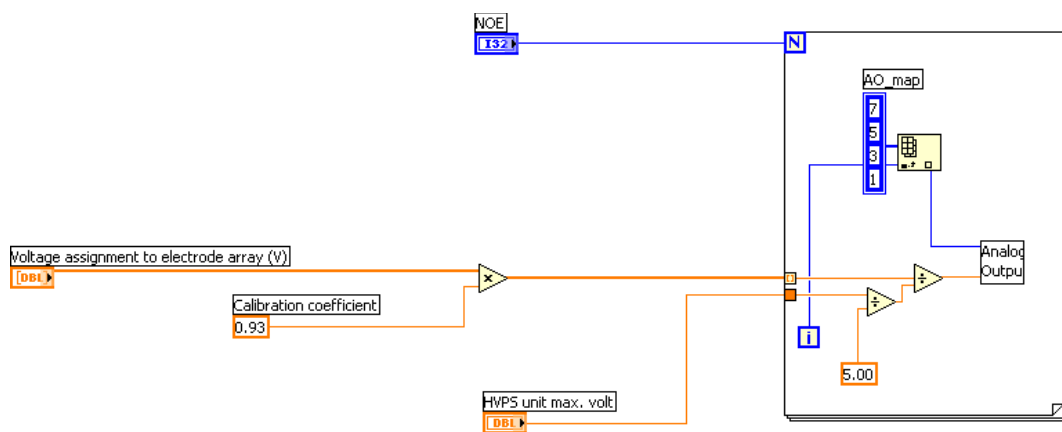


[DBL] HVPS unit max. volt

[I32] NOE

[DBL] Voltage assignment to electrode array (V)

[DBL] ch1





AnalogOutput.vi

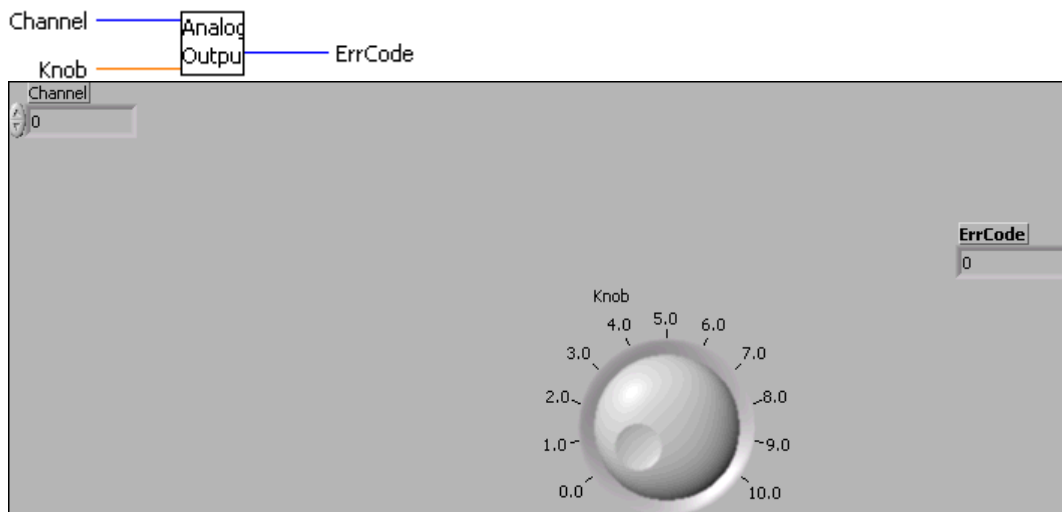
C:\Documents and Settings\Lab Pc\Desktop\DfGF controller V2\Ucontroller.lib\AnalogOutput.vi

"CMDout.vi History"
Current Revision: 6

Position in Hierarchy



AnalogOutput.vi

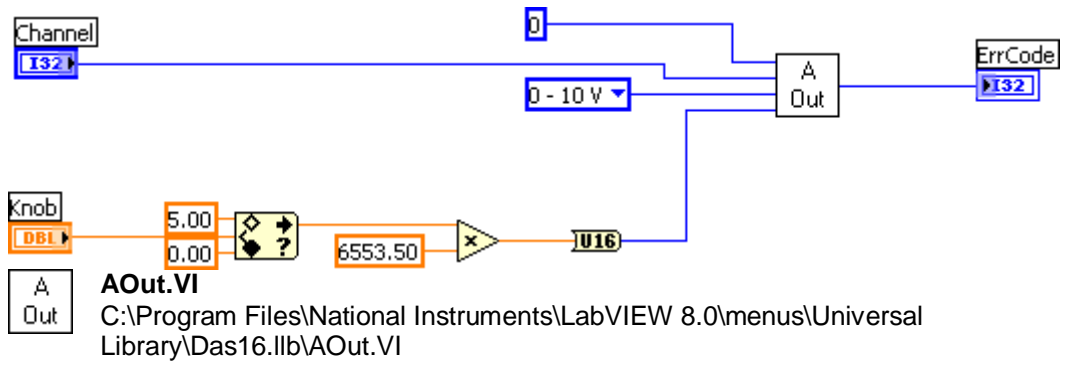


I32 Channel D/A channel number to be updated.

DBL Knob

I32 ErrCode Error code returned from the Universal Library. Zero if no error occurred. Use

the ErrMsg VI to convert ErrCode into a readable string.



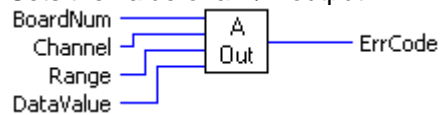
"AnalogOutput.vi History"
 Current Revision: 7

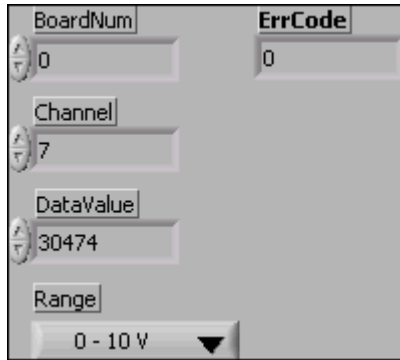
Position in Hierarchy



AOut.VI

Sets the value of a D/A output.





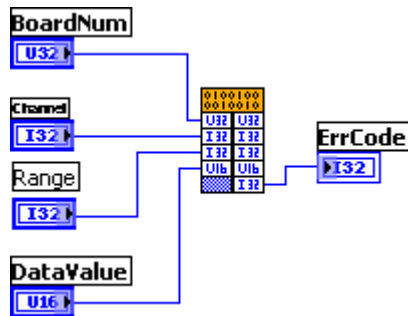
U32 BoardNum The board number used when installed with InstaCal. Can be 0 to 100.

I32 Channel D/A channel number to be updated.

U16 DataValue Value in binary counts to set the D/A to. Use FromEng.VI to convert a value in engineering units to binary counts to be used with this VI.

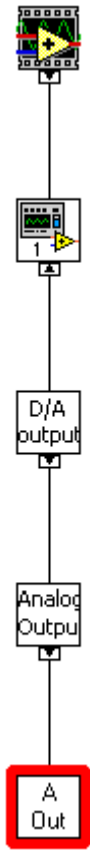
I32 Range The programmable gain/range used when the data was collected.

I32 ErrCode Error code returned from the Universal Library. Zero if no error occurred. Use the ErrMsg VI to convert ErrCode into a readable string.

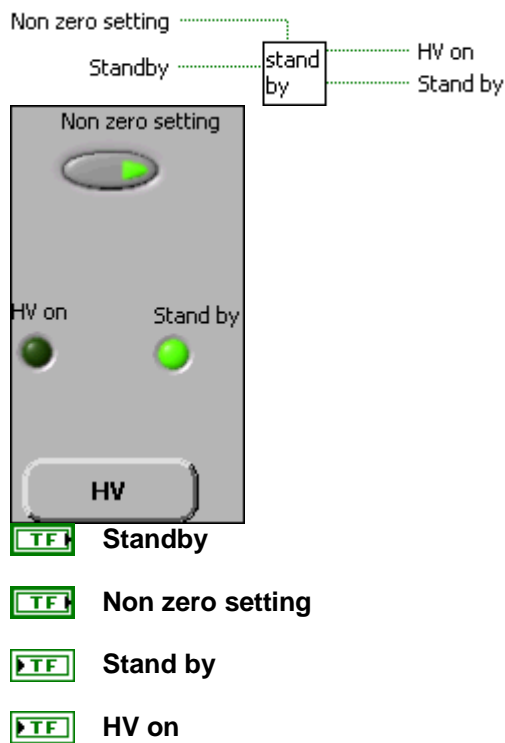


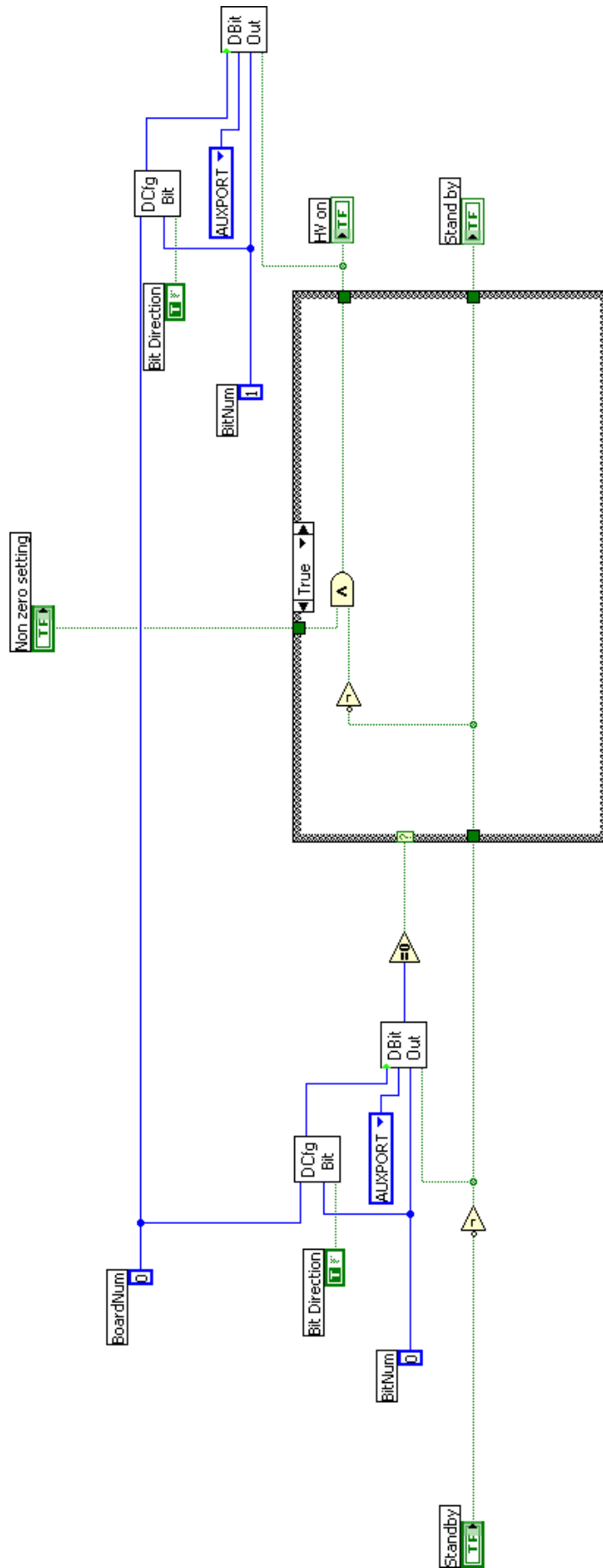
"AOut.VI History"
Current Revision: 26

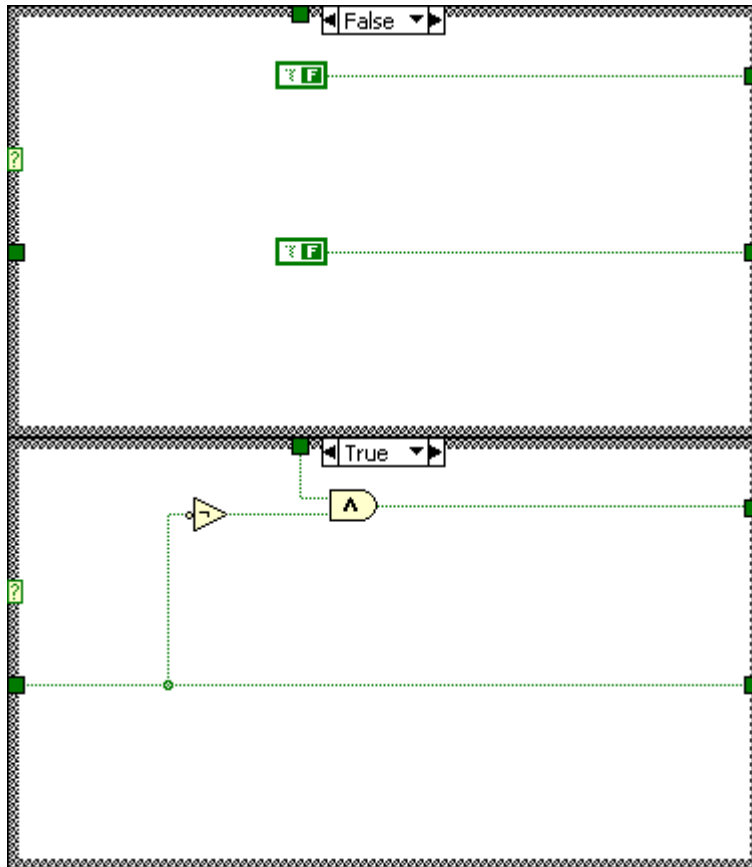
Position in Hierarchy



Standby.vi







DCfg
Bit

DCFGBIT.VI

C:\Program Files\National Instruments\LabVIEW 8.0\menus\Universal Library\Das16.Ilb\DCFGBIT.VI

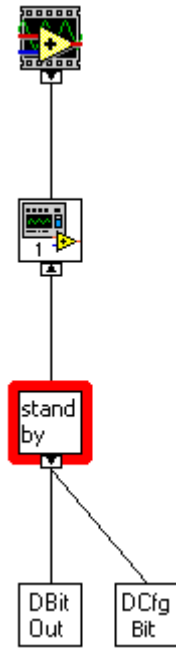
DBit
Out

DBitOut.VI

C:\Program Files\National Instruments\LabVIEW 8.0\menus\Universal Library\Das16.Ilb\DBitOut.VI

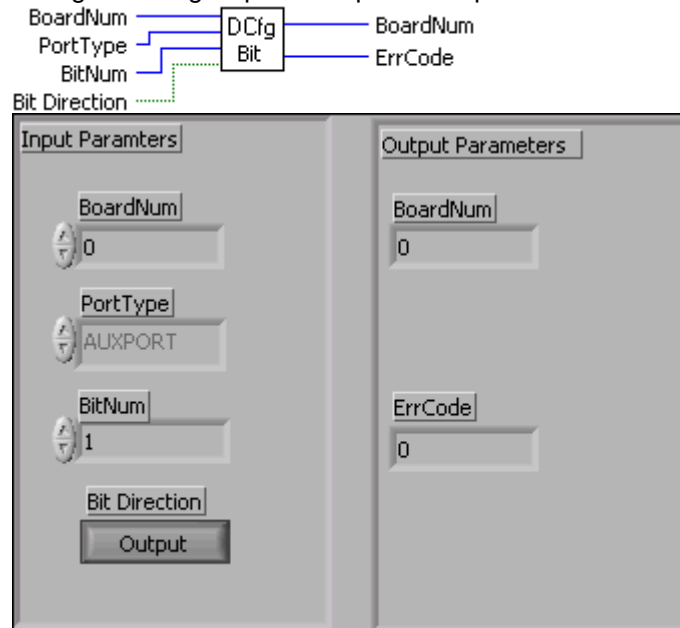
"Standby.vi History"
Current Revision: 7

Position in Hierarchy



DCFGBIT.VI

Configures a digital port as Input or Output.



U32 BoardNum Board number (0..9).

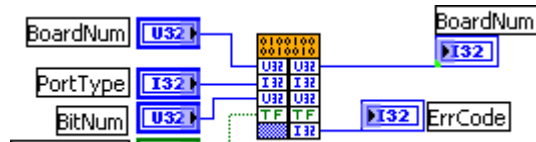
I32 PortType Specifies which digital I/O port to configure. The DCFGBIT.VI supports AUXPORT types only

TF Bit Direction Data direction.

U32 BitNum Specifies which bit to write.
 0-7 : FIRSTPORTA
 ...
 188-191: EIGHTHPORTCH

I32 ErrCode Error code from ComputerBoards Inc. universal library, see ErrMsg.VI.

I32 BoardNum



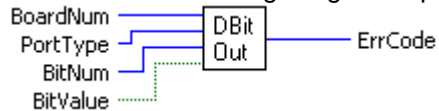
"DCFGBIT.VI History"
Current Revision: 20

Position in Hierarchy



DBitOut.VI

Sets the state of a single digital output bit.



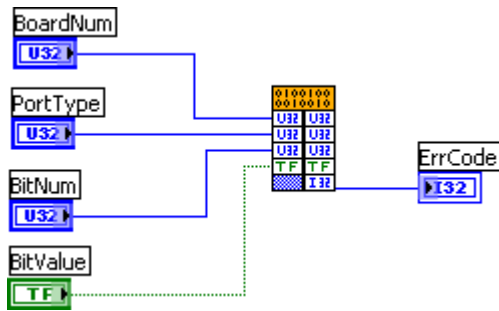
U32 PortType Specifies digital port (AUXPORT, FIRSTPORTA).

U32 BoardNum The board number used when installed with InstaCal. Can be 0 to 100.

U32 BitNum Specifies which bit to set.

TF BitValue The bit's value (0 or 1).

ErrCode Error code returned from the Universal Library. Zero if no error occurred. Use the ErrMsg VI to convert ErrCode into a readable string.



"DBitOut.VI History"
Current Revision: 17

Position in Hierarchy



Appendix C. ImageJ Visual Basic script

```
// Thomas Wray
// Tue 04 Jan 2011 18:28:45 GMT
// Macro will collect profile data from a stack of images and
// output to
// an excel spreadsheet on the desktop

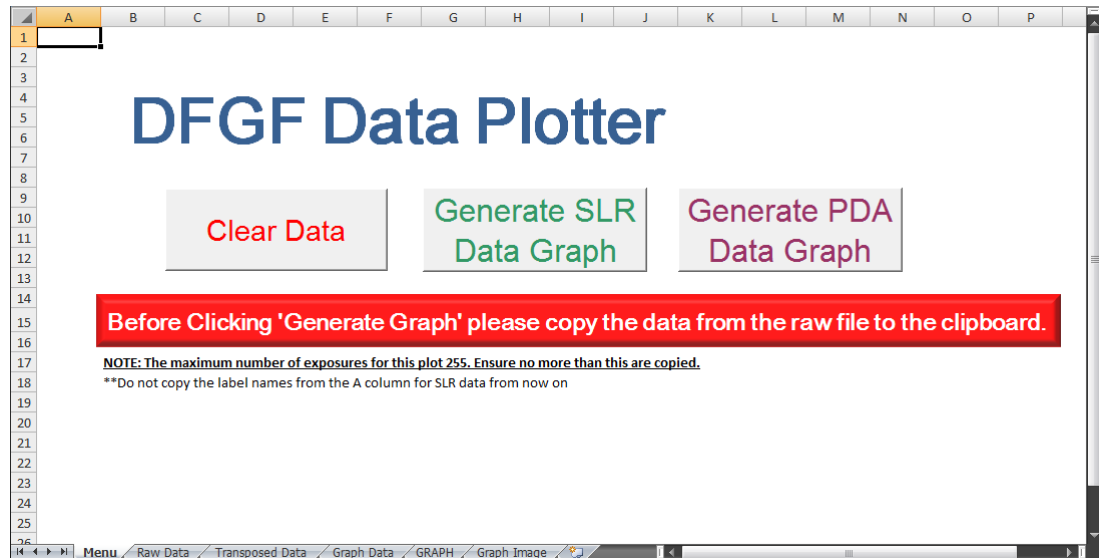
macro "Profile Data File" {
  if (nSlices==1)
    exit("Stack required");
  setBatchMode(true);
  stack1 = getImageID;
  n = nSlices;
  run("Clear Results");
  for (j=1; j<n+1; j++) {
    showProgress(j, n);
    selectImage(stack1);
    setSlice(j);
    run("Select All");
    profile = getProfile();
    for (i=0; i<profile.length; i++)
      setResult(j, i, profile[i]);
  }
  updateResults;

  // Plot profile
  //Plot.create("Profile", "X", "Value", profile);

  // Save as spreadsheet compatible text file
  saveAs("Measurements",
"/home/tom/Desktop/profile_data.xls");

  setSlice(1);
  setBatchMode(false);
  exit("All data collected and saved as Excel spread
sheet");
}
```

Appendix D. VBA MS Excel based system for graph generation



Sub ClearData()

```
Sheets("Raw Data").Select
Cells.Select
Application.CutCopyMode = False
Selection.ClearContents
Range("A1").Select
Sheets("Transposed Data").Select
Cells.Select
Application.CutCopyMode = False
Selection.ClearContents
Range("A1").Select
Sheets("Menu").Select
Range("A1").Select
```

End Sub

Sub PDA_Data_Graph()

```
Sheets("Transposed Data").Select
Range("A1").Select
ActiveSheet.Paste
```

```

Range("A1").Select
    Sheets("Transposed Data").Select
    Range("A1").Select
    Sheets("Graph Data").Select
    Sheets("Graph Data").Select
    Range("B507").Select
    Dim strX As String
    strX = ActiveCell.Value

    Range("A1:" & strX).Select
    ActiveWorkbook.Names.Add Name:="data", RefersTo:=Range("A1:" & strX)
    Sheets("GRAPH").Select
    ActiveSheet.ChartObjects("Chart 1").Activate
    ActiveChart.SetSourceData Source:=Range("Data")
    ActiveSheet.ChartObjects("Chart 1").Activate
    ActiveChart.ChartArea.copy
    Sheets("Graph Image").Select
    Range("A1").Select
    ActiveSheet.Pictures.Paste.Select
    Range("A1").Select
MsgBox ("A graph has been plotted successfully.")

End Sub

Sub GenerateGraphFromNewData()

    Sheets("Raw Data").Select
    Range("A1").Select
    ActiveSheet.Paste
    Range("A1").Select
    Range(Selection, Selection.End(xlDown)).Select
    Range(Selection, Selection.End(xlToRight)).Select
    Application.CutCopyMode = False
    Selection.copy
    Sheets("Transposed Data").Select

Range("A1").Select
    Selection.PasteSpecial Paste:=xlPasteAll, Operation:=xlNone, SkipBlanks:= _

```

```

    False, Transpose:=True
Range("A1").Select
Sheets("Transposed Data").Select
Range("A1").Select
Application.CutCopyMode = False
ActiveCell.FormulaR1C1 = "0"
Range("A1").Select
Sheets("Graph Data").Select
Sheets("Graph Data").Select
Range("B507").Select
Dim strX As String
strX = ActiveCell.Value

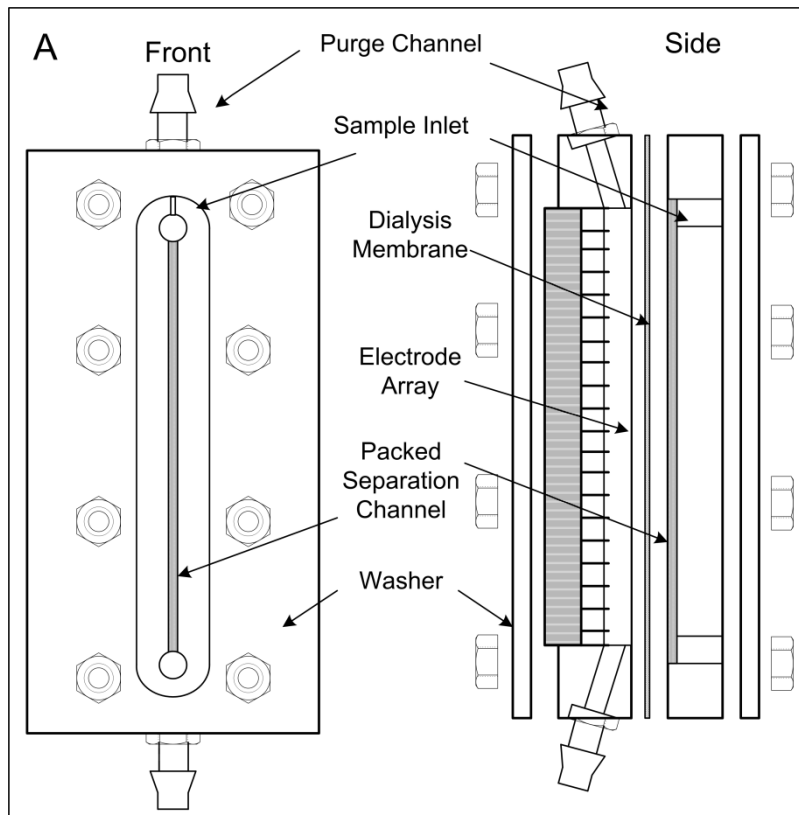
Range("A1:" & strX).Select
ActiveWorkbook.Names.Add Name:="data", RefersTo:=Range("A1:" & strX)
Sheets("GRAPH").Select
ActiveSheet.ChartObjects("Chart 1").Activate
ActiveChart.SetSourceData Source:=Range("Data")
ActiveSheet.ChartObjects("Chart 1").Activate
ActiveChart.ChartArea.Copy
Sheets("Graph Image").Select
Range("A1").Select
ActiveSheet.Pictures.Paste.Select
Range("A1").Select
MsgBox ("A graph has been plotted successfully.")

End Sub

Sheet! Graph Data =('Transposed Data'!B$1)-('Transposed Data'!B1)

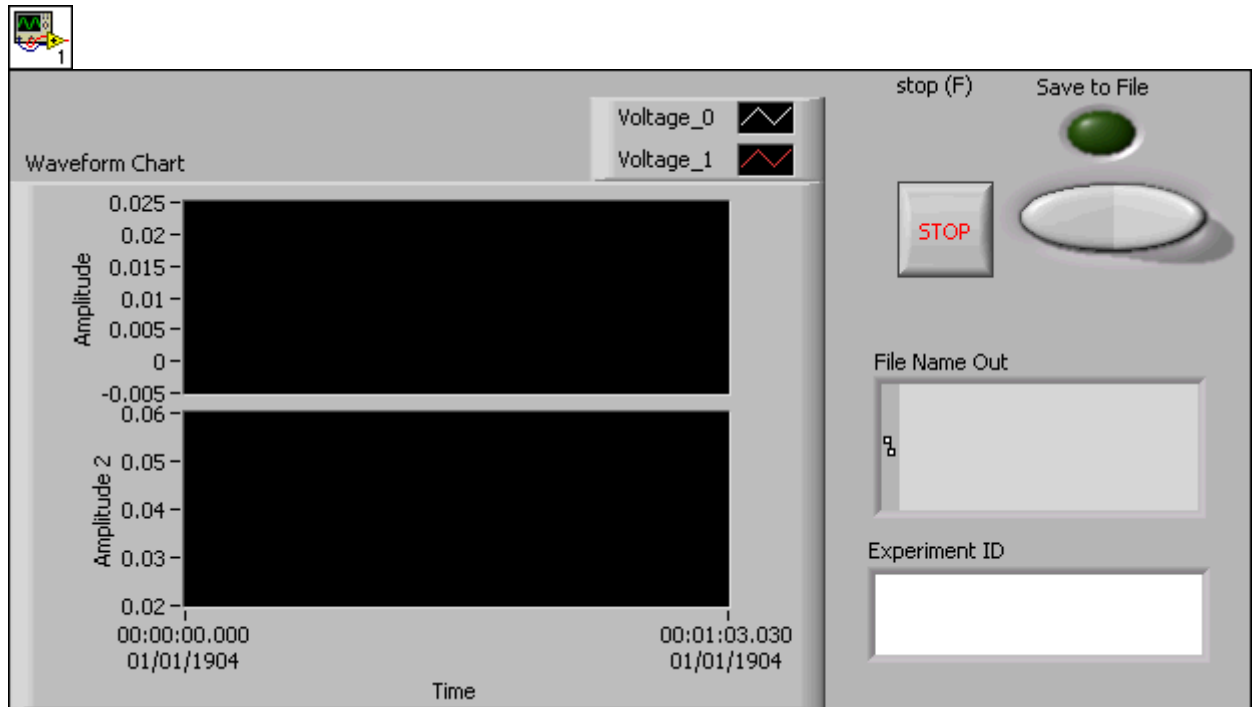
```


Appendix E. First generation DFGF construction




Appendix F. LabView C4D and UV DAQ System

DAQ_Auto.vi



 stop (F)[stop (F)]

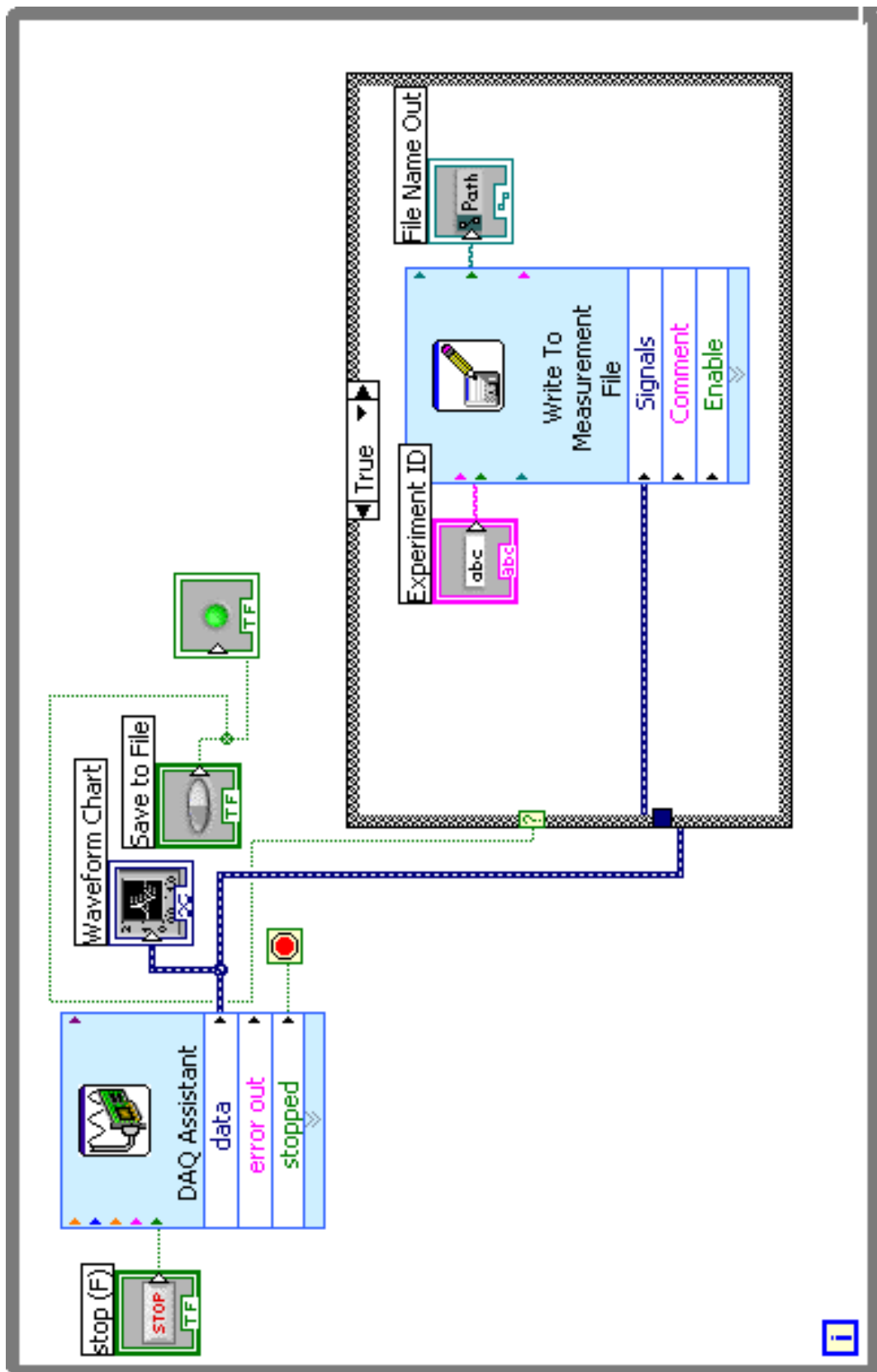
 Comment[Experiment ID] Appends a comment to each data set written to the .lvm or .tdm file.

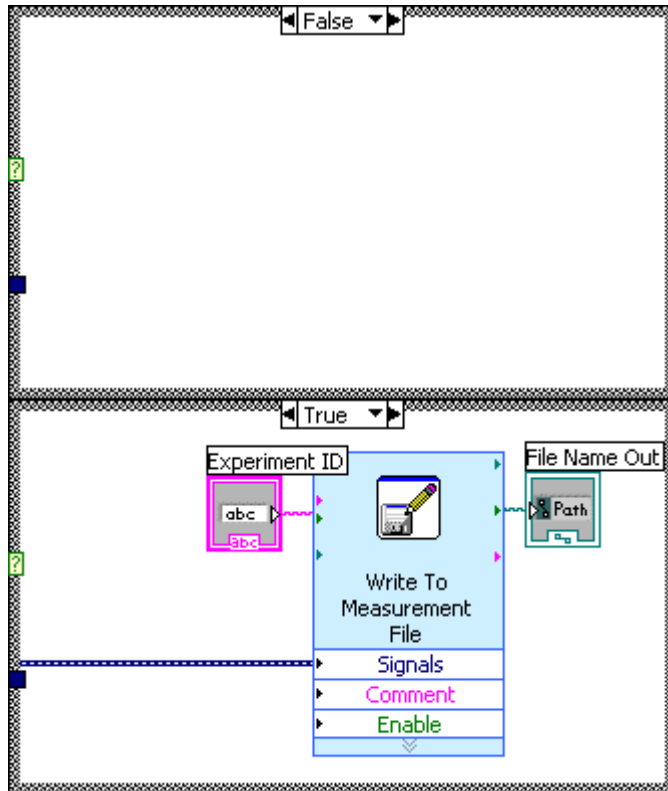
 Save to File

 Waveform Chart

 File Name Out[File Name Out] Returns the name of the file.







"DAQ_Auto.vi History"
Current Revision: 5

Appendix G. List of Software

Ubuntu Linux 11.04

WINE

Libre Office

Mendeley Desktop (Windows and Linux versions)

Microsoft Windows XP

Microsoft Office 2007

ImageJ

Fiji

ImageMagik

GNU Image Manipulation Program (GIMP)

National Instruments LabView 8.0

Nikon Camera Control Pro

Flux Instrument Janeiro 3.0

eDAQ C⁴D Application

OriginLab Origin